Extreme Activation of Androgen Receptor for Prostate Cancer Therapy

By

Mohammadreza Alizadeh Ghodsi
Dame Roma Mitchell Cancer Research Laboratories
Faculty of Health and Medical Sciences
School of Medicine
The University of Adelaide

A thesis submitted to the University of Adelaide in fulfilment of the requirements for the degree of

Doctor of Philosophy
Medicine

May 2021

Table of Contents

Abstract

Prostate cancer (PCa) is the second most common cancer worldwide in men and one of the major causes of cancer-related death among men in Australia. In PCa cells, the androgen receptor (AR) is the key driver of cell proliferation, cell cycle progression, and metabolism; thus, blocking AR activity with androgen deprivation therapy (ADT) is a standard-of-care treatment for metastatic PCa. However, ADT is never curative, with all patients eventually relapsing with lethal castration-resistant prostate cancer (CRPC). In a paradoxical phenomenon, potent activation of AR with high doses of androgens can also inhibit the growth of PCa tumours. However, the exact mechanism(s) by which activation of AR can block PCa growth is poorly understood. Therefore, in my PhD project, I explored the mechanisms underlying PCa growth suppression in response to extreme activation of AR using a potent androgen, methyltestosterone (MeT).

I have found that methyl-testosterone (MeT), a synthetic androgen, can potently transactivate AR and suppress the proliferation of AR-positive prostate cancer cells (LNCaP, C42B, MR49F, and 22RV1) but not an AR-negative cell line (PC3) or a PCa model expressing a version of the AR lacking the ligand-binding domain (R1-D567), suggesting that the growth-inhibitory effects of MeT are AR-dependent. Mechanistically, MeT acts much like high-dose dihydrotestosterone (DHT) in terms of genome-wide AR binding (evaluated by ChIP-seq) and the transcriptional program activated via AR (evaluated by RNA-seq). However, these analyses showed that MeT only extends the AR cistrome and enables AR to act as a potent

transcriptional repressor of genes associated with cell cycle, DNA replication, and DNA damage responses.

Unexpectedly, our RNA-seq data revealed that MeT dysregulates the expression of transposable elements, including endogenous retroviruses (ERVs). Mechanistically, we found that MeT suppresses the expression of DNA methyl-transferases (DNMTs) and EZH2, which are considered to be key factors repressing the expression of transposable elements. Consistent with the proposed hypothesis, my PhD work showed that MeT caused global hypomethylation of DNA and re-distribution of H3K27me3. More specifically, my research supports a model whereby DNA hypomethylation was linked to the induction of endogenous retroviruses (ERVs). Interestingly, I found that ERV induction was associated with a "viral mimicry" response characterised by activation of pattern recognition receptors RIG-I and STING and subsequent activation of interferon (IFN) signalling. Importantly, I also observed increased expression of MHC class I genes with MeT treatment, suggesting that it can enhance tumour immunogenicity. Validating this finding, co-culture of a murine model of PCa (RM1) with tumour-specific $CD8^+$ T cells revealed that MeT promoted enhanced recognition and functional cytokine production by T cells.

Collectively, my work has provided a greater understanding of growth-inhibitory effects of androgens on PCa tumours and uncovers a potential new role for high-dose androgen therapy as an immunosensitisation agent.

Declaration

I certify that this work contains no material which has been accepted for the award of any other degree or diploma in my name, in any university or other tertiary institution and, to the best of my knowledge and belief, contains no material previously published or written by another person, except where due reference has been made in the text. In addition, I certify that no part of this work will, in the future, be used in a submission in my name, for any other degree or diploma in any university or other tertiary institution without the prior approval of the University of Adelaide and where applicable, any partner institution responsible for the joint-award of this degree.

The author acknowledges that copyright of published works contained within the thesis resides with the copyright holder(s) of those works.

I also give permission for the digital version of my thesis to be made available on the web, via the University's digital research repository, the Library Search and also through web search engines, unless permission has been granted by the University to restrict access for a period of time.

I acknowledge the support I have received for my research through the provision of an Australian Government Research Training Program Scholarship.

Mohammadreza Alizadeh Ghodsi

May 2021

Acknowledgements

I would like to express my deepest appreciation to my principal supervisor A/Prof Luke Selth for his excellent mentorship and for offering his expertise on various facets of this project. This thesis would not have been accomplished without his sustained efforts, generous time, and invaluable guidance in all the time of my PhD studies.

I am also greatly indebted to Prof Wayne Tilley, the director of the Dame Roma Mitchell Cancer Research Laboratories, who provided me with an opportunity to work in his Lab and gain substantial benefits from being under his generous tutelage. His enormous support and guidance during my PhD program were greatly appreciated.

I would like to extend my sincere thanks to A/Prof Theresa Hickey and Prof Benjamin Thierry for their interest in my project and their insightful comments.

Special thanks to all previous and current members of Dame Roma Mitchell Cancer Research Labs at the University of Adelaide. I am honoured and extremely fortunate to have worked and interacted with such an amazing team. I also wish to extend my gratitude to members of Parker's lab at Peter MacCallum Cancer Centre. Collaborating with her lab was one of the most exciting parts of my PhD work.

I am grateful to the Australian government for awarding me the Australian Government Research Training Program Scholarship.

I would also like to express my special appreciation to my best friends, Leila HosseinZadeh and Mohammad Pourhassan Moghaddam for being with me in my joys and sorrows. It was their friendship, support, and constant encouragement that have made my life in the Australia a wonderful time.

Last but not least, I would like to express my profound gratitude to my Mom and Dad, Farahnaz and Mahmoud, and lovely sister, Parinaz. Your unwavering love, encouragement, and support are the key to my success. An exceptional thanks to my fiancée, Bahareh, for her tremendous understanding of my absence while I pursue our ambitions and for providing me with continuous encouragement throughout the peaks and valleys of this journey.

Chapter 1: Introduction

1.1. Prostate gland structure and function

The prostate is the largest accessory genital gland that secretes material making up 30-35% of the seminal fluid that protects sperm (Resnick and Thompson 2000). This material includes high levels of divalent cations and several proteases, the most abundant being prostate-specific antigen (PSA or kallikrein-related peptidase-3 (KLK3), encoded by the *KLK3* gene). PSA is responsible for the degradation of the semenogelins I and II in semen after ejaculation, which improves sperm motility (Mattsson, Ravela et al. 2014).

The prostate gland consists of 30 to 50 branched tubule-acinar glands surrounded by a capsule. As shown in figure 1.1, this gland can be divided into three zones histologically: the peripheral zone (about 70% of the glandular tissue of the prostate), central zone (20–25% of the glandular tissue of the prostate), and transition zone (5–10% of the glandular tissue of the prostate). The central zone is the entire base of the prostate and includes the ejaculatory ducts. In the peripheral zone, acini are round to oval and surrounded by a loose stroma of smooth muscle and collagen (Figure 1.2a and 1.2b). Central zone acini are complex and large (Figure 1.2c and 1.2d). Transition zone glands are simple, small, and round and set in a compact stroma (Figure 1.2e and 1.2f).

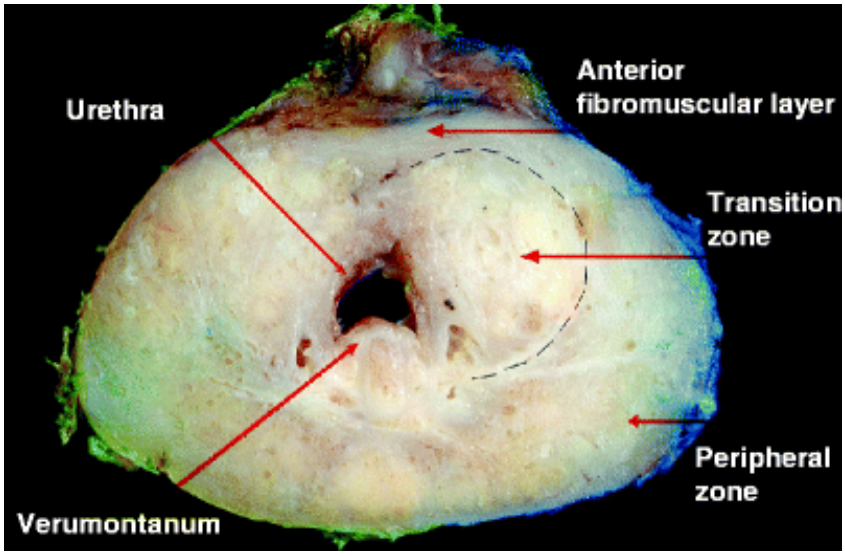

Figure 1.1. Typical anatomy of the prostate gland. The location of prostate zones in the coronal section of the prostate gland (Shah and Zhou 2012).

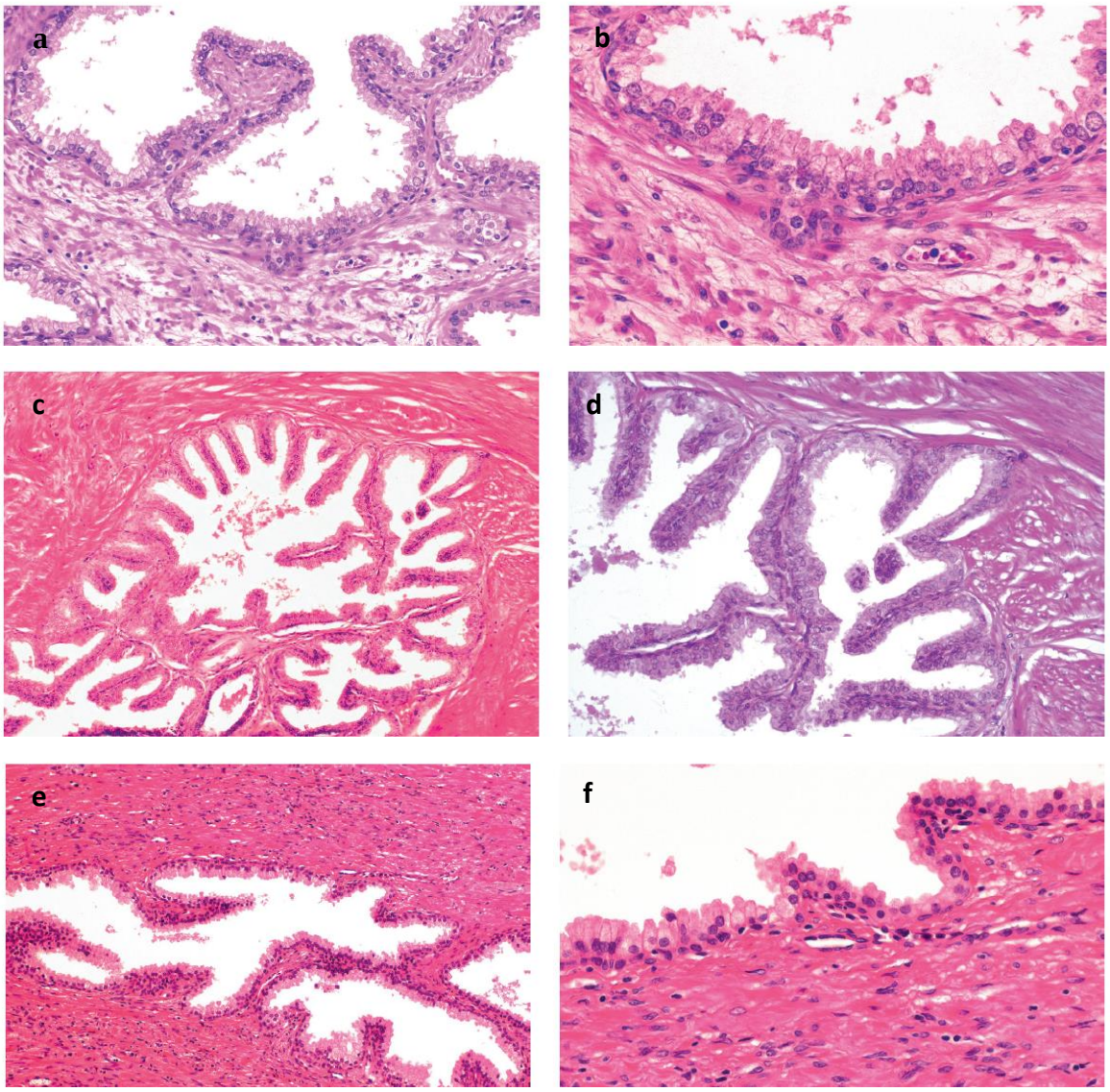

Figure 1.2. Normal Prostate histology. **1.2a.** simple peripheral zone acini. **1.2b.** Columnar epithelium of normal peripheral zone. **1.2c**. Normal, large, complex with papillary infoldings acini of the central zone. **1.2d**. Cuboidal to columnar epithelium of normal central zone. **1.2e.** Normal and simple acini of transition zone with compact stroma. **1.2f**. Cuboidal or low columnar epithelium of normal transition zone (Bostwick and Cheng 2008).

1.2. Androgen receptor (AR) structure and function

Androgen receptor (AR), a member of the steroid and nuclear receptor superfamily (NR3C4, nuclear receptor subfamily 3, group C, gene 4), plays a critical role in the development and homeostasis of the prostate gland. The gene encoding the AR protein is located at the locus Xq11-Xq12 on chromosome X with 8 exons and introns varying between 0.7 to 2.6 kb. AR protein, as a ligand-dependent transcription factor, is a phosphoprotein of 919 amino acids and consists of three main functional domains, including an N-terminal domain (NTD), a DNA-binding domain (DBD), and a C-terminal ligand-binding domain (LBD). A flexible region named hinge connects the LBD domain to the DBD (Lorente, Mateo et al. 2015) (Figure 1.3).

The NTD (residues 1–558) encoded by exon 1 of the AR gene, constitutes approximately 60% of the 110 kDa AR protein (Imamura and Sadar 2016). This domain consists of two regions termed TAU-1 (residues 101–370) and TAU-5 (residues 360–485), which are involved in the transcriptional activity of AR (Jenster, van der Korput et al. 1995). Activation function-1 (AF1) in the TAU-1 domain mediates the protein-protein interactions between AR and coregulatory proteins (Kumar, Betney et al. 2004, Lavery and McEwan 2008, De Mol, Szulc et al. 2018). TAU1 and TAU5 can also mediate the inter-domain interactions between NTD and LBD (N/C interaction), which is an important regulatory mechanism for the expression of some AR target genes (McEwan and Gustafsson 1997, Reid, Murray et al. 2002).

AR exons 5-8 encode the LBD (residues 666–919), consisting of eleven α-helices (H1 to H12) and two β-sheets arranged in a three-layer antiparallel helical sandwich. AR LBD is characterized by a ligand-binding pocket, in which lipophilic ligands are captured in a

hydrophobic cavity (Tan, Li et al. 2015). In response to structurally different AR ligands, hydrophobic amino acids in the LBD can adopt different conformations to maintain the ligand in the steroid-binding cavity. Following the hydrophobic interactions, hydrogen bonds between AR and ligands are formed, firmly tethering the steroid molecule (Pereira de Jésus-Tran, Côté et al. 2006). Structurally, the H12 helix acts as a lid to close the LBP upon ligand binding, leading to the formation of a hydrophobic cleft called the activation function 2 domain (AF2). AF2 acts as a ligand-dependent docking site for AR coactivators such as steroid receptor coactivator-3 (SRC3) (He, Kemppainen et al. 2000, Zhou, Suino-Powell et al. 2010, Tan, Li et al. 2015).

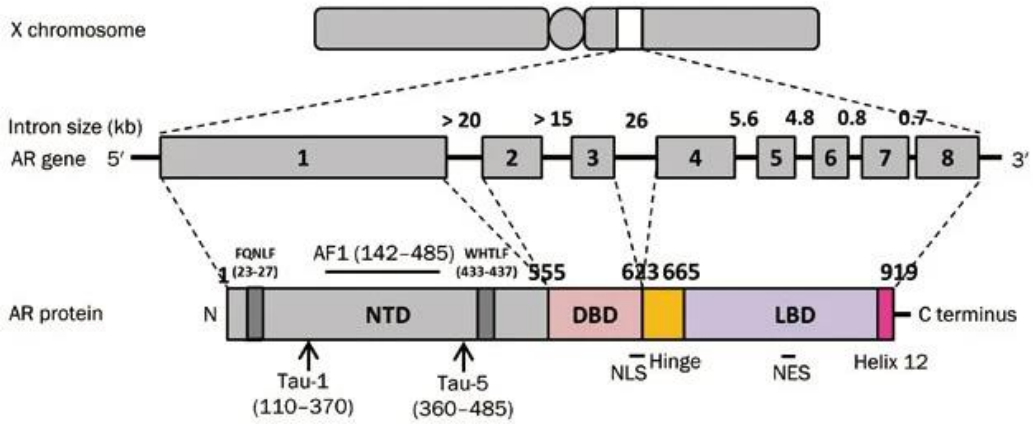

Figure 1.3. A. The structure of the androgen receptor. AR gene consists of 8 exons, encoding three main domains of AR protein including an N-terminal domain (NTD), a DNA-binding domain (DBD), and a C-terminal ligand-binding domain (LBD) (Tan, Li et al. 2015).

The DBD enables AR to bind the androgen response element (ARE) sequences in promoter and enhancer regions of AR-regulated genes. Each ARE consists of two equal, hexameric half-sites (5'-AGAACA-3') separated by a three base-pair spacer. Structurally, AR DBD (residues 556–623) consists of a "core" composed of two Zinc fingers and one carboxyl-terminal extension (CTE) region which is encoded by exon 4 (Khorasanizadeh and Rastinejad 2001, Gelmann, Sawyers et al. 2013). Formed through hydrophobic interactions, DBD Zinc fingers are associated with two zinc ions, leading to the formation of "P-box" and "D-box" in N-terminal and C-terminal Zinc-fingers, respectively. Molecularly, when AR is liganded with an agonist, D-box mediates AR dimerization in a "head-to-head" manner allowing the AR to bind as a dimer to the two half-sites of an ARE (Shaffer, Jivan et al. 2004, Lallous, Dalal et al. 2013). The N-terminal Zinc-finger, termed the Recognition helix, subsequently inserts into the major groove of the chromatin and P-box specifically binds to ARE (Umesono and Evans 1989, Khorasanizadeh and Rastinejad 2001). In addition to Zinc fingers, amino acids residues at CTE are also involved in AR binding to DNA (Gelmann, Sawyers et al. 2013).

1.3. Cellular and molecular phenotypes of prostate epithelial cells

Based on cellular and molecular phenotypes, the glandular prostate epithelium can be categorized into three main cell types including secretory luminal cells, basal cells, and neuroendocrine cells (Van Leenders, Gage et al. 2003). Luminal cells, which can be found in the luminal layer of prostate epithelium, express a high level of androgen receptor (AR) representing the major secretory cells in prostate epithelium. Importantly, in the normal prostate gland, luminal cells are androgen-dependent, terminally differentiated with the lowest proliferation capability. By contrast, basal cells localised in the basal part of glandular epithelium, are androgen-independent, less differentiated, and highly proliferative cells, characterized by a low level of AR and without a significant secretory function. Characterized as the least terminally-differentiated and androgen insensitive cells, neuroendocrine cells can be identified in the prostate epithelium; however, they are less frequent and their function is not completely understood (Table 1.1) (Hudson 2004, Lang, Frame et al. 2009).

Table 1.1. Cellular and molecular phenotypes of prostate epithelial cells

Prostate Epithelial cells	Differentiation/Proliferative status	Key Morphological phenotypes in normal Prostate tissue	Key Molecular phenotypes	Reference (s)
Luminal secretory cells	Terminally-differentiated cells, characterised by lowest proliferative activity and high secretory function; accounting for 73% of the total epithelium volume; androgen-dependent cells	Cuboidal to columnar, with small, round nuclei	High level of AR (+); PSA (+); PAP (+); keratins (K) 8 and 18 (+)	(Van Leenders, Gage et al. 2003, Bostwick and Cheng 2008)
Basal cells	Less common epithelial cells in prostate gland; relatively undifferentiated cells with highest proliferative activity; without secretory function; androgen-independent cells	Flattened and elongate cells surmounting the basement membrane	Low level of AR (+), BCL-2 (+); p63 (+); keratins 5 and 14 (+)	(Robinson, Neal et al. 1998, Bostwick and Cheng 2008)
Neuroendocrine cells	Terminally differentiated epithelial cells in prostate gland; Androgen-insensitive cells	infrequent cells with variability in their morphology; cannot be identified using conventional H&E Staining	Contain both AR-positive and AR-negative cell populations; Serotonin (+); Chromogranin A (+); Neuron-specific enolase (+)	(Nakada, di Sant'Agnese et al. 1993, Bostwick and Cheng 2008, Grigore, Ben-Jacob et al. 2015)

1.4. Androgen receptor agonists

AR agonists consist of small molecules which can interact with AR LBD and stimulate AR transcriptional activity function. These AR interacting compounds can be categorised based on their chemical structure (steroidal versus nonsteroidal) and also the origin of synthesis (endogenous versus synthetic agonist) (Gao, Kim et al. 2006). Testosterone (T) and its potent metabolite, dihydrotestosterone (DHT), are the major male sex hormones acting as endogenous steroidal AR agonists, inducing both androgenic and anabolic effects in a tissue-specific manner (Pihlajamaa, Sahu et al. 2015, Feng and He 2019). Androgenic effects are associated with androgen effects on male sex characteristics and anabolic effects are mainly linked to effects of androgens on skeletal muscle and bones (Bhasin, Taylor et al. 2003).

Another group of AR agonists called anabolic-androgenic steroids (AAS) are synthetic derivatives of T, developed to modulate the androgenic effects of endogenous steroids. In comparison with endogenous androgens, these compounds have improved bioavailability, reduced adverse androgenic effects, and enhanced anabolic features and are clinically used as testosterone analogues for hormone replacement therapies (Patt, Beck et al. 2020). Structurally, AAS hormones are synthesised either through the esterification (e.g. testosterone cypionate) or alkylation (e.g. Methyltestosterone) of the testosterone backbone (Salerno, Cascio et al. 2018). These chemical modifications are mainly affecting the pharmacokinetics of the hormones; for example**,** alkylation or esterification of testosterone structure at 17-alpha position (Figure 1.4), increases the oral bioavailability and decreases the hepatic metabolism of the compound (Fragkaki, Angelis et al. 2009). These chemical

modifications on steroids may also affect the AR conformation, potentially affecting the AR function through the recruitment of different AR-coregulators in a tissue-specific manner (Chang, Norris et al. 1999, Chang and McDonnell 2002, Wang, Lawless et al. 2020).

Another group of synthetic androgens are selective androgen receptor modulators (SARMs). To reduce the undesirable androgenic effects of T on prostate cells, nonsteroidal AR ligands called SARMs have been also developed to help the patients suffering from skeletal muscle wasting. Theoretically, while acting as AR agonist in bone and skeletal muscle, SARMs function either as an antagonist or mild agonist in the prostate gland (Fonseca, Dworatzek et al. 2020). Mechanistically, the exact mechanism(s) involved in tissue-specific activation of AR by SARMs are not fully understood; however, the ligand-dependent surface topology of activated-AR and tissue-specific recruitments of unique coregulators may explain the different effects of DHT and SARMs in prostate cells (Baek, Ohgi et al. 2006, Pihlajamaa, Sahu et al. 2015).

A

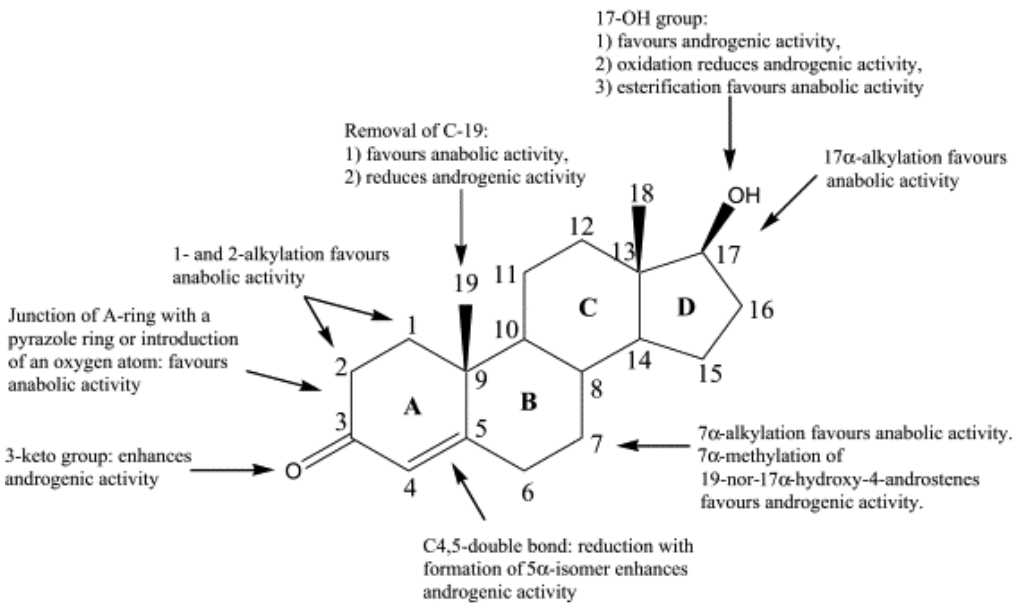

B

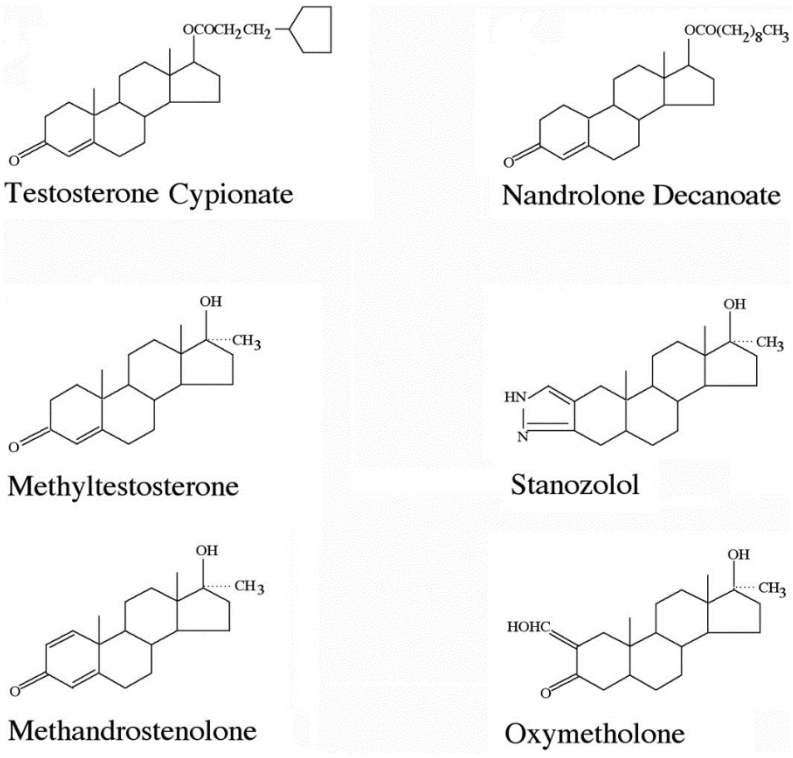

Figure 1.4. A) Chemical modifications on Testosterone backbone. **B)** Chemical structure of synthetic-androgenic AR agonists (Henderson, Penatti et al. 2006, Fragkaki, Angelis et al. 2009).

1.5. AR transcriptional activity

In normal prostate cells, the AR signalling depends on the presence of AR agonists. The inactive form of AR preferentially is located in the cytoplasm while bound to heat shock proteins (HSPs). Heat shock proteins prevent AR translocation and support the permissive conformation of AR for ligand binding (Heinlein and Chang 2002). Upon ligand binding, AR undergoes a conformational change leading to its dimerization in the cytoplasm, followed by translocation into the nucleus and binding to AREs. AR subsequently recruits the basic transcription machinery and related coregulators to trigger the transcription of androgen-responsive genes (Xu, Shimelis et al. 2009) (Figure 1.5).

1.6. Regulation of AR function by co-regulators and post-translational modifications

In the prostate cells, AR coregulators including co-activators and co-repressors are the key determinants of AR function and their quantity and interactions regulate AR's transcriptional activity (Scher, Buchanan et al. 2004). Coactivators consist of a diverse variety of proteins assisting AR in ligand binding, nuclear translocation, DNA binding, and recruitment/stabilizing of the transcription machinery (Heinlein and Chang 2002). Some coactivators, such as SRC-1 from p160/SRC family and CBP/p300, possess a histone modification activity modulating the AR signalling through chromatin remodelling (Spencer, Jenster et al. 1997, Aarnisalo, Palvimo et al. 1998).

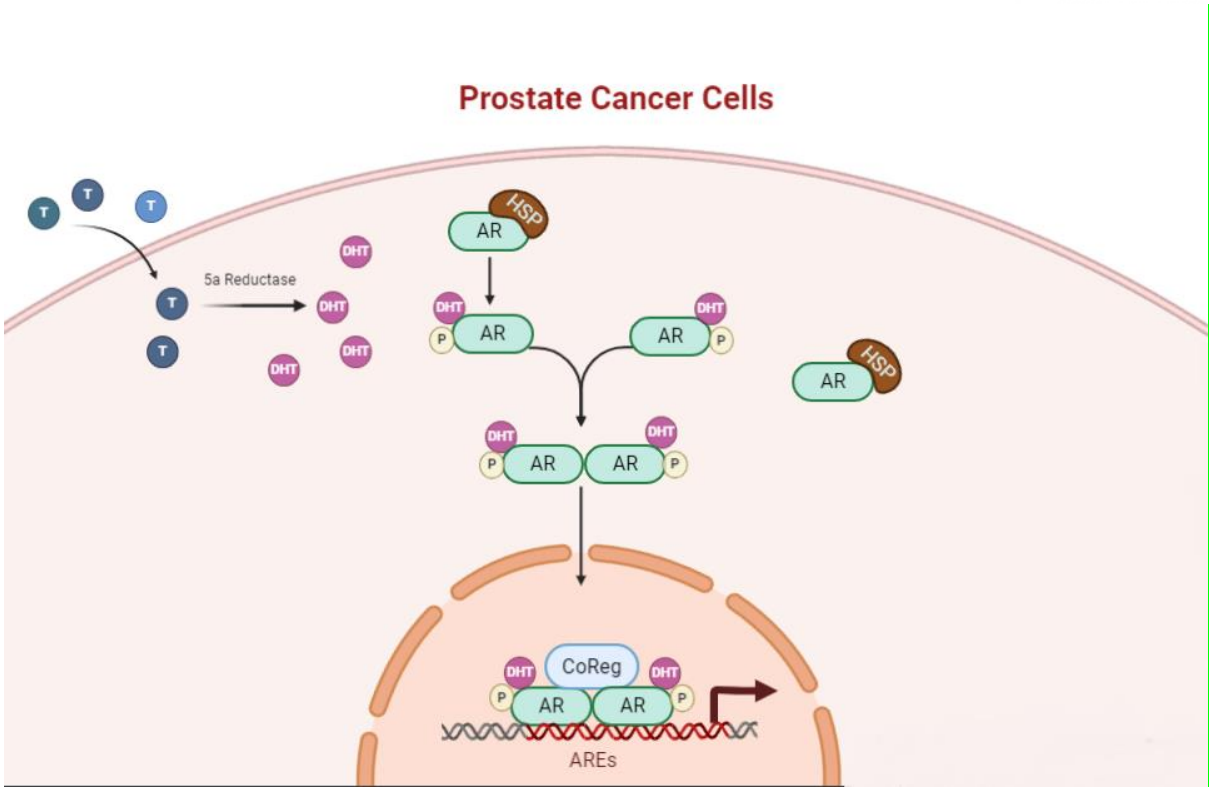

Figure 1.5. Activation of AR signalling by Androgens in prostate cancer cells. T: Testosterone; DHT: Dihydrotestosterone; AR: Androgen receptor; HSP: Heat shock proteins; p: phosphorylation; CoReg: Co-regulator; AREs: Androgen response elements.

Corepressors, in contrast, suppress the transcriptional activity of AR. This group of proteins can modulate the AR signalling by interfering in mechanisms such as AR N/C interactions, translocation, DNA binding, interaction with coactivators, and recruitment of basal transcriptional machinery (Wang, Hsu et al. 2005).

Posttranscriptional modifications of AR protein are another regulatory layer in the fine-tuning of AR function. Phosphorylation, acetylation, methylation, and ubiquitination can either positively or negatively affect AR signalling in response to different signal transduction pathways (Wen, Niu et al. 2019). For example, phosphorylation of Serine 81 (S81) in the AF1 region of the AR NTD domain mediated by different cyclin-dependent kinases (CDKs) regulates AR protein stability, localization, and transactivation (Hsu, Chen et al. 2011).

1.7. AR function in normal prostate gland

Androgens, acting via AR, have a crucial role in male phenotype formation, sexual maturation, and reproductive function. Also, non-reproductive tissues such as muscle, bone, skin, and adipose tissues are affected by androgens (Heemers and Tindall 2007). In the normal prostate gland, AR regulates the homeostasis between cell proliferation and cell death and maintains the differentiated phenotype of prostate epithelial cells (Carson and Rittmaster 2003). To this end, AR in stromal cells induces the expression of growth factors called Andromedins, stimulating the proliferation of epithelial cells in paracrine-manner. By contrast, in luminal cells, while androgens activate AR and stimulate KLK3 expression, however, it causes cell growth suppression (Figure 1.6) (Isaacs and Isaacs 2004). Mechanistically, the growth

inhibitory effect of androgens in normal prostate epithelial cells is linked to AR-mediated repression of *c-Myc* and upregulation of *p21*, *p27*, and *SKP-2*, leading to G0/G1 cell cycle arrest (Vander Griend, Litvinov et al. 2014).

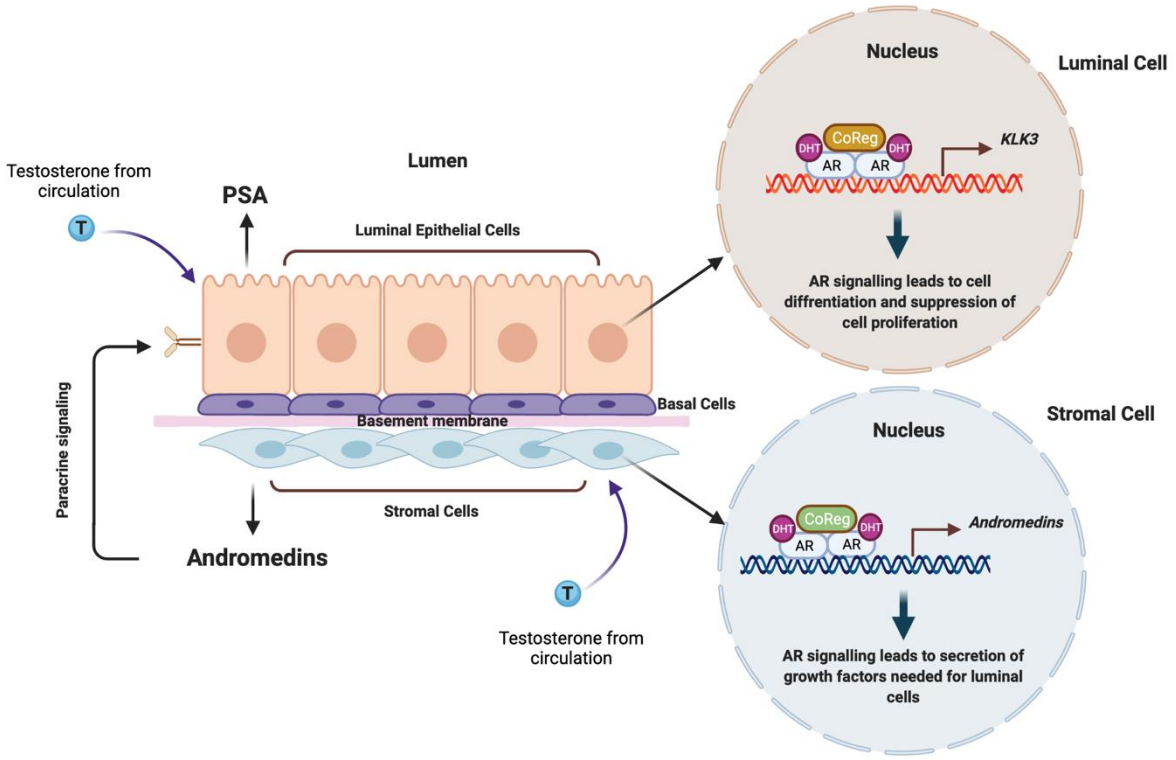

Figure 1.6. AR signalling in normal luminal and stromal cells regulates homeostasis (Isaacs and Isaacs 2004). In normal prostate, AR in stromal cells is activated by androgens, which leads to production of Andromedins, regulating the growth and maintenance of epithelial cells in a paracrine manner. In epithelial cells, however, AR activation by androgens is not associated with growth, but rather mediates the production of secretory proteins such as PSA. T: Testosterone; DHT: Dihydrotestosterone; AR: Androgen receptor; HSP: Heat shock proteins; p: phosphorylation; CoReg: Co-regulator.

1.8. Prostate malignancy

The peripheral zone in the prostate gland is responsible for about 70% to 80% of prostatic intraepithelial neoplasia (PIN) and carcinoma cases (6, 8). Figure 1.7 illustrates the morphologic features of prostate tissue from normal prostatic epithelium to early invasive carcinoma. In low-grade PIN, there is a mild dysplasia which may progress to moderate-to-severe dysplasia, high-grade PIN, and carcinoma. Malignant cell invasion to the stroma, involving disruption of the basal cell layer, is the main feature of early invasive carcinoma (6, 9).

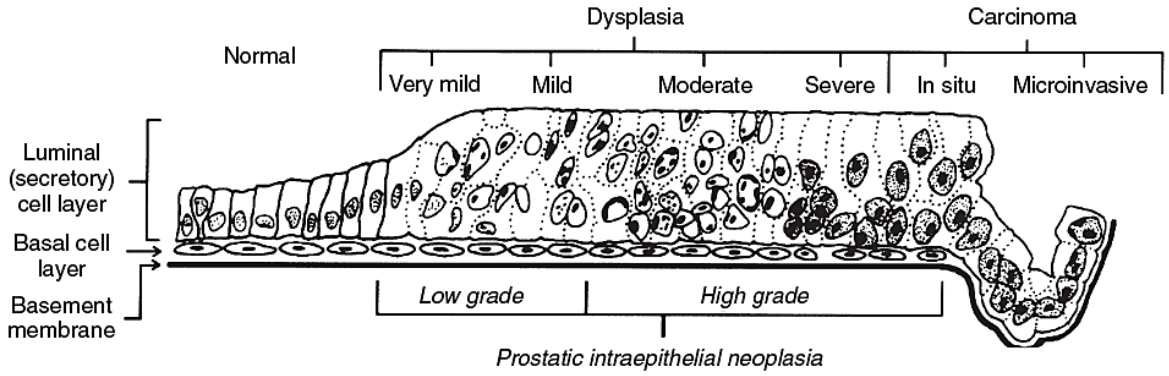

Figure 1.7. Morphologic changes of prostate tissue from normal prostatic epithelium towards early invasive carcinoma (Bostwick and Cheng 2008).

1.8.1. Epidemiology of Prostate cancer:

Prostate cancer is the second most common cancer worldwide in men after lung cancer (Bray, Ferlay et al. 2018) and is one of the major causes of cancer-associated death in men in western countries (Rebello, Oing et al. 2021).

The incidence of PCa in developed western countries is higher than developed Asian nations (e.g. Japan and South Korea) and also developing countries in the rest of the world (Kimura and Egawa 2018). Currently, Australia, New Zealand, North America and Europe, as well as regions in South America such as Brazil, have the highest incidence rates of PCa. Incidence rates are influenced by many factors, including: awareness of prostate cancer and diagnostic screening rates (Loeb, Bjurlin et al. 2014); life expectancy, since risk of prostate cancer is strongly associated with age (i.e. more than 85% of patients newly diagnosed with PCa are more than 60) (Bray, Ferlay et al. 2018); racial differences, as the development and progression of PCa are more likely in African Americans compared to individuals of European ancestry (Hur and Giovannucci 2020); and ethnic diets, since saturated fat intake has been associated with higher risk of developing the disease (Whittemore, Kolonel et al. 1995).

1.9. AR malignancy switch in Prostate Cancer

Changes in the genetic and environment of prostate epithelial cells mediate the carcinogenesis process, which ultimately leads to AR's signalling outputs shift from pro-differentiative and anti-proliferative to anti-differentiative and pro-proliferative (Berger, Febbo et al. 2004). As part of malignant transformation in prostate cells, therefore, AR is switched to an oncogenic factor, considered as a central event in the development and progression of both localized and advanced metastatic prostate cancer (Tomlins, Mehra et al. 2007). The malignancy switch of AR can be characterized by reprogramming of AR cistrome. A comparison of AR cistrome between normal and cancerous cells reveals that the pattern of genome-wide AR binding sites between normal and cancerous tissues is different, which can drive distinct transcriptional programs leading to tumour progression (Pomerantz, Li et al. 2015). Alteration in AR cistrome can be related to the recruitment of unique coregulators in cancerous cells. For example, FOXA1 and HOXB13, only co-expressed in prostate tumour cells, are co-localised with AR at tumor-specific AR binding sites (Pomerantz, Li et al. 2015). This observation suggests that the association of AR with new coregulators such as ERG, FOXA1 and HOXB13 can change the AR function through reprogramming the AR cistrome.

Gene fusions between AR-regulated genes and coding regions of oncogenic transcription factors is another potential oncogenesis process in prostate epithelial cells (Marx 2005, Tomlins, Rhodes et al. 2005). For example, *TMPRSS2–ERG* is the most common gene-fusion occurring in about 50% of all localised prostate cancer, in which promoter region of AR-regulated gene called *TMPRSS2* is fused with the coding region of *ERG*, an ETS transcription

factors (Kumar-Sinha, Tomlins et al. 2008). *TMPRSS2–ERG* expression is constantly induced by androgens, which causes the upregulation of genes associated with cell invasion and epithelial-mesenchymal transition (EMT) (Wang, Cai et al. 2008, Adamo and Ladomery 2016).

1.10. Histologic grading of prostate cancer:

The histologic grade of the tumour is a useful prognostic factor in prostatic adenocarcinoma. Although there are different histologic grading systems, the Gleason system is the best predictor of survival in men suffering from prostate cancer. The Gleason grade is a measure of the level of differentiation in the tumour, ranging from well-differentiated (score 1) to poorly differentiated (score 5). The Gleason score (GS), which ranges from 2-10, is the sum of the primary and secondary Gleason grades which refer to the dominant and second-most frequent pattern of tumour, respectively (Figure 1.8)(Short, Warren et al. 2019). The grading system was modified based on the 2014 ISUP consensus conference and Gleason scores were assigned to 5 prognostically distinct Grade groups for improved prognostication and to reduce overtreatment of indolent cancer (Egevad, Delahunt et al. 2016). The modified ISUP grading system includes all Gleason scores of 6 or less in grade I, Gleason 3+4=7 in grade II, Gleason 4+3=7 in grade III, Gleason 4+4=8 in grade IV, and all Gleason 9 and 10 in grade V (Egevad, Delahunt et al. 2016).

1.11. Treatment of localized prostate cancer

PCa has a highly variable prognosis, which mainly depends on tumour grade at primary diagnosis time. Generally, the majority (~80%) of patient with PCa are diagnosed with organ-confined disease. In patient with localized prostate cancer, the survival expectancy can be about 99% over 10 years if diagnosed at an early stage (Siegel, Miller et al. 2016). However, ~15% of patients are diagnosed with metastases within the region of primary tumours or ~5% with distant metastases (Siegel, Miller et al. 2016). For men diagnosed with metastatic disease, the prognosis is much poorer; indeed, the overall survival rate in PCa patient diagnosed with a distant metastasis is only about 30% at 5 years (Siegel, Miller et al. 2016).

Based on a recommendation by the European Association of Urology, there is a wide variation in treatment intensity that can be applied for localized prostate cancer (Mottet, Bellmunt et al. 2017). Over the last years, active surveillance has been applied as an alternative to intensive treatment of low-risk prostate cancer. Active surveillance is described as close monitoring of cancer progression using PSA and without intensive therapies such as surgery (Haymart, Miller et al. 2017). This strategy is carried on men with low to intermediate grade prostate cancer. However, among these patients, 20% to 41% will need definitive treatment in the following 5 years to control tumour growth. Radical prostatectomy is one of the most common major treatment measures in patients with localized prostate cancer. Mortality and risk of local progression and metastasis are decreased by radical prostatectomy (Bill-Axelson, Holmberg et al. 2005).

Another major treatment method for localised prostate cancer is radiotherapy, comprising radioactive isotopes, photons, and particle beams (Bagshaw, Kaplan et al. 1993). In a study by Hamdy, Freddie C., et al. (Hamdy, Donovan et al. 2016), the effectiveness of external-beam radiotherapy compared to active monitoring and radical prostatectomy was evaluated in terms of mortality and the incidence of metastases and disease progression at a median of 10 years of follow-up. The results of this randomized trial found that radiotherapy (and prostatectomy) were associated with lower rates of disease progression and metastases than active monitoring (Hamdy, Donovan et al. 2016).

However, while surgery and radiation therapies cure a substantial proportion of men, approximately 30% experience recurrence with metastatic disease (Singh, Febbo et al. 2002). Additionally, some men are diagnosed with metastatic PCa, which cannot be treated with surgery or radiation therapy (Aus, Robinson et al. 2005). Androgen deprivation therapy is the key strategy for men who fail treatment for localised disease or who are diagnosed with metastatic disease (see below).

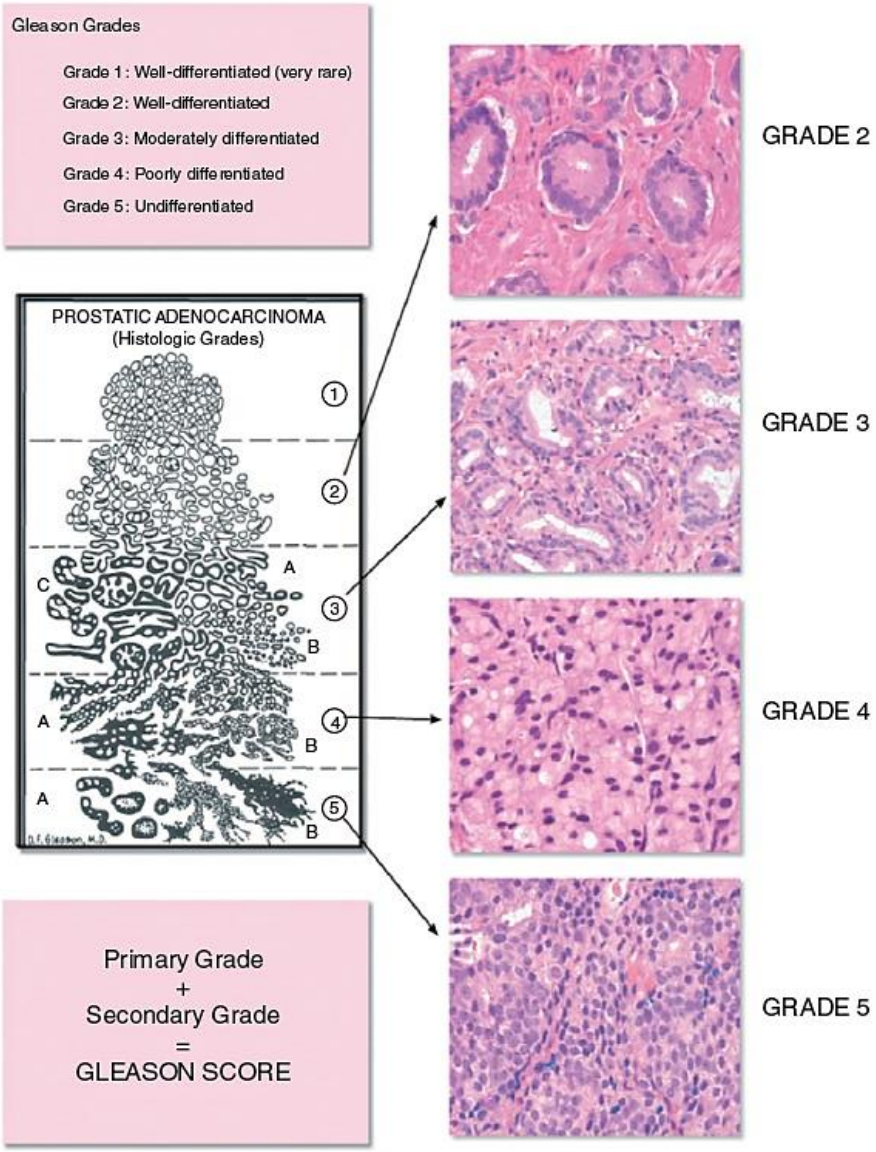

Figure 1.8. The Gleason score ranges and pathological features in different clinical stages of prostate cancer (Bostwick and Cheng 2008).

1.12. Treatment of Metastatic Prostate Cancer

As described earlier, the growth and progression of prostate cancer rely heavily on AR activation by T and DHT. Consequently, androgen deprivation therapy (ADT) has been the main therapeutic strategy for metastatic prostate cancer for many decades (Thompson, Goodman et al. 2003, Vignozzi, Rastrelli et al. 2014). ADT comprises surgical or medical castration, which greatly reduces the levels of circulating testicular androgens and thereby reduces prostate cancer growth (Heinlein and Chang 2004). Surgical castration includes orchiectomy, in which the testicles are removed, but this approach is very rare now. Medical castration is primarily achieved using gonadotropin-releasing hormone (GnRH) agonists (Leuprolide and Goserelin) and antagonists (Degarelix), which act through the anterior pituitary gland. GnRH agonists cause a decrease in luteinizing hormone (LH) levels by down-regulation of GnRH receptors, whereas GnRH antagonists inhibit GnRH receptors. In addition to medical/surgical castration, ADT can also incorporate the application of antiandrogens (AR antagonists), such as cyproterone acetate, bicalutamide, nilutamide, and flutamide, which directly bind to the AR LBD and block its activity (Thomas and Neal 2013). More recently, chemotherapy has been combined with ADT, which can improve outcomes for some patients (Sweeney, Chen et al. 2015). Chemotherapy is a process in which a tumour is treated with one or more cytotoxic drugs (Panda, Chakraborty et al. 2017).

Unfortunately, ADT for metastatic PCa, alone or in combination with chemotherapy, is never curative (Figure 1.9) and patients will eventually relapse with what is termed castration-resistant prostate cancer (CRPC). CRPC is defined as an increase in PSA levels or tumour size despite castrate levels of circulating androgens (<0.50 ng/ml) (Komiya, Yasuda et al. 2013,

Fizazi, Massard et al. 2015). Also, reduction in androgen levels using ADT or antiandrogens have some adverse clinical side effects on a patient's life including a decrease in muscle strength, reduced lean and bone mass, higher risk of fracture and unusual lipid profile (Galvao, Nosaka et al. 2006).

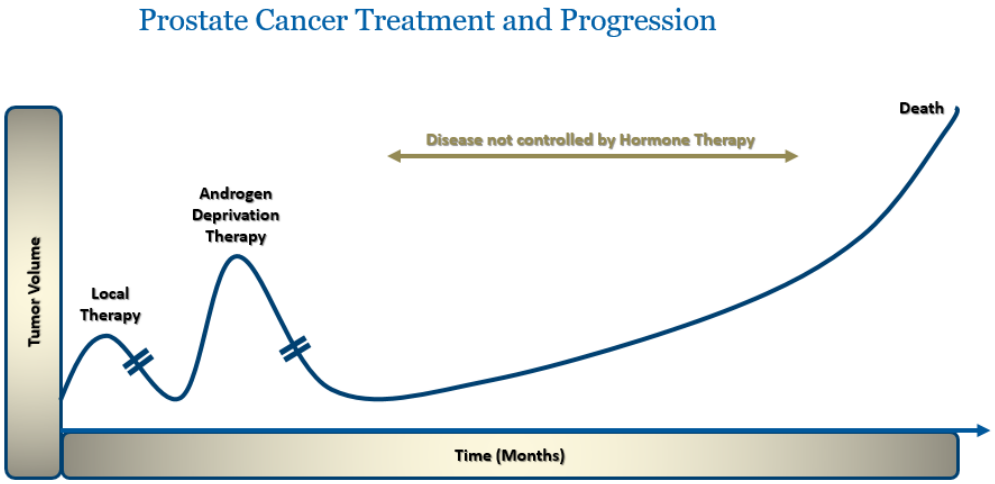

Figure 1.9. The progression pattern of prostate cancer in patients with disease recurrence (Crea, Saidy et al. 2015).

1.13. Treatment of CRPC

In recent years, next-generation ADT agents have been introduced which provide a survival benefit in CRPC. These agents are apalutamide, darolutamide, enzalutamide, as AR antagonists, and abiraterone acetate, a CYP17A1 inhibitor. In CRPC patients and after chemotherapy, administration of AR antagonists blocks the AR signalling by binding to the LBD of AR and inhibiting the transactivation of AR and also by preventing the AR nuclear translocation, which ultimately results in median overall survival by 18.4 months compared to placebo (13.6 months) (Scher, Fizazi et al. 2012). Abiraterone acetate functions as an irreversible inhibitor of CYP17A1, an enzyme that converts pregnenolone to dehydroepiandrosterone (DHEA), a precursor of T and DHT, resulting in a significant decrease in androgen synthesis (Chandrasekar, Yang et al. 2015). After chemotherapy, the median overall survival benefit of Abiraterone acetate was reported as 14.8 months vs. 10.9 months in the placebo group (De Bono, Logothetis et al. 2011). Other therapies for CRPC include the chemotherapeutics docetaxel (Sweeney, Chen et al. 2015) and cabazitaxel (Chandrasekar, Yang et al. 2015). Both Cabazitaxel and Docetaxel belongs to the same family of taxane chemotherapies, however, the TROPIC trial showed that Cabazitaxel was active after docetaxel failure and can prolong overall survival (Shiota, Yokomizo et al. 2016). Radium-223 dichloride is a targeted alpha emitter that can selectively bind to areas of bone with increased turnover and emit alpha particles of extremely short range with high energy. Radium-223 is considered an effective and well-tolerated treatment in men with CRPC and bone metastases (Hoskin, Sartor et al. 2014). However, unfortunately, none of these therapeutic strategies is curative, and all only provide a survival benefit in the order of months. Therefore, there is a major unmet need for new therapies that can effectively control CRPC.

1.14. AR-mediated Therapy Resistance in CRPC:

Persistent AR signalling following the ADT is the major mechanism driving CRPC growth (Coutinho, Day et al. 2016). It has been shown that approximately 80% of CRPC tumours demonstrate persistent AR signalling (Ylitalo, Thysell et al. 2017), highlighting the addiction of prostate cancer cells to this pathway. Illustrating the importance of AR signalling for prostate epithelial cells, therapy-mediated selection pressure causes genomic alterations in genes involved in the regulation of AR signalling such as AR gene itself and AR coregulators such as FOXA1 (pioneer factor) and NCOR1/2 (corepressor), aiming to sustain the AR transcriptional function in cells (Parolia, Cieslik et al. 2019).

ADT-mediated genomic alterations in the AR gene is one of the most frequent mechanisms, leading to the persistent oncogenic function of AR in prostate cancer cells. Despite being castrated, the oncogenic activity of AR following the ADT will be sustained by several mechanisms including hypersensitivity of cancer cells to low levels of androgens, antagonist-agonist switching, AR activation by non-canonical ligands, and ligand-independent transactivation of AR (Table 2). These mechanisms are mainly associated with overexpression or point mutations of the AR gene. AR gene overexpression, which makes cells hypersensitive to very low levels of androgens is achieved either through AR gene copy-number amplification (DNA level) or transcriptional upregulation of the AR gene (RNA level) (Coutinho, Day et al. 2016). Genetic analyses of prostate cancer tumours show that AR gene copy-number amplification is largely present in CRPC but not in primary tumours, accounting for 50% CRPC samples, approximately (Barbieri, Bangma et al. 2013). AR point mutations also can cause oncogenic activation of AR, accounting for 20% of CRPC tumours, approximately (Beltran,

Yelensky et al. 2013). These mutations have been mainly identified in AR ligand-binding domain or AR (AR-LBD) transactivation activity (AR-NTD), which can result in ligand promiscuity causing AR transactivation with a very low level of androgens, AR interaction with non-specific ligands, and/or an antagonist-to-agonist switch (Table 2)(Coutinho, Day et al. 2016). ADT-induced selection pressure is also associated with constitutively active AR variants including AR-V7, AR-V567es and AR-V3 (Jernberg, Bergh et al. 2017).

As an emerging clinical issue, a subpopulation of CRPC patients (accounting for 20%, approximately) can relapse with clinically aggressive variants of prostate cancer, exhibiting an AR-independent phenotype, in which AR expression is reduced or absent (Watson, Arora et al. 2015, Chen, Dong et al. 2018, Handle, Prekovic et al. 2019). Therefore, they are resistant to all current AR signalling inhibitors. Given the continued relevance of AR in the CRPC state and the fact that new AR pathway inhibitors only provide minor survival benefits, smarter AR-targeted therapeutic strategies are needed to treat advanced metastatic prostate cancer.

Table 1.2. ADT-mediated resistance mechanism

ADT-mediated resistance mechanisms	Genetic alteration in the AR gene	Outcome	Representative *in vitro* model	Reference
Hypersensitivity to low levels of androgens	AR gene amplification	Transcriptional upregulation AR gene	VCaP cell line	**(Korenchuk, Lehr et al. 2001, Liu, Xie et al. 2008)**
	T878A gain-of-function mutation	Flutamide and nilutamide act as AR agonists	LNCaP cell line	**(Veldscholte, Ris-Stalpers et al. 1990)**
	H875Y gain-of-function mutation	Nilutamide acts as an AR agonist	22rv1 cell line	**(Marcias, Erdmann et al. 2010)**
	F877L gain-of-function mutation	Enzalutamide act as an AR agonist	MR49F	**(Korpal, Korn et al. 2013, Coleman, Van Hook et al. 2016)**
Antagonist–agonist switching	W742C/L gain-of-function mutation	Bicalutamide acts as an AR agonist	LAPC-4, KuCaP-1	**(Terada, Shimizu et al. 2010, Sugawara, Baumgart et al. 2019)**
	S889G gain-of-function mutation	Flutamide and Bicalutamide act as AR agonists	-	**(Prekovic, Van den Broeck et al. 2018)**
	M896V gain-of-function mutation	Flutamide and Bicalutamide act as AR agonists	-	**(Prekovic, Van den Broeck et al. 2018)**
AR activation by non-canonical ligands	L702H gain-of-function mutation	Glucocorticoids act as an AR agonist	MDA PCa 2b cell line	**(Sumiyoshi, Mizuno et al. 2019)**
	L701H gain-of-function mutation	Cortisol act as an AR agonist	-	**(van de Wijngaart, Molier et al. 2010)**
AR splice variants	AR-V3	Constitutively-active AR variant	-	**(Kallio, Hieta et al. 2018, Tagawa, Antonarakis et al. 2019)**
	AR-V7	Constitutively-active AR variant	22rv1 cell line	
	ARv567es	Constitutively-active AR variant	D567 cell line	

1.15. Bipolar androgen therapy; a potential strategy for prostate cancer therapy

As described above, blocking AR signalling is the main therapeutic strategy for the treatment of patients with advanced metastatic prostate cancer. While attempts to develop more potent AR antagonists are being made, the adaptation mechanisms that lead to the failure of AR pathway inhibitors are a major concern. Therefore, there is an unmet need for an "out of box" approach avoiding the lethal adaptation stage in the treatment of advanced metastatic prostate cancer tumours.

Bipolar Androgen Therapy (BAT) is one of the emerging concepts in the treatment of prostate cancer, which can potentially overcome the innate ability of prostate cancer cells to adapt to castrate level of androgens. In this strategy, rapid cycling between two polar extremes of androgen levels, namely supraphysiologic and castration levels, within a short period can avoid the therapy adaptation due to the abrupt changes in androgen levels. More importantly, while activating the AR transcriptional activity in prostate cancer cells, high-dose of androgens paradoxically inhibits the tumour progression and renders cancer cells vulnerable to death (Schweizer, Antonarakis et al. 2015). This unexpected therapy response is illustrated in figure 1.10 showing the PSA response of a patient who received 16 cycles of BAT having led to a dramatic decrease in tumour progression.

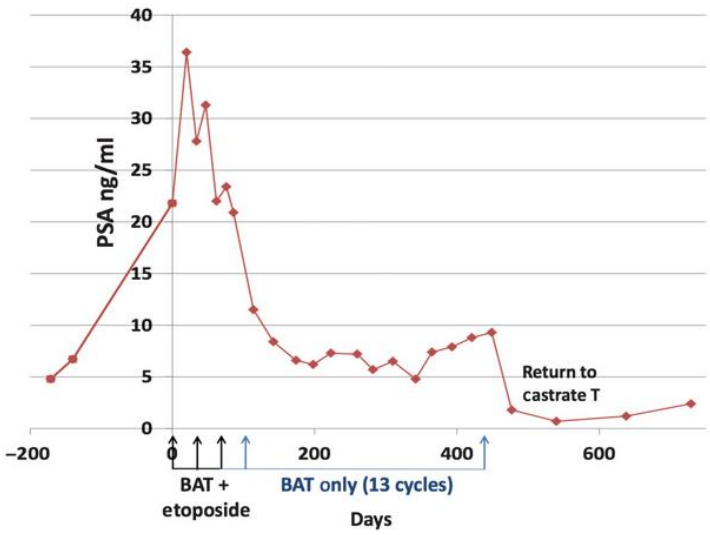

Figure 1.10. PSA response in an individual patient (patient 9) receiving a total of 16 cycles of BAT. (Schweizer, Antonarakis et al. 2015).

Currently, synthetic testosterone derivatives such as Testosterone cypionate and Testosterone Enanthate are widely used in clinical trial studies aiming to treat prostate cancer with high-dose androgen therapy (e.g. NCT03522064, NCT02090114, NCT03554317, NCT03516812, and NCT01750398).

1.16. Proposed Mechanisms for therapeutic effects of high-dose androgens:

Exposing AR-positive prostate cancer cells to a high dose of androgens can inhibit their proliferation (Joly-Pharaboz, Soave et al. 1995). The apparent paradox that AR inhibition and potent activation can both exert anti-cancer effects raises the question as to which mechanisms are involved in tumour suppression by high-dose androgens in CRPC patients. Preclinical studies have proposed some mechanisms for therapeutic effects of high-dose androgen (see below); however, regarding the variation in response to BAT in clinical settings (Schweizer, Antonarakis et al. 2019), the exact tumour suppressive mechanism(s) remains uncertain. Therefore, it is imperative to identify the potential antitumor mechanism following the AR activation by high-dose androgens.

1.16.1. High-dose androgen therapy interrupts cell cycle progression

In prostate cancer cells, liganded-AR has a key role in the progression of the cell cycle either through physical interactions with cell cycle-associated proteins or by driving phase-specific transcriptional networks. Indeed, the interplay between AR and cell cycle proteins induces a phase-specific AR cistrome and transcriptome, governing the proliferation of prostate cancer

cell through the cell cycle progression (Murthy, Wu et al. 2013, McNair, Urbanucci et al. 2017). However, evidence indicates that AR function in the cell cycle depends on the concentration of its agonist. Enigmatically, the proliferative effects of androgens depend on their concentration, exhibiting a biphasic response in prostate cancer cells. More specifically, dose-responses of LNCaP cells treated with R1881 (synthetic androgen) can be divided into proliferative and antiproliferative phases (Figure 1.11). Importantly, cell cycle analysis revealed that antiproliferative doses of androgens cause cell cycle arrest arrested in the G1 phase (De Launoit, Veilleux et al. 1991).

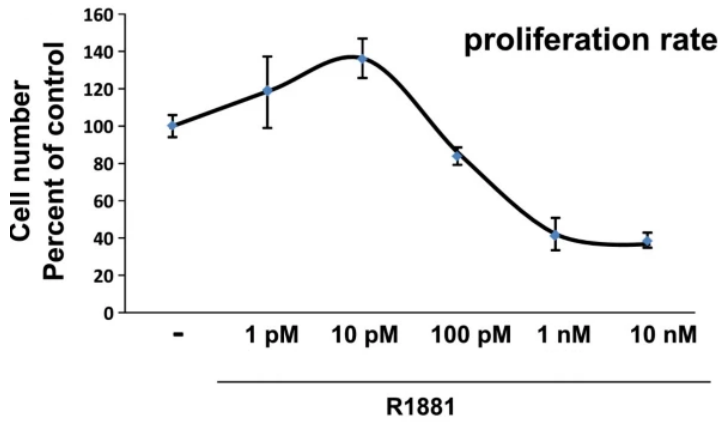

Figure 1.11. Biphasic response of LNCaP cells treated with increasing doses of R1881 for 72h (Roediger, Hessenkemper et al. 2014).

These observations support the idea that AR liganded with an antiproliferative supraphysiologic dose of androgens causes an interruption in the cell cycle progression, leading to cell cycle arrest. Although the key mechanism triggering this cell cycle arrest have not been precisely determined, several mechanisms have been suggested. First, GSEA analysis on transcriptomic data generated from different AR-positive prostate cancer cell lines shows that treatment with 10 nM R188 significantly represses the expression of some gene sets including Myc and E2F1 target genes (Figure 1.12). Since the integrated function of Myc and activated E2F1 is required for S phase entry (Leung, Ehmann et al. 2008), suppression of Myc expression by high-dose androgens may lead to repression of E2F1/E2F1 target genes, which potentially leads to cell cycle arrest (Roediger, Hessenkemper et al. 2014).

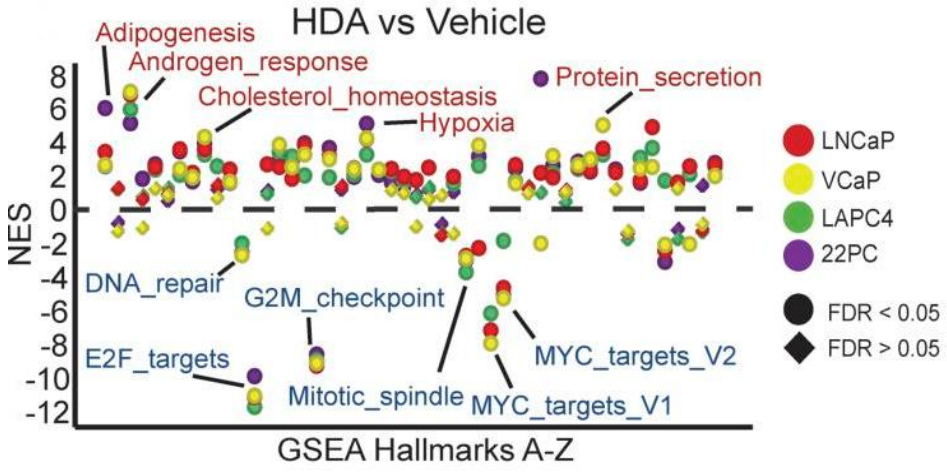

Figure 1.12. Results of GSEA analysis showing enriched significant Hallmark genes sets (FDR < 0.05) in 4 cell lines treated with 10 nM R1881. Red dots: Androgen receptor-related gene sets; Blue dots: cell cycle-related gene sets (Nyquist, Corella et al. 2019)

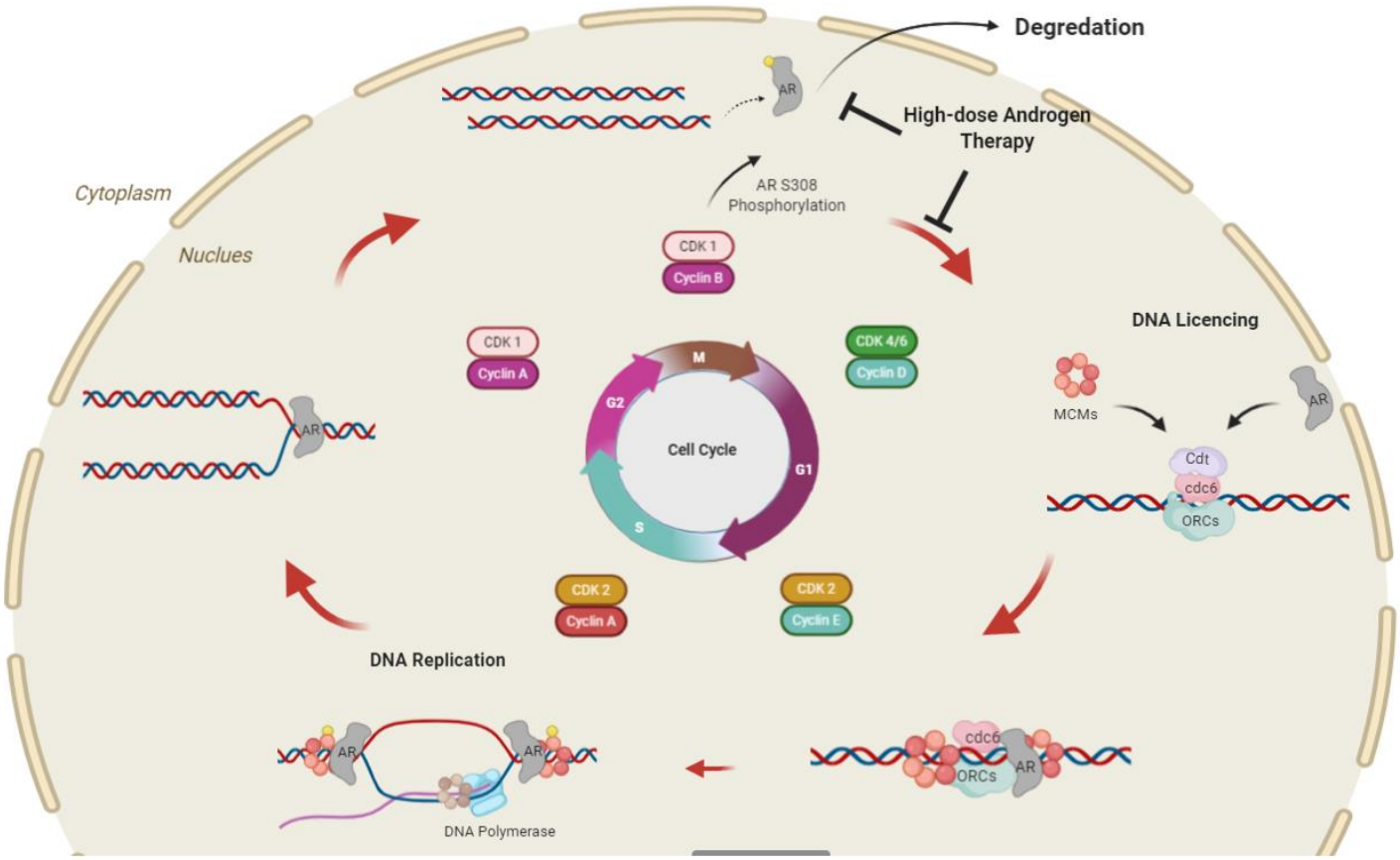

Figure 1.13. Model of AR interaction with replication machinery in the cell cycle. High-dose Androgen therapy may interrupt the AR dissociation from chromatin avoiding DNA re-licensing.

Linked to a non-transcriptional function of AR, another mechanism has been also proposed for cell cycle arrest by high-dose androgens. According to the proposed model, AR has a role in DNA licensing in androgen-sensitive prostate cancer cells, required for DNA replication in the S phase (Litvinov, Vander Griend et al. 2006). This AR function is mediated through the AR interactions with some DNA licensing factors such as Orc2, Cdc6 and MCM7 (Shi, Yan et al. 2008, Jin and Fondell 2009) (Figure 1.13). In this mechanism, liganded-AR binds to the origins of replication sites in the G1 phase and forms a complex with other factors, licensing these sites for replication within the S phase. In the G2 phase, AR remains bound to DNA, which prevents the re-licensing and subsequently re-initiation of DNA replication before the next cell cycle. However, following the G2 phase and in mitosis, AR is excluded from DNA and degraded, which allows the initiation of a new DNA licensing and re-initiation of DNA replication in the next cell cycle (D'Antonio, Vander Griend et al. 2009). Current evidence suggests that high-dose androgens may interrupt the DNA licensing role of AR, arresting the cell cycle progression from G1 to S. In this model, acute increase in the androgen levels up to supraphysiological levels causes insufficient degradation of AR during the mitosis/early G1 leading to interruption in DNA re-licensing and re-initiation of DNA replication (Figure 1.13).

Mechanistically, the function of cell cycle proteins including licensing factors is precisely regulated through the phase-specific cyclin-dependent kinases (CDKs)(Reusswig, Zimmermann et al. 2016). For example, CDK1, overexpressed in prostate cancer tumours, is an M-phase protein involved in G2-to-M transition (Liu, Kao et al. 2008). Expression of CDK1 is induced directly by AR and the association of CDK1 with AR tightly binds to increase the AR stability, localization, and chromatin binding, which are mainly mediated by AR S81

phosphorylation (Lee and Chang 2003, Chen, Xu et al. 2006, Wang, Li et al. 2009, Sharma, Yeow et al. 2010, Chen, Gulla et al. 2012). Suppression of AR transcriptional activity following CDK1 inhibition supports the importance of this CDK1-AR feedback loop (Liu, Gao et al. 2017). Interestingly, a study by Koryakina et al. (Koryakina, Knudsen et al. 2015) demonstrated that AR S308 phosphorylation by CDK1 in the nucleus of mitotic prostate cancer cells is crucial for AR exclusion from chromosomes and nucleus. Therefore, given the proposed role of AR as a licensing factor, high-dose androgens may also, either directly or indirectly, interrupt the post-transcriptional regulation of AR by CDKs, leading to insufficient AR dissociation/degradation in mitosis.

1.16.2. AR-induced cell cycle arrest accumulates activated-Retinoblastoma protein inducing tumour suppressor function to AR

AR activation by a high dose of androgens can trigger the repression of gene sets required for cell cycle progression including DNA repair/replication genes (Niu, Altuwaijri et al. 2008). Analysis of AR binding profiles shows that high-dose androgens cause recruitment of AR proteins to gene sets involved in DNA replication/repair and integration of AR cistrome with transcriptomic data confirms the repression of those gene sets, suggesting a direct tumour suppressor function of AR through its transcriptional activity (Figure 1.14) (Gao, Gao et al. 2016).

AR transcriptional repressor function can be mediated through the recruitment of transcriptional repressor proteins (Cai, He et al. 2011). One of the key transcriptional repressors, which can be activated as a consequence of androgen-induced cell cycle arrest, is

Rb protein. Genomic studies on Rb cistrome revealed that AR and Rb are co-localised on the promotor of DNA replication genes suppressed by high-dose androgens. Given that activated Rb can bind to the promoter of E2F1 target genes (Sharma, Yeow et al. 2010), current evidence suggests that Rb acts as an AR coregulator to repress E2F1 target genes. Importantly, although androgen-induced cell cycle arrest seems to be Rb-independent (Vander Griend, Litvinov et al. 2014); however, Rb deficiency, which is significantly overrepresented in CRPC tumours, may interfere with AR-dependent repression of DNA replication genes (Sharma, Yeow et al. 2010). Therefore, coupling the BAT with other therapeutic strategies can potentially improve the response of patients with Rb-deficiency to BAT.

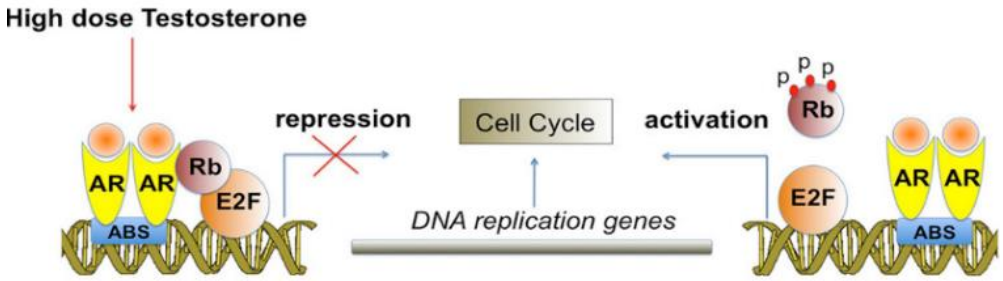

Figure 1.14. Rb activation by high-dose androgens leads to co-localisation of AR and Rb on the promoter of DNA replication/repair genes leading to the suppression of their expression (Gao, Gao et al. 2016).

1.16.3. High dose androgen can induce lethal dsDNA breaks

Chromosomal translocations in prostate epithelial cells is one of the key mechanisms leading to the development and progression of prostate cancer. As described in section 1.8, *ERG-TMPRSS2* fusion is the most frequent genomic rearrangements presented in 50%–70% of prostate tumours resulting in overexpression of ETS oncogenes in an androgen-dependent manner, which can help in the progression of prostate cancer (Carver, Tran et al. 2009, Li, Yuan et al. 2020).

Rearrangements of DNA fragments in prostate cancer cells is mediated by inducing site-specific double-stranded DNA breaks (DSBs)(Kloosterman, Tavakoli-Yaraki et al. 2012). In prostate cancer cells, AR has two key roles in inducing the DSBs: 1) binding to specific regions on DNA and 2) inducing spatial proximity between DNA fragments. Toward this end, liganded-AR binds to specific intronic regions mediating intra- and interchromosomal interactions through the recruitment of enzymes needed for alterations in local epigenetic markers. Local epigenetic remodelling by liganded-AR not only causes chromosomal movement but also makes these regions accessible for enzymes generating DSBs (Lin, Yang et al. 2009).

Multiple enzymes can induce DSBs at AR binding sites. For example, Lin et al (Lin, Yang et al. 2009) reported that exogenous genotoxic stresses can cause the expression of genotoxic-associated enzymes including activation-induced cytidine deaminase (AID) and LINE-I repeat-encoded ORF2 endonucleases, which can bind to AR-induced accessible sites on DNA and establish DSBs. In this study, the presence of genotoxic stresses has been shown to be crucial

for causing the genomic breaks. However, a study by Haffner et al. (Haffner, De Marzo et al. 2011) supports the notion that intrinsic androgen signalling could also be sufficient to generate transient genomic breaks needed for genomic rearrangement in prostate cancer cells. Based on this mechanism, androgen stimulation causes the recruitment of TOP2B at specific AR binding sites inducing extremely fleeting recombinogenic DSBs. Subsequently, androgen-induced DSBs are quickly targeted by DSB repair machinery. More importantly, TOP2B-mediated DSBs has been shown to be crucial for AR transcriptional activity since targeting TOP2B leads to the interruption in the expression of AR-target genes (Ju, Lunyak et al. 2006, Haffner, De Marzo et al. 2011).

In the context of bipolar androgen therapy, current evidence suggests that cyclic activation of AR by supraphysiologic levels of an androgen and castration may lead to unrepaired DSBs, which can induce cell cycle arrest and cell death (Chatterjee, Schweizer et al. 2019). Theoretically, DNA damage could be exacerbated by AR's ability to down-regulate DNA repair gene pathways (see section above) (Gao, Gao et al. 2016). This hypothesis can explain why a patient with BRCA2/ATM deficiency showed an extreme response to high-dose androgen therapy (Teply, Kachhap et al. 2017).

However, the negative feedback loop between androgen level and AR gene expression and/or a lower level of AR protein in a subset of tumours with AR-indifferent phenotype may attenuate the DSBs generation (Chatterjee, Schweizer et al. 2019, Handle, Prekovic et al. 2019). More importantly, the highest frequency of Rb deficiency in a patient with CRPC can also restrict the repression of DNA repair/replication genes in an Rb-dependent manner

(section 1.14.2) (McNair, Xu et al. 2018). Another important point to raise is that, although patients with a deficiency in DNA repair pathways are expected to show better response; however, there is a considerable variation among patients with different genomic aberrations in terms of response to BAT (Figure 1.15) (Schweizer, Antonarakis et al. 2019), indicating that genomic deficiency in DNA repair pathways cannot be a reliable index for segregation of patients in terms of response to BAT. Therefore, the exact mechanism(s) involved in response to high-dose androgen therapy remains imprecise.

Biomarker panel	PSA50 response rate	P-value	Median PFS, mo	Hazard Ratio (95% CI)
HRD	14/30 (47%)	0.02	5.48	0.90 (0.53 - 1.52, P = 0.69)
No HRD	6/32 (19%)		5.34	
TP53 mutation	11/27 (41%)	0.12	5.38	0.70 (0.40 - 1.22, P = 0.21)
No *TP53* mutation	7/32 (22%)		5.44	
HRD and/or *TP53* mutation	20/47 (43%)	0.008	5.51	0.59 (0.33 - 1.08, P = 0.087)
No HRD or *TP53* mutation	1/16 (6.3%)		4.62	

Figure 1.15. PSA response rate of CRPC patients received BAT (Schweizer, Antonarakis et al. 2019).

1.17. Hypothesis and aims

The preliminary data from high-throughput screening of nuclear receptor ligands by my host lab suggests that a synthetic Testosterone analogue, named Methyl-Testosterone (MeT), potently suppresses the proliferation of LNCaP cells. Therefore, we hypothesized that MeT acts as a potent androgen suppressing cell proliferation. As outlined above, while several mechanisms underlying the efficacy of supraphysiological androgen treatment in PCa have been described, many questions still remain. We hypothesised that a potent androgen like MeT could be a useful tool to gain a more complete understanding of these mechanisms as well as having potential as a therapeutic. With this in mind, the specific aims of my project are:

Aims:

1. Characterise the antiproliferative effects of MeT in different prostate cancer models.

2. Define the AR cistrome and AR-induced transcriptome after activation with MeT.

3. Further elucidate the major mechanisms involved in the therapeutic efficacy of high-dose androgens.

Chapter 2: Material and Methods

2.1. Material

Table 2.1: Common chemical and reagents

Reagents	Supplier	Catalogue number
Dulbecco's Modified Eagle's Medium-high glucose	Sigma Aldrich	D6429
RPMI 1640 liquid media	Sigma Aldrich	R8758
RPMI 1640 phenol red free	Sigma Aldrich	R7509
Trypsin EDTA solution	Sigma Aldrich	T4049
Bradford assay reagent	BioRad	500-0006
BSA (bovine serum albumin)	Sigma Aldrich	A9647
Chloroform	Sigma Aldrich	C2432
DMSO (dimethyl sulfoxide)	BDG Laboratory Supplies	D2650
Ethanol, molecular grade	Scharlau	ET00110500
FBS (fetal bovine serum)	Sigma Aldrich	14M357
Glycerol	Chem Supply	GA010-2.5L-P
iScirpt cDNA synthesis kit	BioRad	170-8891
iQ SYBR Green Supermix	BioRad	170-8885
Inactivation buffer (supplied with Turbo free)	Ambion Inc.	AM1907
Methanol	Chem Supply	MA004-2.5L-P
Nitrocellulose membrane (0.4 µm)	Amersham	GEHE10600016
Nuclease free water	Qiagen	129114
PBS (phosphate-buffered saline)	Gibco	14190
Ponceau S	Sigma Aldrich	P3504
LEGENDplex™ Human Type 1/2/3 Interferon Panel (5-plex) with V-bottom Plate	Biolegend	740396
SDS (sodium dodecyl sulphate)	Sigma Aldrich	75746
Triton-X 100	Sigma Aldrich	T8787
TRIZOL Reagent	Sigma Aldrich	T9424
100 bp DNA ladder	New England Biolabs	N3231S
Agarose, analytical grade	Sigma Aldrich	A6013
Poly(I:C) (LMW) / LyoVec™	Invivogen	tlrl-picwlv
Criterion precast gel (4-12%)	BioRad	567-1084
DAPI prolong gold mount media	Molecular Probes (Life Tech)	P26935
17α-Methyltestosterone/ Mesterone	Sigma Aldrich	M7252

Table 2.2: Commonly Used Buffers and Media

Buffer/Medium Name	Buffer/Medium Components
RIPA Buffer for protein extraction	1 g SDS; 0.93 g DTT; 1.2 mg Bromophenol blue; 7 mL Tris-Cl/SDS (4x); 3 mL Glycerol, 10 mL Milli-Q water; Store at -20°C
Running Buffer (10x)	77.5 g Tris Base; 360g Glycine; 25g SDS; 2.5L RO H2O
TBS (10x)	151.5 g Tris ; 219 g NaCl ; Volume to 2.5 L with water (pH 7.4)
TBST (1x)	2.5 mL Tween20 ; 250 mL 10x TBS ; 2.25L RO H2O
Transfer Buffer (10x)	77.5 g Tris ; 360 g Glycine ; Volume to 2.5 L with water
Tris-HCl (0.5M), pH 8.0 and pH 7.6	12.1 g Tris-HCl; 200 ml Milli-Q water
HEPES-KOH (0.5M), pH 7.5	59.5 g HEPES; 500 ml Milli-Q water
NaCl (5M)	29 g NaCl; 100 ml Milli-Q water
EDTA (0.5M)	9.3 g EDTA; 50 ml Milli-Q water
EGTA (0.1M)	1.9 g EGTA; 50 ml Milli-Q water
LiCl (5M)	21.1 g LiCl; 100 ml Milli-Q water
SDS (10%)	20g SDS; 200 ml Milli-Q water
Na-Deoxycholate (5%)	10 g Na-Deoxycholate; 200 ml Milli-Q water
N-laurylsarcosine (5%)	10 g N-laurylsarcosine; 200 ml Milli-Q water
PBS + PI	1x tablet of Complete Mini Protease Inhibitor Cocktail in 10 ml PBS
Triton Extraction Buffer (TEB)	0.5% Triton-X 100, 2 mM phenylmethylsulfonyl fluoride (PMSF), and 0.02% (w/v) NaN3
NaCl 500mM	2 µl of NaCl 5M ; 18 µl sterile water
Triton X-100 (10 %)	1 ml of 100 % Triton X-100; 9 ml Milli-Q water

Table 2.3: Chromatin immunoprecipitation (ChIP) Buffers

Solution name	Final Conc	Stock concentration	Volume
Solution A	1% Formaldehyde	40%	2ml
	50mM HEPES-KOH, pH 7.5	0.5M	8ml
	100mM NaCl	5M	1.6ml
	1mM EDTA	0.5M	160ml
	0.5mM EGTA	0.1M	400ml
	water		67.84ml
	Total volume		80ml
Block Solution	0.5% BSA		250mg
	PBS		to 50ml
LB1	50mM HEPES-KOH, pH 7.5	0.5M	10ml
	140mM NaCl	5M	2.8ml
	10% glycerol	100%	10ml
	1mM EDTA	0.5M	200ml
	0.5% NP-40	100%	500ml
	0.25% Triton X-100	100%	250ml
	water		76.25ml
	Total volume		100ml
LB2	10mM Tris-HCl, pH 8.0	0.5M	2ml
	200mM NaCl	5M	4ml
	1mM EDTA	0.5M	200ml
	0.5mM EGTA	0.1M	500ml
	water		93.3ml
	TOTAL		100ml
LB3	10mM Tris-HCl, pH 8.0	0.5M	1ml
	100mM NaCl	5M	1ml
	1mM EDTA	0.5M	100ml
	0.5mM EGTA	0.1M	250ml
	0.1% Na-Deoxycholate	5%	1ml
	0.5% N-laurylsarcosine	5%	5ml
	water		41.65ml
	Total volume		50ml
RIPA Buffer	50mM HEPES-KOH, pH 7.5	0.5M	10ml
	500mM LiCl	5M	10ml
	1mM EDTA	0.5M	200ml
	1% NP40	100%	1ml
	0.7% Na-Deoxycholate	5%	14ml
	water		64.8ml
	Total volume		100ml
TBS	20mM Tris-HCl, pH 7.6	0.5M	2ml

	150mM NaCl	5M	1.5ml
	water		46.5ml
	Total volume		50ml
Elution Buffer	50mM Tris-HCl, pH 8.0	0.5M	1ml
	10mM EDTA	0.5M	200ml
	1% SDS	10%	1ml
	water		7.8ml
	Total volume		10ml

Table 2.4: Primers

Primer Name	Sequence	Use
FANCI-RT-Fwd	CTGCCCTGGCTACGAAAAAG	ChIP-PCR
FANCI-RT-Rev	CATATTGCTGATCCCACCTGC	ChIP-PCR
LMNB1-RT-Fwd	TGCCCTTTGTGCTGTAATCG	ChIP-PCR
LMNB1-RT-Rev	GACCGTGATAAGGAGGGGAC	ChIP-PCR
MCM7-RT-Fwd	CCTACCAGCCGATCCAGTCT	ChIP-PCR
MCM7-RT-Rev	CCTCCTGAGCGGTTGGTTT	ChIP-PCR
BLM-RT-Fwd	CAGCAGCGGAACATAAGAAGG	ChIP-PCR
BLM-RT-Rev	GCCAAGAAGACTGGCATCAC	ChIP-PCR
FANCI-Fwd	CTGCCCTGGCTACGAAAAAG	qRT-PCR
FANCI-Rev	CATATTGCTGATCCCACCTGC	qRT-PCR
LMNB1-Fwd	TGCCCTTTGTGCTGTAATCG	qRT-PCR
LMNB1-Rev	GACCGTGATAAGGAGGGGAC	qRT-PCR
MCM7-Fwd	CCTACCAGCCGATCCAGTCT	qRT-PCR
MCM7-Rev	CCTCCTGAGCGGTTGGTTT	qRT-PCR
CCNA2-Fwd	CAGAAAACCATTGGTCCCTC	qRT-PCR
CCNA2-Rev	CACTCACTGGCTTTTCATCTTC	qRT-PCR
STING-Fwd	AGCATTACAACAACCTGCTACG	qRT-PCR
STING-Rev	GTTGGGGTCAGCCATACTCAG	qRT-PCR
ERV3-env-Fwd	CCATGGGAAGCAAGGGAACT	qRT-PCR
ERV3-env-Rev	CTTTCCCCAGCGAGCAATAC	qRT-PCR
HERV-W-Fwd	TGAGTCAATTCTCATACCTG	qRT-PCR
HERV-W-Rev	AGTTAAGAGTTCTTGGGTGG	qRT-PCR
HERVE Fwd	GGTGTCACTACTCAATACAC	qRT-PCR
HERVE-Rev	GCAGCCTAGGTCTCTGG	qRT-PCR
HERV F-Fwd	CCTCCAGTCACAACAACTC	qRT-PCR
HERV F-Rev	TATTGAAGAAGGCGGCTGG	qRT-PCR
ERVL-Fwd	ATATCCTGCCTGGATGGGGT	qRT-PCR
ERVL-Rew	GAGCTTCTTAGTCCTCCTGTGT	qRT-PCR
HERV-K-Fwd	ATTGGCAACACCGTATTCTGCT	qRT-PCR
HERV-K-Rev	CAGTCAAAATATGGACGGATGGT	qRT-PCR
DNMT1-Fwd	GCGTTCCGGCTGAACAAC	qRT-PCR
DNMT1-Rev	GCATCTCCACGTCTCCCT	qRT-PCR
EZH2--RT-fwd	GTGGAGAGATTATTTCTCAAGATG	qRT-PCR
EZH2-RT-Rev	CCGACATACTTCAGGGCATCAGCC	qRT-PCR
B2M-RT-fwd	TGACTTTGTCACAGCCCAAG	qRT-PCR
B2M-RT-Rev	AGCAAGCAAGCAGAATTTGG	qRT-PCR
HLA-A-RT-fwd	GGCCCTGACCCAGACCTG	qRT-PCR
HLA-A-RT-Rev	GCACGAACTGCGTGTCGTC	qRT-PCR
HLA-B-RT-fwd	ACTGAGCTTGTGGAGACCAGA	qRT-PCR
HLA-B-RT-Rev	GCAGCCCCTCATGCTGT	qRT-PCR
HLA-C-RT-fwd	CTGGCCCTGACCGAGACCTG	qRT-PCR
HLA-C-RT-Rev	CGCTTGTACTTCTGTGTCTCC	qRT-PCR
IFN-beta-RT-fwd	GCCATCAGTCACTTAAACAGC	qRT-PCR
IFN-beta-RT-Rev	GAAACTGAAGATCTCCTAGCCT	qRT-PCR

ISG15-RT-fwd	CCTTCAGCTCTGACACC	qRT-PCR
ISG15-RT-Rev	CGAACTCATCTTTGCCAGTACA	qRT-PCR
IRF7-RT-fwd	GTGGACTGAGGGCTTGTAG	qRT-PCR
IRF7-RT-Rev	TCAACACCTGTGACTTCATGT	qRT-PCR
MDA5-RT-fwd	GAGCAACTTCTTTCAACCACAG	qRT-PCR
MDA5-RT-Rev	CACTTCCTTCTGCCAAACTTG	qRT-PCR
MAVS-RT-fwd	AGGAGACAGATGGAGACACA	qRT-PCR
MAVS-RT-Rev	CAGAACTGGGCAGTACCC	qRT-PCR
RIG-I-RT-fwd	CCAGCATTACTAGTCAGAAGGAA	qRT-PCR
RIG-I-RT-Rev	CACAGTGCAATCTTGTCATCC	qRT-PCR

Table 2.5: Antibodies

Primary Antibody	**Dilution**	**Application**	**Catalogue number/Supplier**
mouse anti-dsRNA	1:1000	IF	Scicons English
MHC class I	1:1000	Flow cytometry	BioLegend
p-STAT1	1:1000	Western Blotting	Cell Signalling Technology
STAT1	1:1000	Western Blotting	Cell Signalling Technology
Phospho-Rb (Ser780) Antibody	1:1000	Western Blotting	Cell signalling
Rb (4H1) Mouse mAb	1:1000	Western Blotting	Cell signalling
TBK1/NAK Antibody	1:1000	Western Blotting	Cell signalling (#3013)
Phospho-TBK1/NAK (Ser172) (D52C2) XP®	1:1000	Western Blotting	Cell signalling (#5483)
Tri-Methyl-Histone H3 (Lys27) (C36B11)	1:1000	ChIP, Western Blotting	Cell signalling
Anti-phospho-Histone H2A.X	1:1000	Western Blotting	Merck Millipore
Tubulin	1:5000	Western Blotting	Merck Millipore
GAPDH	1:5000	Western Blotting	MAB374, Merck Millipore
Goat anti-rabbit	1:2000	Western Blotting	PO448, DAKO
Goat anti-mouse	1:2000	Western Blotting	PO161, DAKO

2.2. Methods

2.2.1. Reviving, maintaining, passaging and freezing of cell lines

The human prostate carcinoma cell lines, LNCaP, VCaP, PC3, and, 22Rv1 C4-2B, were obtained from the American Type Culture Collection (ATCC). The LNCaP-V16D, LNCaP-MR42D and LNCaP-MR49F cell lines were obtained from Dr Amina Zoubeidi's lab at the Vancouver Prostate Centre. WPMY-1 was obtained from Dr Mitchell Lawrence's lab at Monash University and CWR-R1-D567 was obtained from Dr Scott Dehm's lab at Masonic Cancer Centre of the University of Minnesota.

C4-2B, 22Rv1, LNCaP, and LNCaP-V16D cell lines were maintained in RPMI-1640 containing 10% Fetal Bovine Serum (FBS) and 2 mM L-Glutamine. PC3 and WPMY-1 cell lines were cultured in RPMI-1640 containing 5% FBS and 2 mM L-Glutamine. LNCaP-MR42D and LNCaP-MR49F were maintained in RPMI-1640 containing 10% FBS, 10 uM Enzalutamide and 2 mM L-Glutamine. CWR-R1-D567 cells were maintained in RPMI-1640 containing 10% CSS and 2 mM L-Glutamine. VCaP cells were maintained in DMEM high glucose containing 10% FBS, 2 mM L-Glutamine, 2 mM Sodium Pyruvate, and 2 mM of non-essential amino acids solution. All cell lines were authenticated by short tandem repeat profiling by CellBank Australia and were regularly screened for potential mycoplasma contamination. Cell revival was carried out through a quick throwing of vials in a 37°C water bath, followed by slowly mixing with 7ml of appropriate cell culture media. The cell suspension was centrifuged at 252 *g* for 5 minutes, and then, pellets were resuspended in 2ml of media and transferred into a T25 culture flask with 5 ml fresh media. Flasks were incubated at 37 °C and 5% CO_2 to be passaged when 70-

80% confluency was reached. Passaging was initiated by removing the media, washing the cells with PBS, and trypsinization with 0.25% trypsin. After a short incubation time after trypsinization, trypsin was neutralized with a full medium containing 10% FBS and cell suspension were spun down at 252 *g* for 5 minutes to resuspend and plate the required number of cells into flasks or plates. For cryopreserving cultured cells, a flask with about 70-80% cell confluency was washed and trypsinized, and after trypsin neutralization, the cell suspension was centrifuged at 252 *g* for 5 minutes and cell pellets were suspended in freezing media containing 10% DMSO, 40% FBS, 50% culture media at a cell density of 1-2 million cells/ml. Finally, 1 ml of cell suspension was added to labelled cryo-vials, and placed in isopropanol filled freezing container at -80 °C before transferring the frozen cells into liquid nitrogen.

2.2.2. Trypan blue exclusion assay

Depending on the doubling time and length of proliferation assay, cells were seeded at specific densities in multi-well plates. After cell seeding, plates were incubated at 37 °C and 5% CO_2 for at least 24 hours to allow cells to be attached to the plate surface before treatment. At the appropriate time-points, cells were treated with androgens prepared freshly in cell culture media, followed by incubation at 37 °C and 5% CO_2 until the next time-point. Past studies indicate that for1 nM DHT is considered to recapitulate a physiological dose (i.e. a dose replicating normal DHT levels in prostate tumours) whereas 100 nM is used to recapitulate a supraphysiological level of DHT (Jaaskelainen, Deeb et al. 2006, Li, Chan et al. 2013, Schweizer, Antonarakis et al. 2015, Hedayati, Haffner et al. 2016). We used these

studies to guide our dosing of *in vitro* PCa models to mimic physiological and supraphysiological conditions.

At the end of each time-point, cell viability in allocated plates was assessed using the Trypan blue exclusion assay. To determine the number of live cells in allocated plates, the culture media, and the PBS used for washing were collected followed by treatment of cells with 0.25% trypsin. After 2-3 minutes of incubation at 37°C, trypsin was neutralised through adding a culture media containing FBS or CSS, and then the cell suspension was added to the previously collected media and PBS. Subsequently, the cell suspension was spun down at 252 *g* for 5 minutes and after removing the supernatants, cell pellets were re-suspended in an appropriate volume of media. The cell suspension was mixed with Trypan Blue at a 1:1 ratio and live cells were counted using the haemocytometer.

2.2.3. Cell growth assay using an IncuCyte platform

IncuCyte is a live-cell imaging and analysis platform, allowing to monitor and quantify the cell behaviour over time. For assessment of cell proliferation using the IncuCyte, 50 µl of cell suspension at the appropriate cell density was seeded in 96-well plates and plates were incubated overnight at 37 °C and 5% CO_2. On day 0, 50 µl of media containing freshly prepared drugs and IncuCyte dyes were added to the wells. IncuCyte™ NucLight™ (1:1500) was used for labelling the live cells, and Sytox Green dye (1:1000 from 100 nM stock) was used to identify the dead cells. Following the treatment at day 0, automated imaging was carried out until day 7 as the final time-point. Drug re-treatment was carried out on day 3. Image analysis was performed using IncuCyte™ software.

2.2.4. Western Blotting

2.2.4.1. Preparation of Cell Lysates

To prepare protein lysates, cells were plated at the appropriate seeding density in 6-well plates. To collect cells, media was removed and cells were washed with ice-cold PBS and subsequently, cells were scrapped on ice into 100 µl of RIPA buffer. Protein lysates were spun down at 10,000 *g* for 10 min and supernatants were stored at -80 °C.

2.2.4.2. Bradford Assay

The total protein concentration of extracted cell lysates was determined using the Bradford assay. The assay was carried out in a 96-well flat-bottomed plate. In this experiment, 1 µl of each sample was added in wells contained 159 µl Baxter water for irrigation. To quantify the protein concentration in cell lysates, a standard curve was prepared by adding an increasing amount of Bovine Serum Albumin (BSA) (1 mg/mL) ranging from 0 to 6 µg in wells allocated for standard samples (in duplicate). 40 µl of Bradford reagent was pipetted into each well to a total volume of 200 µl. The plate was mixed and incubated at RT for 5 min before being read at 595 nm on a PolarStar microplate reader. The quantification of protein in each sample was performed using the standard curve.

2.2.4.3. Sodium Dodecyl Sulphate Polyacrylamide Gel Electrophoresis (SDS-PAGE)

Western immunoblotting was carried out in BioRad precast SDS-PAGE gels (4–12%). 20 µg of total protein was mixed with 6x loading dye and heated at 95 °C for 5 minutes, after which samples were loaded in the gel to run at a constant 120V for 90 min. Gels were run in an

immunoblotting running buffer. 6 µl of Precision Plus Protein Dual Color Standards was used as a size marker.

2.2.4.4. Western Transfer and Immunoblotting

After running the SDS-PAGE gel, proteins were transferred to a nitrocellulose membrane in a 1x Transfer Buffer using the BioRad Criterion Blotter at a constant 400 mA for 60 minutes. To verify the protein transfer, the membrane was stained with Ponceau S, followed by overnight blocking at 4 °C in a blocking buffer containing 1% skim milk powder or 2% BSA dissolved in TBST (1x). Subsequently, the membrane was probed using primary and then HRP-conjugated secondary antibodies at room temperature (for 2 hours each). HRP-bound antibody-protein complex was detected using ECL solution, imaged on a BioRad Chemidoc MP imaging system and analysed using Image Lab Software.

2.2.5. Gene expression and transcriptome analysis

2.2.5.1. RNA isolation from cell lines

To isolate RNA from cells, they were grown and treated in 6-well plates. At appropriate time points, media was removed from wells and cells were harvested in 1 mL Trizol per well and collected into 1.5 ml Eppendorf tubes. Following a 15-minutes incubation at 37 °C, 200 µl of chloroform was added into each tube which was then vigorously shaken for 15 s before a 3 min incubation at room temperature. Then, samples were centrifuged at 12,000 *g* at 4 °C to isolate the aqueous phase on the top layer. The supernatant was transferred into a new tube containing 2 µl of Glyco-blue (Life Technologies), 2.5 volume 100% ethanol, 10 mM $MgCl_2$, and 0.1 volume 5M NaCl. Samples were incubated overnight at -20 ˚C, followed by spinning

down at 12,000 *g* for 30 min at 4 °C. RNA pellets then were washed using 80% EtOH and resuspended in 20 µl nuclease-free water. RNA concentration and quality were quantified using Thermo Scientific NanoDrop 2000. Samples were stored at -80 ˚C until further use for qRT-PCR or sequencing (RNA-seq).

2.2.5.2. DNase Treatment

To avoid the interference of DNA in downstream applications, RNA samples were treated with a TURBO DNA-free™ DNase Treatment kit according to the manufacturer's instruction (Ambion cat#AM1907). For DNase treatment, 2 to 4 ug of RNA dissolved in 44 µl RNase free water was mixed with DNase reaction mixture containing 5 µl of 10xTurbo DNAse Buffer and 1 µl TURBO DNase enzyme, followed by a 30-minutes incubation at 37 °C. Following the incubation, 5 µl of DNase inactivation reagent was added to the samples and after a 5-minutes incubation at room temperature, samples were spun down at 10000 *g* for 1.5 minutes. 47 µl of supernatant was transferred into new tubes containing 50 µl 75% isopropanol and 2 µl Glycoblue and incubated overnight at -80 °C. Samples were centrifuged at 16.1 *g* for 20 minutes at 4 °C and RNA pellets were dried after washing with 1 ml of 75% ethanol. Dried RNA pellets were re-suspended in 20 µl of TE buffer, and after a 10 minutes incubation at 55 °C, they were quantified using the Nanodrop.

2.2.5.3. Reverse Transcription

Using the iScriptTM Reverse Transcription kit, DNase-treated RNA samples were converted into cDNA according to the manufacturer's instruction. For a reverse transcriptase (RT) reaction, 500 ng of RNA sample (diluted to 15 µl with TE buffer) was mixed with iScript master

mix containing 4 µl of iScript reaction mix and 1 µl of reverse transcriptase enzyme. Two control samples also were prepared including one "No-RNA" sample and one "No-RT" sample; the No-RNA sample contained 15 µl nuclease-free water and 5 µl iScript master mix and the No-RT sample contained all components (including RNA) except for reverse transcriptase. RT reactions were performed by incubating samples at room temperature for 5 minutes, 42 °C for 30 minutes and 85 °C for 5 minutes. The prepared cDNA samples were diluted 1:5 in nuclease-free water and stored at -20 °C until running the polymerase chain (PCR) reaction.

2.2.5.4. Quantitative polymerase chain reaction (qRT-PCR)

Gene expression was examined via quantitative RT-PCR (qRT-PCR) assay using a BioRad C1000 Thermal Cycler and CFX384TM Real-Time System. The qRT-PCR reaction was performed by preparing a mixture of 0.5 µl forward primer (5 pmol/ µl), 0.5 µl reverse primer (5 pmol/ µl), 5 µl iQ-SYBR Green Supermix, 2 µl RNase free water, and 2 µl cDNA. The qRT-PCR samples were prepared in three biological and three technical replicates, followed by a 3-step PCR program including 1) 3 minutes in at 95 °C, 2) 40 cycles of 15 sec at 95 °C, 15 sec at 55 °C- 62 ˚C (depending on the annealing temperature of primers used), and 30 sec at 72 °C and 3) 1 minute at 95 °C, 1 minute at 55 °C and 10 sec 60 °C. Data were analysed using CFX Manager Software Version 3.0 (Bio-Rad Laboratories, Inc.). Expression of target genes was calculated by the 2-ΔΔCt method relative to the expression of *GAPDH* (reference gene) as described previously (Schmittgen and Livak 2008).

2.2.5.5. RNA-seq

LNCaP cells were seeded at the appropriate seeding density in 6-well plates and treated with Vehicle, MeT 1 nM, DHT 1 nM, and a combination of MeT 1 nM + DHT 1 nM and total RNA was extracted at 6 hours and 24 hours after treatment as described in section 2.2.5.1. For each treatment condition, three biological replicates were used to generate samples for RNA-seq. RNA concentration was quantified by Nanodrop 2000 (Thermo Fisher Scientific) and total RNA (2 µg) was supplied to the South Australian Health and Medical Research Institute (SAHMRI) for RNA integrity check, library preparation and high throughput sequencing. The integrity of RNA samples was assessed using The 2100 Bioanalyzer system (The Agilent). RNA sequencing libraries were constructed with TruSeq® Total RNA HT kit (Illumina) and libraries were sequenced on the Illumina NextSeq 500 platform with the stranded, paired-end read of 80bp.

2.2.6. Immunofluorescence

LNCaP cells were seeded on glass coverslips in 6-well plates. To improve cell adhesion, glass coverslips were coated with 1:8 diluted L-Poly-Lysine. After treating the cells, at appropriate time points, cells were fixed in 4% paraformaldehyde for 10 minutes, permeabilized in 0.1% Triton X-100 for 15 minutes, and blocked in 2.5% BSA solution for 1 hour. The coverslips then were incubated with a primary antibody and incubated overnight at 4 °C, followed by washing (twice with 5 min intervals) and then incubation with a fluorescent-tagged secondary antibody for 1 hour at room temperature. Cell nuclei were visualised by co-staining the cells with 4´-6-Diamidino-2-phenylindole (DAPI; Invitrogen) for 1 min. Imaging was carried out

using a confocal microscope (Olympus FV3000 Confocal Microscope) and analysed using the Image J software (Schneider, Rasband et al. 2012).

2.2.7. Cell cycle analysis by fluorescence-activated cell sorting (FACS)

Cells were seeded in 6-well plates and incubated overnight at 37 °C and 5% CO_2. At appropriate time points, cells were trypsinized after washing with a freshly prepared wash buffer containing PBS with 2% FBS. After trypsin treatment, the cells were pipetted to resuspend and break up any clumps. The cell suspension was added to a 5 ml FACS tube (containing previously collected cell culture media), each well was washed with PBS, and then this wash was added to tubes. Tubes were centrifuged at 700 *g* for 5 min. Cell pellets were re-suspended and washed with 1ml PBS, followed by centrifugation at 700 *g* for 5 minutes. After removing supernatants, cell pellets were resuspended in residual liquid by flicking the tubes and at the end, 1ml ice-cold 70% EtOH in PBS was added into each tubes containing the cell suspension to be fixed overnight at 4 °C. Following cell fixation with ethanol, cells were centrifuged at 700 *g* for 5 minutes and the cell pellets were washed twice with 1 ml HBSS + 2% FBS. Cells were then stained with 1 ml of DAPI (10 ug/mL). The prepared cell suspension was used for cell cycle analysis based on DNA content using BD FACSCanto II flow cytometer (Analyser). Following values/options were applied as a Cytometer Settings: FSC (forward scatter): 284, linear, signal height (H) and area (A) were measured; SSC (side scatter): 236, log, signal height (H) and area (A) were measured; DAPI: 277, linear, signal height (H), width (W) and area (A) were measured. FSC threshold was adjusted to 1200. After acquiring 50,000 events from each tube, the analysis was carried out using the FlowJo software program.

2.2.8. LINE-I ELISA assay for assessment of DNA methylation

The Global DNA Methylation-LINE-I Kit was used to assess the DNA methylation status of Long Interspersed Nucleotide Element 1 (LINE-I) repeat elements, which serves as a proxy for global DNA methylation level.

2.2.8.1. Extraction of genomic DNA

Genomic DNA was isolated using the QIAamp® DNA Mini kit according to the manufacturer's instruction. Cells were grown and treated in a 6-well plate and at the appropriate time points, (see Chapter 3) media was removed. Cells were washed with PBS and then treated with trypsin as described above, followed by the addition of media containing FBS to neutralise the trypsin. Subsequently, the cell suspension was centrifuged at 300 *g* for 5 min, and the supernatant was removed. Cell pellets were re-suspended in 200 µl PBS and 20 µl proteinase K was added into cell suspension. After adding the proteinase K, 200 µl of Buffer AL was added and the mixture was mixed by pulse-vortexing for 15 sec, followed by incubation at 56 °C for 10 minutes. After brief centrifugation, 200 µl of 96–100% ethanol was added to the samples and mixed by pulse-vortexing for 15 sec. Samples were then applied to a QIAamp Mini spin column and spun down at 6000 *g* for 1 minute. The tubes containing the filtrates were discarded and the spin columns were placed in clean 2 ml collection tubes. 500 µl of Buffer AW1 was then added into each column, which was followed by spinning down at 6000 *g* for 1 minute, and then replacing the tubes containing the filtrates with clean 2 ml collection tubes. 500 µl of Buffer AW2 was then added into the columns, after which they were centrifuged at 16.1 *g* speed for 3 minutes. After replacing the collection tubes with clean

tubes, columns were centrifuged at 16.1 *g* speed for 1 minute and then collection tubes were replaced with 1.5 ml microcentrifuge tubes. Finally, 200 µl of AE buffer was added to each column and after incubation at room temperature for 1 min the columns centrifuged at 6000 *g* for 1 min to elute DNA. DNA yield was assessed by Nanodrop and samples were stored at -20 °C.

2.2.8.2. MseI Digestion of Genomic DNA

The methylation status of LINE-I elements is detected through the hybridization of LINE-I probes with DNA fragments generated by MseI-mediated digestion reaction. Digestion reactions were performed by adding 10 µl of genomic DNA (100 ng/ µl) into a reaction mixture consisting of 2 µl reaction buffer (10x), 0.5 µl of MseI enzyme (10U/ µl), and 7.5 µl sterile water. Sample tubes were mixed by pipetting and incubated at 37°C. After 4 hours of incubation, MseI enzymatic activity was stopped by heating the tubes at 65°C for 20 minutes. After digestion, DNA concentration was measured by Nanodrop. Digested DNA samples were stored at -20 °C until further use.

2.2.8.3. DNA Sample Hybridization

For DNA hybridization, 25 µl of digested DNA samples (4 ng/ µl) was added into 0.2 ml PCR tubes (in triplicates) followed by adding 25 µl of LINE-I probe solution. For quantification of DNA methylation in experimental samples, a standard curve was needed to be prepared using standards provided in the kit. Methylated and non-methylated DNA standards were mixed in different combinations to prepare seven standard samples with a known DNA methylation status. Then, in labelled PCR tubes, 25 µl of each standard sample (100 ng DNA/well) was

mixed with 25 µl of LINE-I probe solution. Finally, all samples were placed in a thermal cycler and incubated as following: 98 °C for 10 minutes, 68 °C for 1 hour, and a quick ramp to 25 °C.

2.2.8.4. DNA binding to the streptavidin-coated plate and colorimetric detection

After DNA hybridization, the content of each PCR tube was transferred into an allocated well coated with streptavidin and then the plate was incubated at room temperature for 1 hour with mild agitation. Subsequently, the contents of each well were removed by quickly inverting the plate, followed by washing wells 3x with 200 µl 1X Buffer W (10 minutes each wash). After each wash, the contents of wells were removed by pipette and 200 µl of Assay Buffer AM3 (blocking buffer) was added to each well and then incubated for 30 minutes. After removing the blocking buffer, 100 µl of diluted 5-Methylcytosine antibody was added per well and incubated for 1 hour, followed by 3x washes with 200 µl 1X Wash Buffer. 100 µl of diluted HRP-conjugated anti-mouse antibody was then added to each well for 1 hour at room temperature. Wells were then washed 3x using 200 µl of 1X Wash Buffer before adding 100 µl developing solution to each well. The reaction was stopped by adding 100 µl of stop solution when a medium to dark blue colour was evident in the standard well with the highest concentration of methylated DNA. Absorbance was read using a spectrophotometer at 450nm. The percentage of 5-mC associated with each sample was analysed using the prepared standard curve.

2.2.9. Chromatin immunoprecipitation (ChIP)

2.2.9.1. Cell treatment and cross-linking

LNCaP cells were seeded in 15 cm culture dishes at 5×10^6/plate (for AR-ChIP; three plates per replicate) and $\times10^6$/plate (for H3K27me3-ChIP; one plate per replicate) in their normal growth medium. For AR-ChIP, phenol-red-free medium supplemented with 5% DCC-stripped FBS was used and cells were allowed to grow for 2 days prior to treatment with Vehicle (Ethanol), MeT 1 nM, and DHT 1 nM for 4 hours. For H3K27me3 ChIP, phenol-red-free medium supplemented with 5% FBS was used and cells were allowed to grow for 1 day before treating the cells with Vehicle (Ethanol), MeT (1nM and 100nM), and DHT (1nM and 100nM) for 72 hours. To cross-link, the target protein to DNA, 20ml of pre-warmed Solution A containing freshly added 1% formaldehyde was added to each 15cm-cell culture dish. Plates were incubated for 10 minutes in the fume hood, and then formaldehyde was quenched by adding 2 ml of 1 M glycine (pH 7.5) and incubating for 5 minutes. Subsequently, cells were washed twice with ice-cold PBS, after which cells were scraped into 500 µl PBS + PI per 15 cm dish. After transferring the harvested cells into 2.0 ml Eppendorf tubes, they were centrifuged at 7,168 *g* for 3 minutes at 4 ºC and cell pellets were resuspended in 500 µl PBS + PI. Centrifugation and removal of the supernatant were repeated and then cell pellets were frozen in liquid nitrogen and stored at -80 ºC until further use.

2.2.9.2. Preparation of magnetic beads

Dynabeads (Protein A, Invitrogen) were used for conjugation with AR antibody (Abcam; ab108341) or H3K27me3 antibody (cell Signalling; C36B11). Dynabeads were vortexed to be ensured they were fully resuspended. Then, 100 µl per ChIP was added into a 2 ml, round-

bottomed, Eppendorf tube and put in a magnetic stand, on ice. The supernatant was removed and beads were washed and blocked three times with cold 1ml PBS + 5 mg/ml BSA. After washing, beads were re-suspended in 500 µl of cold PBS/BSA and 10 µg /IP of AR antibody or 7.5 µg /IP H3K27me3 antibody was added into the tubes containing the prepared dynabeads. Tubes were rotated at 12-20 rpm overnight at 4 °C.

2.2.9.3. Sonication and immunoprecipitation

Cell pellets were resuspended in 1 ml of Lysis Buffer 1 (LB1) + PI and then tubes were rotated at 4 C for 10 minutes, centrifuged at 2,000 *g* for 5 min at 4 ºC, after which supernatants were removed. Cell pellets were then resuspended in 1 ml LB2 + PI, rotated at 4 ºC for 10 minutes, centrifuged at 2000 *g* for 5 minutes at 4 ºC, after which supernatants were removed. Cell pellets were then resuspended in 300 µl of LB3 + PI per each 15 cm plate. 300 µl of cell suspension from each replicate were transferred into 1.5 ml TPX sonication tubes (Diagenode) and they were sonicated (Bioruptor Plus, Diagenode) as follows: 30s on and 30s off, on high, for 10 cycles. Ice was added to water in the sonicator after every round to avoid increasing the temperature. Sonicated samples from each replicate were re-pooled and 10 µl aliquot of the sonicated chromatin was evaluated by agarose gel electrophoresis as following protocol. 5 µl of sonicated DNA was transferred into a 250 µl PCR tube containing 2 µl of NaCl 500 mM and the final volume was adjusted to 20 µl with sterile water. Samples were heated in a thermocycler at 100 ºC for 20 minutes, followed by ramping the temperature down to 50 ºC. Then, tubes were removed from the thermocycler and incubated at room temperature for 5 minutes. Reverse cross-linked samples were run on 1.2% agarose gel to check the sonication. Fragment sizes should be ideally approximately 200-500 bp.

After confirming the sonication efficiency on an agarose gel, 10% Triton X-100 dissolved in LB3+PI was added into pooled sonicated samples to a final concentration of 1%. Tubes were then centrifuged at 20,000 *g* for 10 minutes at 4 ºC. In the meantime, magnetic beads prepared in 2.2.9.2 were washed 3x using 1ml ice-cold PBS/BSA using a magnetic stand to remove unbound antibodies, followed by re-suspending in 100 µl of LB3+PI+1% triton. Sonicated chromatin supernatants were transferred into fresh 2ml tubes and 50 µl from each sample was kept as an Input sample. Then, 100 µl of conjugated magnetic beads were added to the tubes containing sonicated chromatin and diluted with LB3 (+PI) with a final concentration of 1% Triton X-100 to ~1.8 ml. tubes were rotated overnight at 4 ºC.

2.2.9.3. Reverse cross-linking and DNA isolation

After overnight incubation of beads with chromatin samples, beads were washed 6x with 1ml ice-cold ChIP-RIPA buffer using a magnetic stand. 200 µl of elution buffer was then added into each tube and incubated on a thermal shaker at 65 °C for 15 min, with a brief vortexing every 5 min. Reverse crosslinking of samples was performed by 18 hours incubation at 65 °C. At the same time, 150 µl of elution buffer was also added to each Input sample which was prepared after sonication and had been stored at -80 °C, followed by 18 hours incubation at 65 °C. After incubation time, tubes were placed on a magnetic stand and supernatants containing eluted antibody: target: DNA complexes were transferred into fresh Eppendorf tubes.

In the next step, 200 µl of TE buffer and 8 µl of 1mg/ml RNAse A were added into each sample, and then the tubes were incubated at 37 ºC for 1 hour. Subsequently, 4 µl of 20 mg/ml Proteinase K was added per sample and tubes were incubated at 55 ºC for 2 hours. 400 µl of

Phenol: Chloroform: Isoamyl alcohol (25:24:1) was added per tube and after mixing for 15 sec the suspension was added into pre-spun 5PRIME phase-lock gel column (Quanta Biosciences). Phase-lock columns were centrifuged for 5 minutes at 10,000 *g* at room temperature, followed by transferring the upper layer (~ 400 µl) into an Eppendorf tube containing 16 µl of 5 M NaCl and 2 µl glycogen (20 µg/ µl). 800 µl 100% ethanol was added per tube and samples were incubated overnight at -80 ºC. The next day, samples were centrifuged at 4 ºC at 16.1 *g* for 20 minutes. The supernatant was removed and DNA pellets were washed using 500 µl cold 70% ethanol. After spinning down at full speed for 5 minutes at 4 ºC, ethanol was removed and pellets were air-dried at room temperature. After drying the pellets, DNA samples were resuspended in 20 µl of 10mM Tris HCl pH 8.0. Samples were stored at -80 ºC until analysis by qPCR or Illumina sequencing.

2.2.9.4. Preparing the ChIP DNA samples for next-generation sequencing

DNA concentration was measured by Qubit dsDNA HS assay, according to the manufacturer's instruction (Thermo Fisher Scientific). Briefly, 200 µl of Qubit working Solution for each standard and sample was prepared by diluting the fluorescent reagent 1:200 in the kit buffer. To prepare the standards, 10 µl of each standard vials (low and high) were mixed with a 190 µl working solution. Qubit samples were prepared by mixing 1 µl of each sample with 199 µl of working solution. Samples were vortexed briefly and incubated for 2 minutes at room temperature. Using the standards, DNA concentration in each sample was measured by the Qubit Fluorometer. 5 ng of ChIP DNA (ChIP-enriched or input) were used for ChIP-sequencing library preparation using an Illumina TruSeq ChIP Library Prep kit (Illumina). Prepared samples

were sequenced on the Illumina Nextseq 500 platform using the single-end protocol with a read length of 75 bp at the South Australian Health and Medical Research Institute (SAHMRI).

2.2.9.5. PCR analysis of ChIP DNA

For ChIP–PCR reactions, iQ SYBR Green Supermix (BIO-RAD) and primers as listed in Table 2.5 were used. For the AR-ChIP PCR experiment, KLK3 was used as a positive control for AR binding, and a non-coding region of DNA named NC2 was used as a negative control. PCR was performed using the CFX384 Real-Time PCR Detection System (BIO-RAD) and standard cycling conditions at the optimised annealing temperature. Enrichment of target factor in ChIP–PCR was analysed as the percentage of input.

2.2.10. RNA-seq analysis:

The quality of raw data was initially assessed using the FastQC platform (http://www.bioinformatics.babraham.ac.uk/projects/fastqc/). The raw FASTQ files were then filtered for short sequences using Cutadapt v1.16.6 (Martin 2011) with the following settings: minimum overlap length in Adaptor options: 3, Minimum length in filter options: 20, maximum error rate: 0.1, quality cut-off: 20. The quality of filtered FASTQ files (averaging 30 million read pairs per sample) were checked again using the FastQC program. Reads were mapped against the human reference genome (hg38) using the STAR spliced alignment algorithm version 2.6.0 b-2 (Dobin, Davis et al. 2013) with default parameters. FeatureCounts was used to count and assign the reads in generated BAM files to genomic features (Liao, Smyth et al. 2014). Count tables generated by featureCount were used for differential expression analysis using DESeq2 (Love, Huber et al. 2014). Statistically, p-adj ≤ 0.05 were

used to identify the differentially expressed genes (DEGs). Principal component analysis and the gene expression visualisation were performed using ClustVis (Metsalu and Vilo 2015).

2.2.11. ChIP-seq analysis:

The quality of raw FastQ files was checked using FastQC v0.72 (https://www.bioinformatics.babraham.ac.uk/projects/fastqc/). The poor-quality reads were removed using Trimmomatic Galaxy v.0.35 (Bolger, Lohse et al. 2014) and subsequently, raw data were aligned to GRCh37 (hg19) genome assembly using Bowtie2 version: 2.3.4.3 with default parameters (Langmead, Trapnell et al. 2009). SAMtools was used to remove the low-quality mapped reads (MAPQ < 10), multi-mapping reads, and PCR duplicates (Li, Handsaker et al. 2009). Peak calling from alignment results were carried out using MACS2 callpeak v 2.1.1.20160309.6, with minimum FDR (q-value) cutoff for peak detection 0.05 (Zhang, Liu et al. 2008, Feng, Liu et al. 2012). BAMCoverage was used to convert BAM files to bigwig, followed by data visualisation using the Integrative Genomics Viewer (Ji, Jiang et al. 2008, Robinson, Thorvaldsdóttir et al. 2011). deepTools was used to generate the Heatmaps (Galaxy Version 3.3.2.0.0) (Ramírez, Ryan et al. 2016). Peak annotations were performed using Cisgenome v2.0 (Ji, Jiang et al. 2008).

2.2.12. Statistical analyses:

Statistical analyses were done using GraphPad Prism 9. Detailed methods for statistical analysis are included in figure legends or the individual Chapter methods.

Chapter 3: Potent stimulation of the androgen receptor instigates a viral mimicry response in prostate cancer

THE UNIVERSITY of ADELAIDE

Statement of Authorship

Title of Paper	Potent stimulation of the androgen receptor instigates a viral mimicry response in prostate cancer
Publication Status	☐ Published ☐ Accepted for Publication ☐ Submitted for Publication ☑ Unpublished and Unsubmitted work written in manuscript style
Publication Details	

Principal Author

Name of Principal Author (Candidate)	Mohammadreza Alizadeh Ghodsi		
Contribution to the Paper	Performed experiments (cell culture, growth assays, Western blots, apoptosis assays, qRT-PCR, ChIP-PCR, ChIP-seq, RNA-seq, transactivation assays, immunofluorescence), analysed and interpreted data (including bioinformatics analysis of ChIP-seq and RNA-seq); designed experiments; generated figures; co-wrote manuscript.		
Overall percentage (%)	70%		
Certification:	This paper reports on original research I conducted during the period of my Higher Degree by Research candidature and is not subject to any obligations or contractual agreements with a third party that would constrain its inclusion in this thesis. I am the primary author of this paper.		
Signature		Date	26/05/2021

Co-Author Contributions

By signing the Statement of Authorship, each author certifies that:

i. the candidate's stated contribution to the publication is accurate (as detailed above);

ii. permission is granted for the candidate in include the publication in the thesis; and

iii. the sum of all co-author contributions is equal to 100% less the candidate's stated contribution.

Name of Co-Author	Katie L. Owen		
Contribution to the Paper	Designed and conducted RM1 experiments; contributed to data analysis and interpretation.		
Signature		Date	13/5/21

Name of Co-Author	Scott Townley		
Contribution to the Paper	Assisted with experimental design and performed experiments (cell culture, qRT-PCR, transactivation assay, growth assays).		
Signature		Date	20/5/21

Please cut and paste additional co-author panels here as required.

Name of Co-Author	Damien Zanker		
Contribution to the Paper	Designed and conducted RM1 experiments; contributed to data analysis and interpretation.		
Signature		Date	13-05-2021

Name of Co-Author	Adrienne Hanson		
Contribution to the Paper	Assisted with experimental design and performed experiments (cell culture, qRT-PCR, LINE-1 DNA methylation assays).		
Signature		Date	17-05-21

Name of Co-Author	Raj Shrestha		
Contribution to the Paper	Assisted with experimental design and performed experiments (apoptosis assays).		
Signature		Date	13/05/2021

Name of Co-Author	John Toubia		
Contribution to the Paper	Assisted with analysis of RNA-seq and ChIP-seq data.		
Signature		Date	13/05/2021

Name of Co-Author	Tessa Gargett		
Contribution to the Paper	Assisted with multiplex IFNs measurement by FACS.		
Signature		Date	19/05/21

Name of Co-Author	Kaylene Simpson		
Contribution to the Paper	Generated preliminary data; assisted with experimental design.		
Signature		Date	17/5/21

Name of Co-Author	Igor Chernukhin		
Contribution to the Paper	Assisted with analysis of RNA-seq data (expression of repetitive elements); assisted with interpretation of transcriptomic data.		
Signature		Date	17.05.21

Name of Co-Author	Jason Carroll		
Contribution to the Paper	Assisted with analysis of RNA-seq data (expression of repetitive elements); assisted with interpretation of transcriptomic data.		
Signature		Date	17/5/21

Name of Co-Author	Jean M. Winter		
Contribution to the Paper	Generated preliminary data; assisted with experimental design.		
Signature		Date	13/05/2021

Name of Co-Author	Lisa M. Butler		
Contribution to the Paper	Generated preliminary data (primary tumour explant study); assisted with experimental design.		
Signature		Date	May 13, 2021

Name of Co-Author	Benjamin Thierry		
Contribution to the Paper	Project co-supervisor; assisted with experimental design.		
Signature		Date	13/05/2021

Name of Co-Author	Mitchell G. Lawrence		
Contribution to the Paper	Generated preliminary data; assisted with experimental design.		
Signature		Date	14 May 2021

Name of Co-Author	Gail Risbridger
Contribution to the Paper	Generated preliminary data; assisted with experimental design.
Signature	Date 17.5.21

Name of Co-Author	Renea Taylor
Contribution to the Paper	Generated preliminary data; assisted with experimental design.
Signature	Date 13th May 2021

Name of Co-Author	Theresa E. Hickey
Contribution to the Paper	Project conceptualization and funding; assisted with experimental design and data interpretation.
Signature	Date 24/05/2021

Name of Co-Author	Belinda S. Parker
Contribution to the Paper	Designed and conducted RM1 experiments; contributed to data analysis and interpretation.
Signature	Date 13/05/21

Name of Co-Author	Wayne Tilley
Contribution to the Paper	Project supervisor; project conceptualization and funding; assisted with experimental analysis and data interpretation.
Signature	Date 24/05/2021

Name of Co-Author	Luke A. Selth
Contribution to the Paper	Project principal supervisor; conceived project; designed experiments; (including bioinformatics analysis of ChIP-seq and RNA-seq); generated figures; co-wrote the manuscrip.
Signature	Date 21/5/21

Potent stimulation of the androgen receptor instigates a viral mimicry response in prostate cancer

Mohammadreza Alizadeh Ghodsi[1], Katie L. Owen[2,3], Scott Townley[1,4], Damien Zanker[2,3], Adrienne Hanson[4], Raj Shrestha[1,4], John Toubia[5,6], Tessa Gargett[5], Igor Chernukhin[7], Jason Carroll[7], Kaylene Simpson[8], Jean M. Winter[1], Mitchell G. Lawrence[9,10], Lisa M. Butler[11,12], Gail Risbridger[9,10,12], Benjamin Thierry[13,14], Renea Taylor[9,15], Theresa E. Hickey[1], Belinda S. Parker[2,12], Wayne D. Tilley[1] and Luke A. Selth[1,3,11*]

1. Dame Roma Mitchell Cancer Research Laboratories and Freemasons Centre for Male Health and Wellbeing, Adelaide Medical School, The University of Adelaide, Adelaide, SA 5005, Australia.
2. Cancer Immunology Program, Peter MacCallum Cancer Centre, Melbourne, VIC 3000, Australia.
3. Sir Peter MacCallum Department of Oncology, The University of Melbourne, Parkville, VIC 3000, Australia.
4. Flinders Health and Medical Research Institute, Flinders University, Bedford Park, SA 5042, Australia.
5. Centre for Cancer Biology, University of South Australia and SA Pathology, Adelaide, SA 5000, Australia.
6. ACRF Cancer Genomics Facility, Centre for Cancer Biology, SA Pathology and University of South Australia, Frome Road, Adelaide, SA, 5000, Australia
7. Cancer Research UK Cambridge Institute, University of Cambridge, Cambridge, UK.
8. Peter MacCallum Cancer Centre, Victorian Centre for Functional Genomics, Melbourne, VIC 3000, Australia.

9. Department of Anatomy and Developmental Biology, Monash Partners Comprehensive Cancer Consortium, Monash Biomedicine Discovery Institute, Prostate Cancer Research Group, Monash University, Clayton, VIC 3168, Australia.
10. Cancer Research Program, Cancer Research Division, Peter MacCallum Cancer Centre, University of Melbourne, Melbourne, VIC 3000, Australia.
11. South Australian Health and Medical Research Institute, Adelaide, SA 5000, Australia.
12. Faculty of Health and Medical Sciences, The University of Adelaide, Adelaide, SA 5000, Australia.
13. ARC Centre of Excellence in Convergent Bio and Nano Science and Technology, University of South Australia, Frome Road, Adelaide, SA 5000, Australia.
14. Future Industries Institute, University of South Australia, Mawson Lakes, SA 5095, Australia.
15. Department of Physiology, Monash Partners Comprehensive Cancer Consortium, Monash Biomedicine Discovery Institute, Prostate Cancer Research Group, Monash University, Clayton, VIC 3168, Australia.

*For correspondence: luke.selth@flinders.edu.au

ABSTRACT

Inhibiting the androgen receptor (AR), a ligand-activated transcription factor, with androgen deprivation therapy is a standard-of-care treatment for metastatic prostate cancer (PCa). Paradoxically, recent studies have suggested that “extreme” activation of AR using high doses of androgens can - similarly to suppression of AR activity - inhibit the growth of PCa. This study exploited a potent synthetic androgen, methyltestosterone (MeT), to investigate the mechanism of action of high dose androgen therapy. MeT strongly inhibited the growth of PCa cells expressing AR, but not AR-negative models. By integrating ChIP-seq and RNA-seq data, we found that the genes and pathways regulated by MeT were highly analogous to those regulated by DHT, although MeT educed a quantitatively greater androgenic response. The transcriptomic analysis also revealed that MeT caused dysregulation of transposable element expression, with long-term treatment resulting in upregulation of endogenous retroviruses (ERVs). Mechanistically, increased expression of ERVs was linked to MeT-mediated down-regulation of DNA methyltransferases and global DNA hypomethylation. Increased ERV expression was associated with accumulation of double-stranded RNA and a “viral mimicry” response that resulted in activation of interferon signalling, upregulation of MHC Class I molecules and enhanced tumor cell immunogenicity as measured by enhanced recognition by tumour-specific $CD8^+$ T cells. Importantly, we identified positive associations between AR activity and ERVs/anti-viral pathways in clinical datasets. Collectively, our study reveals that the potent androgen MeT can activate innate immune responses in PCa cells, a finding that has potential implications for the development of androgen-mediated strategies to sensitize PCa to immunotherapies.

INTRODUCTION

Prostate cancer (PCa) cells are exquisitely dependent on androgens and the androgen receptor (AR) for growth and survival, which explains the efficacy of androgen deprivation therapy (ADT) as a treatment for advanced PCa. ADT is comprised of hormonal manipulations that reduce circulating androgen levels and/or directly block AR activity. While almost all men initially respond to ADT, the development of a therapy resistant disease state, referred to as castration-resistant prostate cancer (CRPC), is inevitable. In the vast majority of cases, resistance to ADT is mediated by adaptive alterations to the AR signalling axis, highlighting addiction to this pathway as a hallmark of PCa (Coutinho, Day et al. 2016).

AR is a transcription factor that, upon binding to androgen, translocates from the cytoplasm to the nucleus and interacts with specific cis-regulatory elements (termed androgen response elements) on chromatin to regulate a gene expression program that promotes growth, survival and metabolism of PCa cells. The transcriptional output of AR can be influenced by a multitude of parameters, including hundreds of co-regulators (Liu, Kumari et al. 2017), epigenetic factors (Gao and Alumkal 2010) and the concentration and composition of the androgenic milieu (Auchus and Sharifi 2020). Additional complexity arises from the evolution of AR signalling axis components during progression to CRPC. For example, direct changes to the *AR* gene (mutation, amplification and rearrangements that result in AR splicing alterations) alter cellular responses to androgens, alternative ligands and anti-androgens, collectively enabling high AR activity despite ongoing ADT (Coutinho, Day et al. 2016).

Not surprisingly, most work on AR to date has focussed on its oncogenic functions. However, it is important to consider that in normal adult prostate epithelial cells AR promotes cellular quiescence by preserving luminal differentiation and protein-secretory activity. This understanding may explain the decades-old observation that administration of high doses of testosterone can result in clinical responses in men with CRPC (Huggins 1965). This apparent paradox is supported by pre-clinical studies demonstrating that low androgen levels promote growth of PCa whereas high androgen concentrations are growth-inhibitory (Langeler, van Uffelen et al. 1993, Kokontis, Hay et al. 1998, Mohammad, Nyquist et al. 2017). The concept of therapeutic application of androgens in PCa has culminated in recent clinical trials testing supraphysiological levels of testosterone (SupraT), which have yielded promising results in a subset of patients (Schweizer, Antonarakis et al. 2015, Teply, Wang et al. 2018, Denmeade, Wang et al. 2021, Markowski, Wang et al. 2021, Sena, Wang et al. 2021). In the clinic, SupraT is often combined with ADT such that patients are cycled between near-castrate and very high serum T levels, a treatment strategy referred to as bipolar androgen therapy (BAT) (Schweizer, Antonarakis et al. 2015, Teply, Wang et al. 2018, Denmeade, Wang et al. 2021, Markowski, Wang et al. 2021, Sena, Wang et al. 2021).

A detailed understanding of the mechanism(s) by which androgens can inhibit PCa growth is important to optimise clinical benefit of SupraT/BTA. Numerous processes have been purported to explain the activity of SupraT, including AR transcriptional reprogramming (Gao, Gao et al. 2016, Nyquist, Corella et al. 2019) and AR's effects on the DNA damage response (Chatterjee, Schweizer et al. 2019), DNA replication (D'Antonio, Vander Griend et al. 2009) and oxidative stress (Bui, Huang et al. 2017), but the relative importance of each and whether

or not other anti-cancer effects exist are poorly understood. In this study, we investigated the mode of action of a synthetic androgen, 17α-methyl-testosterone (MeT), which can potently inhibit PCa growth. By dissecting the transcriptome of MeT-activated AR, we uncovered a novel response of PCa cells to potent androgen action. Specifically, we demonstrate that MeT down-regulated DNA methyltransferases and hence reduced DNA methylation throughout the genome, an effect that was associated with increased expression of endogenous retrovirus transcripts, activation of interferon (IFN) signalling and enhanced immunogenicity of PCa cells. Thus, our findings demonstrate that potent androgenic action can cause viral mimicry in PCa cells, which may provide a basis for new targeted investigations into combining androgen therapies with immunotherapies.

RESULTS

Methyl-testosterone is a potent activator of AR activity and suppressor of prostate cancer cell growth

In studies interrogating the therapeutic potential of AR ligands in PCa, we noted that MeT has strong growth-inhibitory activity in LNCaP cells grown in full serum (i.e. androgen replete conditions) at doses as low as 1 nM (Fig. 1A). Conversely, DHT only suppressed cell growth only at doses greater than 1 nM (Fig. 1A). Growth of the CRPC cell lines C42B, MR49F, and 22Rv1 was also inhibited by MeT at doses ranging from 1-100 nM (Fig. 1B). DHT also suppressed the growth of C42B and MR49F cells but had no effect on 22Rv1 cells (Supplementary Fig. 1A). Importantly, neither the AR-negative model PC3 nor the R1-D567 model, which expresses an AR variant that lacks the ligand-binding domain (ARv567es), were affected by MeT (Supplementary Fig. 1B), indicating that growth suppression was a consequence of binding of MeT to AR.

To better understand the activity of MeT in PCa cells, we undertook a series of molecular assays. First, we compared MeT and DHT in a classic transcriptional activation assay using a probasin promoter:luciferase reporter construct (PB3-luc; (Jia, Kim et al. 2003)). At lower doses (0.1 nM and 0.5 nM), MeT more potently activated endogenous AR in LNCaP cells and exogenously-supplied AR in PC3 cells AR (Fig. 1C). No difference in transcriptional activity was observed between the 1 nM MeT and DHT treatments (Fig. 1C), possibly because of signal saturation, which is known to occur with these types of luciferase assays (Rakotondrafara and Miller 2008, Heise, Oppermann et al. 2013, Meliani, Leborgne et al. 2015). This experiment provided evidence that MeT could more potently induce the transcriptional activity of AR compared to the physiological ligand DHT.

Subsequently, to evaluate MeT regulation of AR at a global level and in a more physiological setting, we conducted AR ChIP-seq and RNA-seq in LNCaP cells. The AR-MeT cistrome was ~3-fold larger than the equivalent AR-DHT cistrome (Fig. 1D). However, heat maps and density plots of sequencing tags (Fig. 1E) revealed that the majority of MeT-induced AR binding sites were also targeted, albeit more weakly, by DHT-activated AR; hence, we refer to these as “MeT-enriched” (Fig. 1E). For both ligands, AR cistromes were mainly comprised of binding sites distal from gene promoters (Supplementary Table 1), which mirrors what has been reported previously (Tewari, Yardimci et al. 2012, Stelloo, Bergman et al. 2019). Although we cannot rule out the possibility that MeT creates additional AR binding sites in the LNCaP genome, our findings suggest that, in general, MeT did not lead to new AR binding events but rather enhanced its interaction with canonical regulatory elements. This concept was supported by transcriptomic analysis, which revealed that genes differentially expressed in response to MeT ($n = 1212$, FDR ≤ 0.05) were also altered by DHT in a directionally-consistent manner albeit to a lesser degree (Fig. 1F; Supplementary Data 1). This effect was most striking when assessing the 285 genes that were differentially expressed by DHT compared to vehicle (FDR ≤ 0.05): 99%

(282/285) of these genes were also regulated by MeT, all of those 282 genes were regulated in the same direction by both hormones, and 99% (280/282) were more strongly regulated by MeT than by DHT (average 1.6-fold stronger downregulated and 1.1-fold stronger upregulated (Supplementary Data 1). The majority of genes altered by either hormone were downregulated (Fig. 1F and Supplementary Data 1). Collectively, these findings suggest that MeT is a potent activator of canonical AR functions that largely exhibits quantitative, rather than qualitative, differences to the endogenous ligand DHT.

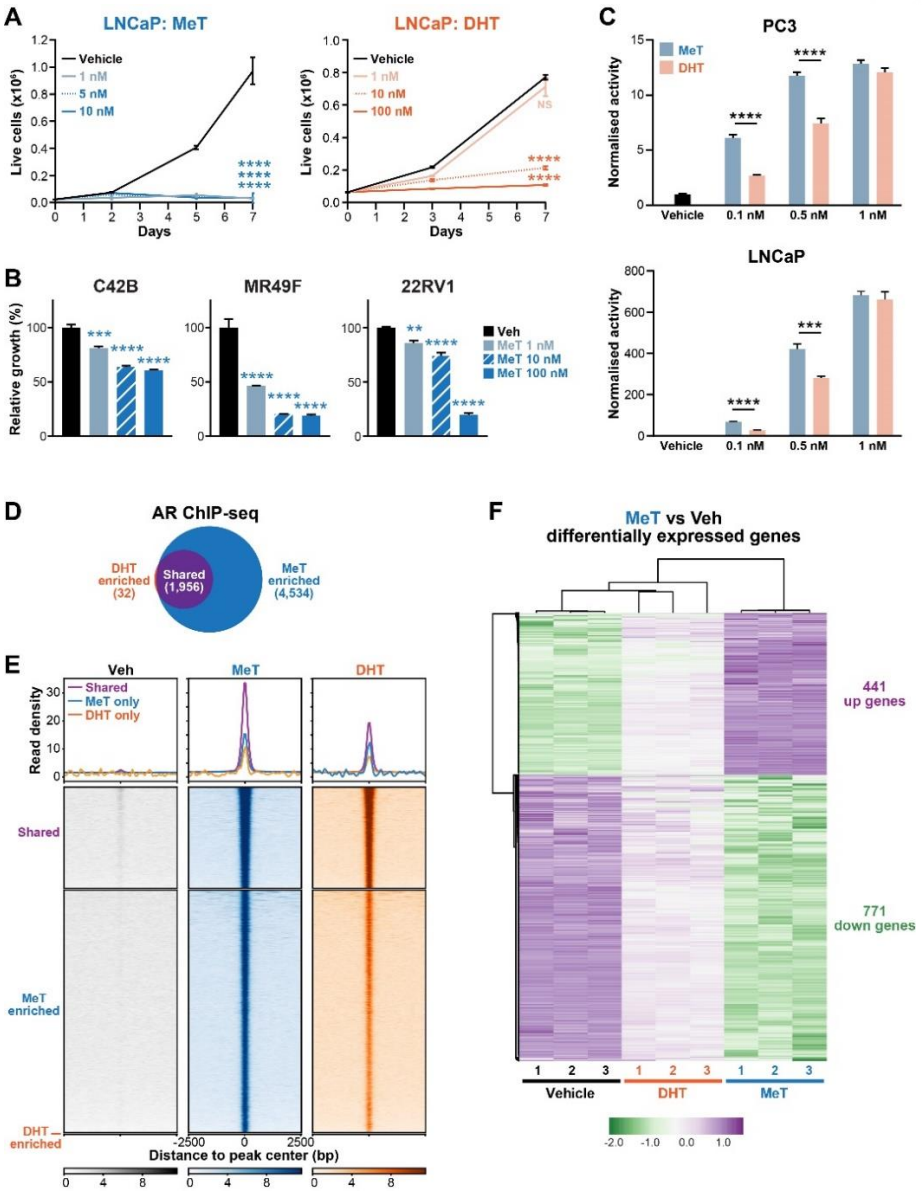
A
LNCaP: MeT
Vehicle
1 nM
5 nM
10 nM
Live cells (x10⁶)
Days
LNCaP: DHT
Vehicle
1 nM
10 nM
100 nM
NS
B
C42B
MR49F
22RV1
Relative growth (%)
Veh
MeT 1 nM
MeT 10 nM
MeT 100 nM
C
PC3
MeT
DHT
Normalised activity
Vehicle
0.1 nM
0.5 nM
1 nM
LNCaP
D
AR ChIP-seq
DHT enriched (32)
Shared (1,956)
MeT enriched (4,534)
E
Veh
MeT
DHT
Read density
Shared
MeT only
DHT only
Shared
MeT enriched
DHT enriched
-2500
0
2500
Distance to peak center (bp)
F
MeT vs Veh
differentially expressed genes
441
up genes
771
down genes
Vehicle
DHT
MeT
-2.0
-1.0
0.0
1.0

Fig. 1. Methyl-testosterone has potent androgenic and growth suppressive activity in prostate cancer cells. (A) MeT potently suppresses the growth of LNCaP cells (left graph), as determined by Trypan blue growth assay. The response of cells to DHT is shown on the right. Error bars are ± SEM. P values (day 7) were determined using ANOVA and Dunnett's multiple comparisons tests (*, $p < 0.05$; **, $p < 0.01$; ***, $p < 0.001$; ****, $p < 0.0001$). NS, not significant. **(B)** MeT inhibits the growth of CRPC models of PCa (C42B, MR49F and 22Rv1), as determined by Trypan blue growth assay. Statistical analysis was as for (A). **(C)** Activation of AR transcriptional activity by MeT in PC3 cells (top) and LNCaP cells (bottom). PC-3 cells were transfected with plasmids expressing or AR and a probasin-luciferase reporter for 4 h prior to a 20 h treatment with 1 nM DHT; LNCaP cells were transfected only with the probasin-luciferase reporter. Transcriptional activity values represent the mean of six biological replicates; results are representative of three independent experiments. Error bars are SEM. Unpaired t tests were used to compare MeT and DHT (***, $p < 0.001$; ****, $p < 0.0001$). **(D)** Venn diagram showing the overlap of AR cistromes in LNCaP cells treated with DHT or MeT (1 nM each). **(E)** Read density plots (top panels) and heatmaps (bottom panels) representing AR ChIP-seq peak sets from (D). **(F)** Heatmap of RNA-seq data for genes differentially expressed by 24 hours of MeT treatment (compared to Vehicle; FDR < 0.05). The heatmap was generated using ClustVis (Metsalu and Vilo 2015) after applying unit variance scaling to each gene.

A

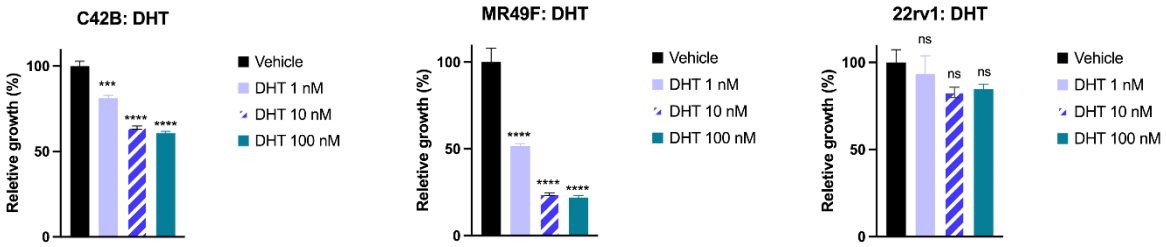

B

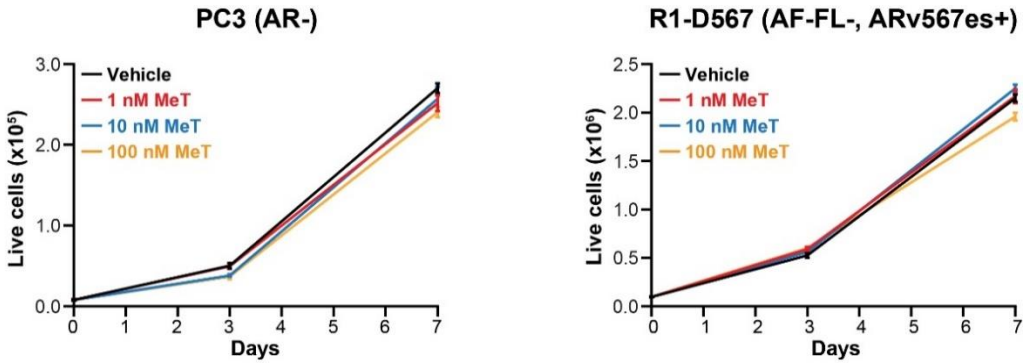

Supplementary Fig. 1. Anti-proliferative effects of MeT and DHT in prostate cancer models. (**A)** DHT inhibits the growth of C42B and MR49F, but not 22RV1, as determined by Trypan blue growth assays. Error bars are +SEM. P values were determined using ANOVA and Dunnett's multiple comparisons tests (*, $p < 0.05$; **, $p < 0.01$; ***, $p < 0.001$; ****, $p < 0.0001$). NS, not significant. **(B)** Methyltestosterone does not affect the growth of PC3 or R1-D567 prostate cancer cells, as determined by Trypan blue growth assays. . Error bars are ± SEM.

Supplementary Table 1. Genomic distribution of AR cistromes

	MeT-AR peaks	DHT-AR peaks	MeT and DHT Shared AR binding sites
Total Peak number (FDR < 0.05)	6491	1993	4123
Intergenic (%)	51.13	51.33	51.30
Intragenic (%)	48.87	48.67	48.70
Exon (%)	2.67	2.91	2.67
Intron (%)	46.50	45.96	46.35
CDS (%)	0.94	0.75	0.82
UTR (%)	1.74	2.16	1.89
5'UTR (%)	0.18	0.25	0.15
3'UTR (%)	1.57	1.96	1.77

* Peak locations were assessed using the CisGenome software.

Methyl-testosterone suppresses DNA replication and repair pathways in prostate cancer cells

Given its potent growth-inhibitory activity, we hypothesised that further dissecting the transcriptomic readouts of MeT-bound AR could yield new insights into mechanisms underlying the activity of high-dose androgen therapy in PCa. Gene set enrichment analysis (GSEA) (Subramanian, Tamayo et al. 2005) was used to identify 'Hallmark' gene sets (Liberzon, Birger et al. 2015) altered by treatment with this potent androgen. Providing further evidence that MeT regulates a transcriptional program that is highly similar to endogenous androgens, the most upregulated hallmarks for both MeT and DHT were 'androgen response', 'protein secretion' and 'apical junction (Fig. 2A). Hallmarks that were robustly repressed by MeT/DHT were related to DNA replication and repair (i.e. E2F targets, MYC targets, G2M checkpoint, mitotic spindle, DNA repair; Fig. 2A), analogous to what has been reported for high-dose androgen treatment previously (Gao, Gao et al. 2016, Chatterjee, Schweizer et al. 2019, Nyquist, Corella et al. 2019). When we examined curated DNA repair (Chatterjee, Schweizer et al. 2019) and DNA replication (Gao, Gao et al. 2016) gene sets that were reported to be repressed by high-dose androgen treatment, we observed that MeT down-regulated these to a considerably greater extent than DHT (Fig. 2B-C). Many of these genes have been purported to be directly regulated by AR on the basis of its binding to proximal regulatory elements (Gao, Gao et al. 2016). Indeed, we found that AR binding near these genes was strongly stimulated by MeT and, to a lesser extent, DHT (Fig. 2D and Supplementary Fig. 2).

A reported consequence of suppression of DNA repair and replication pathways by high-dose androgen treatment is cell cycle arrest (Tsihlias, Zhang et al. 2000, Chatterjee, Schweizer et

al. 2019). Flow cytometry revealed that MeT caused accumulation of cells in G1 phase and consequent reduction of cells in S and G2/M phases (Fig. 2E). The same dose of DHT did not have a significant effect on cell cycle (Fig. 2E), providing additional evidence that MeT is a more potent, yet canonical, androgen than DHT in terms of PCa cell growth suppression. One proposed mediator of G1 arrest by high-dose androgen treatment is increased DNA damage, occurring via a combination of AR-mediated double-stranded breaks (DSBs) (Haffner, De Marzo et al. 2011) and down-regulation of DNA repair genes (Chatterjee, Schweizer et al. 2019). However, MeT did not significantly increase the number of γH2AX foci (Fig. 2F), a marker of DSBs, suggesting that DNA damage is not a major mechanism underlying its growth-suppressive activity in PCa cells. Low dose, but not high dose, DHT caused a minor increase in the number of γH2AX foci (Fig. 2F), potentially representing a differential mode of action between the two androgens in relation to DNA damage and repair.

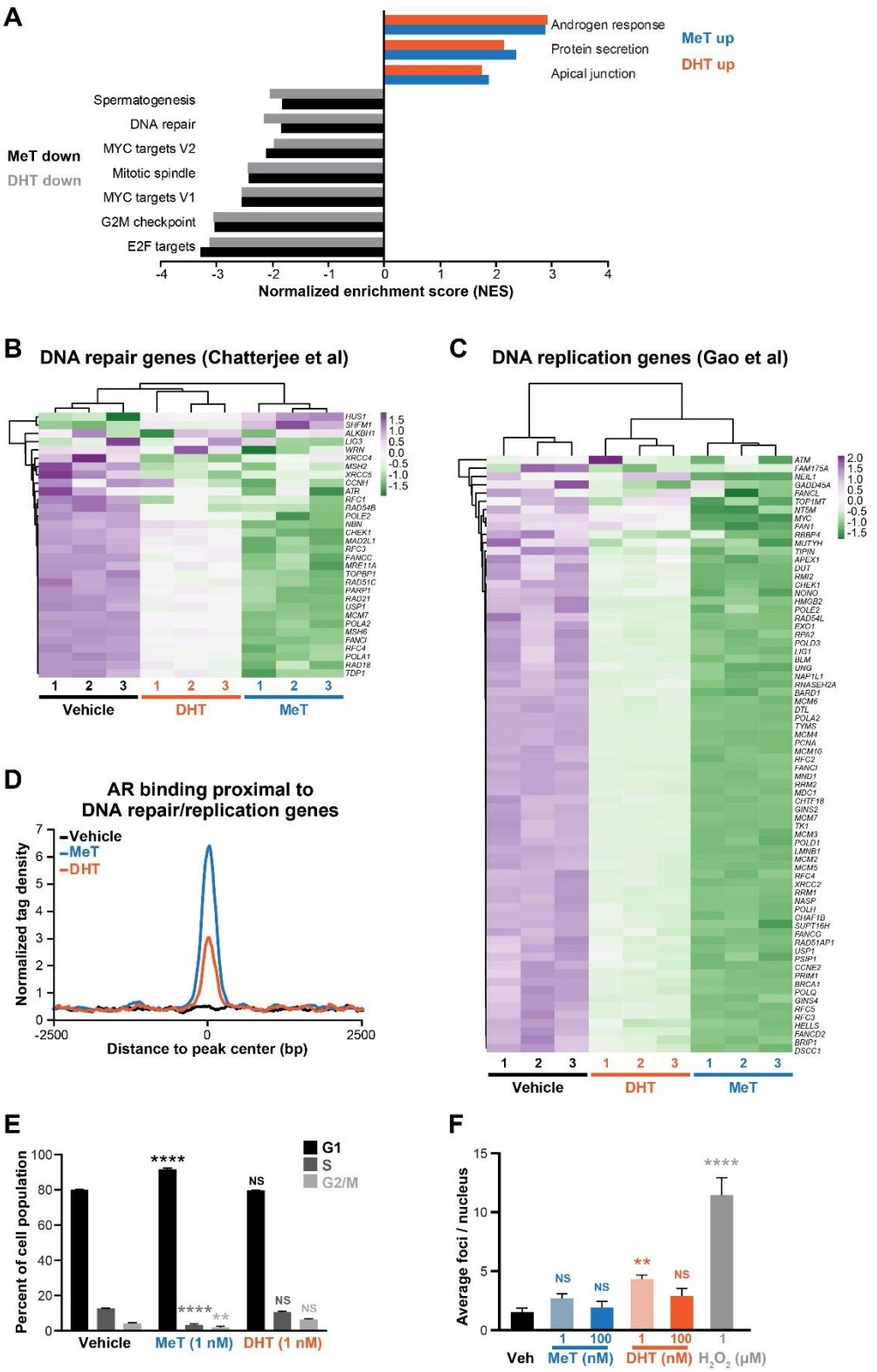
A
Androgen response
Protein secretion
Apical junction
MeT up
DHT up
Spermatogenesis
DNA repair
MYC targets V2
Mitotic spindle
MYC targets V1
G2M checkpoint
E2F targets
MeT down
DHT down
-4 -3 -2 -1 0 1 2 3 4
Normalized enrichment score (NES)
B
DNA repair genes (Chatterjee et al)
1 2 3 1 2 3 1 2 3
Vehicle
DHT
MeT
C
DNA replication genes (Gao et al)
1 2 3 1 2 3 1 2 3
Vehicle
DHT
MeT
D
AR binding proximal to
DNA repair/replication genes
Vehicle
MeT
DHT
Normalized tag density
-2500 0 2500
Distance to peak center (bp)
E
G1
S
G2/M
Percent of cell population
****
NS
****
**
NS
NS
Vehicle
MeT (1 nM)
DHT (1 nM)
F
Average foci / nucleus
****
NS
NS
**
NS
1 100 1 100 1
Veh
MeT (nM)
DHT (nM)
H2O2 (μM)

Fig. 2. DNA replication and repair pathways are repressed by potent androgenic stimulation of prostate cancer cells. (A) Normalized enrichment scores (NES) for top-ranked Hallmark gene sets (Liberzon, Birger et al. 2015) representing RNA-seq data from LNCaP cells treated with 1 nM MeT for 24 hours. **(B-C)** Heatmap of RNA-seq data for androgen-regulated genes associated with DNA repair (Chatterjee, Schweizer et al. 2019) and DNA replication (Gao, Gao et al. 2016) in LNCaP cells treated with 1 nM MeT or 1 nM DHT for 24 hours. Heatmaps were generated using ClustVis (Metsalu and Vilo 2015) after applying unit variance scaling to each gene. (**D**) Average read density plots for AR chromatin binding proximal (<100 kb) to DNA repair/replication genes in LNCaP cells treated with 1 nM MeT or 1 nM DHT for 4 hours. (**E**) Cell cycle analysis by DAPI labelling and flow cytometry after 72 hours of treatment with 1 nM MeT or 1 nM DHT. Unpaired t tests were used to compare data at different cell cycle phases (i.e. G1, S and G2/M) between treatment groups (**, $p < 0.01$; ****, $p < 0.0001$). **(F)** Assessment of DNA double-strand breaks after potent androgen treatments. γH2AX foci were quantitated in LNCaP cells 6 hours after treatment with MeT, DHT or a positive control (H_2O_2). Error bars are SEM. P values (day 7) were determined using ANOVA and Dunnett's multiple comparisons tests (*, $p < 0.05$; **, $p < 0.01$; ***, $p < 0.001$; ****, $p < 0.0001$). NS, not significant.

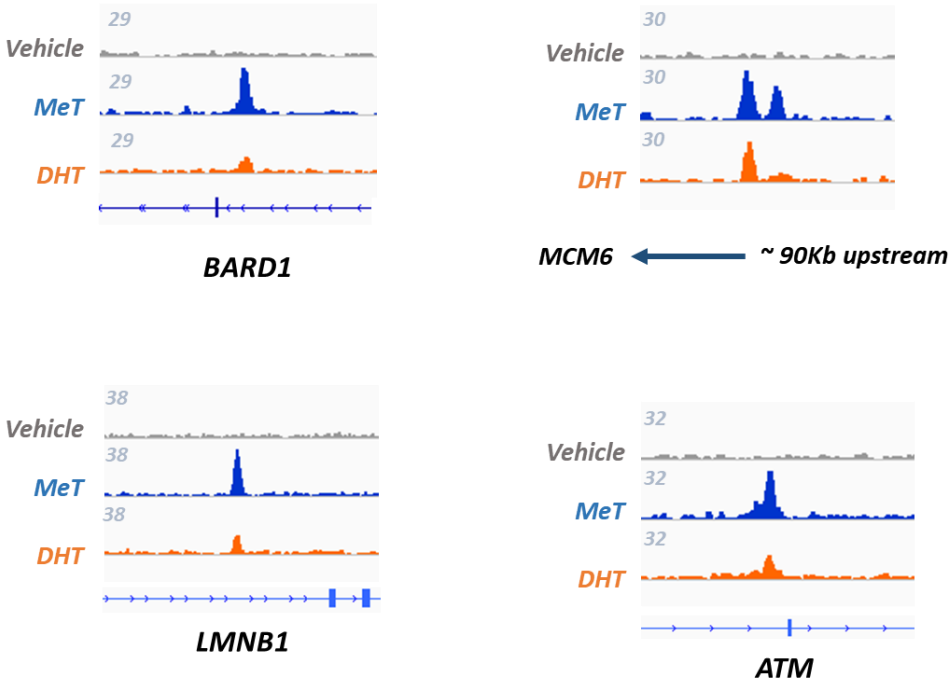

Supplementary Fig 2. **Androgen treatments mediates AR binding to genes involved in DNA replication andrepair.** Genome browser images showing AR ChIP-seq signals at binding sites associated with *BARD1*, *MCM6*, *LNMB1* and *ATM* in LNCaP cells treated with Vehicle, 1 nM MeT or 1 nM DHT for 4 hours.

Methyl-testosterone causes DNA hypomethylation in prostate cancer cells

AR has a major role in regulating the epigenome via interplay with and transcriptional regulation of chromatin remodelling factors (Cai, Yuan et al. 2013), although little is known about how these mechanisms are altered in the context of high-dose androgen treatment. Our RNA-seq data revealed that MeT strongly down-regulated the DNA methyltransferases *DNMT1* and *DNMT3b* in LNCaP cells (Fig. 3A), which we validated by qRT-PCR (Fig. 3B) and Western blotting (Fig. 3C and Supplementary Fig. 3). Gene signatures of response to DNMT inhibitors (Missiaglia, Donadelli et al. 2005, Kim, Zhong et al. 2006) were altered by MeT (Fig. 3D), suggesting that DNA hypomethylation and subsequent effects on transcription were occurring downstream of DNMT down-regulation. To directly test this idea, we assayed for 5-Methylcytosine at long interspersed nuclear elements (LINEs), a proxy for global DNA methylation. In support of our expression profiling data, a decrease in global DNA methylation levels was observed in response to MeT and, to a lesser extent, DHT (Fig. 3E).

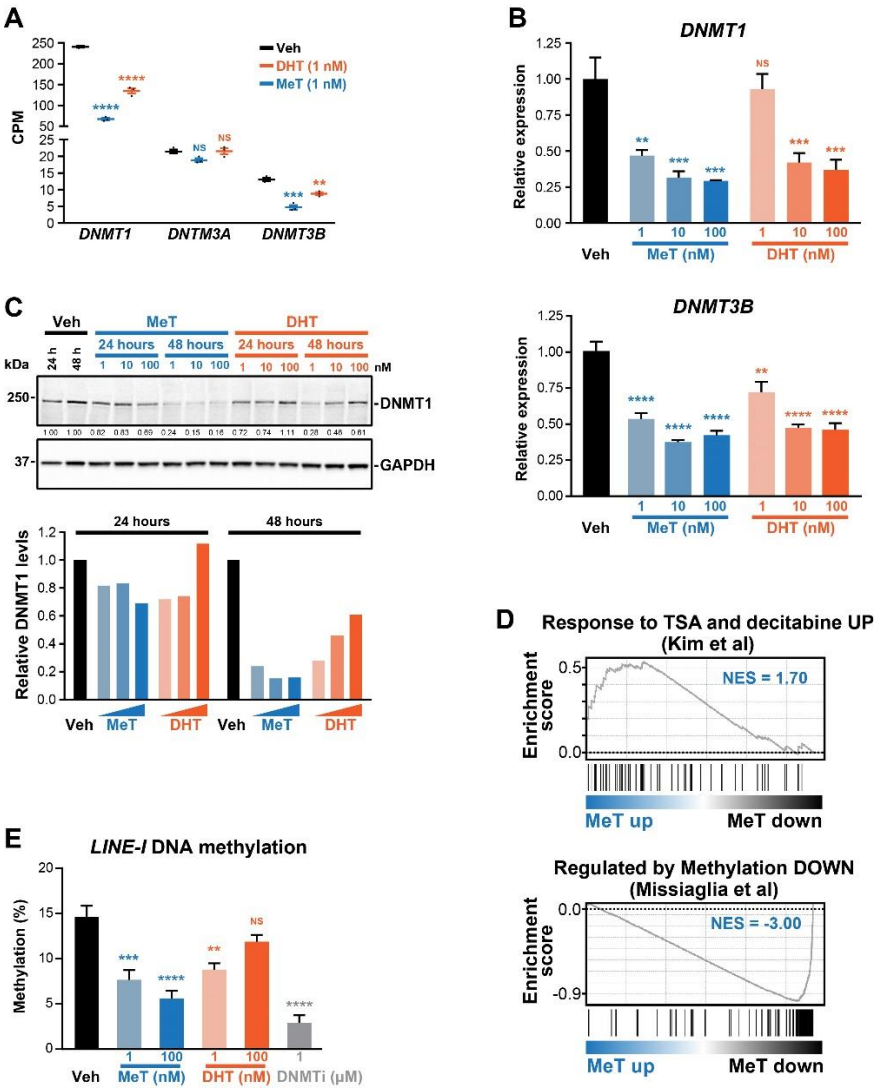
A
CPM
Veh
DHT (1 nM)
MeT (1 nM)
DNMT1
DNTM3A
DNMT3B
B
DNMT1
Relative expression
Veh
MeT (nM)
DHT (nM)
DNMT3B
C
Veh
MeT
DHT
24 hours
48 hours
kDa
nM
DNMT1
GAPDH
Relative DNMT1 levls
D
Response to TSA and decitabine UP
(Kim et al)
Enrichment score
NES = 1.70
MeT up
MeT down
Regulated by Methylation DOWN
(Missiaglia et al)
NES = -3.00
E
LINE-I DNA methylation
Methylation (%)
DNMTi (μM)

Fig. 3. Methyl-testosterone down-regulates DNA methyltransferases and causes DNA hypomethylation. (A) Expression of *DNMT1*, *DNTM3A* and *DNMT3B*, as determined by RNA-seq, of LNCaP cells following 24 hours of treatment with MeT or DHT (1 nM each) or a vehicle control. CPM, counts per million reads. Middle line, mean; above and below, ± SEM. P values (treatment compared to vehicle) were determined using ANOVA and Dunnett's multiple comparisons tests (*, $p < 0.05$; **, $p < 0.01$; ***, $p < 0.001$; ****, $p < 0.0001$). **(B)** Expression of *DNMT1* (top) and *DNMT3B* (bottom), as determined by qRT-PCR, following 24 hours of treatment with MeT or DHT (1 nM each) or a vehicle control. Gene expression was normalized to *GAPDH*; expression for Vehicle was set to 1. Error bars are SEM; P values (treatment compared to vehicle) were determined using ANOVA and Dunnett's multiple comparisons tests (*, $p < 0.05$; **, $p < 0.01$; ***, $p < 0.001$; ****, $p < 0.0001$). **(C)** Representative Western blot showing DNMT1 protein levels following treatment of LNCaP cells with the indicated doses of MeT or DHT or vehicle control for 24 and 48 hours. GAPDH is shown as a loading control; each sample was pooled from two replicates. Quantification of DNMT1 protein (normalised to GAPDH) is shown on right. **(D)** Association between MeT-induced genes and a gene set upregulated by TSA and Decitabine (left) (Kim, Zhong et al. 2006) and between MeT-repressed genes and a set of genes downregulated following treatment with Decitabine (Missiaglia, Donadelli et al. 2005), as demonstrated by GSEA. NES, normalised enrichment score. **(E)** Global DNA methylation (5 mC; % methylation of *LINE-I* elements) in LNCaP cells treated with indicated doses of MeT or DHT for 6 days. Decitabine (1 µM) was used as a positive control. P values (treatment compared to vehicle) were determined using ANOVA and Dunnett's multiple comparisons tests (*, $p < 0.05$; **, $p < 0.01$; ***, $p < 0.001$; ****, $p < 0.0001$).

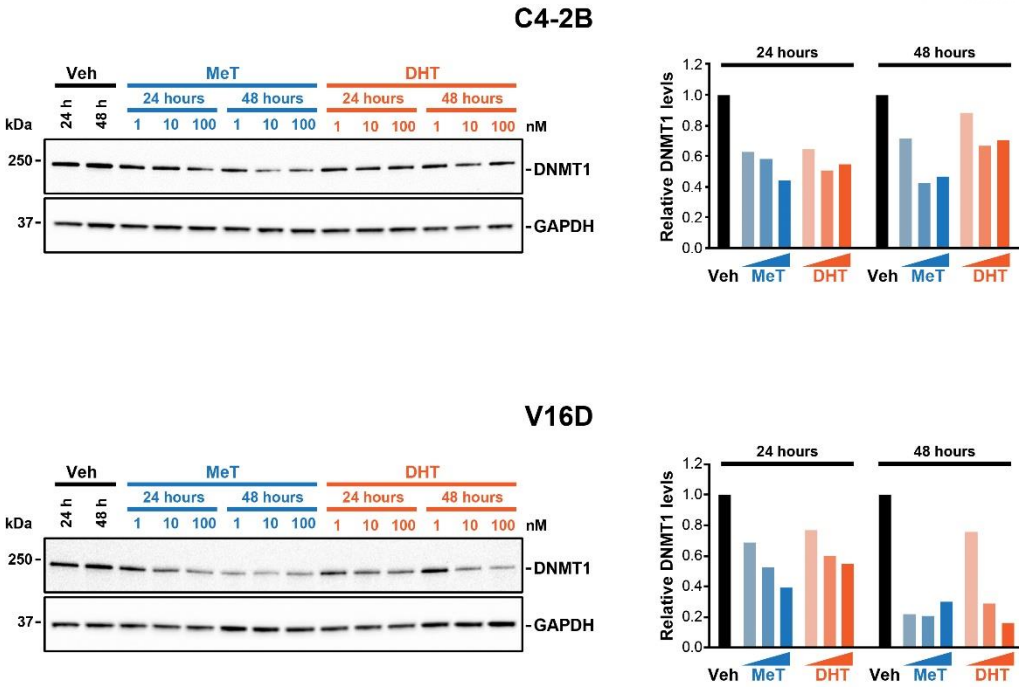

Supplementary Fig. 3. Methyl-testosterone down-regulates DNMT1. Western blots showing DNMT1 protein levels following treatment of C4-2B (top) and V16D (bottom) cells with the indicated doses of MeT or DHT or vehicle control for 24 and 48 hours; each sample was pooled from two replicates. GAPDH is shown as a loading control. Quantification of DNMT1 protein (normalised to GAPDH) is shown on right.

Methyl-testosterone induces transcription of transposable elements and causes accumulation of dsRNA

The transcription of transposable elements (TEs), which constitute ~45% of the human genome (Criscione, Zhang et al. 2014) and are comprised of distinct families including endogenous retroviruses (ERVs), LINEs and Short Interspersed Nuclear Elements (SINEs), is heavily influenced by DNA methylation (Reik 2007). Thus, we hypothesised that loss of DNA methylation in response to MeT could lead to altered TE expression. To test this hypothesis, we first interrogated levels of different TE classes within the ERV/LINE/SINE families in our short-term (24 hour) RNA-seq data. Similar to our analyses of the coding transcriptome, MeT caused substantial changes to expression of TEs whereas DHT had a less pronounced effect (Fig. 4A).

Having established that potent androgen treatment could alter the expression of TEs in 24 hours, we measured specific transcripts after 3-6 days of treatment, based on the earlier observation that loss of DNA methylation occurred over an equivalent period (Fig. 3E). We initially focussed our attention on LINEs, since these elements were specifically evaluated in the DNA methylation assays. *LINE-I* was weakly induced by MeT after 6 days of treatment, but its expression was not altered by DHT treatment (Supplementary Fig. 4A), a finding that was recapitulated in the CRPC cell line C4-2B (Supplementary Fig. 4B). Subsequently, we measured the expression of the major family members of ERVs, since these sequences of viral origin are known to influence various biological processes in cancer cells, including innate immune responses (Bannert, Hofmann et al. 2018). MeT induced *ERV3-1* and *HERV-K* transcripts in LNCaP cells (Fig. 4B); *HERV-E* and *HERV-W* were not significantly altered but exhibited a trend

towards upregulation (Supplementary Fig. 4C). Analogous results – significant induction of *ERV3-1* and *HERV-K* but not *HERV-E* or *HERV-W* – were observed in the C4-2B model, suggesting this is a general response of PCa cells to MeT (Fig. 4C, Supplementary Fig. 4D). As for protein-coding transcripts, equivalent doses of DHT caused similar qualitative changes to LINE/ERV expression but quantitatively weaker effects (Figs. 4B-C, Supplementary Fig. 4). Collectively, these findings demonstrate that the potent synthetic androgen MeT can induce expression of transposable elements, including ERVs, in a context-dependent manner in PCa cells.

Expression of some ERVs occurs bi-directionally and can thereby result in generation of dsRNA (Chiappinelli, Strissel et al. 2015). Since potent androgen treatment led to increased levels of the major classes of ERVs over a period of 3-6 days, we speculated that this could cause accumulation of dsRNA. Using an immunofluorescent approach with a dsRNA-specific antibody (J2), we found that MeT treatment elicited a profound increase in the level of cellular dsRNA (Fig. 4D). Indeed, 1 nM MeT resulted in more detectable dsRNA than 100 nM DHT and 1 µM of Decitabine, a DNMT inhibitor (DNMTi) previously reported to induce dsRNA in other cancer cell types (Chiappinelli, Strissel et al. 2015, Roulois, Loo Yau et al. 2015, Topper, Vaz et al. 2017) (Fig. 4D). Collectively, these findings reveal that potent androgenic stimulation of PCa cells leads to dysregulation of TE transcription that is associated with accumulation of ERV transcripts and dsRNA.

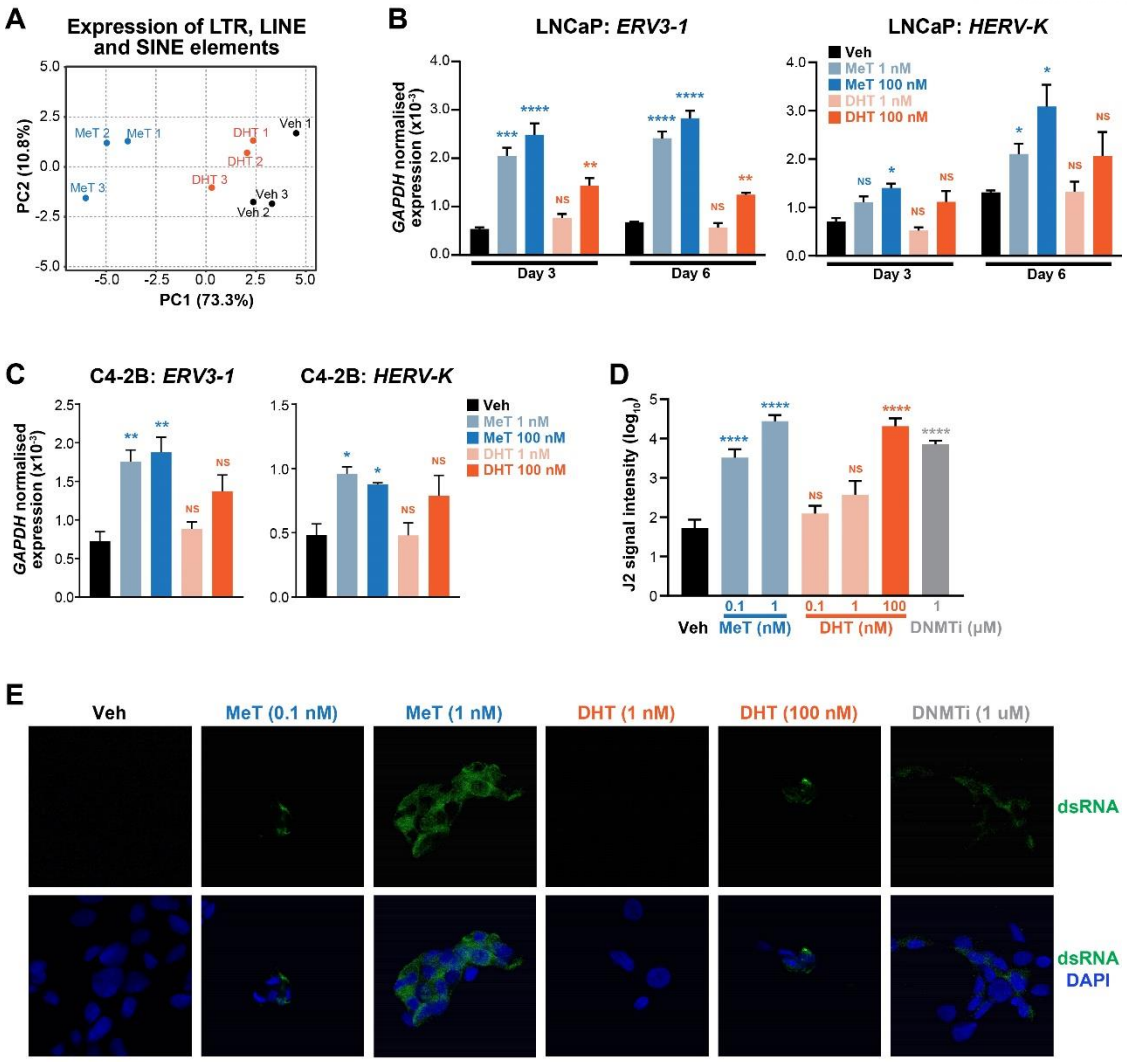

Fig. 4. Induction of transposable element expression by methyl-testosterone is associated with production of dsRNA. (A) Principal component analysis (PCA) of transposable element expression (long terminal repeats, LINE and SINE elements) from RNA-seq data following treatment of LNCaP cells with MeT or DHT (1 nM each) for 24 hours. The plot was generated using ClustVis (Metsalu and Vilo 2015) after applying unit variance scaling to each element. **(B)** Expression of *ERV3-1* and *HERV-K*, as determined by qRT-PCR, following 3 or 6 days of treatment with MeT or DHT (1 nM each) or a vehicle control. Expression of ERVs was normalized to *GAPDH*. Error bars are SEM; P values (treatment compared to vehicle) were determined using ANOVA and Dunnett's multiple comparisons tests (*, $p < 0.05$; **, $p < 0.01$; ***, $p < 0.001$; ****, $p < 0.0001$). **(C)** Expression of ERV3-1 and HERV-K, as determined by qRT-PCR, following 3 days of treatment with MeT or DHT (1 nM each) or a vehicle control. Expression of ERVs was normalized to *GAPDH*. Error bars are SEM; statistical testing was as in (B). **(D)** Quantitation of cellular dsRNA by immunofluorescent staining with J2 monoclonal antibody following 72 hours of treatment with MeT, DHT or a DNMT inhibitor (DNMTi), Decitabine. Error bars are SEM; P values (treatment compared to vehicle) were determined using ANOVA and Dunnett's multiple comparisons tests (****, $p < 0.0001$). **(E)** Representative images of J2 immunofluorescence. J2 signal, representing cellular dsRNA, is in green. Nuclei were counterstained with DAPI (blue).

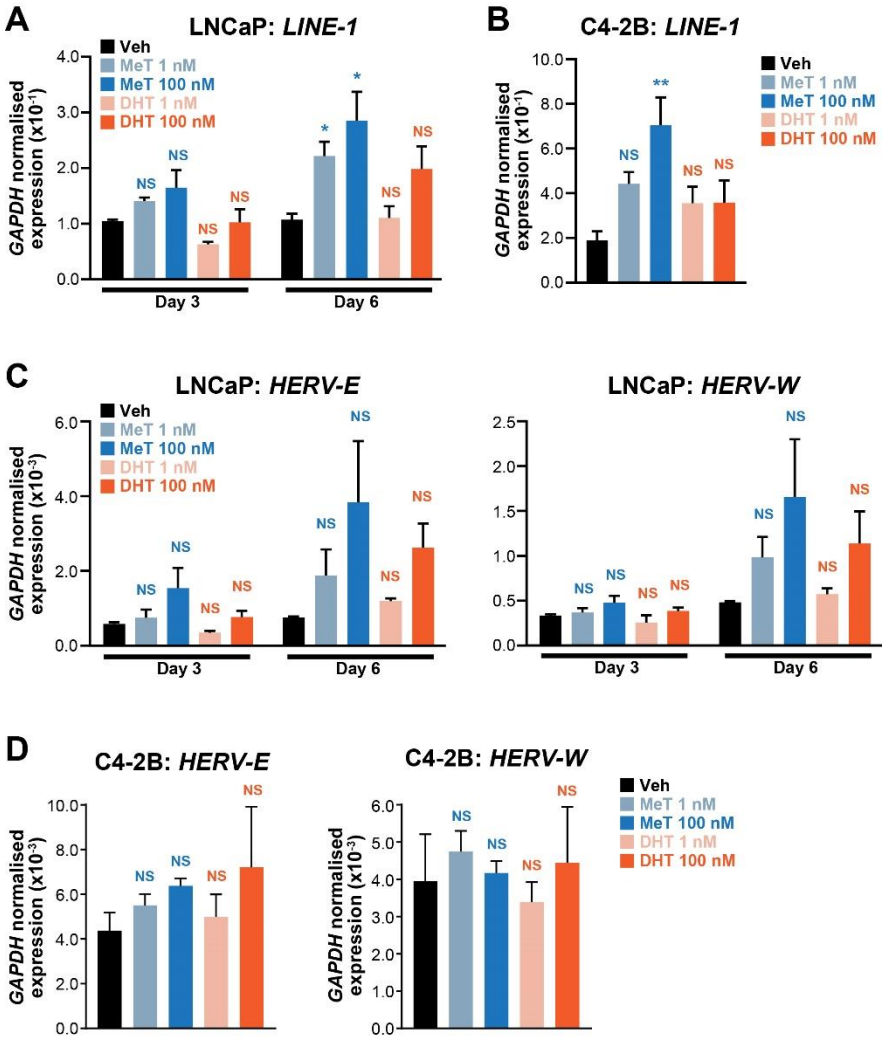

Supplementary Fig. 4. Induction of transposable element expression by methyl-testosterone. (A-B) Expression of *LINE-I*, as determined by qRT-PCR, following treatment with MeT or DHT in LNCaP (A) and C4-2B (B) cells. Expression of *LINE-I* was normalized to *GAPDH*. Error bars are SEM; P values (treatment compared to vehicle) were determined using ANOVA and Dunnett's multiple comparisons tests (*, $p < 0.05$; **, $p < 0.01$). **(C)** Expression of HERV-E and HERV-W, as determined by qRT-PCR, following treatment with MeT or DHT in LNCaP cells. Expression of ERVs was normalized to *GAPDH*. Error bars are SEM; significance (treatment compared to vehicle) was determined using ANOVA and Dunnett's multiple comparisons tests. **(D)** Expression of HERV-E and HERV-W, as determined by qRT-PCR, following treatment with MeT or DHT in C4-2B cells. Expression of ERVs was normalized to *GAPDH*. Error bars are SEM; significance (treatment compared to vehicle) was determined using ANOVA and Dunnett's multiple comparisons tests.

Methyl-testosterone activates interferon signalling

Induction of ERV transcription and accumulation of dsRNA can activate cellular responses similar to those elicited by infection with an exogenous virus, a phenomenon termed "viral mimicry" (Bannert, Hofmann et al. 2018). Given the ability of MeT to modulate ERV transcription and induce dsRNA, we speculated that it could cause a viral mimicry response. To test this hypothesis, we first measured mRNA levels of the cytosolic pattern recognition receptor (PRR) RIG-I (encoded by the *DDX58* gene), which is a major sensor of dsRNA produced during viral infection. We observed induction of *RIG-I* in response to MeT and, to a lesser extent, DHT (Fig. 5A), which was confirmed by Western blotting (Fig. 5B). Another PRR involved in antiviral responses, STING, is best known for its role in sensing of cytosolic DNA but also serves as a detector of RNA viruses and can interact with RIG-I (Ni, Ma et al. 2018): similarly to RIG-I, STING was strongly upregulated by MeT in PCa cells (Fig. 5C). Downstream of PRRs, the mitochondrial antiviral signalling protein (MAVS) and TANK Binding Kinase 1 (TBK-1) are required to activate innate immune anti-viral responses (Sun, Sun et al. 2006). As expected, MeT treatment increased the levels of *MAVS* mRNA and phosphorylated (active) TBK-1; DHT again caused analogous but blunted responses (Figs. 5C-D). Sensing of dsRNA by PRRs leads to activation of Type I IFN signalling (Gonzalez-Cao, Karachaliou et al. 2018). MeT treatment caused induction of IFN-β (encoded by *IFNB1*) as well as *IRF3* and *IRF7*, transcription factors that can activate IFN expression (Fig. 5E). Upregulation of IFN signalling by MeT was also observed in an independent cell line model, C4-2B (Supplementary Fig. 5). Collectively, these findings reveal that MeT activates an anti-viral response, likely due to its ability to increase cellular levels of dsRNA.

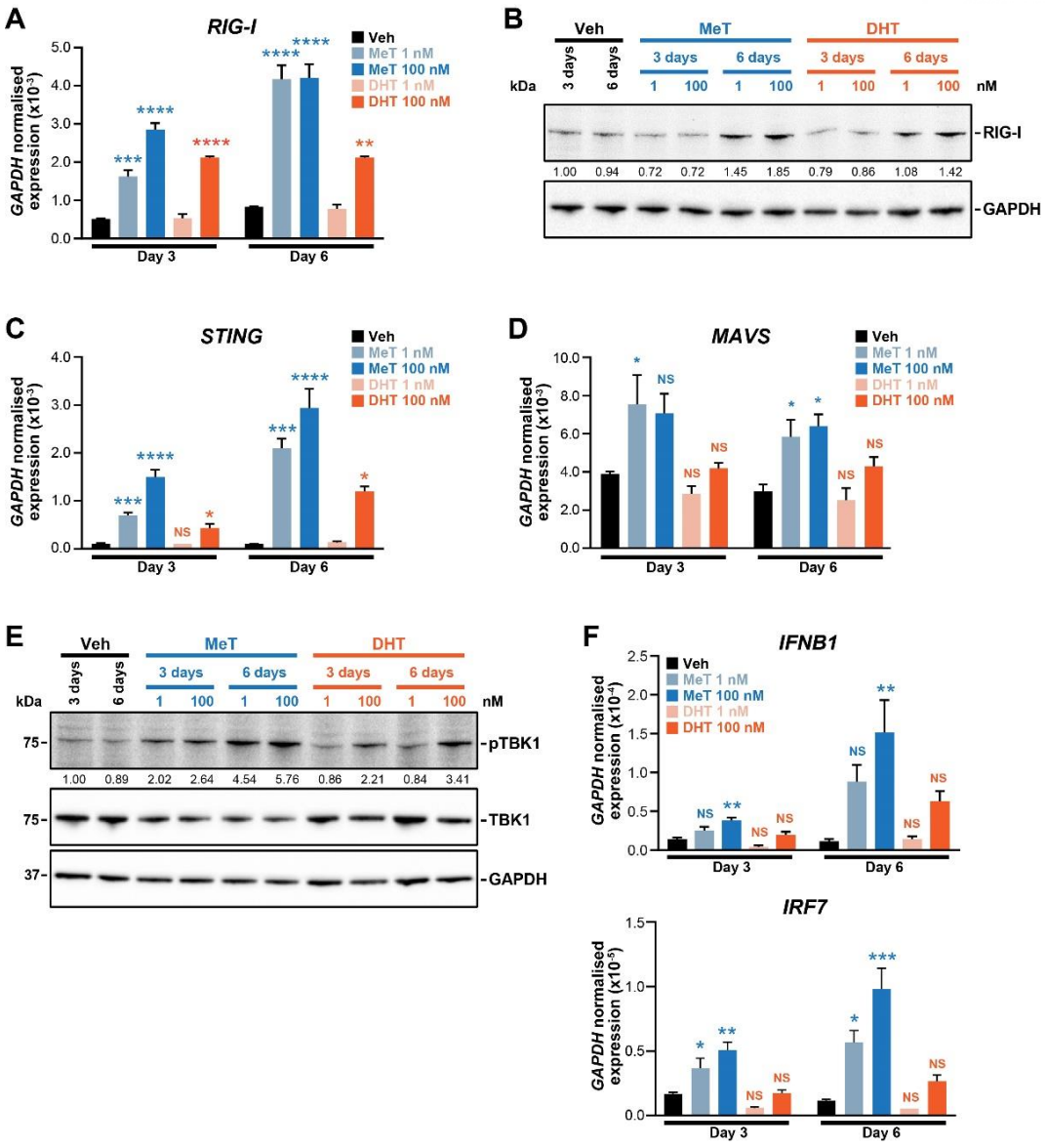
A
RIG-I
GAPDH normalised expression (x10⁻³)
Veh
MeT 1 nM
MeT 100 nM
DHT 1 nM
DHT 100 nM
Day 3
Day 6
B
Veh
MeT
DHT
3 days
6 days
kDa
nM
RIG-I
GAPDH
1.00 0.94 0.72 0.72 1.45 1.85 0.79 0.86 1.08 1.42
C
STING
D
MAVS
E
pTBK1
TBK1
GAPDH
1.00 0.89 2.02 2.64 4.54 5.76 0.86 2.21 0.84 3.41
F
IFNB1
GAPDH normalised expression (x10⁻⁴)
IRF7
GAPDH normalised expression (x10⁻⁵)

Fig. 5. Methyl-testosterone activates an interferon-mediated anti-viral response. (A) Expression of *RIG-I* as determined by qRT-PCR following 3 or 6 days of treatment with the indicated doses of MeT or DHT or a vehicle control. Gene expression was normalized to *GAPDH*. Error bars are SEM; P values (treatment compared to vehicle at each time-point) were determined using ANOVA and Dunnett's multiple comparisons tests (**, $p < 0.01$; ***, $p < 0.001$; ****, $p < 0.0001$). **(B)** Western blot showing RIG-I protein levels following treatment of LNCaP cells with the indicated doses of MeT or DHT or vehicle control for 3 or 6 days. GAPDH is shown as a loading control. **(C)** Expression of *STING* as determined by qRT-PCR following 3 or 6 days of treatment with the indicated doses of MeT or DHT or a vehicle control. Gene expression was normalized to *GAPDH*. Error bars are SEM. Statistical analysis was as for (A) (***, $p < 0.001$; ****, $p < 0.0001$). **(D)** Expression of MAVS as determined by qRT-PCR following 3 or 6 days of treatment with the indicated doses of MeT or DHT or a vehicle control. Gene expression was normalized to *GAPDH*. Error bars are SEM. Statistical analysis was as for (A) (*, $p < 0.05$). **(E)** Western blot showing levels of total and phosphorylated TBK1 following treatment of C4-2B cells with the indicated doses of MeT or DHT or vehicle control for 3 or 6 days. GAPDH is shown as a loading control. **(F)** Expression of *IFNβ* and *IRF7* as determined by qRT-PCR following 3 or 6 days of treatment with the indicated doses of MeT or DHT or a vehicle control. Gene expression was normalized to *GAPDH*. Error bars are SEM. Statistical analysis was as for (A) (*, $p < 0.05$; **, $p < 0.01$; ***, $p < 0.001$; ****, $p < 0.0001$).

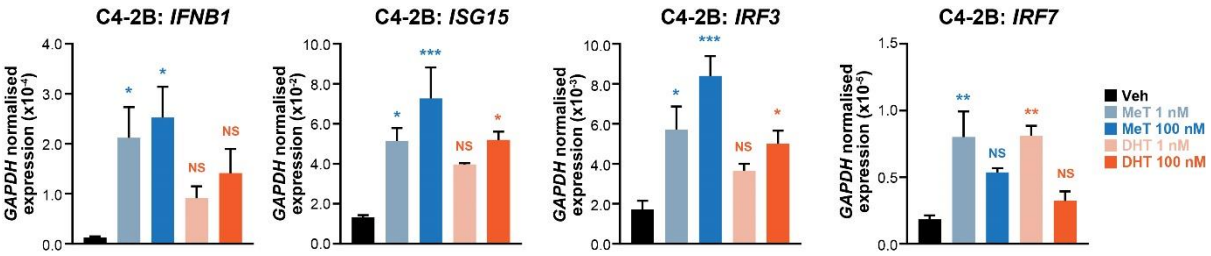

Supplementary Fig. 5. Induction of IFN signalling by methyl-testosterone in C4-2B cells. Expression of IFNβ (encoded by *IFNB1*), *ISG15*, *IRF3* and *IRF7*, as determined by qRT-PCR, following treatment with MeT or DHT in C4-2B cells. Expression of genes was normalized to *GAPDH*. Error bars are SEM; P values (treatment compared to vehicle) were determined using ANOVA and Dunnett's multiple comparisons tests (*, $p < 0.05$; **, $p < 0.01$; ***, $p < 0.001$).

Association between AR activity and anti-viral responses in clinical prostate cancer

Our mechanistic investigations using PCa cell lines suggested that high AR activity could activate a viral mimicry response involving IFN signalling. To gain evidence for this concept in a more clinically-relevant setting, we analysed large transcriptomic datasets from patients with primary prostate cancer (TCGA) and metastatic CRPC (SU2C). Supporting our pre-clinical mechanistic work, we found a significant correlation between AR activity and Reactome's "antiviral mechanism by IFN-stimulated genes" gene set (Fig. 6A). Moreover, by exploiting a study in which ERVs were quantitated in TCGA samples (Rooney, Shukla et al. 2015), we discovered a strong positive correlation between AR activity and the expression of ERVs in the ERV3-1 and HERV-K classes (Fig. 6B). No association between AR signalling and HERV-E ($r = 0.079$, $p = 0.30$) or HERV-W ($r = -0.047$, $p = 0.54$) classes was observed, corroborating our earlier findings that these classes of ERVs were not robustly induced by high dose androgen treatment (Supplementary Fig. 4).

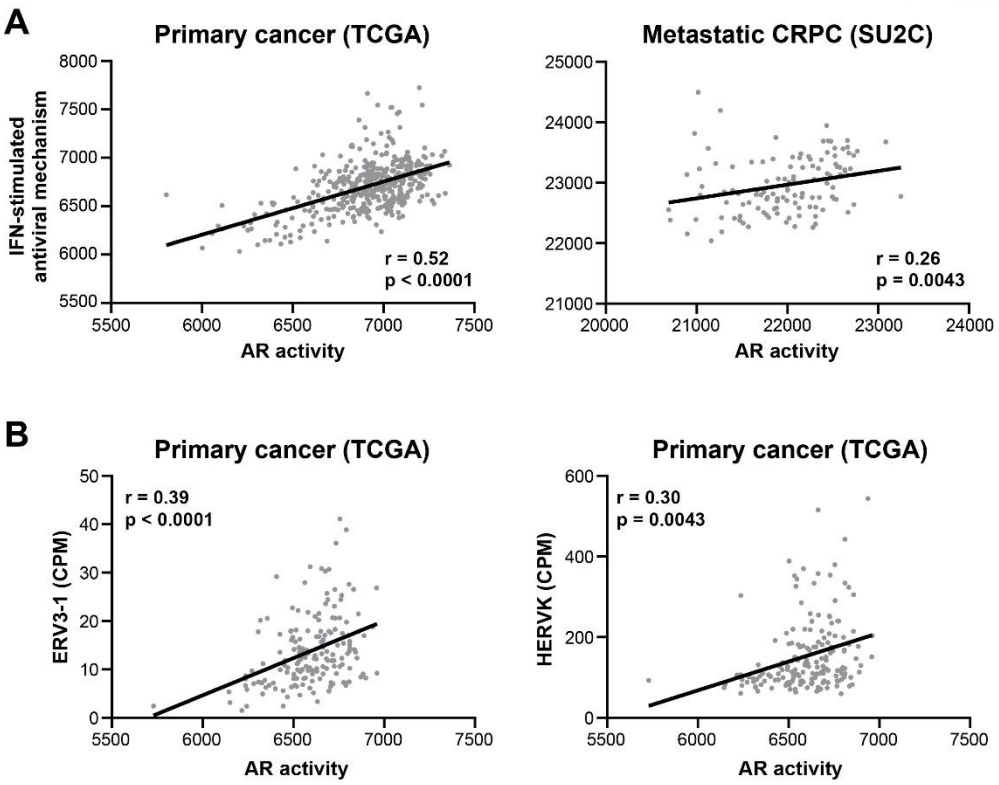

Fig. 6. Positive association between AR signalling and anti-viral responses in patient tumours. (A) AR activity, based on a 267-gene signature (Sowalsky, Ye et al. 2018), is associated with the Reactome "antiviral mechanism by IFN-stimulated genes" gene set in the TCGA (left) and SU2C (right) datasets. Activity scores were calculated using ssGSEA. P and r values were determined using Pearson's correlation tests. **(B)** AR activity is associated with the levels of ERV3-1 (left) and HERVK in the TCGA dataset. AR activity scores were calculated using ssGSEA. Counts per million (CPM) reads for ERV3-1 and HERVK (sum of all HERVK transcripts) were obtained from a published study (Rooney, Shukla et al. 2015). P and r values were determined using Pearson's correlation tests.

Methyl-testosterone can enhance the interaction between prostate cancer cells and T cells

IFN-mediated anti-viral defense signalling is associated with increased immunogenicity of solid tumours and improved responses to immune checkpoint therapy (Chiappinelli, Strissel et al. 2015, Stone, Chiappinelli et al. 2017, Topper, Vaz et al. 2017, Sheng, LaFleur et al. 2018, Morel, Sheahan et al. 2021). Indeed, we found that MeT treatment caused increased expression of MHC class I antigen processing and presentation genes over a period of 3-6 days (Fig. 7A). Moreover, AR activity was positively correlated with Class I (but not Class II: $r = 0.003$ and $p = 0.96$ for TCGA; $r = 0.174$ and $p = 0.06$ for SU2C) MHC-mediated antigen processing and presentation in the TCGA and SU2C cohorts (Fig. 7B).

To determine whether type I IFN-driven modulation of immune signalling in PCa in response to MeT influences T cell function, we utilised the murine RM1 model of CRPC (Owen, Gearing et al. 2020). We first confirmed that RM1 cells expressed AR (Fig. 7C) and were growth-inhibited by MeT/DHT (Fig. 7D, Supplementary Fig. 6A), which collectively highlight the suitability of this model as a tool to understand the impact of high dose androgens on PCa biology. Mirroring the findings from human PCa cell lines, MeT increased expression of ERVs (murine *ERV-L*, *MTA*, *RLTR1B* and *RLTR45*), *LINE-I* elements, *Rig-I* and *Irf7* in RM1 cells (Fig. 7E). Despite DHT having equivalent growth-suppressive effects, it did not influence the expression of transposable elements, *Rig-I* or interferon pathway genes (Supplementary Fig. 6B). We next used an *ex vivo* co-culture system to assess whether viral mimicry induced by MeT could lead to T cell activation. Whilst DHT-treatment had no effect on T cell response, MeT-treatment of RM1 cells increased the immunogenicity of RM1 cells, resulting in enhanced $CD8^+$ T cell recognition and functional cytokine production (Fig. 7F).

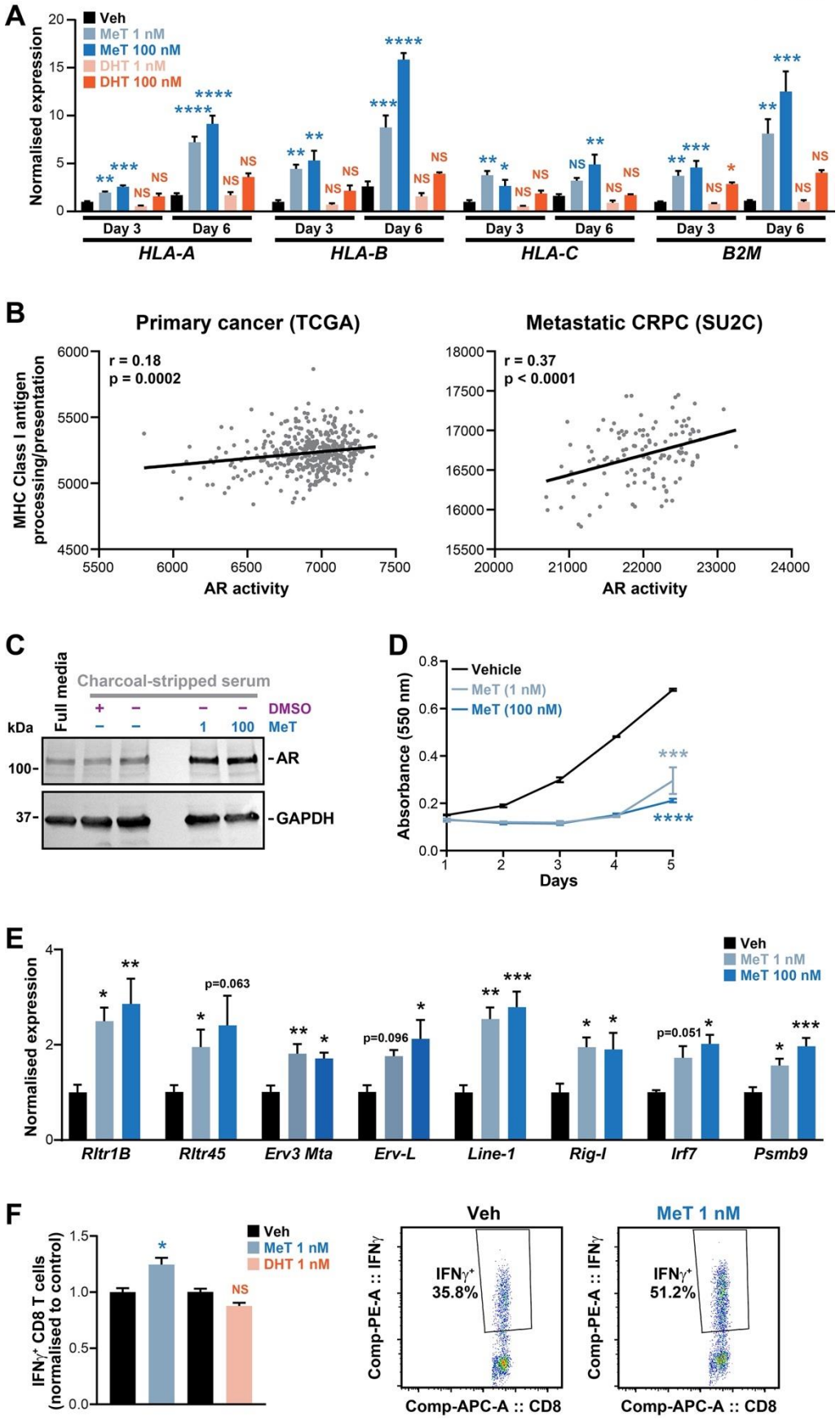
A
Veh
MeT 1 nM
MeT 100 nM
DHT 1 nM
DHT 100 nM
Normalised expression
Day 3
Day 6
HLA-A
HLA-B
HLA-C
B2M
B
Primary cancer (TCGA)
Metastatic CRPC (SU2C)
r = 0.18
p = 0.0002
r = 0.37
p < 0.0001
MHC Class I antigen processing/presentation
AR activity
C
Full media
Charcoal-stripped serum
DMSO
MeT
kDa
100-
37-
AR
GAPDH
D
Vehicle
MeT (1 nM)
MeT (100 nM)
Absorbance (550 nm)
Days
E
Normalised expression
Rltr1B
Rltr45
Erv3 Mta
Erv-L
Line-1
Rig-I
Irf7
Psmb9
p=0.063
p=0.096
p=0.051
F
IFNγ+ CD8 T cells (normalised to control)
DHT 1 nM
Veh
MeT 1 nM
IFNγ+ 35.8%
IFNγ+ 51.2%
Comp-PE-A :: IFNγ
Comp-APC-A :: CD8

Fig. 7. Methyl-testosterone elicits viral mimicry and enhances interferon-γ (IFN-γ) expression in T cells in a mouse model of prostate cancer. (A) Expression of *HLA* genes and *B2M* as determined by qRT-PCR following 3 or 6 days of treatment with the indicated doses of MeT or DHT or a vehicle control. Gene expression was normalized to *GAPDH*. Error bars are SEM; P values (treatment compared to vehicle at each time-point) were determined using ANOVA and Dunnett's multiple comparisons tests (*, $p < 0.05$; **, $p < 0.01$; ***, $p < 0.001$; ****, $p < 0.0001$). **(B)** AR activity is associated with the Reactome "Class I MHC-mediated antigen processing and presentation" gene set in the TCGA (left) and SU2C (right) datasets. Activity scores were calculated using ssGSEA. P and r values were determined using Pearson's correlation tests. **(C)** Western blot showing AR protein expression in RM1 cells following treatment with the indicated doses of MeT or vehicle control (in both full and charcoal-stripped media). GAPDH is shown as a loading control. **(D)** MeT suppresses the growth of RM1 cells, as determined by Sulforhodamine B colorimetric assay mean absorbance (550 nm) is shown at the indicated time-points; error bars are ± SEM. P values were determined using unpaired t tests at day 5 (***, $p < 0.001$; ****, $p < 0.0001$). **(E)** Expression of ERVs (*Rltr1B*, *Rltr45, Erv-L, Erv3 Mta*), *LINE-I*, *RIG-I IRF7* and *ISG15* in RM1 cells as determined by qRT-PCR following 3 of treatment with the indicated doses of MeT. Gene expression was normalized to *Hprt.* Vehicle for each gene was set to 1. Error bars are SEM; P values (treatment compared to vehicle at each time-point) were determined using ANOVA and Dunnett's multiple comparisons tests (*, $p < 0.05$; **, $p < 0.01$; ***, $p < 0.001$; ****, $p < 0.0001$). **(F)** Intracellular cytokine staining (ICS) assay demonstrating IFN-γ^+ in $CD8^+$ following activation by RM1 cells treated with indicated doses of MeT or DHT for 3 days. Vehicle control for each AR ligand was set to 1. Error bars are SEM; P values (treatment compared to vehicle at each time-point) were determined using ANOVA and Dunnett's multiple comparisons tests (*, $p < 0.05$; **, $p < 0.01$; ***, $p < 0.001$; ****, $p < 0.0001$).

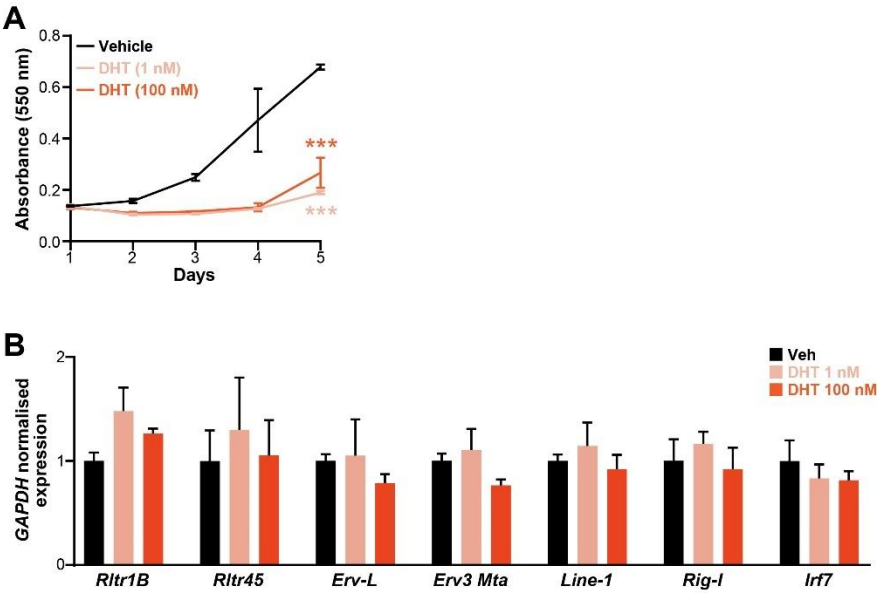

Supplementary Fig. 6. Effects of DHT on RM1 murine model of prostate cancer. (A) DHT suppresses the growth of RM1 cells, as determined by Sulforhodamine B colorimetric assay Mean absorbance (550 nm) is shown at the indicated time-points; error bars are ± SEM. P values were determined using unpaired t tests at day 5 (***, $p < 0.001$). **(B)** Expression of ERVs (*Rltr1B*, *Rltr45, Erv-L, Erv3 Mta*), *LINE-I*, *RIG-I IRF7* and *ISG15* in RM1 cells as determined by qRT-PCR following 3 of treatment with the indicated doses of MeT. Gene expression was normalized to *Hprt.* Vehicle for each gene was set to 1. Error bars are SEM; P values (treatment compared to vehicle at each time-point) were determined using ANOVA and Dunnett's multiple comparisons tests (no significant differences for any transcripts with either dose of DHT).

DISCUSSION

Although the mainstay treatment for advanced prostate cancer relies on suppression of AR activity, there is accumulating evidence that potent activation of AR by treating CRPC patients with high doses of testosterone can also be of therapeutic benefit. The molecular mechanisms underlying this apparent paradox remain to be fully elucidated. Here, by using a synthetic and highly potent androgen, MeT, we provide new insights into the consequences of hyper-activation of AR in PCa.

Molecular dissection of AR activity revealed that MeT elicits remarkably similar activity to DHT in terms of qualitative effects on the transcriptome and AR cistrome. Strikingly, however, MeT's effect on transcription was considerably stronger than DHT's for almost every AR-regulated gene and when evaluated by transcriptional activation assays using a synthetic androgen-responsive reporter gene, the latter observation being consistent with previous work (Wolf, Diel et al. 2011). The potency of MeT was manifested by robust regulation of DNA damage/repair and replication pathways and gene sets that are known to respond to high doses of T and DHT and have been purported to (at least partly) underpin growth suppression and cell death caused by high dose androgen treatment (Gao, Gao et al. 2016, Chatterjee, Schweizer et al. 2019, Nyquist, Corella et al. 2019). Interestingly, despite strong down-regulation of DNA repair genes, we did not observe increased staining of the DNA damage marker γH2AX in response to MeT. Increased DNA damage has been purported to be a mechanism by which high dose androgens cause cell death (Chatterjee, Schweizer et al. 2019), synergise with agents that inhibit DNA repair (Chatterjee, Schweizer et al. 2019) and elicit therapeutic responses in PDXs (Lam, Nguyen et al. 2020) or patients with defective

homology-directed repair (HDR) (Teply, Kachhap et al. 2017, Markowski, Shenderov et al. 2020). This concept has led to a prevailing belief that HDR gene defects could be useful predictive biomarkers of BAT (Chatterjee, Schweizer et al. 2019) and that combining BAT with DNA damaging therapies, such as radiotherapy (e.g. NCT04704505), is a rational therapeutic strategy. By contrast, other studies failed to detect heightened DNA damage in response to high doses of physiological or synthetic (i.e. R1881) androgens (Polkinghorn, Parker et al. 2013), and a recent analysis of BAT clinical trials failed to demonstrate improved progression-free survival in patients with HDR gene defects (Schweizer, Antonarakis et al. 2019). We propose that definitively establishing the relevance of DNA damage, as a mediator of therapeutic response to androgen therapies (including MeT) is imperative to maximise clinical impact. Interestingly, in our experiments low dose (1 nM) but not high dose (100 nM) DHT resulted in a significant increase in DNA damage. Since 1 nM DHT did not substantially impact on PCa cell proliferation, this also argues against DNA damage being important in androgen-mediated growth suppression.

In addition to its effects on DNA replication and repair pathways, our data revealed that MeT caused a major shift in the expression profile of TEs, including ERVs such as ERV3-1 and HERV-K. This occurred concomitantly with down-regulation of DNMT enzymes, including DNMT and DNMT3b, and loss of DNA methylation at LINE-I elements. Given the well-established role of DNA methylation is suppressing the expression (and mobility) of ERVs and other TEs (Reik 2007), we propose that inhibition of DNMTs is a key mechanism underlying our observation. A negative association between the expression/activity of AR and DNMTs has been reported previously (e.g. (Chu, Chang et al. 2014)), but the molecular underpinnings of this

phenomenon are not known. One plausible explanation is that hyper-active AR decreases DNMT expression via its interplay with Rb and E2F. More specifically, it has been reported that high dose androgen treatment leads to AR and Rb binding to, and transcriptionally repressing, a series of E2F-regulated genes involved in DNA replication (Gao, Gao et al. 2016), a finding that we recapitulated with MeT. Since DNMT1 is a well-established target of E2F (Kimura, Nakamura et al. 2003, McCabe, Davis et al. 2005), it is reasonable to expect that it would be down-regulated by AR-mediated perturbation of the Rb/E2F1 axis. Such a mechanism is reminiscent of an earlier study demonstrating that the CDK4/6 inhibitor abemaciclib reduces E2F activity and thereby decreases DNMT1 expression (Goel, DeCristo et al. 2017).

Upregulation of ERVs can result in accumulation of cellular dsRNA (Chiappinelli, Strissel et al. 2015), which is sensed by PRRs (i.e. RIG-I, STING) that signal via MAVS/TBK-1 to activate IFN signalling. We propose that this “viral mimicry” response is a key mechanism by which MeT activates IFN, although we cannot rule out the possibility that host lncRNAs and/or microRNAs induced by MeT play a role in RIG-I activation, as has been described recently (Rehwinkel and Gack 2020). Viral mimicry is thought to be an important mediator of tumour innate immunity in response to epigenetic therapies such as DNMT inhibitors, histone deacetylate inhibitors, CDK4/6 inhibitors and EZH2 inhibitors (Chiappinelli, Strissel et al. 2015, Roulois, Loo Yau et al. 2015, Goel, DeCristo et al. 2017, Krug, De Jay et al. 2019, Morel, Sheahan et al. 2021). In support of this, we demonstrated that MeT enhanced the immunogenicity of murine PCa cells leading to increased T cell responses in a co-culture system, providing *in vitro* evidence that a viral mimicry response induced by this androgen could modulate the tumour immune

microenvironment. A limitation of this experiment is that we only measured IFN-γ in T cells, and hence it is unknown whether the viral mimicry response induced by MeT leads to cancer cell killing by T-cells. We propose to test whether MeT leads to increased cytotoxic T cell mediate cancer cell killing using IncuCyte immune cell killing assays in co-culture condition (Cichocki, Bjordahl et al. 2020, Granger and Appledorn 2021).

PCa is recognised as an immunologically "cold" cancer type based on its tumour microenvironment (i.e. few infiltrating cytotoxic T cells and a predominance of immunosuppressive cells, such as regulatory T cells and M2 macrophages), low immunogenicity and down-regulation of MHC Class I antigen processing/presenting machinery in tumour cells (de Almeida, Fong et al. 2020). These characteristics likely explain the limited impact of immunotherapies in this disease to date (de Almeida, Fong et al. 2020). A cellular immunotherapy, Sipuleucel-T, is approved for men with mCRPC but only confers a survival benefit of ~4 months (Kantoff, Higano et al. 2010). Similarly, multiple trials of immune checkpoint inhibitors (ICIs) have failed to demonstrate overall survival benefits (de Almeida, Fong et al. 2020), although some patients have experienced extraordinary responses to this treatment strategy (Graff, Alumkal et al. 2016, Markowski, Shenderov et al. 2020). With this background in mind, there is considerable interest in developing combinatorial treatment strategies that would sensitize CRPC tumours to immunotherapy. Our study found that MeT enhanced expression of MHC Class I genes and increased T cell cytotoxicity, suggesting that this regulator of viral mimicry could increase tumour cell immunogenicity, which is critical to improve response to ICIs. In support of this concept, a recent study found that inhibition of EZH2 activated a dsRNA–STING–IFN stress response that increased intratumoral trafficking of

activated $CD8^+$ T cells and sensitized PCa cells to PD-1 checkpoint blockade (Morel, Sheahan et al. 2021). Moreover, there is evidence that both AR activation (i.e. BAT) and AR inhibition (i.e. Enzalutamide) could sensitize tumours to PD-1 inhibitors, albeit in very small studies (Graff, Alumkal et al. 2016, Markowski, Shenderov et al. 2020). Whether response to ICIs in patients previously treated with BAT is a result of viral mimicry is an enticing possibility that warrants further investigation, either using pre-clinical models and/or by molecular analysis of samples from patients being treated by BAT/ICI in ongoing clinical trials (e.g. COMBAT-CRPC, NCT03554317).

Immunological priming by BAT has been hypothesised to be a consequence of androgen-mediated DNA damage, which can be sensed by the dsDNA sensor protein cGAS that can in turn activate IFN signalling (Markowski, Shenderov et al. 2020). At least 2 lines from our study of evidence suggest that this hypothesis should be modified to consider dsRNA as an alternative trigger of IFN signalling. First, MeT (and to a lesser extent DHT) induced ERVs, RIG-I and MAVS and caused accumulation of dsRNA. Second, we did not observe increased DNA damage – using γH2AX as a molecular marker of DNA damage - in response to MeT or high-dose DHT (100 nM) in LNCaP cells. However, it must be noted that the absence of γH2AX foci does not preclude MeT-mediated DNA damage, nor did we specifically measure cytoplasmic DNA. Additionally, STING, which is traditionally thought of as a sensor of cytoplasmic DNA, was strongly induced by MeT, although it must be noted that emerging evidence suggests that this factor also plays a key role in dsRNA-based immune responses (Ni, Ma et al. 2018, Morel, Sheahan et al. 2021). In short, it is plausible that the multifactorial impact on transcription and genome organisation caused by MeT (or high doses of DHT/T) would result

in both dsRNA accumulation and DNA damage, both of which could elicit viral mimicry and IFN signalling.

An important question that still needs to be addressed is whether, and to what extent, activation of IFN signalling contributes to MeT-mediated suppression of PCa cell growth. Type I IFNs can elicit cell cycle arrest and apoptosis in malignant cells (Kotredes and Gamero 2013), therefore it is possible that induction of this pathway at least partly explains the efficacy of MeT. However, MeT (and high doses of T/DHT) cause growth suppression within 1-2 days, whereas we observed induction of *IFNβ* and *IRF7* 3-6 days after treatment, an observation that is consistent with a stepwise activation of IFN involving epigenomic remodelling, ERV transcription and sensing of dsRNA. Moreover, growth suppression of RM1 cells by MeT and DHT was equivalent, even though the latter hormone did not induce ERVs or the IFN pathway. These observations argue against viral mimicry and IFN pathway activation playing a major role in the growth-inhibitory effects of MeT, at least when PCa cells are grown *in vitro*. Future *in vivo* studies carried out in the context of antagonism or ablation of viral mimicry effectors (e.g. RIG-I, IFNβ) could resolve this outstanding question.

A consistent finding throughout our study was that MeT exhibited greater potency – in terms of PCa cell growth inhibition, AR DNA binding and transcriptional activity, and viral mimicry responses – than DHT. MeT has been reported to have reduced affinity, when compared to DHT, for both the rat AR ligand-binding domain (Fang, Tong et al. 2003, Attardi, Hild et al. 2006) and cytosolic fractions from rat prostate (Saartok, Dahlberg et al. 1984). However, the main pathway for metabolism of testosterone and its derivatives in PCa cells is via

glucuronidation (Smith, Ballard et al. 1994), and MeT is very poorly glucuronidated by human glucuronyl-transferases (Kuuranne, Kurkela et al. 2003). With these early biochemical studies in mind, we propose that the stronger androgenic effects elicited by MeT relate to its increased stability compared to DHT. Moreover, we hypothesise that the increased potency of MeT, as opposed to a differential mode of action, explains why activation of IFN has not been observed in previous studies aimed at dissecting the mode of action of high dose DHT and other androgens (i.e. R1881) (Chatterjee, Schweizer et al. 2019, Nyquist, Corella et al. 2019). This hypothesis is supported by the observation that DHT elicited effects on ERVs, dsRNA production and IFN signalling that were qualitatively analogous to those mediated by MeT but were in almost all cases weaker. In short, we postulate that a certain threshold of AR activation, in terms of both strength and duration, is required to activate a viral mimicry response and that such a threshold can be more readily reached with stable synthetic androgens such as MeT.

Whether MeT could be harnessed as a therapeutic for advanced PCa, either as a monotherapy or in combination with immunotherapy, is an intriguing question. PCa is an immunologically "cold" cancer but it is possible that a MeT-induced viral mimicry response could increase tumour cell immunogenicity, which is critical to improve response to ICIs. In support of this concept, it has been shown that a small subset of patients treated with BAT showed an extreme response to immune checkpoint blockade (Markowski, Shenderov et al. 2020). Further evidence for this concept comes from our observation of a positive association between AR activity and anti-viral responses in patients with primary or metastatic tumours. As shown in Figure 6A, the correlation between AR activity and IFN response is stronger in

localised disease compared to CRPC, which we propose simply reflects the more homogenous nature of localised PCa in comparison with CRPC tumours.

Current medical recommendations suggest that MeT should be explicitly avoided in men with PCa but these are based on the viewpoint that androgens promote tumour progression, which is overly simplistic in the era of SupraT/BAT as a rational, valid treatment for CRPC. As an anabolic-androgenic steroid, MeT has a range of medical uses, including to treat delayed puberty in males (Bertelloni, Baroncelli et al. 2010), as a component of post-menopausal hormone replacement therapy in women (Chiuve, Martin et al. 2004) and, historically, as a treatment for breast cancer (Nevinny-Stickel, Dederick et al. 1964); as such, its pharmacodynamic, pharmacokinetic and safety profiles are relatively well understood. Drawbacks of MeT include high estrogenicity, due to its efficient aromatization into the potent and stable estrogen 17α-methylestradiol (El-Desoky el, Reyad et al. 2016) and hepatotoxicity (Sanchez-Osorio, Duarte-Rojo et al. 2008). Of course, other AR ligands may be even more effective than MeT in terms of growth suppression and modulation of immune responses. In this respect, selective AR modulators (SARMs) are of interest (Christiansen, Lipshultz et al. 2020) since it is conceivable that some may possess the requisite androgenic anti-growth and immunomodulatory activities in prostate cancer cells and favourable anabolic properties in other tissues. In short, we propose that investigation beyond the physiological androgens testosterone and DHT is required to maximise the therapeutic potential of AR activation in PCa.

In summary, our investigations have revealed a novel consequence of potent activation of AR in PCa cells. We propose that this work will expose new avenues of research aimed at elucidating interplay between androgenic and immune responses in the prostate and facilitate the development of new hormonal strategies to sensitize PCa to immunotherapies.

MATERIALS AND METHODS

Cell lines and cell culture

The human prostate carcinoma cell lines LNCaP, VCaP, PC3, 22Rv1 and C4-2B were obtained from the American Type Culture Collection (ATCC). LNCaP-V16D, LNCaP-MR49F and CWR-R1-D567 have been described previously (Nyquist, Li et al. 2013, Bishop, Thaper et al. 2017). C4-2B, 22Rv1, LNCaP, and LNCaP-V16D cells were maintained in RPMI-1640 (Sigma Aldrich) containing 10% fetal bovine serum (FBS) and 2 mM L-Glutamine. PC3 cells were cultured in RPMI-1640 containing 5% FBS and 2 mM L-Glutamine. LNCaP-MR42D and LNCaP-MR49F were maintained in RPMI-1640 containing 10% FBS, 10 µM Enzalutamide and 2 mM L-Glutamine. CWR-R1-D567 cells were maintained in RPMI-1640 containing 10% charcoal-stripped serum (CSS) and 2 mM L-Glutamine. VCaP cells were maintained in DMEM (high glucose) containing 10% FBS, 2 mM L-Glutamine, 2 mM Sodium Pyruvate, and 2 mM of non-essential amino acids solution (Sigma Aldrich). All cell lines were authenticated by short tandem repeat profiling by CellBank Australia in 2017-2020 and were regularly screened for potential mycoplasma contamination.

Cell viability assays

Cells were seeded at varying densities (depending on the doubling time of cell lines and length of the proliferation assay) in 6-well plates and incubated at 37 °C and 5% CO2 for at least 24 hours to allow cells to be attached to the plate surface before treatment. At the appropriate timepoints, cells were treated with freshly prepared drugs (as indicated in Fig. legends), followed by incubation at 37 °C and 5% CO2 until next time-point. Treatments were refreshed every 2–3 days. At the end of each time-point, cell viability was assessed using Trypan blue exclusion assays. The impact on MeT (1 nM and 100 nM) on the proliferation of RM1 cells was assessed in a 96-well format using the sulforhodamine B-binding assay over 5 days with a seeding density of 500 cells per well, as described previously (Houghton, Fang et al. 2007). Treatment commenced 24 hours post-seeding. Endpoint absorbance was measured at 550 nm.

Transactivation assays

AR transactivation assays were performed in 96-well plates essentially as previously described (Buchanan, Yang et al. 2004). LNCaP cells were used to test the transactivation of endogenous AR, whereas PC-3 cells were used to test the transactivation of exogenous AR. Cells were transfected with 1 ng of pcDNA-AR (PC3 only) and 100 ng of a reporter construct containing 3 copies of the Probasin enhancer (pGL4.14-PB3-luc) using LipofectAMINE 2000 (GIBCO-BRL), according to the manufacturer's instructions. Following transfection, cells were treated for 24 h in phenol-red free medium supplemented with the different doses of MeT and DHT, and luciferase activity was determined in cell lysates using the Luciferase™ Reporter Gene Assay Kit (Promega) and a plate reading luminometer (Top Count).

Chromatin immunoprecipitation (ChIP)-sequencing

LNCaP cells were seeded at 5 × 10^6 cells/plate in 15 cm plates phenol-red-free medium supplemented with 5% DCC-stripped FBS and allowed to grow for 2 days prior to treatment with Vehicle (Ethanol), MeT 1nM, and DHT 1nM on 3 biological replicates each for 4 hours. Subsequently, cells were fixed with formaldehyde and chromatin immunoprecipitation (ChIP) was performed essentially as described previously (Paltoglou, Das et al. 2017) using an Abcam AR antibody (ab108341). For each treatment condition, 2 biological replicates were generated. After DNA quantification with Qubit dsDNA HS assay (Thermo-Fisher Scientific), 5 ng of ChIP DNA (ChIP-enriched or input) was used for library preparation using a TruSeq ChIP Library Prep kit (Illumina). Sequencing was performed on an Illumina Nextseq 500 platform (single-end protocol, 75 bp read length) at the South Australian Genomics Centre (SAGC). Mapping and processing of fastq files were performed as described previously (Chan, Selth et al. 2015). Deeptools (Ramírez, Ryan et al. 2016) was used to convert BAM files to bigwig and for visualizing ChIP-seq data as heatmaps. Peak annotations were performed using Cisgenome v2.0 (Ji, Jiang et al. 2008). HOMER (Heinz, Benner et al. 2010) was used to generate histograms of tag density at specific sets of peaks. Alignments were visualised and interrogated using the Integrative Genomics Viewer v2.3.80 (Thorvaldsdóttir et al., 2013).

RNA sequencing

LNCaP were seeded at the 2x10^5 cells/well in 6-well plates and treated with vehicle, 1 nM MeT or 1 nM DHT. Total RNA was extracted at 6 hours and 24 hours after treatment using Trizol. For each treatment condition, 3 biological replicates were generated. The integrity of

RNA was first assessed using a 2100 Bioanalyzer system (Agilent). RNA concentration were quantified by Nanodrop 2000 (Thermo Fisher Scientific) and total RNA (2 µg) was supplied to the South Australian Genomics Centre (SAGC). RNA sequencing libraries were constructed using a TruSeq Total RNA HT kit (Illumina) and libraries were sequenced on the Illumina NextSeq 500 platform (stranded, paired-end 75 bp reads).

The quality of raw data was initially assessed using FastQC (http://www.bioinformatics.babraham.ac.uk/projects/fastqc/). Raw FASTQ files were then filtered for short sequences using Cutadapt v1.16.6 (Martin 2011) with the following settings: minimum overlap length in Adaptor options: 3, Minimum length in filter options: 20, maximum error rate: 0.1, quality cut-off: 20.

To evaluate expression of protein-coding genes, reads were mapped against the human reference genome (hg19) using STAR version 2.6.0b-2 (Dobin, Davis et al. 2013) with default parameters. FeatureCounts was used to count and assign the mapped reads to genomic features (Liao, Smyth et al. 2014). Count tables generated by featureCounts were used for differential expression analysis using R version 3.2.3 and edgeR version 3.3 (Robinson, McCarthy et al. 2010) as described previously (Lun, Chen et al. 2016). Heatmaps summarising RNA-seq data were generated using ClustVis (Metsalu and Vilo 2015).

To evaluate expression of transposable elements (TEs), reads were re-mapped against the human reference genome (hg19) using STAR version 2.6.0b-2 (Dobin, Davis et al. 2013) with parameters that retained multiply mapped reads (--runThreadN 4 --outSAMtype BAM

SortedByCoordinate --runMode alignReads --outFilterMultimapNmax 1000 --outFilterMismatchNmax 3 -- outMultimapperOrder Random --winAnchorMultimapNmax 1000 --alignEndsType EndToEnd --alignIntronMax 1 --alignMatesGapMax 350). HOMER was used to count and assign the mapped reads to different families of TEs (LTR, LINE and SINE). Count tables generated by HOMER were used to make a PCA plot with ClustVis.

Gene set enrichment analysis

Genes were ranked according to expression using the Signal2Noise metric. Gene Set Enrichment Analysis (Preranked analysis) (Subramanian, Tamayo et al. 2005) was implemented using the Broad Institute's public GenePattern server with default parameters.

Flow cytometry for cell cycle analysis

LNCaP cells were seeded in 6-well plates and incubated overnight at 37°C and 5% CO2. Three days after treatment, cells were washed with a freshly prepared wash buffer containing PBS with 2% FBS, followed by trypsinization. The cell suspension was added to a 5 ml FACS tube containing cell culture media that had been collected earlier. Tubes were centrifuged at 700 *g* for 5 min and cell pellets were re-suspended and washed with 1ml PBS, followed by centrifugation at 700 *g* for 5 minutes. After removing supernatants, cell pellets were resuspended in residual liquid by flicking the tubes. Subsequently, 1ml ice-cold 70% EtOH in PBS was added into tubes containing the cell suspensions and fixed overnight at 4°C. Following cell fixation, cells were centrifuged at 700 *g* for 5 minutes and the cell pellets were washed twice with 1 ml Hanks' Balanced Salt Solution + 2% FBS. Cell were then stained with 1 ml of DAPI (10 µg/mL). The prepared cell suspension was used for cell cycle analysis based

on DNA content using a BD FACSCanto II flow cytometer (Analyser); analysis was carried out using FlowJo software.

Quantitative RT-PCR (qRT-PCR) analysis of mRNA from human cells

Total RNA from human cell lines was extracted using TRI Reagent (Sigma), as described previously (Das, Gregory et al. 2017). Total RNA was treated with Turbo DNA-free kit (Invitrogen), and reverse transcribed using iScript Reverse Transcriptase Supermix kit (Bio-Rad). PCR was done in triplicate using a CFX384TM Real-Time System, as described previously (Moore, Buchanan et al. 2012). Levels of *GAPDH* were used for normalization of qRT-PCR data. Primer sequences are listed in Table S1.

Quantitative RT-PCR (qRT-PCR) analysis of mRNA from mouse cells

mRNA was extracted using the Qiagen Rneasy Plus Mini Kit (Qiagen) according to the manufacturer's instructions and reverse transcribed using iScript Reverse Transcriptase Supermix cDNA for qRT-PCR kit (Bio-Rad). qRT-PCR was performed using PowerUp SYBR Green Master Mix (applied biosystems) to quantify gene expression on the CFX384TM Real-Time System (Bio-Rad) as described previously (Owen, Gearing et al. 2020). Gene expression (arbitrary units) was calculated as mean relative transcript abundance (RTA) by methods outlined previously (Bidwell, Slaney et al. 2012) and expressed relative to a housekeeping gene, *Hprt*. Primer sequences are listed in Table S1.

Western blotting

Protein extraction from cells using RIPA buffer (human cell lines) or hypotonic lysis buffer (RM1) and Western blotting was done essentially as described previously (Moore, Buchanan et al. 2012). Primary antibodies used in human Western blotting were: TBK1 Antibody (Cell Signalling; 3013); phospho-Ser172-TBK1 (Cell Signalling; D52C2); RIG-I (Santa Cruz; SC-376845); and GAPDH (Millipore, MAB374). Primary antibodies used in murine Western blotting were: AR (N-20; Santa Cruz; SC-816) and GAPDH XP (Cell Signaling; D16h11). HRP conjugated anti-rabbit and anti-mouse IgG secondary antibodies (Dako) were used and immunoreactive bands visualized using Clarity Western ECL Substrate (Bio-Rad).

Immunofluorescence

LNCaP cells were seeded on glass coverslips in 6-well plates. To improve cell adhesion, glass coverslips were coated with 1:8 diluted L-Poly-Lysine. After treatment, cells were fixed in 4% paraformaldehyde for 10 minutes, permeabilized in 0.1% Triton X-100 for 15 minutes, and blocked in 2.5% BSA (for phospho-Histone H2A.X) or 5% BSA (for J2) solution for 1 hour. The coverslips then were incubated with anti-γH2AX primary antibody (Millipore; 05-636) or J2 antibody (both used at 1:1000) overnight at 4 °C, followed by washing (twice with 5 min intervals) and then incubation with a fluorescent-tagged secondary antibody for 1 hour at room temperature. Cell nuclei were visualised by co-staining the cells with 4´-6-Diamidino-2-phenylindole (DAPI; Invitrogen) for 1 min. Imaging was carried out using a confocal microscope (Olympus FV3000 Confocal Microscope). To quantify the number of γH2AX foci per nucleus, images were analysed using Image J software: i) the number of cells (i.e. DAPI-stained nuclei) were counted in each image by Analyze Particles tool; ii) the number of γH2AX foci in each image was quantified using the Find Maxima tool, which was performed using the

noise tolerance parameter adjusted for positive control; iii) the average number of foci per nucleus for each treatment was calculated by counting γH2AX foci from 70-150 cells per treatment across multiple microscope fields. To quantify J2 signal, Image J (Schneider, Rasband et al. 2012) was used to measure signal intensity at regions of interest (ROI); total signal intensity was normalised to cell counts at each ROI.

Quantification of LINE-I DNA Methylation

Cells were grown and treated in 6-well plates and genomic DNA was isolated using QIAamp DNA Mini kits, according to the manufacturer's instructions. To quantify the DNA methylation in DNA samples, Global DNA Methylation-LINE-I Kits (Active Motif) were used to assess the methylation of 5-mC status at Long Interspersed Nucleotide Element 1 (LINE-I) elements, as specified by the manufacturer.

Intracellular cytokine staining for T-cell specificity

For assessment of androgen effects on antigen presentation in cancer cells, RM1 cells were treated with MeT, DHT or vehicle control as previously described. Following 72 hrs, RM1 cells (5×10^4) were co-cultured with *in vitro* expanded RM1-specific $CD8^+$ T cells for 5 hrs in the presence of 10 µg/mL Brefeldin A. Intracellular cytokine staining assays for production of IFN-γ were carried out as previously described (Owen, Gearing et al. 2020).

Analysis of prostate cancer clinical transcriptomic data

Clinical transcriptomic datasets (TCGA (Abeshouse, Ahn et al. 2015) and SU2C (Robinson, Van Allen et al. 2015)) were downloaded from cBioportal (Gao, Aksoy et al. 2013). The activity of

AR signalling and other pathways (i.e. antiviral mechanism by IFN-stimulated genes, MHC class I antigen processing and presentation) in these datasets was estimated by single sample GSEA (ssGSEA) (Barbie, Tamayo et al. 2009); ssGSEA was implemented using the Broad Institute's public GenePattern server, using rank normalisation and default parameters.

Statistical analysis

Statistical analyses for grouped quantitative data were carried out using two-tailed unpaired t-test or ANOVA (GraphPad Prism 9). The relationships between activity scores were determined using Pearson's correlation coefficient (Graphpad Prism 9). Further details of statistical tests are provided in the figure legends. Statistical significance was defined as $p < 0.05$.

ACKNOWLEDGEMENTS

This work was supported by a Movember & National Breast Cancer Foundation Collaboration Initiative grant (MNBCF-17-012 to WDT, LAS, GPR, TEH and JSC), the National Health and Medical Research Council of Australia (1145777 to WDT, TEH and LAS) and the Cancer Council of South Australia (Beat Cancer Project Grant 1185012 to LAS). The research programs of LAS, WDT and LMB are supported by the Movember Foundation and the Prostate Cancer Foundation of Australia through a Movember Revolutionary Team Award. LAS is supported by a Principal Cancer Research Fellowship awarded by Cancer Council's Beat Cancer project on behalf of its donors, the South Australian Government through the Department of Health,

and the Australian Government through the Medical Research Future Fund. MAG was supported by an Australian Government Research Training Program Scholarship.

The authors thank: Mark van der Hoek (South Australian Genomics Centre) for assistance with ChIP-seq and RNA-seq; and Zoya Kikhtyak, Geraldine Laven-Law and Marie Pickering (University of Adelaide) for expert technical assistance. The results published here are in part based on data generated by The Cancer Genome Atlas, established by the National Cancer Institute and the National Human Genome Research Institute, and we are grateful to the specimen donors and relevant research groups associated with this project.

Supplementary Data1.
A) MeT vs Vehicle

No	gene_id	logFC	logCPM	LR	PValue	FDR
1	KLK3	1.102505	12.20737	308.6007	4.41E-69	1.87E-67
2	DHCR24	1.013861	11.28665	246.4704	1.53E-55	4.95E-54
3	TUBB	-1.14484	11.22334	344.2626	7.53E-77	3.77E-75
4	KRT8	2.755782	10.91338	1419.69	1.10584753499914e-310	3.14E-307
5	TUBA1B	-1.02658	10.47486	150.4516	1.38E-34	2.46E-33
6	KRT18	1.933156	10.33859	567.1592	2.33E-125	2.39E-123
7	ABHD2	1.056565	10.32729	165.8682	5.91E-38	1.16E-36
8	SORD	1.524395	10.12226	722.6912	3.48E-159	5.81E-157
9	TMPRSS2	1.9133	10.07856	889.5421	1.84E-195	5.66E-193
10	ODC1	1.919991	9.933507	959.7237	1.02E-210	3.52E-208
11	BRP44	1.025034	9.9108	132.7389	1.03E-30	1.61E-29
12	ATP1A1	1.083749	9.856039	378.8471	2.22E-84	1.34E-82
13	FKBP5	2.826146	9.752285	1374.943	5.85E-301	9.50E-298
14	SLC45A3	1.794352	9.685641	692.9592	1.02E-152	1.44E-150
15	ACSL3	2.530338	9.582629	990.3053	2.30E-217	9.01E-215
16	SPDEF	1.81474	9.384326	542.9447	4.31E-120	4.15E-118
17	CENPN	1.577379	9.320023	686.6329	2.41E-151	3.30E-149
18	ELOVL5	1.175085	9.248209	224.8435	7.94E-51	2.31E-49
19	KLK2	1.68128	9.239738	551.3755	6.32E-122	6.25E-120
20	ABCC4	1.138322	9.135198	170.3646	6.16E-39	1.27E-37
21	UAP1	1.075357	9.142776	369.5943	2.29E-82	1.32E-80
22	COPG1	1.079653	9.135934	351.0871	2.46E-78	1.28E-76
23	DBI	1.346483	9.101579	226.7449	3.06E-51	9.05E-50
24	PEX10	1.45545	9.027251	442.5256	3.05E-98	2.21E-96
25	SSR2	1.130174	9.028995	167.2236	2.99E-38	5.99E-37
26	GDF15	1.246685	8.914849	279.276	1.08E-62	3.96E-61
27	PPAP2A	1.767033	8.874552	822.3957	7.29E-181	1.97E-178
28	HM13	1.006956	8.816252	257.3113	6.62E-58	2.24E-56
29	MIA3	1.093211	8.716466	242.8354	9.47E-55	3.02E-53

30	SLC41A1	2.693377	8.666302	1377.688	1.48E-301	2.81E-298
31	NDRG1	3.390736	8.62771	2448.34	0	0
32	RRBP1	1.016748	8.673835	219.8926	9.55E-50	2.68E-48
33	C17orf28	1.257265	8.646756	316.6161	7.91E-71	3.48E-69
34	APP	1.034228	8.639645	174.5952	7.34E-40	1.54E-38
35	TRPM4	1.215836	8.641616	243.4252	7.04E-55	2.26E-53
36	SLC39A7	1.04882	8.640004	305.2606	2.35E-68	9.76E-67
37	MAP7D1	1.082256	8.637467	229.6355	7.16E-52	2.14E-50
38	SMS	2.166353	8.558071	1116.133	1.03E-244	6.50E-242
39	NCAPD3	2.267871	8.563809	785.0907	9.41E-173	2.15E-170
40	ABCC1	1.147796	8.538649	182.54	1.35E-41	2.99E-40
41	PMEPA1	1.11535	8.391103	342.0117	2.33E-76	1.14E-74
42	CORO1B	1.425981	8.376904	447.3255	2.76E-99	2.01E-97
43	H2AFX	-2.20271	8.459112	653.4829	3.91E-144	4.99E-142
44	SCAP	1.273117	8.345523	332.9503	2.19E-74	1.03E-72
45	SLC9A3R2	1.002723	8.347771	192.8273	7.68E-44	1.82E-42
46	ARF4	1.032718	8.209469	223.9967	1.22E-50	3.49E-49
47	CREB3L4	1.261963	8.198118	334.1976	1.17E-74	5.57E-73
48	PACS1	1.984219	8.161179	785.0768	9.48E-173	2.15E-170
49	TBRG1	1.002711	8.188979	329.6456	1.15E-73	5.30E-72
50	CAPZB	1.40817	8.153803	400.5794	4.12E-89	2.72E-87
51	MLPH	1.392538	8.15998	431.327	8.36E-96	5.97E-94
52	TPD52	1.212396	8.161516	161.0796	6.57E-37	1.25E-35
53	SERP1	1.173807	8.131943	203.6154	3.40E-46	8.59E-45
54	MCM7	-2.19755	8.226906	1113.188	4.49E-244	2.69E-241
55	MBOAT2	1.139948	8.12853	357.0327	1.25E-79	6.71E-78
56	SLC50A1	1.091445	8.081225	197.1609	8.70E-45	2.11E-43
57	BAIAP2	1.104676	8.073449	281.5848	3.39E-63	1.26E-61
58	ECI2	1.115146	8.068436	275.6245	6.75E-62	2.42E-60
59	PRKDC	-1.1474	8.09885	125.4546	4.05E-29	5.94E-28
60	MICAL1	3.059149	8.011749	1554.8	0	0
61	SAT1	2.303927	7.935712	1025.171	6.07E-225	2.55E-222
62	SSR3	1.011443	7.960082	177.1866	1.99E-40	4.26E-39
63	GLUD1	1.262113	7.952331	417.6326	7.99E-93	5.51E-91
64	B2M	1.47189	7.95434	233.8719	8.53E-53	2.64E-51
65	HMGXB3	1.139274	7.964506	299.9471	3.38E-67	1.36E-65
66	TMED9	1.202777	7.943769	335.741	5.40E-75	2.58E-73

67	SERINC2	1.072148	7.951807	202.9951	4.64E-46	1.17E-44
68	NANS	1.015961	7.925586	215.8399	7.31E-49	1.99E-47
69	ANKH	1.285997	7.921012	535.9416	1.44E-118	1.38E-116
70	TACC3	-1.35228	7.958916	356.1131	1.98E-79	1.05E-77
71	VPS26B	1.615397	7.865412	616.6265	4.05E-136	4.47E-134
72	CHPF	1.246516	7.86973	230.7004	4.19E-52	1.26E-50
73	HERC3	1.180985	7.824053	150.1779	1.59E-34	2.82E-33
74	KPNA2	-1.66235	7.896057	632.5545	1.39E-139	1.68E-137
75	TNFRSF10B	1.020375	7.780281	233.4449	1.06E-52	3.26E-51
76	HEBP2	1.10033	7.754269	227.2638	2.36E-51	7.01E-50
77	MYC	-1.56335	7.759253	519.0624	6.77E-115	6.11E-113
78	TPM1	1.073725	7.72101	302.3249	1.03E-67	4.20E-66
79	MKI67	-2.67576	7.768959	714.567	2.03E-157	3.16E-155
80	MTOR	1.122382	7.6254	138.3406	6.14E-32	1.01E-30
81	FN1	-1.19125	7.680013	156.4909	6.61E-36	1.23E-34
82	SEC11C	1.23395	7.613902	153.3484	3.21E-35	5.85E-34
83	RHOU	2.167109	7.623098	804.5011	5.67E-177	1.43E-174
84	NCAPD2	-1.80916	7.689602	606.4034	6.78E-134	7.34E-132
85	GFM1	1.338574	7.593172	256.3054	1.10E-57	3.69E-56
86	PAK1IP1	2.387798	7.594383	1117.176	6.11E-245	4.08E-242
87	FOXM1	-1.63477	7.674485	716.9346	6.21E-158	9.94E-156
88	SYVN1	1.000653	7.593092	203.8742	2.98E-46	7.58E-45
89	CSE1L	-1.35737	7.623052	365.7079	1.61E-81	9.06E-80
90	AIDA	-1.10573	7.598071	140.4468	2.13E-32	3.55E-31
91	RBMX	-1.0122	7.594585	288.9231	8.53E-65	3.23E-63
92	PPAPDC1B	1.110143	7.50677	233.6865	9.36E-53	2.89E-51
93	CBWD1	1.778387	7.492296	510.5037	4.93E-113	4.34E-111
94	TBC1D1	1.357368	7.505586	486.5281	8.11E-108	6.40E-106
95	HMGB2	-1.92992	7.56376	551.252	6.72E-122	6.59E-120
96	SAPCD2	-1.20272	7.481292	303.6156	5.37E-68	2.21E-66
97	MYBL2	-2.2685	7.505904	777.8938	3.45E-171	7.55E-169
98	C1orf21	1.443016	7.405648	450.1608	6.65E-100	4.88E-98

99	HIST2H2BE	1.478518	7.37175	488.6229	2.84E-108	2.26E-106
100	NASP	-1.54286	7.471485	513.7376	9.75E-114	8.66E-112
101	MDC1	-1.96038	7.471565	527.8025	8.49E-117	7.98E-115
102	RANBP1	-1.13948	7.46558	148.3011	4.08E-34	7.17E-33
103	LMNB2	-1.38575	7.447536	328.1175	2.47E-73	1.13E-71
104	DNMT1	-1.84248	7.449779	530.912	1.79E-117	1.69E-115
105	SEC61B	1.012905	7.358126	128.9505	6.95E-30	1.05E-28
106	RRM1	-1.70327	7.388294	592.5655	6.93E-131	7.29E-129
107	TPX2	-2.55077	7.409799	1190.686	6.45E-261	5.23E-258
108	ELL2	1.290407	7.311118	217.7268	2.83E-49	7.78E-48
109	ARRDC1	1.224093	7.306428	191.5759	1.44E-43	3.38E-42
110	TSC22D1	1.504501	7.305186	624.1406	9.40E-138	1.08E-135
111	SPAG5	-1.96586	7.378592	1009.157	1.84E-221	7.45E-219
112	MCM2	-3.25425	7.370048	1314.99	6.25E-288	7.10E-285
113	CTBP1	-1.73532	7.339669	691.7332	1.88E-152	2.63E-150
114	LRIG1	1.541028	7.277218	281.3816	3.75E-63	1.39E-61
115	AZGP1	1.55445	7.246189	294.3881	5.50E-66	2.15E-64
116	HERPUD1	1.178085	7.267212	376.2176	8.29E-84	4.93E-82
117	RPA1	-1.00348	7.292358	257.4977	6.03E-58	2.05E-56
118	PCNA	-2.29076	7.316584	775.344	1.24E-170	2.66E-168
119	TK1	-2.40243	7.319267	690.508	3.47E-152	4.80E-150
120	CHRNA2	1.634173	7.192927	371.8103	7.55E-83	4.40E-81
121	C1orf85	1.194064	7.180633	307.9533	6.10E-69	2.58E-67
122	C1orf122	1.067236	7.18229	95.62431	1.39E-22	1.54E-21
123	PRKD1	-1.05385	7.215452	233.2838	1.15E-52	3.52E-51
124	CCNB1	-1.73838	7.235568	454.2172	8.72E-101	6.47E-99
125	ATAD2	-1.20414	7.210836	233.0338	1.30E-52	3.96E-51
126	SEPP1	1.597374	7.116772	412.4631	1.07E-91	7.26E-90
127	SMC1A	-1.02717	7.173127	116.4915	3.71E-27	5.06E-26
128	ZG16B	1.157092	7.107736	169.2795	1.06E-38	2.16E-37
129	BIRC5	-1.81075	7.177067	346.1707	2.89E-77	1.45E-75
130	ELOVL7	1.139251	7.068933	170.6596	5.31E-39	1.10E-37

131	PLK1	-2.34233	7.175124	981.4612	1.92E-215	6.83E-213
132	PPFIBP2	1.405403	7.071177	421.265	1.29E-93	8.97E-92
133	CENPF	-2.65802	7.146804	669.8106	1.10E-147	1.45E-145
134	PSAT1	-1.31278	7.101152	233.2423	1.17E-52	3.58E-51
135	IGF1R	1.227603	7.023089	154.2994	1.99E-35	3.64E-34
136	WFS1	1.091063	6.993063	148.7446	3.26E-34	5.76E-33
137	MCM4	-3.26059	7.062613	1688.681	0	0
138	CBX5	-1.05325	7.02122	196.7588	1.06E-44	2.57E-43
139	RABEP2	1.136575	6.971847	210.3371	1.16E-47	3.08E-46
140	LMNB1	-2.84859	7.04996	1317.988	1.39E-288	1.76E-285
141	CDC20	-2.513	7.066853	1110.524	1.70E-243	9.68E-241
142	MEAF6	1.205925	6.967128	272.7044	2.92E-61	1.04E-59
143	SLC35F2	1.672322	6.930858	492.3402	4.41E-109	3.58E-107
144	TIMELESS	-1.19271	7.011181	207.5162	4.78E-47	1.24E-45
145	MCM3	-2.56895	7.015346	1027.143	2.26E-225	9.89E-223
146	RRM2	-2.97438	7.018513	1415.994	7.02808146803033e-310	1.60E-306
147	F5	2.045852	6.905314	503.1163	1.99E-111	1.69E-109
148	PGM3	1.560865	6.89683	450.1969	6.54E-100	4.82E-98
149	DAPK3	1.178791	6.929353	233.1573	1.22E-52	3.73E-51
150	WHSC1	-1.47703	6.966715	324.6563	1.40E-72	6.37E-71
151	RAB4A	1.049846	6.913361	200.7618	1.42E-45	3.53E-44
152	NUSAP1	-2.61455	6.984579	1181.569	6.18E-259	4.68E-256
153	SRP19	1.161849	6.897063	190.4124	2.58E-43	6.04E-42
154	ZWINT	-1.73203	6.975172	708.0898	5.21E-156	7.89E-154
155	MYO19	-1.31371	6.942265	382.666	3.27E-85	2.02E-83
156	GTF2E2	1.04861	6.859239	183.7858	7.23E-42	1.62E-40
157	LRRFIP2	1.137049	6.884022	201.6501	9.11E-46	2.28E-44
158	TCOF1	-2.34301	6.936038	735.5391	5.59E-162	9.93E-160
159	RAD21	-1.11169	6.892567	165.618	6.70E-38	1.31E-36
160	RCC2	-1.34572	6.904302	348.6003	8.55E-78	4.38E-76
161	SLC22A23	1.021756	6.835524	193.8476	4.60E-44	1.10E-42
162	NAMPT	1.123835	6.822034	207.5622	4.67E-47	1.22E-45
163	TP53	-1.60033	6.865286	381.0834	7.23E-85	4.44E-83

164	PRC1	-2.3849	6.878806	865.6275	2.91E-190	8.48E-188
165	TYMS	-2.70844	6.875414	1343.805	3.42E-294	4.86E-291
166	MKLN1	1.048939	6.782135	202.5771	5.72E-46	1.44E-44
167	FEN1	-2.36599	6.856174	1088.94	8.37E-239	4.32E-236
168	OTUD7B	1.258978	6.767622	203.7774	3.13E-46	7.94E-45
169	RCC1	-1.78013	6.813997	618.4277	1.64E-136	1.85E-134
170	HMGCS1	1.447633	6.7105	321.2542	7.72E-72	3.46E-70
171	HMGCS2	2.068509	6.651636	700.2602	2.62E-154	3.87E-152
172	ATP1B1	-1.13926	6.753034	200.1631	1.92E-45	4.74E-44
173	CDK1	-2.71822	6.77637	913.291	1.27E-200	4.00E-198
174	HES6	1.384235	6.654255	133.4881	7.07E-31	1.11E-29
175	NUP205	-1.23592	6.725211	152.3077	5.43E-35	9.77E-34
176	ZYX	1.042066	6.690777	145.4572	1.71E-33	2.91E-32
177	PPM1A	1.279608	6.66174	331.077	5.60E-74	2.61E-72
178	GFPT1	1.01855	6.660885	189.0691	5.08E-43	1.17E-41
179	MCM5	-2.67709	6.75905	789.0616	1.29E-173	3.12E-171
180	NUCB2	1.701794	6.625689	350.1536	3.92E-78	2.03E-76
181	SEC24D	1.449741	6.633217	232.7447	1.50E-52	4.57E-51
182	PPAPDC2	1.37501	6.634727	397.833	1.63E-88	1.07E-86
183	POLE3	-1.299	6.692208	307.3153	8.40E-69	3.52E-67
184	APPBP2	1.575724	6.61907	392.7653	2.07E-87	1.34E-85
185	ACP2	1.066957	6.624005	213.283	2.64E-48	7.11E-47
186	FAM177A1	1.03761	6.615524	185.9647	2.42E-42	5.48E-41
187	DNAJC10	1.078406	6.596172	175.0401	5.87E-40	1.24E-38
188	TMPO	-2.52112	6.683045	726.7627	4.53E-160	7.80E-158
189	ALDH1A3	1.523543	6.573224	338.8383	1.14E-75	5.53E-74
190	SELM	1.054759	6.605823	77.05903	1.66E-18	1.49E-17
191	TMEM97	-1.46271	6.653461	472.8102	7.84E-105	5.98E-103
192	TSKU	1.551399	6.582456	385.3147	8.67E-86	5.50E-84
193	TMEM125	1.5613	6.532456	339.3559	8.81E-76	4.28E-74
194	FANCI	-2.15162	6.62416	787.3054	3.11E-173	7.35E-171
195	DNAJC3	1.097632	6.536444	181.2118	2.64E-41	5.77E-40
196	DHFR	-1.08106	6.583575	180.1067	4.59E-41	1.00E-39
197	CAD	-1.19815	6.577752	148.4543	3.77E-34	6.66E-33
198	RHBDF1	1.231231	6.520357	215.7936	7.48E-49	2.03E-47

199	H1F0	1.184458	6.514215	315.3405	1.50E-70	6.55E-69
200	CHTF18	-1.10213	6.5864	203.456	3.68E-46	9.29E-45
201	TP53I11	1.001571	6.524923	166.8999	3.52E-38	7.00E-37
202	NUDT9	1.297071	6.493919	357.4887	9.92E-80	5.37E-78
203	ARFGAP3	1.03879	6.483907	218.693	1.74E-49	4.85E-48
204	ST6GALNAC1	1.778908	6.465627	545.0317	1.52E-120	1.47E-118
205	FXYD3	1.594635	6.456788	166.4964	4.31E-38	8.49E-37
206	TONSL	-2.7993	6.54392	761.4106	1.33E-167	2.69E-165
207	ERRFI1	2.396972	6.449845	625.5226	4.71E-138	5.46E-136
208	CYP2U1	2.382067	6.438611	752.9833	9.01E-166	1.74E-163
209	STARD10	1.065298	6.46205	90.23963	2.11E-21	2.24E-20
210	LPAR3	1.164568	6.392414	171.2806	3.89E-39	8.04E-38
211	CHAF1A	-2.07606	6.47708	564.767	7.72E-125	7.83E-123
212	KIF20A	-2.47709	6.495192	989.6868	3.13E-217	1.19E-214
213	FAM105A	2.156335	6.395164	636.382	2.05E-140	2.53E-138
214	CREB3	1.330188	6.382446	238.3737	8.90E-54	2.80E-52
215	GMPPA	1.192689	6.389208	240.3809	3.25E-54	1.03E-52
216	ST7	-1.25679	6.434559	243.1134	8.24E-55	2.63E-53
217	RNASEH2A	-1.92643	6.46065	362.4873	8.09E-81	4.46E-79
218	CDC25B	-1.71029	6.455418	414.9696	3.04E-92	2.08E-90
219	C12orf44	1.112789	6.378276	183.236	9.53E-42	2.13E-40
220	SEC61G	1.028399	6.360787	69.52986	7.53E-17	6.10E-16
221	Mar-02	1.094852	6.346342	185.3067	3.36E-42	7.60E-41
222	SMC4	-2.10645	6.403634	425.6532	1.44E-94	1.02E-92
223	MT2A	-1.12949	6.412637	100.5581	1.15E-23	1.35E-22
224	TFDP1	-1.04138	6.384332	209.8179	1.51E-47	3.98E-46
225	REEP4	-1.40724	6.402221	236.9455	1.82E-53	5.72E-52
226	SHMT1	-1.02091	6.384896	219.8868	9.57E-50	2.68E-48
227	POLD4	1.483001	6.301807	234.5942	5.94E-53	1.85E-51
228	CYTH1	1.114964	6.307986	189.9782	3.21E-43	7.49E-42
229	CKS2	-1.83259	6.377009	321.9099	5.56E-72	2.50E-70
230	WDR90	-1.10826	6.328975	160.1325	1.06E-36	1.99E-35
231	ERBB2IP	1.010267	6.249908	62.56129	2.58E-15	1.90E-14
232	TMEM79	1.537379	6.25542	499.5023	1.22E-110	1.02E-108
233	WNT7B	1.149858	6.280866	276.8787	3.60E-62	1.31E-60
234	CNN2	1.05879	6.259797	224.2268	1.08E-50	3.11E-49

235	PCDH1	1.607217	6.239676	248.7152	4.95E-56	1.63E-54
236	TSPYL2	1.123337	6.260646	153.1687	3.52E-35	6.39E-34
237	TELO2	-1.01961	6.287891	131.3721	2.05E-30	3.17E-29
238	UBE2T	-2.08563	6.302109	509.9576	6.48E-113	5.66E-111
239	CBX2	-1.35803	6.268047	300.6352	2.40E-67	9.69E-66
240	MCM6	-1.95161	6.277195	721.3881	6.68E-159	1.10E-156
241	GNMT	2.439455	6.163692	664.9697	1.24E-146	1.60E-144
242	SLC16A6	1.925227	6.220973	366.6904	9.84E-82	5.59E-80
243	UGT2B11	3.381715	6.119025	878.6553	4.29E-193	1.28E-190
244	PTTG1	-1.13815	6.281529	82.99068	8.24E-20	7.97E-19
245	PIK3R3	-1.00472	6.23804	165.9614	5.64E-38	1.11E-36
246	IGBP1	1.009105	6.187094	211.8651	5.38E-48	1.44E-46
247	RECQL4	-2.44567	6.257349	735.0075	7.30E-162	1.28E-159
248	YIPF1	1.350027	6.149532	289.4761	6.47E-65	2.46E-63
249	TCF19	-3.17297	6.252116	1086.997	2.21E-238	1.09E-235
250	ZCCHC6	1.274969	6.147848	222.7858	2.23E-50	6.34E-49
251	GEMIN4	-1.61516	6.20047	372.4269	5.54E-83	3.28E-81
252	CDCA5	-3.10287	6.238124	1261.541	2.58E-276	2.66E-273
253	GADD45G	2.928615	6.156119	1031.987	2.00E-226	9.48E-224
254	MTMR9	1.228813	6.139286	201.2752	1.10E-45	2.74E-44
255	RFC2	-1.66704	6.199762	305.9512	1.66E-68	6.93E-67
256	GREB1	1.294012	6.120287	198.2542	5.02E-45	1.23E-43
257	SMPD2	1.172216	6.124848	167.983	2.04E-38	4.13E-37
258	DEK	-1.93842	6.168683	409.6557	4.36E-91	2.93E-89
259	NEU1	1.000617	6.103164	208.6205	2.75E-47	7.18E-46
260	HLTF	-1.06762	6.134986	100.1209	1.43E-23	1.67E-22
261	SELS	1.197415	6.093093	230.9763	3.65E-52	1.10E-50
262	CRLS1	1.012555	6.076245	129.3629	5.65E-30	8.54E-29
263	DERL2	1.100616	6.086523	93.39008	4.29E-22	4.66E-21
264	TOP2A	-3.27268	6.159168	710.8513	1.31E-156	2.01E-154
265	DDAH2	1.075739	6.082459	185.7827	2.65E-42	6.00E-41
266	DSEL	-1.17527	6.103658	218.1113	2.34E-49	6.47E-48
267	UBE2C	-2.70921	6.167261	695.3527	3.06E-153	4.46E-151
268	Mar-05	1.037374	6.063772	179.1387	7.47E-41	1.61E-39
269	CORO2A	1.020624	6.027818	151.8501	6.83E-35	1.23E-33

270	SASH1	1.207238	6.020806	91.74808	9.84E-22	1.06E-20
271	POLD1	-1.70165	6.096017	268.312	2.65E-60	9.37E-59
272	LONRF1	1.681935	5.992754	378.0212	3.36E-84	2.01E-82
273	EFCAB4A	1.17597	6.025514	167.7012	2.35E-38	4.74E-37
274	PTPRM	1.231821	6.012084	161.7762	4.63E-37	8.80E-36
275	FAM214B	1.221125	6.022107	189.8395	3.45E-43	8.01E-42
276	CCNB2	-2.3793	6.098181	742.9113	1.40E-163	2.52E-161
277	TROAP	-1.69885	6.095553	383.1854	2.52E-85	1.57E-83
278	ACAD8	1.607501	5.987761	323.4961	2.51E-72	1.14E-70
279	PKP4	-1.31	6.026131	206.9198	6.46E-47	1.66E-45
280	EXOSC2	-1.03818	6.02918	209.0109	2.26E-47	5.91E-46
281	RACGAP1	-2.25328	6.047303	631.398	2.48E-139	2.94E-137
282	LRRC45	-1.54626	6.026365	262.478	4.95E-59	1.73E-57
283	SNHG3	-1.12506	6.010091	176.4108	2.95E-40	6.26E-39
284	LSM2	-1.12572	6.01861	97.2629	6.07E-23	6.86E-22
285	MTHFD2	-1.04098	5.985797	131.1138	2.34E-30	3.61E-29
286	CCNF	-2.25008	6.00093	639.0337	5.42E-141	6.77E-139
287	KIFC1	-2.9716	6.000929	1098.194	8.16E-241	4.41E-238
288	XRCC3	-1.43163	5.971976	295.0115	4.02E-66	1.58E-64
289	E2F1	-3.03618	5.996343	1132.469	2.90E-248	2.06E-245
290	RNF185	1.015195	5.888818	145.5135	1.66E-33	2.83E-32
291	KIF2C	-2.92428	5.981083	1030.185	4.93E-226	2.24E-223
292	DTYMK	-1.087	5.963959	86.3344	1.52E-20	1.53E-19
293	CCDC53	1.220078	5.883705	119.2415	9.27E-28	1.30E-26
294	PKMYT1	-3.17892	5.970537	724.0308	1.78E-159	3.02E-157
295	CDC6	-2.71456	5.945206	956.275	5.74E-210	1.92E-207
296	KANK2	-1.39431	5.903333	195.9566	1.59E-44	3.84E-43
297	HMMR	-2.1397	5.923096	390.2568	7.28E-87	4.67E-85
298	NCAPG	-2.75675	5.917118	851.3649	3.67E-187	1.04E-184
299	SNHG1	-1.66199	5.894013	337.8273	1.90E-75	9.13E-74
300	KCNMA1	1.048287	5.817175	92.86631	5.59E-22	6.06E-21
301	NCAPH2	-1.04697	5.901586	146.5628	9.78E-34	1.68E-32
302	KIF4A	-2.00257	5.899307	514.496	6.67E-114	5.97E-112
303	NDFIP2	1.28736	5.815608	166.6536	3.98E-38	7.87E-37

304	CDCA3	-2.43805	5.893867	508.1527	1.60E-112	1.39E-110
305	MLF1IP	-2.59502	5.883664	774.1869	2.21E-170	4.65E-168
306	PARP2	-1.536	5.878172	297.0701	1.43E-66	5.69E-65
307	HJURP	-2.82867	5.888758	816.9411	1.12E-179	2.89E-177
308	IQGAP3	-2.15928	5.881633	558.399	1.87E-123	1.89E-121
309	RWDD2A	1.144425	5.800116	183.9652	6.60E-42	1.48E-40
310	RPA2	-1.20334	5.852203	173.6675	1.17E-39	2.45E-38
311	POLA2	-2.16493	5.857153	617.5233	2.58E-136	2.88E-134
312	C15orf23	-1.11599	5.854737	204.6946	1.97E-46	5.04E-45
313	MCMBP	-1.2245	5.828437	265.1596	1.29E-59	4.53E-58
314	CDK2	-1.50778	5.841479	299.9445	3.39E-67	1.36E-65
315	MESP1	1.055936	5.748554	78.99119	6.24E-19	5.74E-18
316	INCENP	-2.03569	5.835241	378.6788	2.41E-84	1.45E-82
317	DNAJC9	-1.31581	5.825465	206.7788	6.93E-47	1.78E-45
318	FAM83D	-2.45341	5.838418	720.8671	8.67E-159	1.41E-156
319	FOXD4	1.583442	5.745258	364.0671	3.66E-81	2.05E-79
320	FZD5	1.203639	5.723739	129.8697	4.38E-30	6.65E-29
321	AURKA	-2.26681	5.788678	499.3343	1.33E-110	1.10E-108
322	PSIP1	-1.20329	5.755688	162.085	3.96E-37	7.56E-36
323	SNX25	1.518669	5.693395	280.8462	4.91E-63	1.81E-61
324	ASRGL1	1.333319	5.700826	296.8215	1.62E-66	6.43E-65
325	LRRC20	-1.07583	5.746568	178.1508	1.23E-40	2.63E-39
326	MSH6	-1.34492	5.735659	222.0121	3.29E-50	9.31E-49
327	TOPBP1	-1.2495	5.727987	166.7894	3.72E-38	7.38E-37
328	ZNF350	1.54278	5.671632	314.3957	2.41E-70	1.05E-68
329	CBLL1	1.436619	5.675176	221.5112	4.23E-50	1.19E-48
330	C9orf152	1.30564	5.658872	176.9403	2.26E-40	4.81E-39
331	BUB1B	-3.03646	5.738795	753.0286	8.81E-166	1.73E-163
332	CADPS2	2.250906	5.627089	423.0305	5.34E-94	3.73E-92
333	DLGAP5	-2.21023	5.726486	329.2605	1.39E-73	6.41E-72
334	NCAPG2	-1.90439	5.713099	350.935	2.65E-78	1.38E-76
335	C14orf80	-1.35272	5.711237	247.3248	9.95E-56	3.24E-54
336	ASF1B	-3.8302	5.735445	1225.607	1.66E-268	1.45E-265
337	UNG	-1.42818	5.672245	277.2868	2.93E-62	1.07E-60
338	NUP85	-1.46517	5.692248	291.8036	2.01E-65	7.78E-64

339	TMEM201	-1.33915	5.678676	172.2282	2.41E-39	5.01E-38
340	SLC29A1	-2.77261	5.661481	778.4889	2.56E-171	5.72E-169
341	MAF	2.932162	5.575168	507.8834	1.83E-112	1.58E-110
342	LIFR	2.752187	5.555242	489.2013	2.13E-108	1.70E-106
343	FANCD2	-2.13342	5.646963	494.3288	1.63E-109	1.33E-107
344	PNMA1	1.241846	5.553088	265.5523	1.06E-59	3.73E-58
345	CCNA2	-2.98941	5.643516	695.3065	3.14E-153	4.51E-151
346	CAMK2N1	-2.14393	5.616474	459.8053	5.30E-102	3.99E-100
347	CAP2	1.783524	5.53728	276.5103	4.33E-62	1.56E-60
348	MAP9	1.153307	5.546306	115.2109	7.08E-27	9.58E-26
349	ANLN	-2.7275	5.608306	472.6704	8.41E-105	6.37E-103
350	CDT1	-2.6894	5.617058	592.6203	6.74E-131	7.16E-129
351	TFPT	1.03312	5.547885	99.8895	1.61E-23	1.87E-22
352	CHAF1B	-1.83884	5.603972	347.9958	1.16E-77	5.90E-76
353	GALK2	1.006977	5.504204	102.635	4.03E-24	4.83E-23
354	RAD51C	-1.15301	5.562171	138.3002	6.27E-32	1.03E-30
355	WDR62	-2.89153	5.586252	525.3029	2.97E-116	2.77E-114
356	UGT2B17	-1.49002	5.547899	224.8046	8.10E-51	2.35E-49
357	ACPP	1.065064	5.482185	182.4516	1.41E-41	3.12E-40
358	PRR11	-1.93725	5.569425	386.2358	5.46E-86	3.49E-84
359	MELK	-2.7595	5.576693	666.8211	4.91E-147	6.41E-145
360	STC2	-1.45317	5.527638	194.9093	2.70E-44	6.45E-43
361	TTC39A	1.531964	5.457682	308.8245	3.94E-69	1.68E-67
362	CKAP2	-1.2193	5.532953	141.2153	1.44E-32	2.43E-31
363	DDC	-1.59046	5.532478	148.0825	4.55E-34	7.97E-33
364	NDC80	-2.66059	5.558103	634.4423	5.40E-140	6.60E-138
365	PRPF4	-1.12161	5.51558	140.7936	1.79E-32	3.00E-31
366	LRRC16A	1.282402	5.462036	166.5632	4.17E-38	8.22E-37
367	TCEAL3	1.027348	5.460493	126.2593	2.70E-29	4.00E-28
368	TMEM48	-1.79609	5.505487	320.863	9.40E-72	4.19E-70
369	ERLEC1	1.236214	5.424797	154.3849	1.91E-35	3.50E-34
370	AURKB	-2.99083	5.525203	569.7318	6.42E-126	6.63E-124
371	SLC2A12	1.710115	5.413684	343.7637	9.67E-77	4.80E-75

372	HAUS5	-1.60938	5.507433	236.6324	2.13E-53	6.68E-52
373	SNAPC4	-1.04952	5.472485	112.4805	2.80E-26	3.69E-25
374	POLR1E	-1.49621	5.46638	245.2165	2.87E-55	9.23E-54
375	NR4A1	1.671129	5.435144	289.9536	5.09E-65	1.94E-63
376	PFAS	-1.32278	5.45572	113.5676	1.62E-26	2.16E-25
377	ESPL1	-3.35512	5.494887	823.629	3.93E-181	1.09E-178
378	NUP155	-1.28387	5.441691	134.8934	3.48E-31	5.55E-30
379	FANCG	-1.86435	5.473524	361.5053	1.32E-80	7.23E-79
380	PRKCA	2.027003	5.384767	343.0186	1.40E-76	6.94E-75
381	NRARP	-1.16411	5.441732	162.6872	2.93E-37	5.62E-36
382	KIAA0513	1.392395	5.380875	211.8561	5.41E-48	1.45E-46
383	PLXNA3	1.091541	5.397839	66.45759	3.58E-16	2.78E-15
384	TRIP13	-1.96282	5.45135	479.7892	2.37E-106	1.86E-104
385	RRAS	1.256704	5.388401	126.1676	2.83E-29	4.18E-28
386	CDKN3	-1.23991	5.455793	106.8736	4.74E-25	5.97E-24
387	GMNN	-1.74604	5.450182	366.4446	1.11E-81	6.29E-80
388	DDX11	-1.61283	5.438654	192.4068	9.48E-44	2.24E-42
389	C5orf4	1.226262	5.38173	93.28493	4.53E-22	4.91E-21
390	ITPKC	1.012044	5.381158	125.0619	4.93E-29	7.23E-28
391	BCAP29	1.127326	5.365335	111.3899	4.86E-26	6.32E-25
392	RABAC1	1.299533	5.358938	90.53673	1.82E-21	1.93E-20
393	WIPI1	3.085675	5.320718	715.7274	1.14E-157	1.79E-155
394	CENPE	-2.55539	5.416865	398.9942	9.12E-89	5.99E-87
395	SMAP1	1.128774	5.354387	180.4406	3.88E-41	8.47E-40
396	OAZ3	1.101403	5.338351	70.90724	3.74E-17	3.09E-16
397	RAP1GAP	1.973047	5.301951	290.4567	3.95E-65	1.52E-63
398	EZH2	-1.82731	5.393788	342.9186	1.48E-76	7.26E-75
399	CDCA8	-2.75916	5.409472	817.8243	7.19E-180	1.90E-177
400	SMC2	-1.93674	5.364923	247.6822	8.31E-56	2.71E-54
401	ZBTB24	1.112941	5.319554	155.8564	9.10E-36	1.68E-34
402	NETO2	-1.08871	5.353325	181.9619	1.81E-41	3.98E-40
403	EMP2	-1.2952	5.364514	157.3889	4.21E-36	7.82E-35
404	CENPO	-1.63327	5.363486	303.6638	5.24E-68	2.17E-66
405	YWHAH	-1.00771	5.334659	129.9422	4.22E-30	6.43E-29
406	EDEM2	1.234739	5.287493	149.0135	2.85E-34	5.04E-33
407	TECPR1	1.002065	5.270997	95.51449	1.47E-22	1.63E-21
408	PBK	-2.07243	5.352495	361.7017	1.20E-80	6.59E-79
409	NCAPH	-3.25505	5.350564	989.5939	3.28E-217	1.20E-214

410	RFC4	-1.93463	5.343251	371.91	7.18E-83	4.21E-81
411	LOC150776	-1.07254	5.331821	92.46693	6.85E-22	7.39E-21
412	NUP160	-1.42056	5.301647	134.1115	5.17E-31	8.21E-30
413	ADAM7	1.202614	5.265882	222.1598	3.06E-50	8.66E-49
414	NOTCH1	-1.23504	5.292124	74.77103	5.29E-18	4.57E-17
415	CDC45	-3.02432	5.344925	626.7053	2.60E-138	3.05E-136
416	RGS3	-1.12618	5.30241	166.0001	5.53E-38	1.09E-36
417	BUB1	-2.40453	5.320551	457.2626	1.89E-101	1.42E-99
418	PHF1	1.034168	5.262987	87.6755	7.71E-21	7.94E-20
419	PIAS1	1.229291	5.251054	129.4538	5.40E-30	8.17E-29
420	SLC7A5	-1.38152	5.277115	164.1857	1.38E-37	2.67E-36
421	GTSE1	-2.46696	5.299098	672.4993	2.86E-148	3.82E-146
422	SLC25A20	1.181722	5.2054	195.5404	1.96E-44	4.72E-43
423	MDN1	-1.04446	5.224759	57.79713	2.91E-14	1.98E-13
424	BHLHA15	1.509403	5.167879	142.853	6.33E-33	1.07E-31
425	POC1A	-1.59785	5.245995	225.6205	5.38E-51	1.57E-49
426	CKS1B	-1.54118	5.228513	135.1903	3.00E-31	4.81E-30
427	BRCA1	-3.09521	5.210567	524.7953	3.83E-116	3.54E-114
428	HLA-DMA	1.88914	5.125523	210.2816	1.19E-47	3.16E-46
429	PTPN21	2.308262	5.107155	294.9429	4.16E-66	1.63E-64
430	SLC39A8	-1.38282	5.177939	211.3398	7.01E-48	1.87E-46
431	PODXL	-1.29161	5.175001	152.7887	4.26E-35	7.72E-34
432	AFF3	1.782135	5.101864	226.5547	3.36E-51	9.93E-50
433	KIF11	-2.75344	5.181224	380.6875	8.82E-85	5.39E-83
434	BTG2	-1.39522	5.161335	189.0626	5.09E-43	1.17E-41
435	ARID5B	1.397515	5.090399	133.0787	8.69E-31	1.36E-29
436	PGC	2.199557	5.097379	383.2945	2.39E-85	1.49E-83
437	FAM64A	-2.30997	5.174444	407.6541	1.19E-90	7.94E-89
438	MAD2L1	-2.46985	5.137843	307.9156	6.21E-69	2.62E-67
439	TBC1D8	1.127747	5.102788	104.3703	1.68E-24	2.05E-23
440	C4orf34	1.345178	5.04361	139.8938	2.81E-32	4.67E-31
441	PPP2R5B	1.027742	5.075568	107.2249	3.97E-25	5.02E-24
442	CENPM	-1.42535	5.135223	112.4281	2.88E-26	3.78E-25
443	EAF2	2.160754	5.067209	286.3176	3.15E-64	1.18E-62
444	TFAP4	-1.15115	5.088297	159.2153	1.68E-36	3.14E-35
445	PSRC1	-2.30736	5.139266	497.618	3.14E-110	2.58E-108
446	CDC25A	-1.00609	5.098526	101.1647	8.46E-24	9.98E-23
447	BCL2L12	-1.34974	5.126352	129.9842	4.13E-30	6.30E-29
448	ECT2	-1.9274	5.101833	273.0659	2.44E-61	8.68E-60

449	FANCA	-2.6372	5.118483	522.419	1.26E-115	1.15E-113
450	WRAP53	-1.46638	5.10507	223.492	1.57E-50	4.47E-49
451	CXCR7	-2.41898	5.08734	473.6052	5.26E-105	4.04E-103
452	FN3KRP	-1.12619	5.078632	117.5823	2.14E-27	2.95E-26
453	KIAA1731	-1.00206	5.066189	86.95609	1.11E-20	1.13E-19
454	SLC10A7	1.739501	5.006378	230.9897	3.63E-52	1.10E-50
455	UGT2B15	-1.58315	5.06843	205.6687	1.21E-46	3.10E-45
456	ARHGAP19	-1.43039	5.083822	169.5721	9.18E-39	1.88E-37
457	EXOSC8	-1.59109	5.079829	251.7733	1.07E-56	3.55E-55
458	MCM8	-1.40254	5.061522	170.138	6.90E-39	1.42E-37
459	SLC44A1	-1.12636	5.041781	103.331	2.84E-24	3.43E-23
460	KIAA0101	-1.34067	5.069066	124.7198	5.86E-29	8.56E-28
461	EML1	1.08568	5.004544	122.2279	2.06E-28	2.96E-27
462	TFAM	-1.0786	5.03236	98.67487	2.98E-23	3.41E-22
463	DEPDC1	-2.58639	5.061649	323.2672	2.81E-72	1.27E-70
464	METTL7A	-1.13267	5.040264	114.7384	8.98E-27	1.21E-25
465	NET1	-1.0463	5.030003	83.96344	5.04E-20	4.93E-19
466	ARHGAP11A	-2.7988	5.052337	337.3679	2.39E-75	1.15E-73
467	CIT	-3.02174	5.062757	791.295	4.21E-174	1.04E-171
468	NUP107	-1.49223	5.022358	183.0315	1.06E-41	2.35E-40
469	GINS1	-2.84708	5.043659	771.3359	9.21E-170	1.90E-167
470	ZWILCH	-1.62127	5.026318	281.7203	3.17E-63	1.18E-61
471	LIG1	-1.91338	5.034235	286.6422	2.68E-64	1.01E-62
472	RAD54L	-3.46275	5.045544	704.0766	3.88E-155	5.81E-153
473	TYMP	1.257953	4.937592	138.6267	5.32E-32	8.74E-31
474	C20orf72	-1.84753	5.008939	287.6562	1.61E-64	6.08E-63
475	DDB2	-2.00279	5.021673	351.6334	1.87E-78	9.78E-77
476	CDKN2C	-1.84896	5.018923	262.1932	5.71E-59	1.99E-57
477	CEP55	-2.71222	4.997699	490.714	9.96E-109	8.03E-107
478	LBR	-1.38069	4.970888	127.4202	1.50E-29	2.24E-28
479	CCDC14	-1.51614	4.983164	163.7695	1.70E-37	3.29E-36
480	ZNF395	-1.03166	4.954544	106.0548	7.17E-25	8.92E-24
481	C2orf76	1.034981	4.903542	57.65162	3.13E-14	2.12E-13
482	C10orf47	1.017365	4.910119	95.87337	1.22E-22	1.37E-21
483	CLSPN	-3.80621	4.974504	746.4599	2.36E-164	4.47E-162
484	KNTC1	-2.78784	4.965225	618.9634	1.26E-136	1.43E-134

485	DNAJB9	1.724768	4.8996	247.8891	7.49E-56	2.45E-54
486	HIST1H2AC	1.196452	4.885308	91.65938	1.03E-21	1.10E-20
487	PRKCH	1.275291	4.868928	132.4279	1.21E-30	1.88E-29
488	RFC5	-2.38398	4.949173	368.6632	3.66E-82	2.09E-80
489	BCHE	-2.25651	4.92801	361.2371	1.51E-80	8.23E-79
490	USP1	-1.47739	4.921063	167.0937	3.19E-38	6.37E-37
491	LYAR	-1.50544	4.932251	181.5964	2.17E-41	4.77E-40
492	CDCA7L	-2.18438	4.924996	521.7968	1.72E-115	1.56E-113
493	C9orf100	-2.58737	4.944562	502.9781	2.14E-111	1.80E-109
494	DSN1	-1.64178	4.924662	228.1293	1.53E-51	4.55E-50
495	HIST1H2BD	1.566302	4.834448	146.6505	9.36E-34	1.61E-32
496	GINS2	-2.26059	4.922295	331.6574	4.19E-74	1.97E-72
497	SYNJ1	1.018524	4.845336	60.85368	6.15E-15	4.40E-14
498	ATP11A	-1.44176	4.870624	102.0676	5.37E-24	6.39E-23
499	STEAP4	6.927834	4.757507	1233.643	2.98E-270	2.82E-267
500	LUZP2	-1.56074	4.866457	188.7955	5.82E-43	1.34E-41
501	SOCS2	2.464368	4.823498	333.6941	1.51E-74	7.14E-73
502	POLH	-1.43982	4.871978	146.7418	8.94E-34	1.54E-32
503	TNFRSF19	1.533254	4.816737	209.0766	2.18E-47	5.73E-46
504	CDYL2	1.046766	4.821179	70.01139	5.90E-17	4.81E-16
505	MVP	1.144575	4.810926	133.6722	6.44E-31	1.02E-29
506	MYNN	-1.19668	4.842375	120.8719	4.08E-28	5.78E-27
507	NR2C2AP	-1.3963	4.865353	155.1469	1.30E-35	2.39E-34
508	CCDC99	-1.96585	4.875761	290.7999	3.33E-65	1.28E-63
509	ELOVL6	-1.48167	4.847384	200.1887	1.90E-45	4.70E-44
510	E2F3	-1.01918	4.843824	87.62695	7.90E-21	8.12E-20
511	UGT2B28	3.893655	4.738447	744.1228	7.61E-164	1.39E-161
512	FAM101B	-1.3925	4.84779	201.9817	7.72E-46	1.93E-44
513	ZNF18	1.154333	4.817943	146.4863	1.02E-33	1.74E-32
514	MCM10	-4.32466	4.855	744.3193	6.90E-164	1.28E-161
515	FAM198B	-1.66277	4.815321	146.1116	1.23E-33	2.10E-32
516	TRADD	1.31002	4.778269	105.8736	7.86E-25	9.71E-24
517	RAI14	-1.22035	4.817695	105.8037	8.14E-25	1.00E-23
518	UHRF1	-3.61134	4.827836	758.5996	5.41E-167	1.08E-164
519	INPP4B	1.779542	4.737244	206.9816	6.26E-47	1.62E-45
520	C16orf59	-1.75965	4.835931	290.2952	4.29E-65	1.64E-63
521	RAD1	-1.02587	4.794676	98.62368	3.05E-23	3.49E-22

522	KIF18B	-3.75678	4.830277	596.9025	7.90E-132	8.47E-130
523	CDCA2	-2.75471	4.817123	439.4649	1.42E-97	1.02E-95
524	NAT1	2.105876	4.757416	251.384	1.30E-56	4.30E-55
525	LIN7B	1.602485	4.752415	181.8536	1.91E-41	4.20E-40
526	C17orf96	-1.26239	4.767808	111.6182	4.33E-26	5.64E-25
527	MANEA	-1.21951	4.745592	111.0307	5.83E-26	7.56E-25
528	TTF2	-1.38898	4.759101	162.1472	3.84E-37	7.34E-36
529	C21orf58	-2.35905	4.785925	507.6473	2.06E-112	1.76E-110
530	WDHD1	-2.5941	4.763399	611.5602	5.12E-135	5.60E-133
531	ACOX3	1.074054	4.689627	61.81209	3.78E-15	2.75E-14
532	ZNF812	2.544403	4.648766	584.373	4.20E-129	4.38E-127
533	MTHFD1L	-1.11124	4.7318	97.74967	4.75E-23	5.42E-22
534	PUS7	-1.00813	4.693314	68.98917	9.90E-17	7.97E-16
535	MEX3D	-1.08268	4.704777	98.24086	3.70E-23	4.24E-22
536	MEX3A	-1.35255	4.700962	101.3829	7.58E-24	8.95E-23
537	SHCBP1	-2.76888	4.72046	423.2217	4.86E-94	3.41E-92
538	NAT8L	-1.28146	4.682233	73.65812	9.29E-18	7.92E-17
539	MXD3	-1.73475	4.718974	215.1305	1.04E-48	2.82E-47
540	HAUS6	-1.36579	4.67344	131.8728	1.60E-30	2.47E-29
541	BAHCC1	-1.01076	4.676828	61.13839	5.32E-15	3.83E-14
542	POLA1	-1.59616	4.684699	200.1805	1.91E-45	4.71E-44
543	TUBGCP3	-1.17059	4.680888	117.0667	2.78E-27	3.81E-26
544	SUV39H1	-1.65967	4.690893	231.6669	2.58E-52	7.82E-51
545	RFWD3	-2.07941	4.677295	226.5095	3.44E-51	1.01E-49
546	KIF23	-2.97371	4.685966	651.689	9.59E-144	1.21E-141
547	BMPR1A	1.150621	4.60637	92.87615	5.57E-22	6.03E-21
548	ORC6	-3.34711	4.683425	674.5864	1.01E-148	1.36E-146
549	PIGW	-1.24672	4.638507	130.511	3.17E-30	4.87E-29
550	PLK2	-1.41448	4.671327	128.4041	9.16E-30	1.37E-28
551	POLQ	-3.26326	4.655492	385.0002	1.01E-85	6.41E-84
552	RBBP8	-1.76981	4.640005	216.371	5.60E-49	1.53E-47
553	NUF2	-2.40672	4.651253	301.1723	1.83E-67	7.45E-66
554	NEK2	-2.46444	4.648609	341.503	3.00E-76	1.46E-74
555	PRIM2	-1.14901	4.629397	81.60635	1.66E-19	1.58E-18
556	PSMC3IP	-2.44706	4.631968	347.0801	1.83E-77	9.30E-76
557	DTL	-4.49669	4.61236	954.0361	1.76E-209	5.71E-207

558	CDCA4	-2.9533	4.610723	479.5007	2.74E-106	2.12E-104
559	CDC7	-2.0867	4.595561	309.8759	2.32E-69	9.97E-68
560	MRE11A	-1.08835	4.584518	75.07879	4.52E-18	3.92E-17
561	TUBA3D	2.335066	4.537442	380.21	1.12E-84	6.81E-83
562	SKA3	-2.30676	4.585329	330.5552	7.28E-74	3.37E-72
563	STIL	-2.05411	4.582942	248.6831	5.03E-56	1.65E-54
564	LAMA1	2.261857	4.505519	404.8368	4.88E-90	3.24E-88
565	VRK1	-1.63239	4.572572	256.6143	9.39E-58	3.17E-56
566	TARBP1	-1.0655	4.544414	89.33701	3.33E-21	3.50E-20
567	CABLES2	-1.25456	4.561123	133.9291	5.66E-31	8.98E-30
568	OAS3	-2.25464	4.56786	240.3174	3.35E-54	1.06E-52
569	PCTP	1.26239	4.519361	134.8077	3.64E-31	5.79E-30
570	TMEM194A	-2.42661	4.547988	352.4024	1.27E-78	6.72E-77
571	UACA	-1.14131	4.536448	68.28635	1.41E-16	1.13E-15
572	CCDC34	-1.26032	4.551422	70.07553	5.71E-17	4.66E-16
573	PVT1	-1.13798	4.528861	86.51544	1.39E-20	1.40E-19
574	MAPK11	1.126087	4.475094	84.29218	4.27E-20	4.19E-19
575	PRKX	-1.16917	4.511738	68.34921	1.37E-16	1.09E-15
576	SEC14L2	2.358778	4.44341	309.6495	2.60E-69	1.11E-67
577	PAQR6	1.064693	4.495225	64.28098	1.08E-15	8.16E-15
578	NDE1	-1.15307	4.505692	91.76889	9.74E-22	1.05E-20
579	DUSP1	1.116623	4.459056	81.90146	1.43E-19	1.36E-18
580	SLC25A19	-1.84023	4.490555	291.9924	1.83E-65	7.10E-64
581	RIF1	-1.18942	4.470228	77.44654	1.36E-18	1.23E-17
582	ANP32E	-1.16421	4.482062	68.30151	1.40E-16	1.12E-15
583	SKP2	-2.16685	4.483818	276.831	3.68E-62	1.33E-60
584	ACD	-1.00083	4.491429	57.18785	3.96E-14	2.67E-13
585	KRT19	1.52064	4.433102	106.5317	5.64E-25	7.06E-24
586	CD3EAP	-1.20903	4.461233	106.5053	5.71E-25	7.14E-24
587	ID2	1.114766	4.451093	86.96935	1.10E-20	1.12E-19
588	DCK	-1.36039	4.467973	79.68538	4.39E-19	4.07E-18
589	ADCY3	-1.26148	4.462304	71.77503	2.41E-17	2.02E-16
590	CEP57	-1.02447	4.45679	63.1173	1.95E-15	1.45E-14
591	CHEK1	-2.67607	4.48128	307.0872	9.41E-69	3.93E-67
592	HAUS1	-1.45359	4.484391	152.0858	6.07E-35	1.09E-33
593	TARP	2.0082	4.394865	293.1411	1.03E-65	4.00E-64
594	BTG3	-1.44741	4.458835	139.2849	3.82E-32	6.29E-31
595	ORAI3	1.406972	4.385888	129.0624	6.57E-30	9.92E-29
596	GUSBP1	-1.70377	4.420452	204.5126	2.16E-46	5.51E-45
597	RCCD1	-1.22891	4.442964	125.0822	4.88E-29	7.16E-28
598	FAM107B	-1.1013	4.418613	72.64276	1.55E-17	1.31E-16

599	YEATS4	-1.37125	4.4016	89.13679	3.68E-21	3.87E-20
600	GINS4	-2.83117	4.410119	370.9958	1.14E-82	6.59E-81
601	LOC100132247	-1.22548	4.371449	5.883853	0.01528	0.027177
602	FANCC	-1.8619	4.390391	189.7382	3.63E-43	8.41E-42
603	DBF4B	-2.06223	4.401455	256.8599	8.30E-58	2.81E-56
604	CCDC141	2.787908	4.324552	174.0387	9.71E-40	2.04E-38
605	SH2D3A	1.225514	4.317489	91.76856	9.74E-22	1.05E-20
606	DBF4	-1.85695	4.362105	207.1958	5.62E-47	1.45E-45
607	RAD18	-1.16233	4.356835	86.0776	1.73E-20	1.73E-19
608	CSPG5	-1.06289	4.354519	90.54889	1.80E-21	1.92E-20
609	SH3BP1	-1.06124	4.359435	70.7006	4.16E-17	3.42E-16
610	MIR22HG	1.593397	4.321499	179.503	6.22E-41	1.34E-39
611	DEPDC1B	-2.69309	4.373182	344.0621	8.32E-77	4.15E-75
612	PRSS16	1.029776	4.309015	57.0447	4.26E-14	2.86E-13
613	BMPR1B	1.288273	4.299067	90.54056	1.81E-21	1.93E-20
614	GCNT2	1.101548	4.295841	61.31621	4.86E-15	3.50E-14
615	HAUS7	-1.16574	4.337564	42.28691	7.88E-11	4.11E-10
616	FGD4	1.577784	4.287323	111.3836	4.88E-26	6.33E-25
617	TEAD4	-1.08412	4.32635	68.56459	1.23E-16	9.84E-16
618	ORC1	-2.92149	4.352869	384.9004	1.07E-85	6.70E-84
619	TRIM52	1.313995	4.273618	112.1945	3.24E-26	4.24E-25
620	RMI1	-1.514	4.316916	102.4814	4.35E-24	5.21E-23
621	SPC24	-2.63448	4.336883	372.2121	6.17E-83	3.64E-81
622	ZFAND2A	1.068566	4.277248	72.57435	1.61E-17	1.36E-16
623	POLD3	-1.93025	4.315872	212.8788	3.23E-48	8.69E-47
624	WEE1	-2.12736	4.312252	174.0315	9.74E-40	2.04E-38
625	IL10RB	1.10843	4.257556	97.425	5.59E-23	6.33E-22
626	DST	-1.04814	4.306202	32.04447	1.51E-08	6.38E-08
627	NRM	-1.93358	4.31834	198.1546	5.28E-45	1.29E-43
628	EME1	-3.06517	4.314727	346.9957	1.91E-77	9.66E-76
629	RFC3	-2.85784	4.302175	320.0803	1.39E-71	6.18E-70
630	TMEM237	-1.63188	4.288242	191.3249	1.63E-43	3.83E-42
631	TRERF1	-1.22385	4.251048	74.02023	7.73E-18	6.64E-17
632	FIGNL1	-2.51617	4.277732	225.5112	5.68E-51	1.66E-49
633	ASPM	-3.05577	4.279402	223.4129	1.63E-50	4.64E-49
634	CCNE1	-1.48767	4.267012	166.8232	3.66E-38	7.26E-37
635	ZNF43	-1.08378	4.256483	75.80417	3.13E-18	2.76E-17
636	ZNF385B	1.068493	4.22953	69.82443	6.48E-17	5.28E-16
637	CDC25C	-2.27893	4.290442	264.1282	2.16E-59	7.58E-58
638	URB2	-1.11889	4.236503	38.19154	6.41E-10	3.10E-09
639	ANKRD37	2.81022	4.170971	283.5484	1.27E-63	4.73E-62
640	DIAPH3	-2.22925	4.25633	369.7869	2.08E-82	1.20E-80

641	TTK	-2.90284	4.256631	311.6591	9.50E-70	4.11E-68
642	ANO7	1.582033	4.185993	108.8021	1.79E-25	2.30E-24
643	ERN1	1.068375	4.156414	25.92961	3.54E-07	1.29E-06
644	G2E3	-1.24851	4.193824	60.09737	9.03E-15	6.40E-14
645	CHEK2	-2.14126	4.214408	301.1367	1.86E-67	7.56E-66
646	AJUBA	-1.16244	4.188373	94.40761	2.57E-22	2.81E-21
647	TNFRSF21	-1.02892	4.174664	66.25842	3.96E-16	3.06E-15
648	FICD	1.800882	4.140731	199.2631	3.02E-45	7.41E-44
649	APLN	-1.2229	4.181197	96.93863	7.15E-23	8.06E-22
650	ISG20	1.287618	4.128919	78.58197	7.67E-19	7.03E-18
651	MFHAS1	-1.02568	4.160037	58.37976	2.16E-14	1.49E-13
652	HNRNPU-AS1	-1.19214	4.163327	101.998	5.56E-24	6.61E-23
653	C1orf112	-1.62682	4.174699	153.3047	3.29E-35	5.98E-34
654	LRR1	-1.19925	4.168088	114.8618	8.44E-27	1.14E-25
655	RAB27A	1.065875	4.133523	59.69147	1.11E-14	7.81E-14
656	AGR2	1.385475	4.086989	87.89266	6.91E-21	7.15E-20
657	MIS18A	-1.9019	4.160942	175.9537	3.71E-40	7.84E-39
658	GPSM2	-2.34426	4.158148	244.1555	4.88E-55	1.57E-53
659	PARVA	1.101712	4.083544	73.80191	8.64E-18	7.37E-17
660	SGK1	2.090041	4.126749	152.5369	4.84E-35	8.72E-34
661	ERCC6L	-2.15891	4.124497	131.4457	1.98E-30	3.06E-29
662	SGOL2	-2.27281	4.126562	258.6919	3.31E-58	1.14E-56
663	KDM5B-AS1	1.06292	4.077932	57.56826	3.26E-14	2.21E-13
664	CEP78	-1.87971	4.117113	172.2264	2.41E-39	5.01E-38
665	PHTF2	-1.2045	4.090515	59.43018	1.27E-14	8.87E-14
666	PDSS1	-1.36548	4.099026	128.4645	8.88E-30	1.33E-28
667	MERTK	2.4027	4.034444	217.7853	2.75E-49	7.57E-48
668	PSCA	1.005194	4.080927	60.38523	7.80E-15	5.54E-14
669	KIF20B	-2.91237	4.10426	356.1447	1.95E-79	1.04E-77
670	CENPH	-1.60544	4.09512	154.3255	1.97E-35	3.60E-34
671	EXO1	-4.22236	4.094591	631.448	2.42E-139	2.90E-137
672	NEDD1	-1.27383	4.062327	68.38542	1.34E-16	1.07E-15
673	MASTL	-1.77061	4.07329	161.707	4.79E-37	9.10E-36
674	TMEM150A	1.039055	4.032263	77.84202	1.12E-18	1.01E-17
675	A1BG	1.398434	4.026405	41.66666	1.08E-10	5.57E-10
676	HSPG2	-1.09465	4.046511	77.21183	1.54E-18	1.38E-17
677	ACACB	-1.32703	4.04808	62.16556	3.16E-15	2.31E-14
678	SLC5A3	-1.34694	4.027646	47.76811	4.80E-12	2.78E-11
679	NEURL1B	-1.66536	4.042715	126.2141	2.76E-29	4.08E-28
680	SKA1	-2.95702	4.036338	348.6993	8.14E-78	4.18E-76
681	C1orf96	-1.62557	4.011396	118.7362	1.20E-27	1.67E-26

682	QSER1	-1.19693	3.992907	76.32404	2.41E-18	2.15E-17
683	C11orf82	-2.4944	4.00667	188.4001	7.11E-43	1.63E-41
684	TIPARP	2.133877	3.963071	165.3256	7.77E-38	1.51E-36
685	PIF1	-2.52455	4.027417	217.1512	3.78E-49	1.04E-47
686	C15orf42	-3.64515	4.010447	410.3408	3.09E-91	2.09E-89
687	SLITRK3	-2.73803	3.984061	351.9018	1.63E-78	8.59E-77
688	RELL2	1.165997	3.956934	56.75353	4.94E-14	3.30E-13
689	CEP85	-1.24208	3.990531	54.28541	1.73E-13	1.11E-12
690	C9orf40	-1.6649	3.979057	142.6632	6.96E-33	1.18E-31
691	FAM123B	-1.16898	3.947375	50.20149	1.39E-12	8.42E-12
692	PLK4	-2.60187	3.956852	219.7499	1.03E-49	2.86E-48
693	KIF15	-3.3208	3.955213	424.9456	2.05E-94	1.44E-92
694	HERC5	1.284517	3.886767	130.0925	3.91E-30	5.97E-29
695	DCLRE1B	-2.14993	3.928038	234.2715	6.98E-53	2.17E-51
696	RASD1	2.236472	3.863466	169.5251	9.40E-39	1.92E-37
697	PLEKHA7	-1.03048	3.912357	43.92	3.42E-11	1.85E-10
698	FBXO5	-2.25191	3.919201	200.8726	1.35E-45	3.35E-44
699	DFFB	-1.03534	3.895758	42.13086	8.54E-11	4.44E-10
700	DEFB132	1.299497	3.856532	81.5667	1.69E-19	1.61E-18
701	SERTAD1	1.155962	3.876137	62.81318	2.27E-15	1.68E-14
702	C17orf107	1.615546	3.823275	156.3913	6.95E-36	1.29E-34
703	CDH26	-1.22118	3.859626	70.65852	4.25E-17	3.49E-16
704	MYCL1	1.088066	3.837652	56.65464	5.19E-14	3.46E-13
705	CCP110	-1.34822	3.860193	80.912	2.36E-19	2.22E-18
706	HIST1H2BC	1.438715	3.811325	76.83254	1.86E-18	1.67E-17
707	SDC4	-1.41598	3.854239	124.185	7.67E-29	1.12E-27
708	STXBP5L	-1.379	3.84011	118.6546	1.25E-27	1.73E-26
709	NCOA7	-1.06508	3.840618	52.72481	3.84E-13	2.42E-12
710	PRIM1	-2.7987	3.862068	274.9707	9.37E-62	3.35E-60
711	FANCE	-1.44336	3.857833	118.6963	1.22E-27	1.70E-26
712	RAD51AP1	-3.10514	3.858318	311.8686	8.55E-70	3.71E-68
713	TIPIN	-1.37836	3.843579	73.74915	8.87E-18	7.57E-17
714	SLC7A2	-1.75815	3.830496	86.37052	1.49E-20	1.50E-19
715	KIF24	-2.95619	3.858929	303.4058	5.97E-68	2.45E-66
716	OIP5	-2.26235	3.853208	230.1571	5.51E-52	1.65E-50
717	FAM176B	1.516353	3.800912	89.7365	2.72E-21	2.87E-20
718	DUSP9	-1.16083	3.809888	58.29823	2.25E-14	1.55E-13
719	HAUS8	-2.79464	3.827204	310.7765	1.48E-69	6.37E-68
720	TRAIP	-2.20067	3.817425	180.5902	3.60E-41	7.87E-40
721	TTN	2.614608	3.775705	258.7871	3.15E-58	1.09E-56
722	WNT10B	-1.14977	3.778618	90.63025	1.73E-21	1.84E-20
723	SUV39H2	-1.60642	3.784435	135.8789	2.12E-31	3.42E-30

724	B3GALT4	2.832441	3.720288	328.9995	1.59E-73	7.27E-72
725	SMC6	-1.5804	3.776707	82.32832	1.15E-19	1.10E-18
726	DPYSL2	-1.26224	3.758385	59.14969	1.46E-14	1.02E-13
727	IQCC	-1.51402	3.759863	116.9337	2.97E-27	4.07E-26
728	FLJ41484	-1.5235	3.741278	84.19088	4.49E-20	4.40E-19
729	GINS3	-1.73824	3.756026	119.3809	8.64E-28	1.21E-26
730	RAD51	-2.98367	3.756982	395.1846	6.15E-88	4.00E-86
731	MNS1	-2.44062	3.749475	184.9116	4.10E-42	9.25E-41
732	LOC728554	-1.30577	3.73998	107.1871	4.05E-25	5.11E-24
733	LOC219347	-1.01781	3.749536	48.77995	2.86E-12	1.69E-11
734	E2F2	-3.57466	3.755456	479.6686	2.52E-106	1.96E-104
735	CTDSPL2	-1.27314	3.720102	44.89663	2.08E-11	1.14E-10
736	SLC27A2	-1.61449	3.725654	128.8359	7.37E-30	1.11E-28
737	SH3D21	2.647745	3.671158	234.1186	7.54E-53	2.34E-51
738	KIAA1524	-2.11234	3.73011	165.4529	7.28E-38	1.42E-36
739	SPC25	-2.5445	3.737694	215.2429	9.86E-49	2.67E-47
740	GSTCD	-1.99654	3.706872	143.8889	3.76E-33	6.39E-32
741	LRCH1	1.206261	3.675248	44.32163	2.79E-11	1.51E-10
742	SYBU	-1.16677	3.678905	66.81248	2.99E-16	2.33E-15
743	HIST1H4H	1.486856	3.628909	48.00753	4.25E-12	2.47E-11
744	KIF14	-2.71377	3.700978	226.7791	3.00E-51	8.92E-50
745	PRKD3	-1.19138	3.679304	69.00198	9.84E-17	7.93E-16
746	TBX15	2.031142	3.649352	186.9746	1.45E-42	3.31E-41
747	ESCO2	-3.55128	3.678045	255.0783	2.03E-57	6.78E-56
748	ORM1	4.646724	3.584169	558.3566	1.91E-123	1.91E-121
749	CASC5	-3.54596	3.668182	281.3416	3.83E-63	1.41E-61
750	ZFP36L2	-1.40277	3.646974	107.2857	3.85E-25	4.87E-24
751	BRI3BP	-1.04553	3.644973	38.75384	4.81E-10	2.35E-09
752	CA12	-1.41513	3.646291	119.7792	7.07E-28	9.95E-27
753	CCNE2	-3.26585	3.647541	258.1389	4.37E-58	1.49E-56
754	NRGN	-1.17895	3.657298	49.72338	1.77E-12	1.07E-11
755	JDP2	-1.15876	3.63517	58.98903	1.59E-14	1.10E-13
756	CSGALNACT1	3.40068	3.570962	363.437	5.03E-81	2.80E-79
757	KHK	-1.37881	3.631483	61.99874	3.44E-15	2.51E-14
758	ERI1	-1.72734	3.606816	160.2264	1.01E-36	1.91E-35
759	MMP16	-2.2333	3.620427	137.2339	1.07E-31	1.75E-30
760	CHML	-1.2323	3.599155	44.99648	1.97E-11	1.09E-10
761	HPGD	2.109722	3.546501	143.4881	4.60E-33	7.81E-32
762	WDR67	-1.25399	3.621995	55.63943	8.71E-14	5.72E-13
763	PARPBP	-2.4475	3.618575	156.3664	7.04E-36	1.30E-34
764	NUP35	-1.19488	3.598997	66.57558	3.37E-16	2.62E-15

765	DSCC1	-2.13346	3.614539	182.6449	1.28E-41	2.85E-40
766	SLC15A2	1.385816	3.573008	87.0846	1.04E-20	1.06E-19
767	KLF5	1.288376	3.562063	62.57721	2.56E-15	1.89E-14
768	IL17RB	-1.99178	3.581358	160.1375	1.06E-36	1.99E-35
769	ENPP1	-1.21258	3.559328	62.39313	2.81E-15	2.06E-14
770	SPTBN4	1.395943	3.522144	108.7891	1.81E-25	2.31E-24
771	LAT2	2.427611	3.494342	149.5321	2.19E-34	3.90E-33
772	ORM2	4.097867	3.458973	353.356	7.88E-79	4.18E-77
773	SNHG12	-1.30454	3.53138	75.89123	3.00E-18	2.65E-17
774	CENPL	-1.79845	3.539967	99.88182	1.62E-23	1.88E-22
775	HSPA4L	-1.67534	3.524468	59.37183	1.31E-14	9.13E-14
776	LRRN1	-1.61001	3.495236	76.19264	2.57E-18	2.29E-17
777	BARD1	-2.55148	3.507466	129.8716	4.37E-30	6.65E-29
778	KCNQ4	-1.01167	3.498545	33.61509	6.72E-09	2.94E-08
779	CAMK2B	-1.14934	3.51744	58.65534	1.88E-14	1.30E-13
780	CKAP2L	-2.74072	3.497197	218.0685	2.39E-49	6.58E-48
781	EXPH5	-1.15146	3.457627	52.61518	4.06E-13	2.55E-12
782	CECR6	2.186917	3.43316	78.76437	7.00E-19	6.42E-18
783	LOC100128191	-2.64894	3.508863	224.3989	9.93E-51	2.86E-49
784	HS3ST1	1.066131	3.47225	54.76213	1.36E-13	8.81E-13
785	NT5C3	-1.00783	3.470744	34.14562	5.11E-09	2.27E-08
786	OSGEPL1	-1.16074	3.469654	51.25061	8.13E-13	5.03E-12
787	C14orf132	-1.01481	3.467186	35.43416	2.64E-09	1.20E-08
788	HAUS3	-1.43001	3.459513	101.3935	7.54E-24	8.91E-23
789	CDC14B	1.323304	3.421135	65.15301	6.93E-16	5.31E-15
790	TAF5	-1.16492	3.458455	55.89393	7.65E-14	5.05E-13
791	SGOL1	-2.76634	3.475341	261.1823	9.48E-59	3.29E-57
792	KLF10	-1.1361	3.443025	62.58935	2.55E-15	1.88E-14
793	ADCY1	-1.64174	3.444643	130.4402	3.28E-30	5.03E-29
794	ZNF107	-1.66983	3.428667	96.52452	8.81E-23	9.90E-22
795	RNF43	-1.28268	3.445817	63.50381	1.60E-15	1.19E-14
796	RMI2	-3.02067	3.453655	276.6049	4.13E-62	1.49E-60
797	ZAK	-1.94421	3.440323	118.3677	1.44E-27	1.99E-26
798	CENPA	-2.92953	3.460974	297.4671	1.17E-66	4.68E-65
799	APOBEC3B	-1.35257	3.444421	85.66577	2.13E-20	2.13E-19
800	DDX12P	-2.2256	3.44998	158.0284	3.05E-36	5.68E-35
801	KLF4	1.189636	3.388472	52.24152	4.91E-13	3.07E-12
802	TRIM59	-1.45269	3.408551	122.5707	1.73E-28	2.50E-27
803	VLDLR	1.481824	3.381713	115.8754	5.06E-27	6.88E-26
804	DONSON	-2.00066	3.413257	158.1582	2.86E-36	5.33E-35
805	SWT1	1.644071	3.366704	73.42668	1.04E-17	8.88E-17
806	DNA2	-2.76689	3.405734	150.8371	1.14E-34	2.03E-33

807	LIN54	-1.04281	3.402325	31.36063	2.14E-08	8.94E-08
808	GEN1	-1.9078	3.395221	136.0877	1.91E-31	3.08E-30
809	EPB41L2	-1.04174	3.39408	52.91812	3.48E-13	2.19E-12
810	FAM134B	-1.29243	3.367858	58.6655	1.87E-14	1.29E-13
811	E2F8	-3.81998	3.392733	317.5903	4.85E-71	2.15E-69
812	ZNF367	-4.32813	3.380485	299.4173	4.41E-67	1.77E-65
813	NNMT	1.047581	3.347602	41.63383	1.10E-10	5.66E-10
814	ZNF100	-1.04783	3.352851	24.02709	9.50E-07	3.32E-06
815	ABCG1	1.105241	3.311829	28.89807	7.63E-08	3.02E-07
816	BLM	-3.41356	3.366816	279.0465	1.21E-62	4.43E-61
817	SPATA5	-1.32015	3.348486	71.99	2.16E-17	1.81E-16
818	GSG2	-3.4629	3.364504	362.7189	7.20E-81	3.99E-79
819	SNHG4	-1.14853	3.330395	57.11487	4.11E-14	2.77E-13
820	SLC6A6	-1.40983	3.336926	52.14168	5.16E-13	3.23E-12
821	PRKY	-1.60872	3.323492	99.28248	2.19E-23	2.53E-22
822	CENPJ	-1.85117	3.341224	63.57473	1.54E-15	1.15E-14
823	NKPD1	1.02814	3.292974	34.08192	5.28E-09	2.34E-08
824	ANKRD32	-1.16676	3.32541	38.79946	4.70E-10	2.29E-09
825	ZIK1	-1.29188	3.317349	87.37181	8.99E-21	9.22E-20
826	SCLT1	-1.33599	3.308964	73.59365	9.60E-18	8.18E-17
827	CRISPLD2	2.077797	3.259313	107.2989	3.83E-25	4.85E-24
828	C17orf48	1.018594	3.271453	37.04864	1.15E-09	5.42E-09
829	SASS6	-1.95293	3.282375	115.6829	5.58E-27	7.56E-26
830	LRRCC1	-1.39311	3.277272	51.58085	6.87E-13	4.26E-12
831	COLEC12	-1.32371	3.262694	86.10465	1.71E-20	1.71E-19
832	MND1	-3.12209	3.307658	199.8417	2.26E-45	5.55E-44
833	DNMT3B	-1.44814	3.284436	76.21404	2.55E-18	2.27E-17
834	PKIB	-1.07747	3.267757	49.06057	2.48E-12	1.48E-11
835	C18orf56	-1.22464	3.292778	39.3162	3.60E-10	1.78E-09
836	CDH24	-1.19277	3.281354	44.90404	2.07E-11	1.14E-10
837	ADAT2	-1.02294	3.251893	37.47591	9.25E-10	4.41E-09
838	TRNP1	-1.25211	3.254968	44.57074	2.45E-11	1.34E-10
839	CCDC15	-1.00268	3.260078	33.55018	6.94E-09	3.04E-08
840	SLC2A3	4.014408	3.21207	331.2792	5.06E-74	2.37E-72
841	KIAA1656	1.186426	3.234862	50.09021	1.47E-12	8.89E-12
842	NEIL3	-3.04605	3.264715	255.398	1.73E-57	5.80E-56
843	MAPRE2	-1.00429	3.23097	49.70027	1.79E-12	1.08E-11
844	LRRC37A4	-1.16917	3.225988	40.99446	1.53E-10	7.78E-10
845	LOC401431	-1.08407	3.196361	38.23166	6.28E-10	3.04E-09
846	C4orf46	-3.12073	3.184868	187.1242	1.35E-42	3.07E-41
847	WDR76	-2.68684	3.182243	224.8671	7.85E-51	2.29E-49
848	ANG	1.814142	3.110239	102.8918	3.54E-24	4.26E-23

849	OPTN	1.691043	3.098588	105.9395	7.60E-25	9.41E-24
850	CEP152	-2.1307	3.15379	94.95323	1.95E-22	2.15E-21
851	RBL1	-2.58173	3.150147	110.088	9.37E-26	1.21E-24
852	TMEM107	-1.16554	3.156484	43.78547	3.66E-11	1.97E-10
853	TRPV1	-1.04874	3.148863	34.01874	5.46E-09	2.41E-08
854	NOC3L	-1.00389	3.126805	58.27829	2.28E-14	1.56E-13
855	ARMC12	2.123023	3.118034	143.9772	3.59E-33	6.12E-32
856	RELL1	-1.27884	3.118836	50.25672	1.35E-12	8.23E-12
857	SNAI2	2.481717	3.122005	204.8473	1.83E-46	4.68E-45
858	TEX30	-1.4719	3.122972	64.3744	1.03E-15	7.80E-15
859	XRCC2	-3.57366	3.10956	315.5248	1.37E-70	6.00E-69
860	BEND3	-1.3985	3.096632	64.15968	1.15E-15	8.66E-15
861	PTPRN2	2.082654	3.083282	176.1122	3.42E-40	7.26E-39
862	BRCA2	-3.54997	3.112857	295.2399	3.59E-66	1.42E-64
863	POLR3G	-1.45319	3.092283	70.21691	5.31E-17	4.35E-16
864	HELLS	-3.3891	3.100935	162.3502	3.47E-37	6.64E-36
865	PART1	1.712935	3.060102	77.45019	1.36E-18	1.23E-17
866	CDCA7	-3.07772	3.091576	202.5467	5.81E-46	1.46E-44
867	SLC45A1	1.032657	3.046409	39.69559	2.97E-10	1.48E-09
868	KIAA1211	-1.41924	3.092965	57.84276	2.84E-14	1.93E-13
869	LOC642846	-2.5479	3.100182	114.2246	1.16E-26	1.57E-25
870	NR1D1	-1.21055	3.063159	49.29168	2.21E-12	1.32E-11
871	SLC31A2	1.143838	3.039866	39.33853	3.56E-10	1.76E-09
872	PER2	-1.27893	3.059703	42.4396	7.29E-11	3.82E-10
873	CASP8AP2	-1.132	3.045985	34.18097	5.02E-09	2.23E-08
874	FAM178A	-1.261	3.030438	44.4955	2.55E-11	1.39E-10
875	CLDN8	1.161157	3.026854	59.4506	1.25E-14	8.79E-14
876	ODF3B	1.054682	3.018693	45.6125	1.44E-11	8.00E-11
877	LOC100129480	1.568523	2.993878	57.22885	3.88E-14	2.62E-13
878	CEP128	-2.23337	3.035504	123.0141	1.38E-28	2.00E-27
879	C16orf55	-1.27736	3.024729	51.41188	7.49E-13	4.64E-12
880	CHRNA5	-1.24955	3.008231	57.56419	3.27E-14	2.22E-13
881	CEP68	-1.2034	2.994158	46.65497	8.47E-12	4.79E-11
882	ABTB1	1.586115	2.970268	107.5077	3.45E-25	4.38E-24
883	RNASE4	1.730216	2.948282	60.43789	7.59E-15	5.40E-14
884	S100P	2.105736	2.925508	96.50694	8.89E-23	9.98E-22
885	MMS22L	-2.38191	3.000201	117.5078	2.22E-27	3.06E-26
886	FANCM	-1.23901	2.987179	49.32213	2.17E-12	1.30E-11
887	NHSL1	-1.06838	2.98745	34.67221	3.90E-09	1.75E-08
888	SPATA18	-1.43826	2.974484	69.01939	9.75E-17	7.86E-16
889	ZNF704	-1.00002	2.96406	28.36926	1.00E-07	3.90E-07
890	PTGER4	1.524584	2.933251	54.94859	1.24E-13	8.03E-13

891	C1QTNF9B-AS1	2.154137	2.922719	113.8169	1.43E-26	1.92E-25
892	CCDC18	-1.80017	2.956273	63.77814	1.39E-15	1.04E-14
893	MTMR11	1.026313	2.937255	21.65315	3.27E-06	1.06E-05
894	E2F7	-4.91385	2.942007	247.2552	1.03E-55	3.34E-54
895	AKAP12	2.532329	2.863866	121.4501	3.05E-28	4.36E-27
896	CENPI	-3.01173	2.932829	251.4544	1.25E-56	4.16E-55
897	ALOXE3	-1.08352	2.913425	36.00663	1.97E-09	9.07E-09
898	CAMK2D	-1.55716	2.911014	80.60872	2.75E-19	2.58E-18
899	ZNF551	-1.54863	2.898383	62.83916	2.24E-15	1.66E-14
900	CENPK	-3.0927	2.918185	154.9931	1.41E-35	2.58E-34
901	ALG10B	-1.09698	2.904789	31.75831	1.75E-08	7.35E-08
902	SORL1	-1.73064	2.907479	82.575	1.02E-19	9.78E-19
903	AZGP1P1	1.403957	2.87277	58.04092	2.57E-14	1.75E-13
904	DOK3	-1.19857	2.904108	26.44425	2.71E-07	1.01E-06
905	ZNF850	-1.43981	2.877071	58.69405	1.84E-14	1.27E-13
906	HIST1H2BG	1.137454	2.850955	14.86339	0.000116	0.000304
907	PAG1	-1.88583	2.895752	81.31123	1.93E-19	1.82E-18
908	FAM40B	-1.56009	2.899425	66.90838	2.84E-16	2.23E-15
909	POLE2	-2.15642	2.88688	67.75599	1.85E-16	1.46E-15
910	C16orf7	1.233663	2.858755	45.09093	1.88E-11	1.04E-10
911	SCML2	-2.04179	2.881585	117.5708	2.15E-27	2.97E-26
912	ADAM22	-1.36209	2.873116	45.25893	1.73E-11	9.55E-11
913	CEP57L1	-1.37994	2.870672	46.51872	9.07E-12	5.11E-11
914	TMCC3	2.885206	2.843765	167.1876	3.04E-38	6.09E-37
915	LIN9	-2.98293	2.863285	172.5152	2.09E-39	4.35E-38
916	AUTS2	-1.69129	2.864932	86.86803	1.16E-20	1.18E-19
917	SORBS2	-1.56091	2.85289	78.51926	7.92E-19	7.25E-18
918	LOC730101	-1.37135	2.832468	75.19295	4.27E-18	3.72E-17
919	SNX16	1.058401	2.809404	25.65605	4.08E-07	1.48E-06
920	SOX8	-1.52318	2.821924	63.5696	1.55E-15	1.16E-14
921	CENPQ	-2.06973	2.832032	102.4547	4.41E-24	5.27E-23
922	PLXDC2	1.159774	2.807117	47.19046	6.44E-12	3.68E-11
923	KIF18A	-2.58675	2.830089	132.4496	1.19E-30	1.86E-29
924	BRIP1	-3.62238	2.817232	209.6381	1.65E-47	4.34E-46
925	KDELC1	-1.19361	2.78665	47.68966	4.99E-12	2.89E-11
926	HSD17B11	1.36911	2.747794	53.85517	2.16E-13	1.38E-12
927	PTPRCAP	1.180093	2.765529	15.88675	6.72E-05	0.000183
928	ZMYM1	-1.20525	2.77071	26.19817	3.08E-07	1.13E-06
929	SERPINI1	-1.30872	2.778014	44.85772	2.12E-11	1.16E-10
930	LOC100288637	-2.51647	2.787301	95.18491	1.73E-22	1.92E-21
931	FAM86B1	-1.08404	2.747808	39.62318	3.08E-10	1.53E-09

932	DPYSL5	-1.27905	2.748075	30.95906	2.64E-08	1.09E-07
933	NANP	-1.35702	2.750439	40.8687	1.63E-10	8.28E-10
934	ZNF530	-1.69082	2.748085	75.36687	3.91E-18	3.42E-17
935	FAM69A	1.22512	2.717053	32.20534	1.39E-08	5.89E-08
936	KLF11	-1.54491	2.741484	46.76429	8.01E-12	4.55E-11
937	AMACR	2.005658	2.704537	66.28415	3.90E-16	3.03E-15
938	SRCIN1	-1.58181	2.725143	84.74002	3.40E-20	3.37E-19
939	ZNF124	-1.45314	2.735325	47.93472	4.41E-12	2.56E-11
940	ENO2	-1.49626	2.725995	49.35197	2.14E-12	1.28E-11
941	LOC100506469	-1.02567	2.717116	28.40661	9.83E-08	3.83E-07
942	RELT	-2.53494	2.732905	65.19319	6.79E-16	5.20E-15
943	RTKN2	-2.06478	2.716191	94.11113	2.98E-22	3.26E-21
944	RNF219	-1.00003	2.694821	23.15978	1.49E-06	5.07E-06
945	DPF1	-1.24215	2.71074	47.67369	5.03E-12	2.91E-11
946	GLDC	-1.13095	2.691858	39.18088	3.86E-10	1.90E-09
947	NUAK2	-1.70525	2.692936	62.80441	2.28E-15	1.69E-14
948	DENND5B	-1.17903	2.673064	37.88917	7.49E-10	3.60E-09
949	PLK3	-1.45445	2.672837	73.33306	1.10E-17	9.30E-17
950	SLMO1	-1.08521	2.67575	37.99684	7.09E-10	3.42E-09
951	ZNF93	-1.11103	2.671161	34.28057	4.77E-09	2.12E-08
952	KHDRBS3	-1.15034	2.672515	25.4356	4.57E-07	1.65E-06
953	LIMD2	1.271281	2.63981	49.16096	2.36E-12	1.41E-11
954	CEP97	-1.05388	2.653911	24.20318	8.67E-07	3.04E-06
955	RTTN	-1.63953	2.656886	71.61399	2.62E-17	2.18E-16
956	ESPN	-1.08073	2.646307	32.31347	1.31E-08	5.59E-08
957	IER5	-1.89334	2.65326	84.15907	4.57E-20	4.47E-19
958	TAF4B	-1.32777	2.630413	39.20987	3.81E-10	1.87E-09
959	C17orf53	-2.47448	2.658987	124.9219	5.29E-29	7.74E-28
960	HLF	-1.60576	2.636684	95.70296	1.33E-22	1.49E-21
961	EPS8L1	2.620432	2.587459	90.74023	1.64E-21	1.75E-20
962	CBLN2	-1.92761	2.632524	96.20168	1.04E-22	1.16E-21
963	CPEB3	1.213971	2.58833	36.86618	1.27E-09	5.92E-09
964	FCHSD1	1.253142	2.608096	33.80884	6.08E-09	2.67E-08
965	ZNF136	-1.01757	2.620838	21.04429	4.49E-06	1.44E-05
966	NPPC	2.723005	2.599821	139.9337	2.75E-32	4.58E-31
967	THBS1	-1.83254	2.637855	52.05617	5.39E-13	3.37E-12
968	RASSF5	-1.12099	2.597728	43.365	4.54E-11	2.41E-10
969	EGLN3	-1.57213	2.609625	68.63082	1.19E-16	9.53E-16
970	SFTPA2	-1.00607	2.601936	39.58828	3.14E-10	1.56E-09
971	FERMT2	1.690235	2.570251	39.15683	3.91E-10	1.92E-09
972	WLS	-1.03426	2.598078	25.16743	5.26E-07	1.88E-06
973	MYBPC1	1.523943	2.566469	58.62965	1.90E-14	1.31E-13

974	NOVA1	-1.0091	2.59571	32.33856	1.30E-08	5.53E-08
975	IL1RN	-2.1615	2.568722	102.6374	4.02E-24	4.83E-23
976	ZNF738	-1.45842	2.59568	50.2456	1.36E-12	8.27E-12
977	PPARGC1B	-1.6331	2.565518	42.67018	6.48E-11	3.41E-10
978	FAM72D	-2.61545	2.584525	112.6984	2.51E-26	3.32E-25
979	CDH15	1.391528	2.543718	48.69188	3.00E-12	1.77E-11
980	KCNH2	1.106511	2.54331	23.42814	1.30E-06	4.44E-06
981	LOC100289019	-1.28144	2.565203	39.2761	3.68E-10	1.81E-09
982	GSN	1.332322	2.527229	59.26114	1.38E-14	9.64E-14
983	DOK4	1.13866	2.530696	47.32529	6.01E-12	3.45E-11
984	MYL9	2.356212	2.49094	176.7636	2.47E-40	5.25E-39
985	PBX1	-1.37297	2.539773	32.30585	1.32E-08	5.61E-08
986	DMBX1	-3.31864	2.55599	187.633	1.04E-42	2.38E-41
987	C4orf21	-2.70675	2.540547	118.6437	1.25E-27	1.74E-26
988	SFR1	-1.56724	2.538136	47.53869	5.39E-12	3.11E-11
989	SPIN4	-1.75798	2.517004	53.11968	3.14E-13	1.98E-12
990	PMAIP1	-2.07863	2.526016	99.02954	2.49E-23	2.87E-22
991	PPP1R14C	-1.86232	2.519561	66.34634	3.78E-16	2.94E-15
992	SLC16A10	-1.49963	2.5063	54.31323	1.71E-13	1.10E-12
993	PRSS53	-1.1251	2.485032	28.66805	8.59E-08	3.37E-07
994	STON2	-2.096	2.486208	91.17675	1.31E-21	1.40E-20
995	HES2	1.223881	2.445505	52.51301	4.27E-13	2.68E-12
996	KAZN	-1.26518	2.447172	37.58481	8.75E-10	4.18E-09
997	MAP1A	-1.09005	2.453251	23.67543	1.14E-06	3.94E-06
998	DGKA	1.866233	2.423003	94.02393	3.12E-22	3.41E-21
999	LPCAT4	-1.10384	2.449361	40.44437	2.02E-10	1.02E-09
1000	EPS8	-1.72946	2.417679	74.86677	5.04E-18	4.36E-17
1001	GCFC1-AS1	1.288144	2.399184	50.20985	1.38E-12	8.39E-12
1002	CEP72	-1.9532	2.416237	79.32761	5.26E-19	4.85E-18
1003	ARPM1	-1.6938	2.400956	61.32243	4.85E-15	3.49E-14
1004	SLITRK6	1.716986	2.375405	56.18784	6.59E-14	4.36E-13
1005	SPOCK1	1.862883	2.378154	75.15071	4.36E-18	3.79E-17
1006	PAX1	-1.15955	2.383393	25.69356	4.00E-07	1.45E-06
1007	LOC388588	1.114402	2.351305	22.85323	1.75E-06	5.90E-06
1008	FLJ43663	2.383105	2.350449	103.4788	2.63E-24	3.19E-23
1009	PCDH11Y	-1.0438	2.346546	15.69972	7.42E-05	0.000201
1010	ANK1	1.231433	2.307912	32.85622	9.92E-09	4.28E-08
1011	KANK1	1.113171	2.305604	26.79755	2.26E-07	8.44E-07
1012	FAM54A	-2.9195	2.328249	126.3087	2.63E-29	3.90E-28
1013	C1orf135	-3.51417	2.327583	195.0289	2.54E-44	6.09E-43
1014	FAM72B	-3.14189	2.327372	182.0249	1.75E-41	3.86E-40
1015	NAV3	-2.87294	2.307982	173.5452	1.24E-39	2.60E-38

1016	RPP25	-2.247	2.319348	73.56585	9.73E-18	8.28E-17
1017	FAM110C	1.266511	2.277315	36.74183	1.35E-09	6.30E-09
1018	FERMT1	-1.62606	2.296089	37.68478	8.32E-10	3.98E-09
1019	CCPG1	1.103146	2.264724	16.39262	5.15E-05	0.000143
1020	TLN2	-1.32066	2.295772	41.96012	9.32E-11	4.83E-10
1021	NUP62CL	-1.23328	2.266863	52.39818	4.53E-13	2.84E-12
1022	ATAD5	-3.02111	2.251379	163.2787	2.17E-37	4.20E-36
1023	C18orf54	-3.36421	2.27838	120.4654	5.00E-28	7.07E-27
1024	LRIG3	-1.68613	2.253936	63.85011	1.34E-15	1.01E-14
1025	TUBA3E	1.549677	2.242307	34.19097	5.00E-09	2.22E-08
1026	S1PR3	-2.1669	2.257376	86.43685	1.44E-20	1.46E-19
1027	RGS16	1.144013	2.23219	22.22318	2.43E-06	8.05E-06
1028	FLJ27352	1.440643	2.215473	43.63146	3.96E-11	2.13E-10
1029	RDH12	1.17123	2.198395	28.03445	1.19E-07	4.58E-07
1030	WWTR1	1.395273	2.20958	40.19173	2.30E-10	1.16E-09
1031	SPRY1	-1.39013	2.229203	40.37813	2.09E-10	1.05E-09
1032	HIST1H3E	1.072551	2.199202	24.40843	7.79E-07	2.75E-06
1033	C19orf57	-1.48688	2.232643	39.45573	3.36E-10	1.66E-09
1034	ATG16L2	-1.04803	2.229414	18.44324	1.75E-05	5.17E-05
1035	ABCA12	-2.10961	2.211496	79.61031	4.56E-19	4.22E-18
1036	FAM81A	-2.04924	2.201616	74.27069	6.81E-18	5.86E-17
1037	BAI2	-2.08205	2.210137	67.83247	1.78E-16	1.41E-15
1038	SLC35G1	-1.1792	2.189683	30.6818	3.04E-08	1.25E-07
1039	DOC2A	-1.18475	2.18977	23.712	1.12E-06	3.87E-06
1040	CEL	-1.57992	2.20338	55.45546	9.56E-14	6.25E-13
1041	TNFAIP3	1.815204	2.169242	49.47055	2.01E-12	1.21E-11
1042	MIR210HG	1.020706	2.177146	19.53759	9.86E-06	3.02E-05
1043	ARL6IP6	-1.51766	2.183627	40.6177	1.85E-10	9.37E-10
1044	ACSM1	1.127692	2.158517	34.81551	3.62E-09	1.63E-08
1045	EML5	-1.33987	2.166066	30.82732	2.82E-08	1.17E-07
1046	SPTLC3	-1.13605	2.163615	23.00166	1.62E-06	5.48E-06
1047	SPTB	3.032926	2.147878	135.5347	2.52E-31	4.05E-30
1048	NTNG1	1.119156	2.142932	19.52801	9.91E-06	3.03E-05
1049	ACTA2	2.44597	2.1205	156.0955	8.07E-36	1.49E-34
1050	C3orf67	-1.29347	2.155856	37.66297	8.41E-10	4.03E-09
1051	BORA	-1.72587	2.176648	37.17712	1.08E-09	5.09E-09
1052	B4GALT6	-1.2244	2.154657	25.74113	3.90E-07	1.42E-06
1053	ALG10	-1.39232	2.136098	24.05594	9.36E-07	3.27E-06
1054	RDM1	-1.56178	2.141119	45.98921	1.19E-11	6.63E-11
1055	RPS6KA5	-1.07954	2.128145	21.25958	4.01E-06	1.29E-05
1056	LOC100128361	-2.17419	2.14019	44.19524	2.97E-11	1.61E-10
1057	MAP2K6	-1.53591	2.121205	42.30775	7.80E-11	4.07E-10

1058	DGKH	-1.62531	2.105578	48.41111	3.46E-12	2.03E-11
1059	TMEM198	1.231294	2.101973	25.52855	4.36E-07	1.57E-06
1060	IL36RN	-1.1089	2.081946	20.08638	7.40E-06	2.31E-05
1061	DOCK8	1.663145	2.079418	32.76555	1.04E-08	4.48E-08
1062	FHOD3	-1.31769	2.096363	37.30608	1.01E-09	4.79E-09
1063	C1orf95	-1.35075	2.078048	41.48846	1.19E-10	6.08E-10
1064	C5orf34	-2.76075	2.086564	114.4972	1.01E-26	1.37E-25
1065	CARTPT	1.052406	2.075935	21.50327	3.53E-06	1.15E-05
1066	OSBPL3	-2.34789	2.079187	85.02476	2.95E-20	2.92E-19
1067	FAM83E	2.570063	2.024604	107.6969	3.13E-25	3.99E-24
1068	CENPP	-1.77688	2.063449	54.67616	1.42E-13	9.20E-13
1069	CEP135	-1.27049	2.048791	29.50725	5.57E-08	2.24E-07
1070	HIST1H3D	1.690032	1.974339	49.53411	1.95E-12	1.17E-11
1071	KDELR3	1.558803	1.967166	28.79817	8.03E-08	3.17E-07
1072	FRK	1.02276	1.974574	15.75645	7.20E-05	0.000195
1073	SLCO5A1	-1.09875	1.979989	19.63936	9.35E-06	2.87E-05
1074	FAM72A	-2.5642	1.984398	93.7363	3.60E-22	3.93E-21
1075	KCNRG	1.069423	1.965047	21.55398	3.44E-06	1.12E-05
1076	NKD1	-1.47093	1.974114	37.45952	9.33E-10	4.44E-09
1077	TERT	-4.1561	1.971424	246.2368	1.72E-55	5.55E-54
1078	NDUFA4L2	1.904308	1.937276	41.22357	1.36E-10	6.93E-10
1079	GLS2	-1.38334	1.960414	36.6204	1.44E-09	6.68E-09
1080	C8orf37	-1.2345	1.947375	25.65078	4.09E-07	1.48E-06
1081	VASH2	-1.26784	1.942977	31.99667	1.54E-08	6.53E-08
1082	FAM184A	-1.31369	1.932584	23.43671	1.29E-06	4.43E-06
1083	SPRY4	1.809711	1.907563	58.10853	2.48E-14	1.70E-13
1084	SNORD96A	-1.09602	1.933839	15.86783	6.79E-05	0.000185
1085	FOXN4	-2.57939	1.923733	80.97104	2.29E-19	2.15E-18
1086	LRFN2	-1.52234	1.906427	34.05736	5.35E-09	2.37E-08
1087	FAM86HP	-1.49703	1.901182	24.93247	5.94E-07	2.12E-06
1088	ZPLD1	-1.30848	1.89286	23.56633	1.21E-06	4.16E-06
1089	TACSTD2	1.237194	1.870662	28.80697	8.00E-08	3.16E-07
1090	TLL1	-2.60858	1.876395	108.2262	2.40E-25	3.06E-24
1091	SYP	1.090691	1.866526	23.87587	1.03E-06	3.57E-06
1092	CHAC2	-1.83655	1.881431	41.94793	9.37E-11	4.86E-10
1093	IL1RAP	-1.20648	1.875948	21.87642	2.91E-06	9.55E-06
1094	TNS4	2.242506	1.830132	62.23311	3.05E-15	2.23E-14
1095	BMX	-2.1776	1.871175	64.00359	1.24E-15	9.34E-15
1096	CNKSR2	-1.27943	1.850409	21.95448	2.79E-06	9.20E-06
1097	LOC399815	-1.48621	1.850908	43.12363	5.14E-11	2.72E-10
1098	PLS1	-1.06651	1.836253	22.50702	2.09E-06	7.01E-06
1099	CYP2E1	1.235881	1.832136	23.47648	1.26E-06	4.34E-06

1100	RPL36A	-1.00276	1.831481	19.38397	1.07E-05	3.25E-05
1101	GRID2IP	1.011762	1.81248	21.0586	4.45E-06	1.43E-05
1102	ZNF670	-1.21212	1.826519	24.04651	9.40E-07	3.29E-06
1103	PDE4A	-1.3815	1.818773	31.52318	1.97E-08	8.26E-08
1104	MREG	-1.03493	1.818472	22.39408	2.22E-06	7.40E-06
1105	ZNF273	-1.77619	1.823732	43.52925	4.18E-11	2.23E-10
1106	RIMS4	-1.81132	1.806549	67.9084	1.71E-16	1.36E-15
1107	SP4	-1.38909	1.795308	19.90012	8.16E-06	2.53E-05
1108	SOBP	-1.4504	1.793005	28.3486	1.01E-07	3.94E-07
1109	SCARA3	-2.28258	1.78656	64.34631	1.04E-15	7.90E-15
1110	SSTR5	-2.0986	1.760856	78.42893	8.29E-19	7.58E-18
1111	LTB4R2	-1.07409	1.765178	14.40708	0.000147	0.000382
1112	LOC100505633	-1.34983	1.774233	20.58555	5.70E-06	1.80E-05
1113	SNCG	2.141418	1.739804	86.96288	1.11E-20	1.12E-19
1114	FHIT	1.638182	1.726672	42.47578	7.16E-11	3.75E-10
1115	APCDD1	-1.0052	1.741211	19.11834	1.23E-05	3.71E-05
1116	IRX5	-1.26884	1.752793	23.92784	1.00E-06	3.48E-06
1117	TMOD2	-1.15865	1.73486	21.77992	3.06E-06	1.00E-05
1118	ASPHD2	1.504459	1.715996	35.25951	2.89E-09	1.31E-08
1119	PTCRA	1.930257	1.688935	46.68008	8.36E-12	4.73E-11
1120	CNIH2	-1.21141	1.724738	18.62461	1.59E-05	4.73E-05
1121	BEST1	-2.16933	1.710968	46.46788	9.31E-12	5.25E-11
1122	MTBP	-2.65029	1.698324	89.12618	3.70E-21	3.88E-20
1123	TNNT1	1.092825	1.675933	10.44822	0.001228	0.002736
1124	ZNF695	-2.35394	1.697929	60.84913	6.16E-15	4.41E-14
1125	TG	4.1646	1.638793	192.4292	9.38E-44	2.22E-42
1126	CCDC75	-1.1721	1.673007	20.37489	6.37E-06	2.00E-05
1127	SMYD2	-1.28818	1.677318	19.0658	1.26E-05	3.81E-05
1128	LOC100335030	-1.32428	1.667135	22.52934	2.07E-06	6.93E-06
1129	CADM2	1.0948	1.648612	21.68954	3.21E-06	1.05E-05
1130	LINC00176	-1.03309	1.656477	9.771892	0.001772	0.003834
1131	GJC1	-1.68402	1.651347	42.66762	6.49E-11	3.41E-10
1132	ITIH4	-1.02405	1.640978	17.01973	3.70E-05	0.000104
1133	FAM161A	-1.11544	1.621317	20.49142	5.99E-06	1.89E-05
1134	PLCH1	-2.49368	1.627385	79.40895	5.05E-19	4.66E-18
1135	LOC100507424	-1.33874	1.618079	23.18715	1.47E-06	5.01E-06
1136	C14orf28	1.065	1.604954	17.60773	2.71E-05	7.83E-05
1137	TMEM51	-1.10643	1.60531	13.86745	0.000196	0.0005
1138	GLI3	-1.10048	1.602994	16.66514	4.46E-05	0.000125
1139	LRP4	1.181704	1.564273	24.0128	9.57E-07	3.34E-06
1140	SLC38A4	1.956431	1.574071	45.79123	1.32E-11	7.32E-11
1141	LOC100130522	-1.32239	1.573387	23.25106	1.42E-06	4.85E-06

1142	RIN2	-1.08761	1.548226	17.88452	2.35E-05	6.83E-05
1143	SNORA61	-1.62578	1.560059	37.53262	8.99E-10	4.29E-09
1144	FGD1	-1.40586	1.558773	23.68611	1.13E-06	3.91E-06
1145	RUNX1	2.734274	1.545251	95.17885	1.74E-22	1.92E-21
1146	CDKN1C	1.32803	1.533424	30.07559	4.16E-08	1.69E-07
1147	SLC22A1	1.779197	1.531084	57.15464	4.03E-14	2.72E-13
1148	SERPINB8	1.398553	1.529914	30.32696	3.65E-08	1.49E-07
1149	CHRNB1	1.758455	1.526782	32.44972	1.22E-08	5.23E-08
1150	SLA2	2.549826	1.518812	62.54033	2.61E-15	1.92E-14
1151	FAS	-1.18092	1.527157	12.94238	0.000321	0.000794
1152	MIR17HG	-1.13688	1.521143	17.41567	3.00E-05	8.60E-05
1153	ZC3HAV1L	-1.12874	1.515464	13.74072	0.00021	0.000532
1154	FAM18B2	1.1073	1.510544	23.12508	1.52E-06	5.16E-06
1155	RELB	1.22223	1.485984	32.33023	1.30E-08	5.55E-08
1156	NINL	-2.23201	1.505842	72.21464	1.93E-17	1.62E-16
1157	KSR2	-1.78497	1.505379	53.33565	2.81E-13	1.78E-12
1158	FMNL3	-1.70245	1.509285	46.8384	7.71E-12	4.39E-11
1159	RUNX2	-1.42959	1.497007	26.20327	3.07E-07	1.13E-06
1160	MAP3K8	-1.39547	1.48672	34.76635	3.72E-09	1.67E-08
1161	LOC646862	1.650769	1.44402	33.6782	6.50E-09	2.85E-08
1162	SYCE2	-1.60112	1.472849	29.53277	5.50E-08	2.21E-07
1163	MYB	-2.79468	1.464304	81.6063	1.66E-19	1.58E-18
1164	TMEM92	2.267773	1.424565	72.64822	1.55E-17	1.31E-16
1165	FAM49A	-1.01656	1.446769	12.24935	0.000465	0.00112
1166	OSMR	1.089576	1.42196	9.5673	0.001981	0.004243
1167	KLHL11	-1.75409	1.424296	39.23119	3.76E-10	1.85E-09
1168	CERS1	-1.31818	1.430794	18.26135	1.93E-05	5.66E-05
1169	C1QTNF6	-1.15064	1.413993	12.90532	0.000328	0.000807
1170	NWD1	-1.18629	1.414917	14.98437	0.000108	0.000286
1171	HIST1H1E	2.96548	1.355928	68.5934	1.21E-16	9.71E-16
1172	DNALI1	1.244847	1.363986	26.14563	3.17E-07	1.16E-06
1173	ELOVL2	3.171632	1.352361	88.97125	4.01E-21	4.18E-20
1174	LOC100505815	-1.07858	1.359125	11.0402	0.000892	0.002031
1175	C21orf63	-1.19031	1.366243	12.63672	0.000378	0.000924
1176	LOC728558	-1.17439	1.361073	13.9122	0.000192	0.000489
1177	FAM189A2	2.41436	1.351339	55.57986	8.97E-14	5.88E-13
1178	PBX4	-1.25146	1.340035	18.90357	1.37E-05	4.12E-05
1179	KCNK5	-2.61271	1.321363	80.26566	3.27E-19	3.05E-18
1180	CDC14A	-1.28691	1.317279	17.64996	2.66E-05	7.67E-05
1181	SCNN1G	1.762162	1.303017	45.01709	1.95E-11	1.07E-10
1182	DSE	-1.10457	1.327406	13.21516	0.000278	0.000693
1183	LOC100507634	1.303284	1.305097	22.51538	2.08E-06	6.98E-06

1184	ZNF726	-1.79213	1.314377	51.1638	8.50E-13	5.25E-12
1185	CCDC150	-2.97812	1.32368	69.58955	7.30E-17	5.92E-16
1186	COL5A2	-1.40336	1.313311	22.99794	1.62E-06	5.49E-06
1187	C1QL1	-1.28244	1.30253	24.14731	8.92E-07	3.13E-06
1188	SIX1	-1.78416	1.29539	46.08767	1.13E-11	6.33E-11
1189	STARD9	-1.82016	1.287747	33.36004	7.66E-09	3.34E-08
1190	ODAM	-1.1372	1.276016	18.70473	1.53E-05	4.55E-05
1191	FLT4	-2.63701	1.275186	85.31737	2.54E-20	2.53E-19
1192	GAS2L3	-2.46385	1.266427	57.97387	2.66E-14	1.81E-13
1193	LOC144481	3.840201	1.240202	91.85196	9.34E-22	1.00E-20
1194	FANCB	-3.29328	1.266418	118.7223	1.20E-27	1.68E-26
1195	LOC100507266	-1.69659	1.252319	26.94533	2.09E-07	7.85E-07
1196	ZNF519	-1.76136	1.252172	46.55266	8.92E-12	5.04E-11
1197	BRDT	-2.04241	1.227013	40.47631	1.99E-10	1.00E-09
1198	EDN2	-1.14199	1.204857	10.46637	0.001216	0.002712
1199	REP15	3.918908	1.16051	171.0062	4.46E-39	9.22E-38
1200	FRMPD2	-1.79538	1.173007	30.37788	3.56E-08	1.46E-07
1201	HEY1	-1.22813	1.167951	12.96696	0.000317	0.000784
1202	RADIL	-2.09897	1.161073	56.7567	4.93E-14	3.30E-13
1203	MYBL1	-2.58499	1.132487	53.42557	2.69E-13	1.70E-12
1204	ANTXR1	-1.86435	1.103571	34.02184	5.45E-09	2.41E-08
1205	BCL2	-2.22535	1.09301	36.63148	1.43E-09	6.65E-09
1206	KCNG3	1.628505	1.072403	34.5463	4.16E-09	1.86E-08
1207	ANGPT2	2.571655	1.058679	78.00937	1.03E-18	9.34E-18
1208	NLRC5	-1.43576	1.079631	23.12287	1.52E-06	5.16E-06
1209	TGM3	-3.30533	1.063226	96.72651	7.96E-23	8.97E-22
1210	OXTR	-1.74428	1.004629	27.00498	2.03E-07	7.62E-07
1211	LGI2	-4.03209	0.985462	101.5434	6.99E-24	8.27E-23
1212	HHIPL2	2.978962	0.623952	98.79176	2.80E-23	3.22E-22

B) DHT vs Vehicle

No	gene_id	logFC	logCPM	LR	PValue	FDR
1	KRT8	1.045876	10.91338	226.5447	3.38E-51	1.48E-48
2	TMPRSS2	1.034806	10.07856	270.9375	7.09E-61	4.74E-58
3	FKBP5	1.332703	9.752285	334.1801	1.18E-74	4.48E-71
4	ACSL3	1.3599	9.582629	306.3878	1.34E-68	1.69E-65
5	SLC41A1	1.300349	8.666302	342.749	1.61E-76	9.14E-73
6	NDRG1	1.023857	8.62771	244.7676	3.59E-55	1.94E-52
7	SMS	1.157277	8.558071	330.8652	6.23E-74	1.77E-70
8	H2AFX	-1.03003	8.459112	154.8721	1.49E-35	2.00E-33
9	MCM7	-1.06535	8.226906	286.1939	3.36E-64	2.54E-61
10	MICAL1	1.500391	8.011749	399.6633	6.52E-89	7.41E-85
11	MKI67	-1.19786	7.768959	161.078	6.58E-37	9.97E-35
12	CBWD1	1.060669	7.492296	184.4621	5.14E-42	1.22E-39
13	HMGB2	-1.16852	7.56376	214.2192	1.65E-48	5.68E-46
14	MYBL2	-1.03923	7.505904	181.4944	2.29E-41	5.09E-39
15	TPX2	-1.21605	7.409799	309.4635	2.86E-69	4.64E-66
16	SPAG5	-1.01596	7.378592	295.3601	3.38E-66	3.20E-63
17	MCM2	-1.21199	7.370048	223.1899	1.82E-50	7.14E-48
18	PCNA	-1.04151	7.316584	177.9997	1.32E-40	2.64E-38
19	TK1	-1.06191	7.319267	151.2888	9.06E-35	1.20E-32
20	CHRNA2	1.328367	7.192927	246.8557	1.26E-55	7.15E-53
21	PLK1	-1.02222	7.175124	213.2254	2.72E-48	9.08E-46
22	CENPF	-1.15946	7.146804	144.8989	2.26E-33	2.85E-31
23	MCM4	-1.20808	7.062613	290.5878	3.70E-65	3.24E-62
24	LMNB1	-1.0847	7.04996	229.8125	6.55E-52	3.10E-49
25	CDC20	-1.14647	7.066853	267.8045	3.42E-60	2.16E-57
26	MCM3	-1.03623	7.015346	194.0438	4.17E-44	1.13E-41
27	RRM2	-1.27669	7.018513	315.908	1.13E-70	2.14E-67
28	F5	1.193323	6.905314	174.4316	7.97E-40	1.44E-37
29	NUSAP1	-1.26706	6.984579	321.8234	5.80E-72	1.32E-68
30	TCOF1	-1.06926	6.936038	171.7099	3.13E-39	5.56E-37
31	PRC1	-1.1647	6.878806	234.0694	7.73E-53	3.82E-50
32	TYMS	-1.18347	6.875414	306.6155	1.19E-68	1.69E-65
33	FEN1	-1.16776	6.856174	302.1943	1.10E-67	1.25E-64
34	CDK1	-1.1056	6.77637	178.0335	1.30E-40	2.64E-38
35	MCM5	-1.07627	6.75905	149.1362	2.68E-34	3.50E-32

36	TMPO	-1.12552	6.683045	164.5448	1.15E-37	1.84E-35
37	FANCI	-1.08779	6.62416	224.3811	1.00E-50	4.07E-48
38	ST6GALNAC1	1.035249	6.465627	183.1555	9.92E-42	2.25E-39
39	TONSL	-1.04372	6.54392	125.7227	3.54E-29	3.46E-27
40	CHAF1A	-1.00718	6.47708	146.5049	1.01E-33	1.29E-31
41	KIF20A	-1.16897	6.495192	260.3395	1.45E-58	8.66E-56
42	SMC4	-1.09011	6.403634	123.7541	9.54E-29	9.18E-27
43	GNMT	1.219482	6.163692	167.4938	2.61E-38	4.36E-36
44	UGT2B11	1.518936	6.119025	186.6543	1.71E-42	4.22E-40
45	RECQL4	-1.0609	6.257349	161.6995	4.81E-37	7.49E-35
46	TCF19	-1.29178	6.252116	228.2471	1.44E-51	6.54E-49
47	CDCA5	-1.28337	6.238124	277.8941	2.16E-62	1.53E-59
48	TOP2A	-1.40947	6.159168	161.6144	5.02E-37	7.71E-35
49	UBE2C	-1.25634	6.167261	177.2288	1.95E-40	3.76E-38
50	CCNB2	-1.08107	6.098181	179.9488	4.97E-41	1.07E-38
51	RACGAP1	-1.06619	6.047303	160.3922	9.29E-37	1.34E-34
52	CCNF	-1.04616	6.00093	158.4234	2.50E-36	3.47E-34
53	KIFC1	-1.3823	6.000929	297.1907	1.35E-66	1.39E-63
54	E2F1	-1.17503	5.996343	220.3052	7.76E-50	2.94E-47
55	KIF2C	-1.24228	5.981083	236.2581	2.57E-53	1.33E-50
56	PKMYT1	-1.16667	5.970537	123.9963	8.44E-29	8.20E-27
57	CDC6	-1.12952	5.945206	202.602	5.65E-46	1.69E-43
58	HMMR	-1.07546	5.923096	108.5231	2.06E-25	1.59E-23
59	NCAPG	-1.16227	5.917118	185.3473	3.30E-42	7.97E-40
60	CDCA3	-1.09271	5.893867	118.705	1.22E-27	1.10E-25
61	MLF1IP	-1.12605	5.883664	175.5714	4.49E-40	8.37E-38
62	HJURP	-1.32201	5.888758	217.7788	2.76E-49	1.01E-46
63	POLA2	-1.07986	5.857153	174.5567	7.48E-40	1.37E-37
64	FAM83D	-1.20972	5.838418	204.0482	2.73E-46	8.39E-44
65	AURKA	-1.05393	5.788678	123.5456	1.06E-28	1.01E-26
66	BUB1B	-1.24551	5.738795	157.6552	3.68E-36	5.04E-34
67	CADPS2	1.363656	5.627089	156.1036	8.04E-36	1.09E-33
68	DLGAP5	-1.12252	5.726486	93.95554	3.23E-22	2.03E-20
69	ASF1B	-1.25257	5.735445	197.7686	6.41E-45	1.87E-42
70	MAF	1.508879	5.575168	137.4348	9.69E-32	1.06E-29
71	FANCD2	-1.16644	5.646963	164.0542	1.47E-37	2.32E-35
72	CCNA2	-1.22092	5.643516	143.9444	3.65E-33	4.51E-31
73	CAMK2N1	-1.13657	5.616474	143.1641	5.41E-33	6.61E-31
74	ANLN	-1.15084	5.608306	98.83844	2.74E-23	1.90E-21
75	CDT1	-1.08162	5.617058	115.3649	6.55E-27	5.55E-25
76	WDR62	-1.05034	5.586252	85.81977	1.97E-20	1.10E-18
77	MELK	-1.21792	5.576693	158.7707	2.10E-36	2.95E-34

78	NDC80	-1.35382	5.558103	194.5612	3.21E-44	8.90E-42
79	AURKB	-1.10044	5.525203	97.75995	4.72E-23	3.20E-21
80	ESPL1	-1.37699	5.494887	183.9924	6.51E-42	1.51E-39
81	PRKCA	1.122294	5.384767	103.5093	2.59E-24	1.89E-22
82	WIPI1	1.393275	5.320718	140.8564	1.73E-32	1.99E-30
83	CENPE	-1.15521	5.416865	94.29366	2.72E-22	1.73E-20
84	CDCA8	-1.147	5.409472	179.8694	5.18E-41	1.09E-38
85	PBK	-1.1895	5.352495	131.122	2.33E-30	2.38E-28
86	NCAPH	-1.1707	5.350564	176.9506	2.25E-40	4.25E-38
87	RFC4	-1.03248	5.343251	117.288	2.48E-27	2.17E-25
88	ADAM7	1.02902	5.265882	159.1141	1.77E-36	2.51E-34
89	CDC45	-1.26503	5.344925	138.8939	4.65E-32	5.23E-30
90	BUB1	-1.08608	5.320551	108.5805	2.01E-25	1.56E-23
91	GTSE1	-1.00121	5.299098	138.2256	6.50E-32	7.25E-30
92	BRCA1	-1.32938	5.210567	118.8537	1.13E-27	1.03E-25
93	AFF3	1.025491	5.101864	74.22527	6.97E-18	3.25E-16
94	KIF11	-1.24269	5.181224	91.5732	1.08E-21	6.57E-20
95	PGC	1.437474	5.097379	160.5865	8.42E-37	1.23E-34
96	PSRC1	-1.00039	5.139266	112.9466	2.22E-26	1.85E-24
97	UGT2B15	-1.0213	5.06843	89.53838	3.01E-21	1.78E-19
98	DEPDC1	-1.08531	5.061649	66.14444	4.19E-16	1.62E-14
99	ARHGAP11A	-1.09129	5.052337	61.27484	4.96E-15	1.73E-13
100	CIT	-1.30978	5.062757	194.8121	2.83E-44	8.04E-42
101	GINS1	-1.21617	5.043659	180.5777	3.62E-41	7.92E-39
102	RAD54L	-1.33744	5.045544	144.1264	3.33E-33	4.16E-31
103	DDB2	-1.1311	5.021673	125.9661	3.13E-29	3.12E-27
104	CDKN2C	-1.02241	5.018923	88.19348	5.94E-21	3.41E-19
105	CEP55	-1.16941	4.997699	111.4567	4.70E-26	3.87E-24
106	CLSPN	-1.32154	4.974504	129.0052	6.76E-30	6.86E-28
107	KNTC1	-1.20081	4.965225	142.1741	8.91E-33	1.05E-30
108	RFC5	-1.06755	4.949173	86.16157	1.66E-20	9.33E-19
109	BCHE	-1.00441	4.92801	81.65234	1.62E-19	8.50E-18
110	CDCA7L	-1.05264	4.924996	141.3639	1.34E-32	1.55E-30
111	C9orf100	-1.11235	4.944562	114.9189	8.20E-27	6.90E-25
112	GINS2	-1.02608	4.922295	79.16132	5.72E-19	2.87E-17
113	STEAP4	3.740503	4.757507	286.9926	2.25E-64	1.83E-61
114	SOCS2	1.298868	4.823498	90.77711	1.61E-21	9.72E-20
115	UGT2B28	2.151729	4.738447	224.7092	8.50E-51	3.58E-48
116	MCM10	-1.39635	4.855	117.8871	1.84E-27	1.63E-25
117	UHRF1	-1.24869	4.827836	127.3368	1.57E-29	1.58E-27
118	INPP4B	1.037968	4.737244	69.23793	8.73E-17	3.58E-15
119	KIF18B	-1.24701	4.830277	94.5038	2.45E-22	1.57E-20

120	CDCA2	-1.19934	4.817123	102.1822	5.06E-24	3.64E-22
121	C21orf58	-1.02692	4.785925	116.885	3.04E-27	2.64E-25
122	WDHD1	-1.09878	4.763399	137.4265	9.73E-32	1.06E-29
123	ZNF812	1.188918	4.648766	118.1696	1.59E-27	1.42E-25
124	SHCBP1	-1.21918	4.72046	101.3271	7.80E-24	5.57E-22
125	KIF23	-1.15958	4.685966	133.2985	7.78E-31	8.11E-29
126	ORC6	-1.41043	4.683425	164.9222	9.51E-38	1.54E-35
127	POLQ	-1.45569	4.655492	95.53963	1.45E-22	9.52E-21
128	NUF2	-1.2725	4.651253	96.92885	7.19E-23	4.78E-21
129	NEK2	-1.2653	4.648609	104.8892	1.29E-24	9.66E-23
130	PSMC3IP	-1.06282	4.631968	79.07517	5.98E-19	2.98E-17
131	DTL	-1.46799	4.61236	167.9618	2.06E-38	3.50E-36
132	CDCA4	-1.0423	4.610723	78.2652	9.01E-19	4.43E-17
133	CDC7	-1.00613	4.595561	82.09577	1.30E-19	6.90E-18
134	TUBA3D	1.154626	4.537442	86.83625	1.18E-20	6.70E-19
135	SKA3	-1.19007	4.585329	101.1734	8.43E-24	5.99E-22
136	TMEM194A	-1.07667	4.547988	81.32644	1.91E-19	9.88E-18
137	PAQR6	1.09006	4.495225	66.83885	2.95E-16	1.16E-14
138	TARP	1.388336	4.394865	135.0885	3.16E-31	3.35E-29
139	GINS4	-1.29491	4.410119	95.70459	1.33E-22	8.81E-21
140	CCDC141	1.189939	4.324552	32.11229	1.46E-08	2.44E-07
141	DEPDC1B	-1.1672	4.373182	79.50803	4.80E-19	2.42E-17
142	ORC1	-1.19596	4.352869	81.79847	1.51E-19	7.97E-18
143	SPC24	-1.05033	4.336883	74.50119	6.06E-18	2.85E-16
144	POLD3	-1.01666	4.315872	65.33273	6.33E-16	2.40E-14
145	NRM	-1.03433	4.31834	63.31645	1.76E-15	6.45E-14
146	EME1	-1.26083	4.314727	75.8949	2.99E-18	1.42E-16
147	RFC3	-1.18466	4.302175	67.80551	1.80E-16	7.27E-15
148	FIGNL1	-1.01857	4.277732	43.21601	4.90E-11	1.13E-09
149	ASPM	-1.4306	4.279402	58.03575	2.57E-14	8.31E-13
150	CDC25C	-1.12305	4.290442	75.37873	3.89E-18	1.84E-16
151	DIAPH3	-1.24199	4.25633	132.5798	1.12E-30	1.15E-28
152	TTK	-1.24649	4.256631	70.54799	4.49E-17	1.90E-15
153	ANO7	1.119116	4.185993	53.57236	2.49E-13	7.23E-12
154	C1orf112	-1.11931	4.174699	76.51285	2.19E-18	1.05E-16
155	GPSM2	-1.13496	4.158148	67.0086	2.70E-16	1.07E-14
156	SGOL2	-1.1287	4.126562	73.64056	9.37E-18	4.31E-16
157	CEP78	-1.16272	4.117113	71.18209	3.26E-17	1.41E-15
158	KIF20B	-1.15605	4.10426	71.55151	2.70E-17	1.19E-15
159	EXO1	-1.36995	4.094591	109.6295	1.18E-25	9.45E-24
160	SKA1	-1.24075	4.036338	79.7189	4.32E-19	2.18E-17
161	C15orf42	-1.24883	4.010447	67.63497	1.97E-16	7.90E-15

162	SLITRK3	-1.02532	3.984061	62.39063	2.82E-15	1.01E-13
163	PLK4	-1.37775	3.956852	71.42752	2.88E-17	1.26E-15
164	KIF15	-1.54313	3.955213	122.2659	2.02E-28	1.85E-26
165	FBXO5	-1.19666	3.919201	64.46982	9.80E-16	3.69E-14
166	PRIM1	-1.21125	3.862068	63.49777	1.61E-15	5.92E-14
167	RAD51AP1	-1.15768	3.858318	58.05566	2.55E-14	8.25E-13
168	KIF24	-1.36447	3.858929	81.48532	1.77E-19	9.20E-18
169	OIP5	-1.14958	3.853208	69.36202	8.20E-17	3.41E-15
170	HAUS8	-1.02802	3.827204	56.10902	6.86E-14	2.11E-12
171	TRAIP	-1.07542	3.817425	50.27131	1.34E-12	3.64E-11
172	TTN	1.077946	3.775705	38.66438	5.03E-10	1.01E-08
173	B3GALT4	1.182619	3.720288	50.97522	9.35E-13	2.57E-11
174	RAD51	-1.07935	3.756982	72.57113	1.61E-17	7.21E-16
175	MNS1	-1.09502	3.749475	43.99635	3.29E-11	7.73E-10
176	E2F2	-1.23445	3.755456	85.18558	2.72E-20	1.49E-18
177	SH3D21	1.282619	3.671158	51.82665	6.06E-13	1.69E-11
178	SPC25	-1.07155	3.737694	46.94391	7.30E-12	1.84E-10
179	GSTCD	-1.03503	3.706872	42.86711	5.86E-11	1.32E-09
180	KIF14	-1.36197	3.700978	68.26926	1.43E-16	5.79E-15
181	ESCO2	-1.45165	3.678045	55.81356	7.97E-14	2.44E-12
182	ORM1	2.68578	3.584169	160.9633	6.97E-37	1.04E-34
183	CASC5	-1.26326	3.668182	48.37091	3.53E-12	9.28E-11
184	CCNE2	-1.11895	3.647541	39.64711	3.04E-10	6.31E-09
185	CSGALNACT1	1.467457	3.570962	59.99358	9.52E-15	3.23E-13
186	HPGD	1.189323	3.546501	44.59851	2.42E-11	5.74E-10
187	PARPBP	-1.0267	3.618575	32.07735	1.48E-08	2.47E-07
188	LAT2	1.808413	3.494342	81.74352	1.55E-19	8.15E-18
189	ORM2	2.277915	3.458973	103.6533	2.41E-24	1.78E-22
190	CKAP2L	-1.37663	3.497197	66.26921	3.93E-16	1.53E-14
191	LOC100128191	-1.10586	3.508863	50.82687	1.01E-12	2.76E-11
192	SGOL1	-1.285	3.475341	71.60043	2.63E-17	1.17E-15
193	CENPA	-1.16333	3.460974	63.32866	1.75E-15	6.43E-14
194	DNA2	-1.07637	3.405734	27.57142	1.51E-07	2.12E-06
195	E2F8	-1.45672	3.392733	66.72104	3.13E-16	1.22E-14
196	ZNF367	-1.26754	3.380485	38.95944	4.33E-10	8.69E-09
197	BLM	-1.44642	3.366816	68.87758	1.05E-16	4.27E-15
198	GSG2	-1.15996	3.364504	60.92601	5.93E-15	2.04E-13
199	MND1	-1.27578	3.307658	44.33562	2.77E-11	6.55E-10
200	SLC2A3	1.635052	3.21207	43.81152	3.62E-11	8.47E-10
201	NEIL3	-1.23068	3.264715	57.13893	4.06E-14	1.28E-12
202	C4orf46	-1.09017	3.184868	29.63386	5.22E-08	8.04E-07
203	WDR76	-1.40378	3.182243	74.41954	6.32E-18	2.95E-16

204	RBL1	-1.17563	3.150147	26.45176	2.70E-07	3.67E-06
205	ARMC12	1.379683	3.118034	55.38136	9.93E-14	3.00E-12
206	XRCC2	-1.3023	3.10956	59.86127	1.02E-14	3.42E-13
207	BRCA2	-1.41478	3.112857	66.44681	3.59E-16	1.40E-14
208	HELLS	-1.53223	3.100935	42.13719	8.51E-11	1.89E-09
209	CEP128	-1.24395	3.035504	43.14315	5.09E-11	1.17E-09
210	MMS22L	-1.29335	3.000201	39.26095	3.71E-10	7.57E-09
211	C1QTNF9B-AS1	1.100726	2.922719	27.94559	1.25E-07	1.78E-06
212	E2F7	-1.58824	2.942007	43.0215	5.41E-11	1.23E-09
213	AKAP12	1.100638	2.863866	21.66297	3.25E-06	3.62E-05
214	CENPI	-1.10423	2.932829	46.9114	7.43E-12	1.86E-10
215	CENPK	-1.01082	2.918185	22.05818	2.65E-06	3.01E-05
216	POLE2	-1.12344	2.88688	20.44972	6.12E-06	6.47E-05
217	LIN9	-1.27168	2.863285	40.22044	2.27E-10	4.75E-09
218	CENPQ	-1.09655	2.832032	32.19487	1.39E-08	2.34E-07
219	KIF18A	-1.30277	2.830089	40.64214	1.83E-10	3.88E-09
220	BRIP1	-1.41776	2.817232	44.91719	2.06E-11	4.94E-10
221	LOC100288637	-1.25103	2.787301	27.35663	1.69E-07	2.36E-06
222	AMACR	1.097843	2.704537	19.25968	1.14E-05	0.000114
223	RTKN2	-1.08436	2.716191	29.59898	5.31E-08	8.17E-07
224	RTTN	-1.08787	2.656886	33.65603	6.58E-09	1.16E-07
225	C17orf53	-1.05357	2.658987	29.12903	6.77E-08	1.02E-06
226	EPS8L1	1.487662	2.587459	28.84377	7.85E-08	1.16E-06
227	NPPC	1.455035	2.599821	36.19989	1.78E-09	3.35E-08
228	MYBPC1	1.509729	2.566469	56.84312	4.72E-14	1.48E-12
229	MYL9	1.044808	2.49094	29.31107	6.16E-08	9.37E-07
230	DMBX1	-1.30436	2.55599	42.3223	7.74E-11	1.73E-09
231	C4orf21	-1.11661	2.540547	25.10183	5.44E-07	7.01E-06
232	SPOCK1	1.424415	2.378154	41.58222	1.13E-10	2.47E-09
233	FAM54A	-1.55824	2.328249	44.20212	2.96E-11	7.00E-10
234	C1orf135	-1.33165	2.327583	42.16507	8.39E-11	1.86E-09
235	FAM72B	-1.00685	2.327372	27.98112	1.23E-07	1.76E-06
236	NAV3	-1.30885	2.307982	47.05214	6.91E-12	1.75E-10
237	ATAD5	-1.30778	2.251379	40.39695	2.07E-10	4.36E-09
238	C18orf54	-1.37064	2.27838	27.43676	1.62E-07	2.27E-06
239	TUBA3E	1.058685	2.242307	15.49707	8.26E-05	0.000678
240	WWTR1	1.058971	2.20958	22.2506	2.39E-06	2.74E-05
241	FAM81A	-1.05907	2.201616	22.58194	2.01E-06	2.34E-05
242	BAI2	-1.04187	2.210137	19.65704	9.27E-06	9.44E-05
243	SPTB	1.789417	2.147878	42.50964	7.03E-11	1.58E-09
244	BORA	-1.08328	2.176648	15.66585	7.56E-05	0.000627
245	RDM1	-1.23917	2.141119	29.91662	4.51E-08	7.02E-07

246	LOC100128361	-1.14282	2.14019	13.99811	0.000183	0.001348
247	DOCK8	1.214777	2.079418	17.03475	3.67E-05	0.000327
248	C5orf34	-1.24434	2.086564	30.32367	3.66E-08	5.77E-07
249	FAM83E	1.045876	2.024604	15.80158	7.03E-05	0.000588
250	FAM72A	-1.14168	1.984398	23.18369	1.47E-06	1.75E-05
251	TERT	-1.04564	1.971424	29.50947	5.56E-08	8.52E-07
252	TLL1	-1.43159	1.876395	39.11432	4.00E-10	8.08E-09
253	TNS4	1.09081	1.830132	13.78198	0.000205	0.001496
254	DKFZP586I1420	-1.20672	1.767396	27.97644	1.23E-07	1.76E-06
255	SCARA3	-1.17827	1.78656	20.50021	5.96E-06	6.33E-05
256	SNCG	1.540067	1.739804	40.4059	2.06E-10	4.35E-09
257	CNIH2	-1.14487	1.724738	16.27522	5.48E-05	0.000471
258	BEST1	-1.11194	1.710968	14.15187	0.000169	0.001258
259	MTBP	-1.01201	1.698324	17.09664	3.55E-05	0.000319
260	TG	1.618921	1.638793	20.00753	7.71E-06	8.00E-05
261	PLCH1	-1.60649	1.627385	37.55753	8.88E-10	1.73E-08
262	SLC38A4	1.052922	1.574071	12.12558	0.000497	0.003258
263	RIN2	-1.02774	1.548226	15.7213	7.34E-05	0.00061
264	SLC22A1	1.201327	1.531084	23.64649	1.16E-06	1.41E-05
265	MIR29C	1.252847	1.517626	14.419	0.000146	0.001116
266	TMEM92	1.375662	1.424565	24.06239	9.33E-07	1.15E-05
267	HIST1H1E	1.763121	1.355928	23.05116	1.58E-06	1.87E-05
268	ELOVL2	1.376338	1.352361	14.32076	0.000154	0.001166
269	FAM189A2	1.085025	1.351339	9.386104	0.002186	0.011536
270	LOC100507634	1.070315	1.305097	14.40869	0.000147	0.00112
271	ZNF726	-1.51561	1.314377	37.2321	1.05E-09	2.01E-08
272	CCDC150	-1.68177	1.32368	27.76753	1.37E-07	1.93E-06
273	FLT4	-1.7364	1.275186	43.6101	4.01E-11	9.31E-10
274	LOC144481	2.239074	1.240202	28.52418	9.25E-08	1.36E-06
275	FANCB	-1.22628	1.266418	24.93974	5.92E-07	7.58E-06
276	ZNF519	-1.09469	1.252172	19.82199	8.50E-06	8.71E-05
277	BRDT	-1.30824	1.227013	18.47476	1.72E-05	0.000166
278	REP15	1.131996	1.16051	8.149773	0.004307	0.020351
279	MYBL1	-1.18515	1.132487	14.21853	0.000163	0.001221
280	ANTXR1	-1.00703	1.103571	11.32855	0.000763	0.004684
281	BCL2	-1.31481	1.09301	14.37067	0.00015	0.001139
282	KCNG3	1.095702	1.072403	14.55977	0.000136	0.00105
283	LEF1	-1.31681	1.076696	17.32408	3.15E-05	0.000286
284	TGM3	-1.13365	1.063226	17.29202	3.21E-05	0.00029
285	LGI2	-1.23654	0.985462	17.02595	3.69E-05	0.000329

C) MeT vs DHT

No	gene_id	logFC (DHT_vs_Vehicle)	Direction of change (TRUE= Up-reg/FALSE=Down-reg)	logFC (MeT_vs_Vehicle)	Direction of change (TRUE= Up-reg/FALSE=Down-reg)	Direction of change for DHT and MeT (TRUE= similar/FALSE=diferent)	Potency of MeT vs DHT (TRUE= Yes /FALSE=No)
1	KRT8	1.045876342	TRUE	2.755781922	TRUE	TRUE	TRUE
2	TMPRSS2	1.034805517	TRUE	1.913299628	TRUE	TRUE	TRUE
3	FKBP5	1.332702783	TRUE	2.826146249	TRUE	TRUE	TRUE
4	ACSL3	1.359899873	TRUE	2.530338335	TRUE	TRUE	TRUE
5	SLC41A1	1.300348613	TRUE	2.693377322	TRUE	TRUE	TRUE
6	NDRG1	1.023857137	TRUE	3.390736204	TRUE	TRUE	TRUE
7	SMS	1.1572766	TRUE	2.166352624	TRUE	TRUE	TRUE
8	H2AFX	-1.030028221	FALSE	-2.202710294	FALSE	TRUE	TRUE
9	MCM7	-1.065352573	FALSE	-2.197546713	FALSE	TRUE	TRUE
10	MICAL1	1.500391067	TRUE	3.059148889	TRUE	TRUE	TRUE
11	MKI67	-1.197863921	FALSE	-2.675758539	FALSE	TRUE	TRUE
12	CBWD1	1.060669375	TRUE	1.778386773	TRUE	TRUE	TRUE
13	HMGB2	-1.168522187	FALSE	-1.92991569	FALSE	TRUE	TRUE
14	MYBL2	-1.039232839	FALSE	-2.268501325	FALSE	TRUE	TRUE
15	TPX2	-1.216047638	FALSE	-2.550768441	FALSE	TRUE	TRUE
16	SPAG5	-1.015957159	FALSE	-1.965860952	FALSE	TRUE	TRUE
17	MCM2	-1.211990237	FALSE	-3.254253329	FALSE	TRUE	TRUE
18	PCNA	-1.04151328	FALSE	-2.290764524	FALSE	TRUE	TRUE
19	TK1	-1.061913876	FALSE	-2.402434733	FALSE	TRUE	TRUE
20	CHRNA2	1.32836714	TRUE	1.634172626	TRUE	TRUE	TRUE
21	PLK1	-1.022220803	FALSE	-2.342325954	FALSE	TRUE	TRUE
22	CENPF	-1.159461023	FALSE	-2.65802473	FALSE	TRUE	TRUE
23	MCM4	-1.208081784	FALSE	-3.260585881	FALSE	TRUE	TRUE
24	LMNB1	-1.084695629	FALSE	-2.848586399	FALSE	TRUE	TRUE

25	CDC20	-1.14647327	FALSE	-2.512996723	FALSE	TRUE	TRUE
26	MCM3	-1.036232211	FALSE	-2.568954992	FALSE	TRUE	TRUE
27	RRM2	-1.276686341	FALSE	-2.974381993	FALSE	TRUE	TRUE
28	F5	1.193322934	TRUE	2.045851997	TRUE	TRUE	TRUE
29	NUSAP1	-1.267055087	FALSE	-2.614549279	FALSE	TRUE	TRUE
30	TCOF1	-1.069263668	FALSE	-2.34301276	FALSE	TRUE	TRUE
31	PRC1	-1.164698178	FALSE	-2.384901748	FALSE	TRUE	TRUE
32	TYMS	-1.183465165	FALSE	-2.708440284	FALSE	TRUE	TRUE
33	FEN1	-1.167763126	FALSE	-2.365989503	FALSE	TRUE	TRUE
34	CDK1	-1.105601811	FALSE	-2.718216424	FALSE	TRUE	TRUE
35	MCM5	-1.076269501	FALSE	-2.677088667	FALSE	TRUE	TRUE
36	TMPO	-1.125515723	FALSE	-2.521116016	FALSE	TRUE	TRUE
37	FANCI	-1.087788642	FALSE	-2.151618351	FALSE	TRUE	TRUE
38	ST6GALNAC1	1.035248874	TRUE	1.77890807	TRUE	TRUE	TRUE
39	TONSL	-1.043724519	FALSE	-2.799302478	FALSE	TRUE	TRUE
40	CHAF1A	-1.007177729	FALSE	-2.076061462	FALSE	TRUE	TRUE
41	KIF20A	-1.168971285	FALSE	-2.477091628	FALSE	TRUE	TRUE
42	SMC4	-1.090109412	FALSE	-2.106454983	FALSE	TRUE	TRUE
43	GNMT	1.219481919	TRUE	2.439455122	TRUE	TRUE	TRUE
44	UGT2B11	1.518935699	TRUE	3.381715294	TRUE	TRUE	TRUE
45	RECQL4	-1.060902593	FALSE	-2.445665156	FALSE	TRUE	TRUE
46	TCF19	-1.291775954	FALSE	-3.172965797	FALSE	TRUE	TRUE
47	CDCA5	-1.283365986	FALSE	-3.102866954	FALSE	TRUE	TRUE
48	TOP2A	-1.409466435	FALSE	-3.272675299	FALSE	TRUE	TRUE
49	UBE2C	-1.256344145	FALSE	-2.709209166	FALSE	TRUE	TRUE
50	CCNB2	-1.081067384	FALSE	-2.379299888	FALSE	TRUE	TRUE
51	RACGAP1	-1.066187692	FALSE	-2.253279945	FALSE	TRUE	TRUE
52	CCNF	-1.04615908	FALSE	-2.250083003	FALSE	TRUE	TRUE

53	KIFC1	-1.382295762	FALSE	-2.971603879	FALSE	TRUE	TRUE
54	E2F1	-1.175034137	FALSE	-3.036178507	FALSE	TRUE	TRUE
55	KIF2C	-1.242277497	FALSE	-2.924284205	FALSE	TRUE	TRUE
56	PKMYT1	-1.16667173	FALSE	-3.178917271	FALSE	TRUE	TRUE
57	CDC6	-1.129516281	FALSE	-2.71456379	FALSE	TRUE	TRUE
58	HMMR	-1.075463041	FALSE	-2.13970401	FALSE	TRUE	TRUE
59	NCAPG	-1.162266101	FALSE	-2.756747891	FALSE	TRUE	TRUE
60	CDCA3	-1.09270978	FALSE	-2.438049997	FALSE	TRUE	TRUE
61	MLF1IP	-1.12604774	FALSE	-2.595021465	FALSE	TRUE	TRUE
62	HJURP	-1.322013259	FALSE	-2.828667295	FALSE	TRUE	TRUE
63	POLA2	-1.079861112	FALSE	-2.164926123	FALSE	TRUE	TRUE
64	FAM83D	-1.209719625	FALSE	-2.453405967	FALSE	TRUE	TRUE
65	AURKA	-1.05393423	FALSE	-2.26681424	FALSE	TRUE	TRUE
66	BUB1B	-1.245511491	FALSE	-3.036462965	FALSE	TRUE	TRUE
67	CADPS2	1.363656093	TRUE	2.250906321	TRUE	TRUE	TRUE
68	DLGAP5	-1.122519594	FALSE	-2.210231158	FALSE	TRUE	TRUE
69	ASF1B	-1.252574853	FALSE	-3.830201677	FALSE	TRUE	TRUE
70	MAF	1.50887869	TRUE	2.93216193	TRUE	TRUE	TRUE
71	FANCD2	-1.166438719	FALSE	-2.133415414	FALSE	TRUE	TRUE
72	CCNA2	-1.220920171	FALSE	-2.989407496	FALSE	TRUE	TRUE
73	CAMK2N1	-1.136569859	FALSE	-2.143932843	FALSE	TRUE	TRUE
74	ANLN	-1.150842319	FALSE	-2.727502835	FALSE	TRUE	TRUE
75	CDT1	-1.081618517	FALSE	-2.689396398	FALSE	TRUE	TRUE
76	WDR62	-1.050337128	FALSE	-2.891531589	FALSE	TRUE	TRUE
77	MELK	-1.217921829	FALSE	-2.759500497	FALSE	TRUE	TRUE
78	NDC80	-1.353819497	FALSE	-2.660586973	FALSE	TRUE	TRUE
79	AURKB	-1.100437683	FALSE	-2.990827496	FALSE	TRUE	TRUE
80	ESPL1	-1.376994473	FALSE	-3.355118415	FALSE	TRUE	TRUE
81	PRKCA	1.122294464	TRUE	2.027002763	TRUE	TRUE	TRUE

82	WIPI1	1.393274809	TRUE	3.085674519	TRUE	TRUE	TRUE
83	CENPE	-1.15520954	FALSE	-2.555391363	FALSE	TRUE	TRUE
84	CDCA8	-1.1470038	FALSE	-2.759158596	FALSE	TRUE	TRUE
85	PBK	-1.189499367	FALSE	-2.072426546	FALSE	TRUE	TRUE
86	NCAPH	-1.170698346	FALSE	-3.25505236	FALSE	TRUE	TRUE
87	RFC4	-1.03248118	FALSE	-1.934632068	FALSE	TRUE	TRUE
88	ADAM7	1.029019992	TRUE	1.202613578	TRUE	TRUE	TRUE
89	CDC45	-1.265032209	FALSE	-3.024323883	FALSE	TRUE	TRUE
90	BUB1	-1.086081406	FALSE	-2.404529709	FALSE	TRUE	TRUE
91	GTSE1	-1.001211741	FALSE	-2.466957332	FALSE	TRUE	TRUE
92	BRCA1	-1.329380022	FALSE	-3.095206837	FALSE	TRUE	TRUE
93	AFF3	1.02549085	TRUE	1.782135488	TRUE	TRUE	TRUE
94	KIF11	-1.24269003	FALSE	-2.75344164	FALSE	TRUE	TRUE
95	PGC	1.437473724	TRUE	2.199557138	TRUE	TRUE	TRUE
96	PSRC1	-1.000392831	FALSE	-2.307361535	FALSE	TRUE	TRUE
97	UGT2B15	-1.021296841	FALSE	-1.583153089	FALSE	TRUE	TRUE
98	DEPDC1	-1.085305957	FALSE	-2.58639383	FALSE	TRUE	TRUE
99	ARHGAP11A	-1.091290913	FALSE	-2.798800982	FALSE	TRUE	TRUE
100	CIT	-1.309782345	FALSE	-3.021738838	FALSE	TRUE	TRUE
101	GINS1	-1.216166047	FALSE	-2.8470779	FALSE	TRUE	TRUE
102	RAD54L	-1.337438916	FALSE	-3.462746647	FALSE	TRUE	TRUE
103	DDB2	-1.131098339	FALSE	-2.002790306	FALSE	TRUE	TRUE
104	CDKN2C	-1.022411823	FALSE	-1.848961771	FALSE	TRUE	TRUE
105	CEP55	-1.169409436	FALSE	-2.712221536	FALSE	TRUE	TRUE
106	CLSPN	-1.321541214	FALSE	-3.806210426	FALSE	TRUE	TRUE
107	KNTC1	-1.200814389	FALSE	-2.787840551	FALSE	TRUE	TRUE
108	RFC5	-1.067554271	FALSE	-2.383980383	FALSE	TRUE	TRUE
109	BCHE	-1.004408418	FALSE	-2.256506198	FALSE	TRUE	TRUE

110	CDCA7L	-1.052642899	FALSE	-2.184383218	FALSE	TRUE	TRUE
111	C9orf100	-1.112348742	FALSE	-2.587372724	FALSE	TRUE	TRUE
112	GINS2	-1.026078761	FALSE	-2.260594946	FALSE	TRUE	TRUE
113	STEAP4	3.740503079	TRUE	6.927834265	TRUE	TRUE	TRUE
114	SOCS2	1.298868135	TRUE	2.464368219	TRUE	TRUE	TRUE
115	UGT2B28	2.151729029	TRUE	3.893654774	TRUE	TRUE	TRUE
116	MCM10	-1.396353967	FALSE	-4.324655992	FALSE	TRUE	TRUE
117	UHRF1	-1.24868542	FALSE	-3.611338214	FALSE	TRUE	TRUE
118	INPP4B	1.037968163	TRUE	1.779542035	TRUE	TRUE	TRUE
119	KIF18B	-1.247012844	FALSE	-3.756783914	FALSE	TRUE	TRUE
120	CDCA2	-1.19933997	FALSE	-2.754714744	FALSE	TRUE	TRUE
121	C21orf58	-1.026924267	FALSE	-2.359051929	FALSE	TRUE	TRUE
122	WDHD1	-1.098778331	FALSE	-2.5940982	FALSE	TRUE	TRUE
123	ZNF812	1.18891817	TRUE	2.544402562	TRUE	TRUE	TRUE
124	SHCBP1	-1.219179322	FALSE	-2.768879626	FALSE	TRUE	TRUE
125	KIF23	-1.159581868	FALSE	-2.973708564	FALSE	TRUE	TRUE
126	ORC6	-1.410427813	FALSE	-3.347110046	FALSE	TRUE	TRUE
127	POLQ	-1.45569072	FALSE	-3.263259538	FALSE	TRUE	TRUE
128	NUF2	-1.272495917	FALSE	-2.406721166	FALSE	TRUE	TRUE
129	NEK2	-1.265302279	FALSE	-2.464440633	FALSE	TRUE	TRUE
130	PSMC3IP	-1.062822576	FALSE	-2.447064317	FALSE	TRUE	TRUE
131	DTL	-1.467991792	FALSE	-4.496685228	FALSE	TRUE	TRUE
132	CDCA4	-1.042297429	FALSE	-2.953304223	FALSE	TRUE	TRUE
133	CDC7	-1.006128916	FALSE	-2.086704676	FALSE	TRUE	TRUE
134	TUBA3D	1.154626031	TRUE	2.335065764	TRUE	TRUE	TRUE
135	SKA3	-1.190066862	FALSE	-2.306758982	FALSE	TRUE	TRUE
136	TMEM194A	-1.076674222	FALSE	-2.426610686	FALSE	TRUE	TRUE
137	PAQR6	1.090060223	TRUE	1.064693465	TRUE	TRUE	FALSE
138	TARP	1.388336182	TRUE	2.008199636	TRUE	TRUE	TRUE

139	GINS4	-1.294914823	FALSE	-2.831174567	FALSE	TRUE	TRUE
140	CCDC141	1.189938719	TRUE	2.787907738	TRUE	TRUE	TRUE
141	DEPDC1B	-1.167203464	FALSE	-2.693087157	FALSE	TRUE	TRUE
142	ORC1	-1.195958423	FALSE	-2.92148973	FALSE	TRUE	TRUE
143	SPC24	-1.050331491	FALSE	-2.634475094	FALSE	TRUE	TRUE
144	POLD3	-1.016659061	FALSE	-1.930249025	FALSE	TRUE	TRUE
145	NRM	-1.034326925	FALSE	-1.933576918	FALSE	TRUE	TRUE
146	EME1	-1.260826713	FALSE	-3.065169405	FALSE	TRUE	TRUE
147	RFC3	-1.184657999	FALSE	-2.857837015	FALSE	TRUE	TRUE
148	FIGNL1	-1.018572707	FALSE	-2.516167238	FALSE	TRUE	TRUE
149	ASPM	-1.430598464	FALSE	-3.05576722	FALSE	TRUE	TRUE
150	CDC25C	-1.123047229	FALSE	-2.27892595	FALSE	TRUE	TRUE
151	DIAPH3	-1.241987969	FALSE	-2.229247879	FALSE	TRUE	TRUE
152	TTK	-1.2464924	FALSE	-2.902844566	FALSE	TRUE	TRUE
153	ANO7	1.119115697	TRUE	1.582032662	TRUE	TRUE	TRUE
154	C1orf112	-1.119308744	FALSE	-1.626819576	FALSE	TRUE	TRUE
155	GPSM2	-1.134960417	FALSE	-2.344259362	FALSE	TRUE	TRUE
156	SGOL2	-1.128698025	FALSE	-2.272806317	FALSE	TRUE	TRUE
157	CEP78	-1.162716799	FALSE	-1.879714778	FALSE	TRUE	TRUE
158	KIF20B	-1.156046882	FALSE	-2.91237426	FALSE	TRUE	TRUE
159	EXO1	-1.369954807	FALSE	-4.222356158	FALSE	TRUE	TRUE
160	SKA1	-1.240749167	FALSE	-2.957023834	FALSE	TRUE	TRUE
161	C15orf42	-1.248834863	FALSE	-3.645150154	FALSE	TRUE	TRUE
162	SLITRK3	-1.02532286	FALSE	-2.738033774	FALSE	TRUE	TRUE
163	PLK4	-1.377753449	FALSE	-2.601874761	FALSE	TRUE	TRUE
164	KIF15	-1.543127387	FALSE	-3.320802452	FALSE	TRUE	TRUE
165	FBXO5	-1.196655444	FALSE	-2.251912723	FALSE	TRUE	TRUE
166	PRIM1	-1.211248231	FALSE	-2.798704947	FALSE	TRUE	TRUE
167	RAD51AP1	-1.157676361	FALSE	-3.10514468	FALSE	TRUE	TRUE

168	KIF24	-1.364466375	FALSE	-2.956187902	FALSE	TRUE	TRUE
169	OIP5	-1.14958276	FALSE	-2.262354289	FALSE	TRUE	TRUE
170	HAUS8	-1.02802212	FALSE	-2.794636226	FALSE	TRUE	TRUE
171	TRAIP	-1.075419141	FALSE	-2.200671601	FALSE	TRUE	TRUE
172	TTN	1.077945902	TRUE	2.614607718	TRUE	TRUE	TRUE
173	B3GALT4	1.182618545	TRUE	2.83244062	TRUE	TRUE	TRUE
174	RAD51	-1.079353332	FALSE	-2.983667145	FALSE	TRUE	TRUE
175	MNS1	-1.095024374	FALSE	-2.440617519	FALSE	TRUE	TRUE
176	E2F2	-1.234452908	FALSE	-3.574660124	FALSE	TRUE	TRUE
177	SH3D21	1.282618699	TRUE	2.647745216	TRUE	TRUE	TRUE
178	SPC25	-1.071551589	FALSE	-2.544504359	FALSE	TRUE	TRUE
179	GSTCD	-1.03502589	FALSE	-1.996536631	FALSE	TRUE	TRUE
180	KIF14	-1.361971458	FALSE	-2.713772216	FALSE	TRUE	TRUE
181	ESCO2	-1.451654145	FALSE	-3.551278606	FALSE	TRUE	TRUE
182	ORM1	2.685780251	TRUE	4.646724223	TRUE	TRUE	TRUE
183	CASC5	-1.263255053	FALSE	-3.545964195	FALSE	TRUE	TRUE
184	CCNE2	-1.118945868	FALSE	-3.265852377	FALSE	TRUE	TRUE
185	CSGALNACT1	1.467457205	TRUE	3.400679736	TRUE	TRUE	TRUE
186	HPGD	1.189322791	TRUE	2.10972209	TRUE	TRUE	TRUE
187	PARPBP	-1.026696093	FALSE	-2.44749604	FALSE	TRUE	TRUE
188	LAT2	1.808412928	TRUE	2.427610918	TRUE	TRUE	TRUE
189	ORM2	2.277914574	TRUE	4.097867053	TRUE	TRUE	TRUE
190	CKAP2L	-1.376627724	FALSE	-2.740723603	FALSE	TRUE	TRUE
191	LOC100128191	-1.105860761	FALSE	-2.648944929	FALSE	TRUE	TRUE
192	SGOL1	-1.285003552	FALSE	-2.766338523	FALSE	TRUE	TRUE
193	CENPA	-1.163331502	FALSE	-2.929527833	FALSE	TRUE	TRUE
194	DNA2	-1.076365642	FALSE	-2.766893559	FALSE	TRUE	TRUE

195	E2F8	-1.456717266	FALSE	-3.819975362	FALSE	TRUE	TRUE
196	ZNF367	-1.267542181	FALSE	-4.328131999	FALSE	TRUE	TRUE
197	BLM	-1.446418778	FALSE	-3.413560967	FALSE	TRUE	TRUE
198	GSG2	-1.159958704	FALSE	-3.462901799	FALSE	TRUE	TRUE
199	MND1	-1.275780661	FALSE	-3.12209387	FALSE	TRUE	TRUE
200	SLC2A3	1.635051806	TRUE	4.014407892	TRUE	TRUE	TRUE
201	NEIL3	-1.23067546	FALSE	-3.046048434	FALSE	TRUE	TRUE
202	C4orf46	-1.090166037	FALSE	-3.120734289	FALSE	TRUE	TRUE
203	WDR76	-1.403783484	FALSE	-2.686839002	FALSE	TRUE	TRUE
204	RBL1	-1.175630515	FALSE	-2.581728216	FALSE	TRUE	TRUE
205	ARMC12	1.379682894	TRUE	2.123023084	TRUE	TRUE	TRUE
206	XRCC2	-1.302298458	FALSE	-3.573656338	FALSE	TRUE	TRUE
207	BRCA2	-1.414784046	FALSE	-3.54997446	FALSE	TRUE	TRUE
208	HELLS	-1.532231649	FALSE	-3.389096455	FALSE	TRUE	TRUE
209	CEP128	-1.243949596	FALSE	-2.23337467	FALSE	TRUE	TRUE
210	MMS22L	-1.293353731	FALSE	-2.381910095	FALSE	TRUE	TRUE
211	C1QTNF9B-AS1	1.10072601	TRUE	2.154136878	TRUE	TRUE	TRUE
212	E2F7	-1.588243565	FALSE	-4.913846077	FALSE	TRUE	TRUE
213	AKAP12	1.100637771	TRUE	2.532328524	TRUE	TRUE	TRUE
214	CENPI	-1.104227625	FALSE	-3.011729362	FALSE	TRUE	TRUE
215	CENPK	-1.010823327	FALSE	-3.092695248	FALSE	TRUE	TRUE
216	POLE2	-1.123439223	FALSE	-2.156420233	FALSE	TRUE	TRUE
217	LIN9	-1.271678646	FALSE	-2.982933162	FALSE	TRUE	TRUE
218	CENPQ	-1.096545173	FALSE	-2.069731859	FALSE	TRUE	TRUE
219	KIF18A	-1.30277165	FALSE	-2.58675416	FALSE	TRUE	TRUE
220	BRIP1	-1.41776079	FALSE	-3.622375724	FALSE	TRUE	TRUE
221	LOC100288637	-1.251034885	FALSE	-2.516472719	FALSE	TRUE	TRUE

222	AMACR	1.097842667	TRUE	2.005658133	TRUE	TRUE	TRUE
223	RTKN2	-1.084364609	FALSE	-2.064782461	FALSE	TRUE	TRUE
224	RTTN	-1.087868503	FALSE	-1.639532367	FALSE	TRUE	TRUE
225	C17orf53	-1.053568236	FALSE	-2.474477853	FALSE	TRUE	TRUE
226	EPS8L1	1.487662116	TRUE	2.620431689	TRUE	TRUE	TRUE
227	NPPC	1.455035342	TRUE	2.723004788	TRUE	TRUE	TRUE
228	MYBPC1	1.509729064	TRUE	1.523942741	TRUE	TRUE	TRUE
229	MYL9	1.044807814	TRUE	2.356211967	TRUE	TRUE	TRUE
230	DMBX1	-1.304358586	FALSE	-3.318635318	FALSE	TRUE	TRUE
231	C4orf21	-1.116614217	FALSE	-2.706746464	FALSE	TRUE	TRUE
232	SPOCK1	1.424415309	TRUE	1.86288276	TRUE	TRUE	TRUE
233	FAM54A	-1.558239219	FALSE	-2.919502267	FALSE	TRUE	TRUE
234	C1orf135	-1.331645648	FALSE	-3.514170836	FALSE	TRUE	TRUE
235	FAM72B	-1.006851967	FALSE	-3.141893991	FALSE	TRUE	TRUE
236	NAV3	-1.308845358	FALSE	-2.872938246	FALSE	TRUE	TRUE
237	ATAD5	-1.307776291	FALSE	-3.021105108	FALSE	TRUE	TRUE
238	C18orf54	-1.370639646	FALSE	-3.364205193	FALSE	TRUE	TRUE
239	TUBA3E	1.058685319	TRUE	1.54967697	TRUE	TRUE	TRUE
240	WWTR1	1.058971357	TRUE	1.395273429	TRUE	TRUE	TRUE
241	FAM81A	-1.059074227	FALSE	-2.049243476	FALSE	TRUE	TRUE
242	BAI2	-1.041866526	FALSE	-2.082050513	FALSE	TRUE	TRUE
243	SPTB	1.789417358	TRUE	3.032925756	TRUE	TRUE	TRUE
244	BORA	-1.083276266	FALSE	-1.725870742	FALSE	TRUE	TRUE
245	RDM1	-1.239172797	FALSE	-1.561782172	FALSE	TRUE	TRUE
246	LOC100128361	-1.14281644	FALSE	-2.174185642	FALSE	TRUE	TRUE
247	DOCK8	1.214777253	TRUE	1.663145353	TRUE	TRUE	TRUE
248	C5orf34	-1.244339471	FALSE	-2.760752528	FALSE	TRUE	TRUE
249	FAM83E	1.045875529	TRUE	2.570062662	TRUE	TRUE	TRUE

250	FAM72A	-1.141683692	FALSE	-2.564204856	FALSE	TRUE	TRUE
251	TERT	-1.045640638	FALSE	-4.156096455	FALSE	TRUE	TRUE
252	TLL1	-1.431590211	FALSE	-2.608579968	FALSE	TRUE	TRUE
253	TNS4	1.090810064	TRUE	2.242506408	TRUE	TRUE	TRUE
254	DKFZP586I1420	-1.206721235	FALSE	na	na	na	na
255	SCARA3	-1.178270901	FALSE	-2.282576928	FALSE	TRUE	TRUE
256	SNCG	1.540067338	TRUE	2.141418164	TRUE	TRUE	TRUE
257	CNIH2	-1.144865495	FALSE	-1.211409805	FALSE	TRUE	TRUE
258	BEST1	-1.111941307	FALSE	-2.169326688	FALSE	TRUE	TRUE
259	MTBP	-1.012011262	FALSE	-2.650291204	FALSE	TRUE	TRUE
260	TG	1.618921061	TRUE	4.164600171	TRUE	TRUE	TRUE
261	PLCH1	-1.606490775	FALSE	-2.493679618	FALSE	TRUE	TRUE
262	SLC38A4	1.052921933	TRUE	1.956430774	TRUE	TRUE	TRUE
263	RIN2	-1.027735094	FALSE	-1.087612492	FALSE	TRUE	TRUE
264	SLC22A1	1.201327452	TRUE	1.779196776	TRUE	TRUE	TRUE
265	MIR29C	1.252846758	TRUE	na	na	na	na
266	TMEM92	1.375662294	TRUE	2.26777347	TRUE	TRUE	TRUE
267	HIST1H1E	1.763121375	TRUE	2.965480185	TRUE	TRUE	TRUE
268	ELOVL2	1.376338484	TRUE	3.171632272	TRUE	TRUE	TRUE
269	FAM189A2	1.085025011	TRUE	2.414360391	TRUE	TRUE	TRUE
270	LOC100507634	1.070314585	TRUE	1.30328445	TRUE	TRUE	TRUE
271	ZNF726	-1.515607382	FALSE	-1.792125284	FALSE	TRUE	TRUE
272	CCDC150	-1.681765513	FALSE	-2.978122952	FALSE	TRUE	TRUE
273	FLT4	-1.736401302	FALSE	-2.637010841	FALSE	TRUE	TRUE
274	LOC144481	2.239074443	TRUE	3.840201325	TRUE	TRUE	TRUE
275	FANCB	-1.226284941	FALSE	-3.293278214	FALSE	TRUE	TRUE
276	ZNF519	-1.094688579	FALSE	-1.761359961	FALSE	TRUE	TRUE

277	BRDT	-1.308242704	FALSE	-2.042411341	FALSE	TRUE	TRUE
278	REP15	1.131995532	TRUE	3.918908125	TRUE	TRUE	TRUE
279	MYBL1	-1.18514824	FALSE	-2.584986562	FALSE	TRUE	TRUE
280	ANTXR1	-1.007032067	FALSE	-1.864352091	FALSE	TRUE	TRUE
281	BCL2	-1.314809671	FALSE	-2.225353599	FALSE	TRUE	TRUE
282	KCNG3	1.095702456	TRUE	1.628504918	TRUE	TRUE	TRUE
283	LEF1	-1.316811997	FALSE	na	na	na	na
284	TGM3	-1.133649271	FALSE	-3.30532901	FALSE	TRUE	TRUE
285	LGI2	-1.236536649	FALSE	-4.032093846	FALSE	TRUE	TRUE

Supplementary Table S1. Primer sequences for qRT-PCRs

Primer	Sequence	Application
STING-Fwd	AGCATTACAACAACCTGCTACG	qRT-PCR
STING-Rev	GTTGGGGTCAGCCATACTCAG	qRT-PCR
ERV3-env-Fwd	CCATGGGAAGCAAGGGAACT	qRT-PCR
ERV3-env-Rev	CTTTCCCCAGCGAGCAATAC	qRT-PCR
HERV-W-Fwd	TGAGTCAATTCTCATACCTG	qRT-PCR
HERV-W-Rev	AGTTAAGAGTTCTTGGGTGG	qRT-PCR
HERVE Fwd	GGTGTCACTACTCAATACAC	qRT-PCR
HERVE-Rev	GCAGCCTAGGTCTCTGG	qRT-PCR
HERV F-Fwd	CCTCCAGTCACAACAACTC	qRT-PCR
HERV F-Rev	TATTGAAGAAGGCGGCTGG	qRT-PCR
ERVL-Fwd	ATATCCTGCCTGGATGGGGT	qRT-PCR
ERVL-Rew	GAGCTTCTTAGTCCTCCTGTGT	qRT-PCR
HERV-F-Fwd	CCTCCAGTCACAACAACTC	qRT-PCR
HERV-F-Rev	TATTGAAGAAGGCGGCTGG	qRT-PCR
HERV-K-Fwd	ATTGGCAACACCGTATTCTGCT	qRT-PCR
HERV-K-Rev	CAGTCAAAATATGGACGGATGGT	qRT-PCR
DNMT1-Fwd	GCGTTCCGGCTGAACAAC	qRT-PCR
DNMT1-Rev	GCATCTCCACGTCTCCCT	qRT-PCR
EZH2--RT-fwd	GTGGAGAGATTATTTCTCAAGATG	qRT-PCR
EZH2-RT-Rev	CCGACATACTTCAGGGCATCAGCC	qRT-PCR
B2M-RT-fwd	TGACTTTGTCACAGCCCAAG	qRT-PCR
B2M-RT-Rev	AGCAAGCAAGCAGAATTTGG	qRT-PCR
HLA-A-RT-fwd	GGCCCTGACCCAGACCTG	qRT-PCR
HLA-A-RT-Rev	GCACGAACTGCGTGTCGTC	qRT-PCR
HLA-B-RT-fwd	ACTGAGCTTGTGGAGACCAGA	qRT-PCR
HLA-B-RT-Rev	GCAGCCCCTCATGCTGT	qRT-PCR
HLA-C-RT-fwd	CTGGCCCTGACCGAGACCTG	qRT-PCR
HLA-C-RT-Rev	CGCTTGTACTTCTGTGTCTCC	qRT-PCR
IFN-β-RT-fwd	GCCATCAGTCACTTAAACAGC	qRT-PCR
IFN-β-RT-Rev	GAAACTGAAGATCTCCTAGCCT	qRT-PCR
ISG15-RT-fwd	CCTTCAGCTCTGACACC	qRT-PCR
ISG15-RT-Rev	CGAACTCATCTTTGCCAGTACA	qRT-PCR
IRF7-RT-fwd	GTGGACTGAGGGCTTGTAG	qRT-PCR
IRF7-RT-Rev	TCAACACCTGTGACTTCATGT	qRT-PCR
MAVS-RT-fwd	AGGAGACAGATGGAGACACA	qRT-PCR
MAVS-RT-Rev	CAGAACTGGGCAGTACCC	qRT-PCR
RIG-I-RT-fwd	CCAGCATTACTAGTCAGAAGGAA	qRT-PCR
RIG-I-RT-Rev	CACAGTGCAATCTTGTCATCC	qRT-PCR

Mouse-IRF7-fwd	CCACACCCCCATCTTCGA	qRT-PCR
Mouse-IRF7-Rev	CCTCCGAGCCCGAAACTC	qRT-PCR
Mouse-psmb9-fwd	TAGTAGCTGGCTGGGACCAA	qRT-PCR
Mouse-psmb9-Rev	GATGGTAAAGGGCTGTCGAA	qRT-PCR
Mouse-HPRT-fwd	GGCCAGACTTTGTTGGATTT	qRT-PCR
Mouse-HPRT-Rev	ACTGGCAACATCAACAGGACT	qRT-PCR
Mouse-STING-Fwd	GGTCACCGCTCCAAATATGTAG	qRT-PCR
Mouse-STING-Rev	CAGTAGTCCAAGTTCGTGCGA	qRT-PCR
Mouse-DDX58(RIG-I)-Fwd	AAGAGCCAGAGTGTCAGAATCT	qRT-PCR
Mouse-DDX58(RIG-I)-Rev	AGCTCCAGTTGGTAATTTCTTGG	qRT-PCR
Mouse-DNMT1-Fwd	CCAGGCATTTCGGCTGAA	qRT-PCR
Mouse-DNMT1-Rev	CGTTGCAGTCCTCTGTGAACA	qRT-PCR
Mouse-LINE1-fwd	GGACCAGAAAAGAAATTCCTCCCG	qRT-PCR
Mouse-LINE1-rev	CTCTTCTGGCTTTCATAGTCTCTGG	qRT-PCR
Mouse-ERV-MTA-fwd	TCTGTGGGATGTTGTGTAGGAG	qRT-PCR
Mouse-ERV-MTA-Rev	CCACAGATCTTCACAATCCAAA	qRT-PCR
Mouse-ERV-RLTR1B-fwd	GGTCCACACAAACACCTACCTT	qRT-PCR
Mouse-ERV-RLTR1B-Rev	TTTGAGATACACCCTTCGAGGT	qRT-PCR
Mouse-ERV-RLTR45-fwd	ACCTTGGACCTTTCTCAATACAT	qRT-PCR
Mouse-ERV-RLTR45-Rev	GACCTCCTCCTAATAACCAAATG	qRT-PCR
Mouse-ERV-IAPEZ-fwd	AAATCAATCTGTTGTGTTTCCAC	qRT-PCR
Mouse-ERV-IAPEZ-Rev	ACCACATAACAGGAATCTGACAC	qRT-PCR

Supplementary Data2. GSEA report for top enriched Hallmark genesets (p ≤ 0.05) with a positive NES

	Name	NES	FDR q-val
1	**HALLMARK_ANDROGEN_RESPONSE**	2.8952408	0
2	**HALLMARK_PROTEIN_SECRETION**	2.3557687	0
3	**HALLMARK_APICAL_JUNCTION**	1.8830771	0.02535794
4	**HALLMARK_CHOLESTEROL_HOMEOSTASIS**	1.7936019	0.03255346
5	**HALLMARK_ESTROGEN_RESPONSE_EARLY**	1.788912	0.02765674
6	**HALLMARK_XENOBIOTIC_METABOLISM**	1.7781266	0.02561309
7	**HALLMARK_COAGULATION**	1.7351228	0.02783313
8	**HALLMARK_FATTY_ACID_METABOLISM**	1.7211664	0.02772199
9	**HALLMARK_EPITHELIAL_MESENCHYMAL_TRANSITION**	1.6315349	0.0438025

Supplementary Data3. GSEA report for top enriched Hallmark genesets (p ≤ 0.05) with a Negative NES

	Name	NES	FDR q-val
1	**HALLMARK_E2F_TARGETS**	-3.283671	0
2	**HALLMARK_G2M_CHECKPOINT**	-3.0368714	0
3	**HALLMARK_MYC_TARGETS_V1**	-2.536929	0
4	**HALLMARK_MITOTIC_SPINDLE**	-2.4192386	0
5	**HALLMARK_MYC_TARGETS_V2**	-2.110342	0
6	**HALLMARK_DNA_REPAIR**	-1.8421776	8.29E-04
7	**HALLMARK_SPERMATOGENESIS**	-1.8274815	8.81E-04

REFERENCES

Bannert, N., Hofmann, H., Block, A., and Hohn, O. (2018). HERVs New Role in Cancer: From Accused Perpetrators to Cheerful Protectors. Front Microbiol *9*, 178.

Bishop, J.L., Thaper, D., Vahid, S., Davies, A., Ketola, K., Kuruma, H., Jama, R., Nip, K.M., Angeles, A., Johnson, F.*, et al.* (2017). The Master Neural Transcription Factor BRN2 Is an Androgen Receptor-Suppressed Driver of Neuroendocrine Differentiation in Prostate Cancer. Cancer Discov *7*, 54-71.

Buchanan, G., Yang, M., Cheong, A., Harris, J.M., Irvine, R.A., Lambert, P.F., Moore, N.L., Raynor, M., Neufing, P.J., and Coetzee, G.A. (2004). Structural and functional consequences of glutamine tract variation in the androgen receptor. Human molecular genetics *13*, 1677-1692.

Cai, C., Yuan, X., and Balk, S.P. (2013). Androgen receptor epigenetics. Transl Androl Urol *2*, 148-157.

Chan, S.C., Selth, L.A., Li, Y., Nyquist, M.D., Miao, L., Bradner, J.E., Raj, G.V., Tilley, W.D., and Dehm, S.M. (2015). Targeting chromatin binding regulation of constitutively active AR variants to overcome prostate cancer resistance to endocrine-based therapies. Nucleic Acids Res.

Chatterjee, P., Schweizer, M.T., Lucas, J.M., Coleman, I., Nyquist, M.D., Frank, S.B., Tharakan, R., Mostaghel, E., Luo, J., Pritchard, C.C.*, et al.* (2019). Supraphysiological androgens suppress prostate cancer growth through androgen receptor-mediated DNA damage. The Journal of clinical investigation *129*, 4245-4260.

Chiappinelli, K.B., Strissel, P.L., Desrichard, A., Li, H., Henke, C., Akman, B., Hein, A., Rote, N.S., Cope, L.M., Snyder, A.*, et al.* (2015). Inhibiting DNA Methylation Causes an Interferon Response in Cancer via dsRNA Including Endogenous Retroviruses. Cell *162*, 974-986.

Chu, M., Chang, Y., Li, P., Guo, Y., Zhang, K., and Gao, W. (2014). Androgen receptor is negatively correlated with the methylation-mediated transcriptional repression of miR-375 in human prostate cancer cells. Oncol Rep *31*, 34-40.

Coutinho, I., Day, T.K., Tilley, W.D., and Selth, L.A. (2016). Androgen receptor signaling in castration-resistant prostate cancer: a lesson in persistence. Endocrine-related cancer *23*, T179-T197.

Criscione, S.W., Zhang, Y., Thompson, W., Sedivy, J.M., and Neretti, N. (2014). Transcriptional landscape of repetitive elements in normal and cancer human cells. BMC Genomics *15*, 583.

Das, R., Gregory, P.A., Fernandes, R.C., Denis, I., Wang, Q., Townley, S.L., Zhao, S.G., Hanson, A.R., Pickering, M.A., Armstrong, H.K.*, et al.* (2017). MicroRNA-194 Promotes Prostate Cancer Metastasis by Inhibiting SOCS2. Cancer research *77*, 1021-1034.

de Almeida, D.V.P., Fong, L., Rettig, M.B., and Autio, K.A. (2020). Immune Checkpoint Blockade for Prostate Cancer: Niche Role or Next Breakthrough? Am Soc Clin Oncol Educ Book *40*, 1-18.

Dobin, A., Davis, C.A., Schlesinger, F., Drenkow, J., Zaleski, C., Jha, S., Batut, P., Chaisson, M., and Gingeras, T.R. (2013). STAR: ultrafast universal RNA-seq aligner. Bioinformatics *29*, 15-21.

Gao, S., Gao, Y., He, H.H., Han, D., Han, W., Avery, A., Macoska, J.A., Liu, X., Chen, S., Ma, F.*, et al.* (2016). Androgen Receptor Tumor Suppressor Function Is Mediated by Recruitment of Retinoblastoma Protein. Cell reports *17*, 966-976.

Goel, S., DeCristo, M.J., Watt, A.C., BrinJones, H., Sceneay, J., Li, B.B., Khan, N., Ubellacker, J.M., Xie, S., Metzger-Filho, O.*, et al.* (2017). CDK4/6 inhibition triggers anti-tumour immunity. Nature *548*, 471-475.

Graff, J.N., Alumkal, J.J., Drake, C.G., Thomas, G.V., Redmond, W.L., Farhad, M., Cetnar, J.P., Ey, F.S., Bergan, R.C., Slottke, R.*, et al.* (2016). Early evidence of anti-PD-1 activity in enzalutamide-resistant prostate cancer. Oncotarget *7*, 52810-52817.

Heinz, S., Benner, C., Spann, N., Bertolino, E., Lin, Y.C., Laslo, P., Cheng, J.X., Murre, C., Singh, H., and Glass, C.K. (2010). Simple combinations of lineage-determining transcription factors prime cis-regulatory elements required for macrophage and B cell identities. Molecular cell *38*, 576-589.

Huggins, C. (1965). Two principles in endocrine therapy of cancers: hormone deprival and hormone interference. Cancer research *25*, 1163-1167.

Ji, H., Jiang, H., Ma, W., Johnson, D.S., Myers, R.M., and Wong, W.H. (2008). An integrated software system for analyzing ChIP-chip and ChIP-seq data. Nature biotechnology *26*, 1293-1300.

Jia, L., Kim, J., Shen, H., Clark, P.E., Tilley, W.D., and Coetzee, G.A. (2003). Androgen receptor activity at the prostate specific antigen locus: steroidal and non-steroidal mechanisms. Molecular cancer research : MCR *1*, 385-392.

Kantoff, P.W., Higano, C.S., Shore, N.D., Berger, E.R., Small, E.J., Penson, D.F., Redfern, C.H., Ferrari, A.C., Dreicer, R., Sims, R.B.*, et al.* (2010). Sipuleucel-T immunotherapy for castration-resistant prostate cancer. N Engl J Med *363*, 411-422.

Kimura, H., Nakamura, T., Ogawa, T., Tanaka, S., and Shiota, K. (2003). Transcription of mouse DNA methyltransferase 1 (Dnmt1) is regulated by both E2F-Rb-HDAC-dependent and -independent pathways. Nucleic Acids Res *31*, 3101-3113.

Kotredes, K.P., and Gamero, A.M. (2013). Interferons as inducers of apoptosis in malignant cells. J Interferon Cytokine Res *33*, 162-170.

Krug, B., De Jay, N., Harutyunyan, A.S., Deshmukh, S., Marchione, D.M., Guilhamon, P., Bertrand, K.C., Mikael, L.G., McConechy, M.K., Chen, C.C.L.*, et al.* (2019). Pervasive H3K27 Acetylation Leads to ERV Expression and a Therapeutic Vulnerability in H3K27M Gliomas. Cancer cell *35*, 782-797 e788.

Liao, Y., Smyth, G.K., and Shi, W. (2014). featureCounts: an efficient general purpose program for assigning sequence reads to genomic features. Bioinformatics *30*, 923-930.

Liberzon, A., Birger, C., Thorvaldsdottir, H., Ghandi, M., Mesirov, J.P., and Tamayo, P. (2015). The Molecular Signatures Database (MSigDB) hallmark gene set collection. Cell Syst *1*, 417-425.

Lun, A.T., Chen, Y., and Smyth, G.K. (2016). It's DE-licious: a recipe for differential expression analyses of RNA-seq experiments using quasi-likelihood methods in edgeR. In Statistical genomics (Springer), pp. 391-416.

Madan, R.A., Karzai, F., Donahue, R.N., Al-Harthy, M., Bilusic, M., Rosner, II, Singh, H., Arlen, P.M., Theoret, M.R., Marte, J.L.*, et al.* (2021). Clinical and immunologic impact of short-course enzalutamide alone and with immunotherapy in non-metastatic castration sensitive prostate cancer. J Immunother Cancer *9*.

Markowski, M.C., Shenderov, E., Eisenberger, M.A., Kachhap, S., Pardoll, D.M., Denmeade, S.R., and Antonarakis, E.S. (2020). Extreme responses to immune checkpoint blockade following bipolar androgen therapy and enzalutamide in patients with metastatic castration resistant prostate cancer. The Prostate *80*, 407-411.

Martin, M. (2011). Cutadapt removes adapter sequences from high-throughput sequencing reads. EMBnet journal *17*, 10-12.

McCabe, M.T., Davis, J.N., and Day, M.L. (2005). Regulation of DNA methyltransferase 1 by the pRb/E2F1 pathway. Cancer research *65*, 3624-3632.

Metsalu, T., and Vilo, J. (2015). ClustVis: a web tool for visualizing clustering of multivariate data using Principal Component Analysis and heatmap. Nucleic acids research *43*, W566-W570.

Mohammad, O.S., Nyquist, M.D., Schweizer, M.T., Balk, S.P., Corey, E., Plymate, S., Nelson, P.S., and Mostaghel, E.A. (2017). Supraphysiologic Testosterone Therapy in the Treatment of Prostate Cancer: Models, Mechanisms and Questions. Cancers (Basel) *9*.

Moore, N.L., Buchanan, G., Harris, J.M., Selth, L.A., Bianco-Miotto, T., Hanson, A.R., Birrell, S.N., Butler, L.M., Hickey, T.E., and Tilley, W.D. (2012). An androgen receptor mutation in the MDA-MB-453 cell line model of molecular apocrine breast cancer compromises receptor activity. Endocrine related cancer *19*, 599.

Ni, G., Ma, Z., and Damania, B. (2018). cGAS and STING: At the intersection of DNA and RNA virus-sensing networks. PLoS Pathog *14*, e1007148.

Nyquist, M.D., Corella, A., Mohamad, O., Coleman, I., Kaipainen, A., Kuppers, D.A., Lucas, J.M., Paddison, P.J., Plymate, S.R., Nelson, P.S*., et al.* (2019). Molecular determinants of response to high-dose androgen therapy in prostate cancer. JCI Insight *4*.

Nyquist, M.D., Li, Y., Hwang, T.H., Manlove, L.S., Vessella, R.L., Silverstein, K.A., Voytas, D.F., and Dehm, S.M. (2013). TALEN-engineered AR gene rearrangements reveal endocrine uncoupling of androgen receptor in prostate cancer. Proceedings of the National Academy of Sciences of the United States of America *110*, 17492-17497.

Owen, K.L., Gearing, L.J., Zanker, D.J., Brockwell, N.K., Khoo, W.H., Roden, D.L., Cmero, M., Mangiola, S., Hong, M.K., Spurling, A.J*., et al.* (2020). Prostate cancer cell-intrinsic interferon signaling regulates dormancy and metastatic outgrowth in bone. EMBO Rep *21*, e50162.

Paltoglou, S., Das, R., Townley, S.L., Hickey, T.E., Tarulli, G.A., Coutinho, I., Fernandes, R., Hanson, A.R., Denis, I., and Carroll, J.S. (2017). Novel androgen receptor coregulator GRHL2 exerts both oncogenic and antimetastatic functions in prostate cancer. Cancer research *77*, 3417-3430.

Ramírez, F., Ryan, D.P., Grüning, B., Bhardwaj, V., Kilpert, F., Richter, A.S., Heyne, S., Dündar, F., and Manke, T. (2016). deepTools2: a next generation web server for deep-sequencing data analysis. Nucleic acids research *44*, W160-W165.

Robinson, M.D., McCarthy, D.J., and Smyth, G.K. (2010). edgeR: a Bioconductor package for differential expression analysis of digital gene expression data. Bioinformatics *26*, 139-140.

Roulois, D., Loo Yau, H., Singhania, R., Wang, Y., Danesh, A., Shen, S.Y., Han, H., Liang, G., Jones, P.A., Pugh, T.J*., et al.* (2015). DNA-Demethylating Agents Target Colorectal Cancer Cells by Inducing Viral Mimicry by Endogenous Transcripts. Cell *162*, 961-973.

Schneider, C.A., Rasband, W.S., and Eliceiri, K.W. (2012). NIH Image to ImageJ: 25 years of image analysis. Nature methods *9*, 671-675.

Sheng, W., LaFleur, M.W., Nguyen, T.H., Chen, S., Chakravarthy, A., Conway, J.R., Li, Y., Chen, H., Yang, H., Hsu, P.H*., et al.* (2018). LSD1 Ablation Stimulates Anti-tumor Immunity and Enables Checkpoint Blockade. Cell *174*, 549-563 e519.

Stone, M.L., Chiappinelli, K.B., Li, H., Murphy, L.M., Travers, M.E., Topper, M.J., Mathios, D., Lim, M., Shih, I.M., Wang, T.L*., et al.* (2017). Epigenetic therapy activates type I interferon signaling in murine

ovarian cancer to reduce immunosuppression and tumor burden. Proceedings of the National Academy of Sciences of the United States of America *114*, E10981-E10990.

Subramanian, A., Tamayo, P., Mootha, V.K., Mukherjee, S., Ebert, B.L., Gillette, M.A., Paulovich, A., Pomeroy, S.L., Golub, T.R., and Lander, E.S. (2005). Gene set enrichment analysis: a knowledge-based approach for interpreting genome-wide expression profiles. Proceedings of the National Academy of Sciences *102*, 15545-15550.

Topper, M.J., Vaz, M., Chiappinelli, K.B., DeStefano Shields, C.E., Niknafs, N., Yen, R.C., Wenzel, A., Hicks, J., Ballew, M., Stone, M.*, et al.* (2017). Epigenetic Therapy Ties MYC Depletion to Reversing Immune Evasion and Treating Lung Cancer. Cell *171*, 1284-1300 e1221.

Tsihlias, J., Zhang, W., Bhattacharya, N., Flanagan, M., Klotz, L., and Slingerland, J. (2000). Involvement of p27Kip1 in G1 arrest by high dose 5 alpha-dihydrotestosterone in LNCaP human prostate cancer cells. Oncogene *19*, 670-679.

Abeshouse, A., Ahn, J., Akbani, R., Ally, A., Amin, S., Andry, C.D., Annala, M., Aprikian, A., Armenia, J., and Arora, A. (2015). The molecular taxonomy of primary prostate cancer. Cell *163*, 1011-1025.
Attardi, B.J., Hild, S.A., and Reel, J.R. (2006). Dimethandrolone undecanoate: a new potent orally active androgen with progestational activity. Endocrinology *147*, 3016-3026.
Auchus, R.J., and Sharifi, N. (2020). Sex Hormones and Prostate Cancer. Annu Rev Med *71*, 33-45.
Bannert, N., Hofmann, H., Block, A., and Hohn, O. (2018). HERVs New Role in Cancer: From Accused Perpetrators to Cheerful Protectors. Front Microbiol *9*, 178.
Barbie, D.A., Tamayo, P., Boehm, J.S., Kim, S.Y., Moody, S.E., Dunn, I.F., Schinzel, A.C., Sandy, P., Meylan, E., and Scholl, C. (2009). Systematic RNA interference reveals that oncogenic KRAS-driven cancers require TBK1. Nature *462*, 108.
Bertelloni, S., Baroncelli, G.I., Garofalo, P., and Cianfarani, S. (2010). Androgen therapy in hypogonadal adolescent males. Horm Res Paediatr *74*, 292-296.
Bidwell, B.N., Slaney, C.Y., Withana, N.P., Forster, S., Cao, Y., Loi, S., Andrews, D., Mikeska, T., Mangan, N.E., Samarajiwa, S.A.*, et al.* (2012). Silencing of Irf7 pathways in breast cancer cells promotes bone metastasis through immune escape. Nat Med *18*, 1224-1231.
Bishop, J.L., Thaper, D., Vahid, S., Davies, A., Ketola, K., Kuruma, H., Jama, R., Nip, K.M., Angeles, A., Johnson, F.*, et al.* (2017). The Master Neural Transcription Factor BRN2 Is an Androgen Receptor-Suppressed Driver of Neuroendocrine Differentiation in Prostate Cancer. Cancer Discov *7*, 54-71.
Buchanan, G., Yang, M., Cheong, A., Harris, J.M., Irvine, R.A., Lambert, P.F., Moore, N.L., Raynor, M., Neufing, P.J., and Coetzee, G.A. (2004). Structural and functional consequences of glutamine tract variation in the androgen receptor. Human molecular genetics *13*, 1677-1692.
Bui, A.T., Huang, M.E., Havard, M., Laurent-Tchenio, F., Dautry, F., and Tchenio, T. (2017). Transient exposure to androgens induces a remarkable self-sustained quiescent state in dispersed prostate cancer cells. Cell cycle *16*, 879-893.
Cai, C., Yuan, X., and Balk, S.P. (2013). Androgen receptor epigenetics. Transl Androl Urol *2*, 148-157.
Chan, S.C., Selth, L.A., Li, Y., Nyquist, M.D., Miao, L., Bradner, J.E., Raj, G.V., Tilley, W.D., and Dehm, S.M. (2015). Targeting chromatin binding regulation of constitutively active AR variants to overcome prostate cancer resistance to endocrine-based therapies. Nucleic Acids Res.
Chatterjee, P., Schweizer, M.T., Lucas, J.M., Coleman, I., Nyquist, M.D., Frank, S.B., Tharakan, R., Mostaghel, E., Luo, J., Pritchard, C.C.*, et al.* (2019). Supraphysiological androgens suppress prostate cancer growth through androgen receptor-mediated DNA damage. The Journal of clinical investigation *129*, 4245-4260.

Chiappinelli, K.B., Strissel, P.L., Desrichard, A., Li, H., Henke, C., Akman, B., Hein, A., Rote, N.S., Cope, L.M., Snyder, A.*, et al.* (2015). Inhibiting DNA Methylation Causes an Interferon Response in Cancer via dsRNA Including Endogenous Retroviruses. Cell *162*, 974-986.
Chiuve, S.E., Martin, L.A., Campos, H., and Sacks, F.M. (2004). Effect of the combination of methyltestosterone and esterified estrogens compared with esterified estrogens alone on apolipoprotein CIII and other apolipoproteins in very low density, low density, and high density lipoproteins in surgically postmenopausal women. J Clin Endocrinol Metab *89*, 2207-2213.
Christiansen, A.R., Lipshultz, L.I., Hotaling, J.M., and Pastuszak, A.W. (2020). Selective androgen receptor modulators: the future of androgen therapy? Transl Androl Urol *9*, S135-S148.
Chu, M., Chang, Y., Li, P., Guo, Y., Zhang, K., and Gao, W. (2014). Androgen receptor is negatively correlated with the methylation-mediated transcriptional repression of miR-375 in human prostate cancer cells. Oncol Rep *31*, 34-40.
Coutinho, I., Day, T.K., Tilley, W.D., and Selth, L.A. (2016). Androgen receptor signaling in castration-resistant prostate cancer: a lesson in persistence. Endocrine-related cancer *23*, T179-T197.
Criscione, S.W., Zhang, Y., Thompson, W., Sedivy, J.M., and Neretti, N. (2014). Transcriptional landscape of repetitive elements in normal and cancer human cells. BMC Genomics *15*, 583.
D'Antonio, J.M., Vander Griend, D.J., and Isaacs, J.T. (2009). DNA licensing as a novel androgen receptor mediated therapeutic target for prostate cancer. Endocrine-related cancer *16*, 325-332.
Das, R., Gregory, P.A., Fernandes, R.C., Denis, I., Wang, Q., Townley, S.L., Zhao, S.G., Hanson, A.R., Pickering, M.A., Armstrong, H.K.*, et al.* (2017). MicroRNA-194 Promotes Prostate Cancer Metastasis by Inhibiting SOCS2. Cancer research *77*, 1021-1034.
de Almeida, D.V.P., Fong, L., Rettig, M.B., and Autio, K.A. (2020). Immune Checkpoint Blockade for Prostate Cancer: Niche Role or Next Breakthrough? Am Soc Clin Oncol Educ Book *40*, 1-18.
Denmeade, S.R., Wang, H., Agarwal, N., Smith, D.C., Schweizer, M.T., Stein, M.N., Assikis, V., Twardowski, P.W., Flaig, T.W., Szmulewitz, R.Z.*, et al.* (2021). TRANSFORMER: A Randomized Phase II Study Comparing Bipolar Androgen Therapy Versus Enzalutamide in Asymptomatic Men With Castration-Resistant Metastatic Prostate Cancer. J Clin Oncol *39*, 1371-1382.
Dobin, A., Davis, C.A., Schlesinger, F., Drenkow, J., Zaleski, C., Jha, S., Batut, P., Chaisson, M., and Gingeras, T.R. (2013). STAR: ultrafast universal RNA-seq aligner. Bioinformatics *29*, 15-21.
El-Desoky el, S.I., Reyad, M., Afsah, E.M., and Dawidar, A.A. (2016). Synthesis and chemical reactions of the steroidal hormone 17alpha-methyltestosterone. Steroids *105*, 68-95.
Fang, H., Tong, W., Branham, W.S., Moland, C.L., Dial, S.L., Hong, H., Xie, Q., Perkins, R., Owens, W., and Sheehan, D.M. (2003). Study of 202 natural, synthetic, and environmental chemicals for binding to the androgen receptor. Chem Res Toxicol *16*, 1338-1358.
Gao, J., Aksoy, B.A., Dogrusoz, U., Dresdner, G., Gross, B., Sumer, S.O., Sun, Y., Jacobsen, A., Sinha, R., Larsson, E.*, et al.* (2013). Integrative analysis of complex cancer genomics and clinical profiles using the cBioPortal. Sci Signal *6*, pl1.
Gao, L., and Alumkal, J. (2010). Epigenetic regulation of androgen receptor signaling in prostate cancer. Epigenetics *5*, 100-104.
Gao, S., Gao, Y., He, H.H., Han, D., Han, W., Avery, A., Macoska, J.A., Liu, X., Chen, S., Ma, F.*, et al.* (2016). Androgen Receptor Tumor Suppressor Function Is Mediated by Recruitment of Retinoblastoma Protein. Cell reports *17*, 966-976.
Goel, S., DeCristo, M.J., Watt, A.C., BrinJones, H., Sceneay, J., Li, B.B., Khan, N., Ubellacker, J.M., Xie, S., Metzger-Filho, O.*, et al.* (2017). CDK4/6 inhibition triggers anti-tumour immunity. Nature *548*, 471-475.
Gonzalez-Cao, M., Karachaliou, N., Santarpia, M., Viteri, S., Meyerhans, A., and Rosell, R. (2018). Activation of viral defense signaling in cancer. Ther Adv Med Oncol *10*, 1758835918793105.

Graff, J.N., Alumkal, J.J., Drake, C.G., Thomas, G.V., Redmond, W.L., Farhad, M., Cetnar, J.P., Ey, F.S., Bergan, R.C., Slottke, R.*, et al.* (2016). Early evidence of anti-PD-1 activity in enzalutamide-resistant prostate cancer. Oncotarget *7*, 52810-52817.
Haffner, M.C., De Marzo, A.M., Meeker, A.K., Nelson, W.G., and Yegnasubramanian, S. (2011). Transcription-induced DNA double strand breaks: both oncogenic force and potential therapeutic target? Clinical cancer research : an official journal of the American Association for Cancer Research *17*, 3858-3864.
Heinz, S., Benner, C., Spann, N., Bertolino, E., Lin, Y.C., Laslo, P., Cheng, J.X., Murre, C., Singh, H., and Glass, C.K. (2010). Simple combinations of lineage-determining transcription factors prime cis-regulatory elements required for macrophage and B cell identities. Molecular cell *38*, 576-589.
Houghton, P., Fang, R., Techatanawat, I., Steventon, G., Hylands, P.J., and Lee, C.C. (2007). The sulphorhodamine (SRB) assay and other approaches to testing plant extracts and derived compounds for activities related to reputed anticancer activity. Methods *42*, 377-387.
Huggins, C. (1965). Two principles in endocrine therapy of cancers: hormone deprival and hormone interference. Cancer research *25*, 1163-1167.
Ji, H., Jiang, H., Ma, W., Johnson, D.S., Myers, R.M., and Wong, W.H. (2008). An integrated software system for analyzing ChIP-chip and ChIP-seq data. Nature biotechnology *26*, 1293-1300.
Jia, L., Kim, J., Shen, H., Clark, P.E., Tilley, W.D., and Coetzee, G.A. (2003). Androgen receptor activity at the prostate specific antigen locus: steroidal and non-steroidal mechanisms. Molecular cancer research : MCR *1*, 385-392.
Kantoff, P.W., Higano, C.S., Shore, N.D., Berger, E.R., Small, E.J., Penson, D.F., Redfern, C.H., Ferrari, A.C., Dreicer, R., Sims, R.B.*, et al.* (2010). Sipuleucel-T immunotherapy for castration-resistant prostate cancer. N Engl J Med *363*, 411-422.
Kim, T.Y., Zhong, S., Fields, C.R., Kim, J.H., and Robertson, K.D. (2006). Epigenomic profiling reveals novel and frequent targets of aberrant DNA methylation-mediated silencing in malignant glioma. Cancer research *66*, 7490-7501.
Kimura, H., Nakamura, T., Ogawa, T., Tanaka, S., and Shiota, K. (2003). Transcription of mouse DNA methyltransferase 1 (Dnmt1) is regulated by both E2F-Rb-HDAC-dependent and -independent pathways. Nucleic Acids Res *31*, 3101-3113.
Kokontis, J.M., Hay, N., and Liao, S. (1998). Progression of LNCaP prostate tumor cells during androgen deprivation: hormone-independent growth, repression of proliferation by androgen, and role for p27Kip1 in androgen-induced cell cycle arrest. Molecular endocrinology *12*, 941-953.
Kotredes, K.P., and Gamero, A.M. (2013). Interferons as inducers of apoptosis in malignant cells. J Interferon Cytokine Res *33*, 162-170.
Krug, B., De Jay, N., Harutyunyan, A.S., Deshmukh, S., Marchione, D.M., Guilhamon, P., Bertrand, K.C., Mikael, L.G., McConechy, M.K., Chen, C.C.L.*, et al.* (2019). Pervasive H3K27 Acetylation Leads to ERV Expression and a Therapeutic Vulnerability in H3K27M Gliomas. Cancer cell *35*, 782-797 e788.
Kuuranne, T., Kurkela, M., Thevis, M., Schanzer, W., Finel, M., and Kostiainen, R. (2003). Glucuronidation of anabolic androgenic steroids by recombinant human UDP-glucuronosyltransferases. Drug Metab Dispos *31*, 1117-1124.
Lam, H.M., Nguyen, H.M., Labrecque, M.P., Brown, L.G., Coleman, I.M., Gulati, R., Lakely, B., Sondheim, D., Chatterjee, P., Marck, B.T.*, et al.* (2020). Durable Response of Enzalutamide-resistant Prostate Cancer to Supraphysiological Testosterone Is Associated with a Multifaceted Growth Suppression and Impaired DNA Damage Response Transcriptomic Program in Patient-derived Xenografts. European urology *77*, 144-155.

Langeler, E.G., van Uffelen, C.J., Blankenstein, M.A., van Steenbrugge, G.J., and Mulder, E. (1993). Effect of culture conditions on androgen sensitivity of the human prostatic cancer cell line LNCaP. The Prostate *23*, 213-223.
Liao, Y., Smyth, G.K., and Shi, W. (2014). featureCounts: an efficient general purpose program for assigning sequence reads to genomic features. Bioinformatics *30*, 923-930.
Liberzon, A., Birger, C., Thorvaldsdottir, H., Ghandi, M., Mesirov, J.P., and Tamayo, P. (2015). The Molecular Signatures Database (MSigDB) hallmark gene set collection. Cell Syst *1*, 417-425.
Liu, S., Kumari, S., Hu, Q., Senapati, D., Venkadakrishnan, V.B., Wang, D., DePriest, A.D., Schlanger, S.E., Ben-Salem, S., Valenzuela, M.M*., et al.* (2017). A comprehensive analysis of coregulator recruitment, androgen receptor function and gene expression in prostate cancer. eLife *6*.
Lun, A.T., Chen, Y., and Smyth, G.K. (2016). It's DE-licious: a recipe for differential expression analyses of RNA-seq experiments using quasi-likelihood methods in edgeR. In Statistical genomics (Springer), pp. 391-416.
Markowski, M.C., Shenderov, E., Eisenberger, M.A., Kachhap, S., Pardoll, D.M., Denmeade, S.R., and Antonarakis, E.S. (2020). Extreme responses to immune checkpoint blockade following bipolar androgen therapy and enzalutamide in patients with metastatic castration resistant prostate cancer. The Prostate *80*, 407-411.
Markowski, M.C., Wang, H., Sullivan, R., Rifkind, I., Sinibaldi, V., Schweizer, M.T., Teply, B.A., Ngomba, N., Fu, W., Carducci, M.A*., et al.* (2021). A Multicohort Open-label Phase II Trial of Bipolar Androgen Therapy in Men with Metastatic Castration-resistant Prostate Cancer (RESTORE): A Comparison of Post-abiraterone Versus Post-enzalutamide Cohorts. European urology *79*, 692-699.
Martin, M. (2011). Cutadapt removes adapter sequences from high-throughput sequencing reads. EMBnet journal *17*, 10-12.
McCabe, M.T., Davis, J.N., and Day, M.L. (2005). Regulation of DNA methyltransferase 1 by the pRb/E2F1 pathway. Cancer research *65*, 3624-3632.
Metsalu, T., and Vilo, J. (2015a). ClustVis: a web tool for visualizing clustering of multivariate data using Principal Component Analysis and heatmap. Nucleic Acids Res *43*, W566-570.
Metsalu, T., and Vilo, J. (2015b). ClustVis: a web tool for visualizing clustering of multivariate data using Principal Component Analysis and heatmap. Nucleic acids research *43*, W566-W570.
Missiaglia, E., Donadelli, M., Palmieri, M., Crnogorac-Jurcevic, T., Scarpa, A., and Lemoine, N.R. (2005). Growth delay of human pancreatic cancer cells by methylase inhibitor 5-aza-2'-deoxycytidine treatment is associated with activation of the interferon signalling pathway. Oncogene *24*, 199-211.
Mohammad, O.S., Nyquist, M.D., Schweizer, M.T., Balk, S.P., Corey, E., Plymate, S., Nelson, P.S., and Mostaghel, E.A. (2017). Supraphysiologic Testosterone Therapy in the Treatment of Prostate Cancer: Models, Mechanisms and Questions. Cancers (Basel) *9*.
Moore, N.L., Buchanan, G., Harris, J.M., Selth, L.A., Bianco-Miotto, T., Hanson, A.R., Birrell, S.N., Butler, L.M., Hickey, T.E., and Tilley, W.D. (2012). An androgen receptor mutation in the MDA-MB-453 cell line model of molecular apocrine breast cancer compromises receptor activity. Endocrine related cancer *19*, 599.
Morel, K.L., Sheahan, A.V., Burkhart, D.L., Baca, S.C., Boufaied, N., Liu, Y., Qiu, X., Canadas, I., Roehle, K., Heckler, M*., et al.* (2021). EZH2 inhibition activates a dsRNA-STING-interferon stress axis that potentiates response to PD-1 checkpoint blockade in prostate cancer. Nat Cancer *2*, 444-456.
Nevinny-Stickel, H.B., Dederick, M.M., Haines, C.R., and Hall, T.C. (1964). Comparative Study of 6-Dehydro-17alpha-Methyltestosterone and Testosterone Propionate in Human Breast Cancer. Cancer *17*, 95-99.
Ni, G., Ma, Z., and Damania, B. (2018). cGAS and STING: At the intersection of DNA and RNA virus-sensing networks. PLoS Pathog *14*, e1007148.

Nyquist, M.D., Corella, A., Mohamad, O., Coleman, I., Kaipainen, A., Kuppers, D.A., Lucas, J.M., Paddison, P.J., Plymate, S.R., Nelson, P.S., *et al.* (2019). Molecular determinants of response to high-dose androgen therapy in prostate cancer. JCI Insight *4*.
Nyquist, M.D., Li, Y., Hwang, T.H., Manlove, L.S., Vessella, R.L., Silverstein, K.A., Voytas, D.F., and Dehm, S.M. (2013). TALEN-engineered AR gene rearrangements reveal endocrine uncoupling of androgen receptor in prostate cancer. Proceedings of the National Academy of Sciences of the United States of America *110*, 17492-17497.
Owen, K.L., Gearing, L.J., Zanker, D.J., Brockwell, N.K., Khoo, W.H., Roden, D.L., Cmero, M., Mangiola, S., Hong, M.K., Spurling, A.J., *et al.* (2020). Prostate cancer cell-intrinsic interferon signaling regulates dormancy and metastatic outgrowth in bone. EMBO Rep *21*, e50162.
Paltoglou, S., Das, R., Townley, S.L., Hickey, T.E., Tarulli, G.A., Coutinho, I., Fernandes, R., Hanson, A.R., Denis, I., and Carroll, J.S. (2017). Novel androgen receptor coregulator GRHL2 exerts both oncogenic and antimetastatic functions in prostate cancer. Cancer research *77*, 3417-3430.
Polkinghorn, W.R., Parker, J.S., Lee, M.X., Kass, E.M., Spratt, D.E., Iaquinta, P.J., Arora, V.K., Yen, W.F., Cai, L., Zheng, D., *et al.* (2013). Androgen receptor signaling regulates DNA repair in prostate cancers. Cancer Discov *3*, 1245-1253.
Ramírez, F., Ryan, D.P., Grüning, B., Bhardwaj, V., Kilpert, F., Richter, A.S., Heyne, S., Dündar, F., and Manke, T. (2016). deepTools2: a next generation web server for deep-sequencing data analysis. Nucleic acids research *44*, W160-W165.
Rehwinkel, J., and Gack, M.U. (2020). RIG-I-like receptors: their regulation and roles in RNA sensing. Nat Rev Immunol *20*, 537-551.
Reik, W. (2007). Stability and flexibility of epigenetic gene regulation in mammalian development. Nature *447*, 425-432.
Robinson, D., Van Allen, E.M., Wu, Y.-M., Schultz, N., Lonigro, R.J., Mosquera, J.-M., Montgomery, B., Taplin, M.-E., Pritchard, C.C., and Attard, G. (2015). Integrative clinical genomics of advanced prostate cancer. Cell *161*, 1215-1228.
Robinson, M.D., McCarthy, D.J., and Smyth, G.K. (2010). edgeR: a Bioconductor package for differential expression analysis of digital gene expression data. Bioinformatics *26*, 139-140.
Rooney, M.S., Shukla, S.A., Wu, C.J., Getz, G., and Hacohen, N. (2015). Molecular and genetic properties of tumors associated with local immune cytolytic activity. Cell *160*, 48-61.
Roulois, D., Loo Yau, H., Singhania, R., Wang, Y., Danesh, A., Shen, S.Y., Han, H., Liang, G., Jones, P.A., Pugh, T.J., *et al.* (2015). DNA-Demethylating Agents Target Colorectal Cancer Cells by Inducing Viral Mimicry by Endogenous Transcripts. Cell *162*, 961-973.
Saartok, T., Dahlberg, E., and Gustafsson, J.A. (1984). Relative binding affinity of anabolic-androgenic steroids: comparison of the binding to the androgen receptors in skeletal muscle and in prostate, as well as to sex hormone-binding globulin. Endocrinology *114*, 2100-2106.
Sanchez-Osorio, M., Duarte-Rojo, A., Martinez-Benitez, B., Torre, A., and Uribe, M. (2008). Anabolic-androgenic steroids and liver injury. Liver Int *28*, 278-282.
Schneider, C.A., Rasband, W.S., and Eliceiri, K.W. (2012). NIH Image to ImageJ: 25 years of image analysis. Nature methods *9*, 671-675.
Schweizer, M.T., Antonarakis, E.S., Eisenberger, M.A., Nelson, P., Luo, J., Pritchard, C., and Denmeade, S.R. (2019). Genomic determinants of sensitivity to bipolar androgen therapy (BAT) in castrate-resistant prostate cancer (CRPC). Journal of Clinical Oncology *37*, 200-200.
Schweizer, M.T., Antonarakis, E.S., Wang, H., Ajiboye, A.S., Spitz, A., Cao, H., Luo, J., Haffner, M.C., Yegnasubramanian, S., Carducci, M.A., *et al.* (2015). Effect of bipolar androgen therapy for asymptomatic men with castration-resistant prostate cancer: results from a pilot clinical study. Science translational medicine *7*, 269ra262.

Sena, L.A., Wang, H., Lim Sc, M.S., Rifkind, I., Ngomba, N., Isaacs, J.T., Luo, J., Pratz, C., Sinibaldi, V., Carducci, M.A*., et al.* (2021). Bipolar androgen therapy sensitizes castration-resistant prostate cancer to subsequent androgen receptor ablative therapy. Eur J Cancer *144*, 302-309.
Sheng, W., LaFleur, M.W., Nguyen, T.H., Chen, S., Chakravarthy, A., Conway, J.R., Li, Y., Chen, H., Yang, H., Hsu, P.H*., et al.* (2018). LSD1 Ablation Stimulates Anti-tumor Immunity and Enables Checkpoint Blockade. Cell *174*, 549-563 e519.
Smith, C.M., Ballard, S.A., Wyllie, M.G., and Masters, J.R. (1994). Comparison of testosterone metabolism in benign prostatic hyperplasia and human prostate cancer cell lines in vitro. The Journal of steroid biochemistry and molecular biology *50*, 151-159.
Sowalsky, A.G., Ye, H., Bhasin, M., Van Allen, E.M., Loda, M., Lis, R.T., Montaser-Kouhsari, L., Calagua, C., Ma, F., Russo, J.W*., et al.* (2018). Neoadjuvant-Intensive Androgen Deprivation Therapy Selects for Prostate Tumor Foci with Diverse Subclonal Oncogenic Alterations. Cancer research *78*, 4716-4730.
Stone, M.L., Chiappinelli, K.B., Li, H., Murphy, L.M., Travers, M.E., Topper, M.J., Mathios, D., Lim, M., Shih, I.M., Wang, T.L*., et al.* (2017). Epigenetic therapy activates type I interferon signaling in murine ovarian cancer to reduce immunosuppression and tumor burden. Proceedings of the National Academy of Sciences of the United States of America *114*, E10981-E10990.
Subramanian, A., Tamayo, P., Mootha, V.K., Mukherjee, S., Ebert, B.L., Gillette, M.A., Paulovich, A., Pomeroy, S.L., Golub, T.R., and Lander, E.S. (2005). Gene set enrichment analysis: a knowledge-based approach for interpreting genome-wide expression profiles. Proceedings of the National Academy of Sciences *102*, 15545-15550.
Sun, Q., Sun, L., Liu, H.H., Chen, X., Seth, R.B., Forman, J., and Chen, Z.J. (2006). The specific and essential role of MAVS in antiviral innate immune responses. Immunity *24*, 633-642.
Teply, B.A., Kachhap, S., Eisenberger, M.A., and Denmeade, S.R. (2017). Extreme Response to High-dose Testosterone in BRCA2- and ATM-mutated Prostate Cancer. European urology *71*, 499.
Teply, B.A., Wang, H., Luber, B., Sullivan, R., Rifkind, I., Bruns, A., Spitz, A., DeCarli, M., Sinibaldi, V., Pratz, C.F*., et al.* (2018). Bipolar androgen therapy in men with metastatic castration-resistant prostate cancer after progression on enzalutamide: an open-label, phase 2, multicohort study. Lancet Oncol *19*, 76-86.
Topper, M.J., Vaz, M., Chiappinelli, K.B., DeStefano Shields, C.E., Niknafs, N., Yen, R.C., Wenzel, A., Hicks, J., Ballew, M., Stone, M*., et al.* (2017). Epigenetic Therapy Ties MYC Depletion to Reversing Immune Evasion and Treating Lung Cancer. Cell *171*, 1284-1300 e1221.
Tsihlias, J., Zhang, W., Bhattacharya, N., Flanagan, M., Klotz, L., and Slingerland, J. (2000). Involvement of p27Kip1 in G1 arrest by high dose 5 alpha-dihydrotestosterone in LNCaP human prostate cancer cells. Oncogene *19*, 670-679.
Wolf, S., Diel, P., Parr, M.K., Rataj, F., Schanzer, W., Vollmer, G., and Zierau, O. (2011). Long-term detection of methyltestosterone (ab-) use by a yeast transactivation system. Arch Toxicol *85*, 285-292.

Chapter 4: Modulation of the histone methyltransferase EZH2 by methyl-testosterone in prostate cancer cells

4.1. Introduction

Enhancer of Zeste Homolog 2 (EZH2) is a histone methyl-transferase that forms the catalytic subunit of Polycomb Repressive Complex 2 (PRC2). As part of the canonical function of PRC2, EZH2 mediates tri-methylation of histone H3 lysine 27 (H3K27me3), which causes compaction of chromatin and transcriptional silencing of target genes (Jiao, Shubbar et al. 2020). In proliferative cells, the interplay between Rb and E2Fs govern EZH2 function and thereby regulate the inheritance of H3K27me3 patterns during DNA replication and cell proliferation (Bracken, Pasini et al. 2003, Lanzuolo, Sardo et al. 2011, Mu, Starmer et al. 2018). For example, it has been shown that in skeletal muscle cells, Rb-mediated EZH2 binding to cell cycle genes leads to irreversible cell cycle exit and cell differentiation (Blais, van Oevelen et al. 2007). Additionally, it has been reported that RB protein can recruit PRC2 complex to repress the expression of genes associated with repetitive elements (Ishak, Marshall et al. 2016) and pluripotency (Kareta, Gorges et al. 2015) by tri-methylation of histone H3 at lysine 27. EZH2 can also regulate the expression of genes involved in stem cell differentiation and tumour immunogenicity by altering the ratio of H3K27me3 to H3K4me3; these are referred to as bivalent genes because their promoters harbour histone marks associated with both positive (H3K4me3) and negative (H3K27me3) transcriptional outcomes (Ezhkova, Pasolli et al. 2009, Blanco, González-Ramírez et al. 2020). In short, the canonical function of EZH2 and subsequently the level of H3K27me3 is an important determinant of the balance between cell differentiation and proliferation (Ezponda and Licht 2014).

Dysregulation in the expression and function of EZH2 can lead to carcinogenesis and cancer progression in multiple tumour types. For example, overexpression of *EZH2* in prostate cancer tumours is associated with the progression of clinically localized solid tumours to a lethal, therapy-resistant state (Varambally, Dhanasekaran et al. 2002, Yu, Yu et al. 2007). Mechanistically, several mechanisms can cause dysregulation of both the expression and function of EZH2 in prostate cancer: *TMPRSS2-ERG* fusion genes can cause the overexpression of *EZH2*, inducing a stem-cell-like dedifferentiation program (Yu, Yu et al. 2010), while *SOX4* overexpression in cancer cells can directly upregulate the expression of *EZH2*, which subsequently leads to re-distribution of H3K27me3 and de-repression of genes required for epithelial-mesenchymal transition, a key process in tumour metastasis (Tiwari, Tiwari et al. 2013). Interestingly, overexpression of *EZH2* in castration-resistant prostate cancer has been associated with lower global levels of H3K27me3 suggesting that EZH2 has activity beyond histone modification; indeed, it was found that EZH2 interacts with AR and in this context can act as a transcriptional activator (Xu, Wu et al. 2012). Consistent with this notion, phosphorylation of partially disordered transactivation domain (TAD) in EZH2 causes the recruitment of P300, leading to gene activation rather than repression (Jiao, Shubbar et al. 2020). However, these findings were not supported by mass spectrometry-based analysis of the EZH2 interactome, which recovered all PRC2 related components but did not identify an interaction with AR (Wassef, Luscan et al. 2019). In short, the precise function of EZH2 in PCa cells remains to be fully elucidated.

Other studies of EZH2 have potentially important implications for this project and the results presented in Chapter 3. First, a CRISPR/CAS9 screen revealed that EZH2 depletion can make prostate cancer cells sensitive to high-dose androgen therapy (Nyquist, Corella et al. 2019), suggesting that it has a role in mediating resistance to this therapeutic strategy. Moreover, it has been shown that EZH2 inhibition can lead to the enhanced immunogenicity of tumours through de-repression of *ERVs* and activation of a viral mimicry response (Deblois, Tonekaboni et al. 2020, Janin and Esteller 2020, Ishiguro, Kitajima et al. 2021). EZH2 inhibition can also directly increase tumour immunogenicity by enhancing the expression and presentation of major MHC-I molecules (Burr, Sparbier et al. 2019, Zhou, Mudianto et al. 2020). Consistent with this idea, we showed in Chapter 3 that Decitabine-induced dsRNAs are less strong than MeT 1 nM, suggesting that dsRNA induction by MeT is also amplified by another mechanism. With this background in mind, I hypothesised that the viral mimicry response elicited by MeT (as described in Chapter 3) could at least in part be mediated via reduced expression and/or activity of EZH2. In this Chapter, I tested this hypothesis by characterizing the expression and activity of EZH2 in response to MeT treatment.

4.2. Materials and Methods

Details of cell lines, Western blotting, q-RT-PCR and RNA-seq are described in Chapters 2 and 3.

4.2.1. Histone extraction

Total nucleoplasmic histones were extracted using the acid extraction protocol recommended by Abcam. Briefly, after harvesting the cells, they were washed twice with ice-cold PBS and cell pellets were re-suspended in Triton Extraction Buffer (TEB) (please see Chapter 2), at a cell density of 10^7 cells per ml for 10 min with gentle stirring on ice. Then, the lysate was centrifuged at 6,500 × *g* for 10 min at 4°C to spin down the nuclei. After discarding the supernatant, cell pellets were washed in half the volume of TEB and centrifuged at 6,500 × g for 10 min at 4°C. Subsequently, cell pellets were re-suspended in 0.2 N HCl at a density of 4 ×10^7 nuclei per ml overnight. Samples were centrifuged at 6,500 × *g* for 10 min at 4°C and the supernatant containing total nucleoplasmic H3K27me3 was moved into a new tube. Finally, HCl in samples was neutralised with 2M NaOH at 1/10 of the volume of the supernatant. Protein concentration was measured using the Bradford assay described in Chapter 2 and samples were kept at -80 °C.

4.2.2. H3K27me3 ChIP-seq experiment, analysis and DATA

H3K27me3 ChIP-seq experiment was carried out as described in Chapter 2. Peak calling in Galaxy was performed essentially as described in Chapter 2, except that the “broad” peak parameter was used, with a cutoff for the broad region of 0.1. H3K27me3 ChIP-seq data are

from Augello, M. A et al. (Augello, Liu et al. 2019): GEO accession GSE117430, and Xu K et al. (Xu, Wu et al. 2012): GEO accession GSM969571.

4.2.3. Integrating RNA-seq and H3K27me3 ChIP-Seq data

Integration of H3K27me3 ChIP-seq data with transcriptomic analyses was carried out using the CisGenome software system (Ji, Jiang et al. 2008). The CisGenome software and hg19 genome build were used to annotate H3K27me3 peaks to proximal (+/- 10kb from TSS) genes. Genes marked with H3K27me3 were compared with the list of log normalized counts of genes, generated from the RNA-seq experiment described in Chapter 3.

4.2.4. GO analysis

The PANTHER online platform version 16.0 (Released 2020-12-01) (http://geneontology.org/) was used for gene ontology (GO) analysis (Mi, Muruganujan et al. 2019).

4.2.5. Tag density analysis using HOMER software.

BAM files from the ChIP-seq experiment were converted to bed files using bedtools (version 2.18 (Quinlan and Hall 2010)); “bamToBed.” Bed files were converted to tag directories using HOMER (version 4.11 (Heinz, Benner et al. 2010)); “makeTagDirectory.pl.” Tag density plots were generated using HOMER “annotatePeaks.pl.” (-size 5000 - hist 20).

4.2.6. DiffReps

DiffReps (version 1.55.4) (Shen, Shao et al. 2013) was run according to the developer's protocol using bed files from the androgen-treated samples as the --treatment group and bed files from the vehicle-treated samples as the --control group. The G-test method was used for differential analysis (--meth gt).

4.2.7. H3K27me3 deposition on repetitive elements

To measure H3K27me3 at repetitive elements, genomic coordinates of these elements were directly downloaded from The UCSC Table Browser (Karolchik, Hinrichs et al. 2004). More specifically, after specifying the February 2009 human reference sequence (GRCh37) as a reference genome, RepeatMasker was applied in the annotation track to filter the coordinates of different families (repFamily) of repetitive elements. HOMER (Heinz, Benner et al. 2010) was used to generate histograms of tag density at repetitive elements.

4.2.8. Visualisation of H3K27me3 deposition

The density of H3K27me3 deposition at previously reported coordinates associated with H3K27me3 modification was visualised using deepTools2 (Ramírez, Ryan et al. 2016). Reported gene sets in LNCaP was from Hawkins RD et al. (Hawkins, Hon et al. 2010) and Xu K. et al (Xu, Wu et al. 2012). ComputeMatrix was used to prepare an intermediate Matrix file containing the scores for the signal distribution associated with the centre of genomic regions (reference point). The generated Matrix file was used with plotProfile to plot the signal distributions across genomic regions.

4.2.9. Venn diagram generation for comparing the intervals of two datasets

To compare the overlapping of H3K27me3 ChIP-seq peaks, The Galaxy/Cistrome Venn diagram (version 1.0.0) tool (Liu, Ortiz et al. 2011) was used to compare the overlapping of peaks.

4.2.10. Upset plots

UpSet diagram tool (Galaxy Version 0.6.4) (Conway, Lex et al. 2017) was used to illustrate the unique intersection of genomic regions between different treatment groups as an upset plot based on the order of intersections frequency.

4.2.11. Pairwise intervention analysis

Pairwise intersection tool (Galaxy Version 0.6.4) was used to compute and visualize intersections of multiple sets of genomic regions (Khan and Mathelier 2017). Calculation of overlapping fraction was applied as the metric for the generated heatmap containing the overlapping fraction number. Coordinates associated with H3K27me3 peaks were generated by DiffReps and TSS-associated coordinates were downloaded from UCSC table browser (Karolchik, Hinrichs et al. 2004) as follows: “February 2009 human reference sequence (GRCh37)” was specified as a reference genome, “Regulation” was applied in the group, “SwitchGear TSS” was applied in track, and BED file was generated after adding 100, 1000, and 10,000bp to the upstream. CpG islands coordinates were similarly downloaded from the UCSC Table Browser (26).

4.2.12. Number and location of H3K27me3 deposition

CisGenome software system (Ji, Jiang et al. 2008) was used to assess the genome-wide location of H3K27me3 peaks after specifying the hg19 as a reference genome build.

4.3. Results

4.3.1. Potent activation of AR repressed EZH2 expression in prostate cancer cells

To assess the hypothesis that antiproliferative effects of high-dose androgens could be mediated by altered *EZH2* expression and/or activity, we first checked the expression status of PRC2 subunits including *EZH2*/1, *SUZ12*, *EED*, and *RBBP4/7* in our RNA-seq data (described in Chapter 3). The analysis of differentially expressed genes in LNCaP cells shows that *EZH2*, *EED*, *SUZ12*, and *RBBP4/7* were all significantly repressed by both androgens, whereas *EZH1* was not changed significantly (Figure 4.1A to F). This suggests that androgens modulate the function of the PRC2 complex. *EZH2* downregulation in RNA-seq analysis was confirmed using qRT-PCR (Figure 4.2A). Consistent with PRC2 downregulation, GSEA analysis shows that expression of EZH2 target genes (Liao, Chen et al. 2020) was downregulated by MeT (1 nM) and DHT (1 nM) (Figure 4.2B). Also, RNA-seq results showed that the expression of genes associated with growth inhibitory effects of EZH2 inhibitor was repressed by MeT (Figure 4.2C), indicating that MeT caused the repression of genes activated by EZH2.

Mechanistically, overexpression of *EZH2* is reported to be caused by the transcription factors E2F1 or SOX4 (Bracken, Pasini et al. 2003, Tiwari, Tiwari et al. 2013, Mu, Starmer et al. 2018). To test whether these known associations could explain EZH2 downregulation by high-dose

androgens in our experiments, we examined our RNA-seq data. This revealed that MeT 1 nM and DHT 1nM significantly repressed the expression *E2F1*; however, significant repression of *SOX4* was only mediated after MeT 1 nM treatment (Figure 4.2D). These observations suggest that *E2F1* repression may explain androgen-mediated down-regulation of *EZH2*.

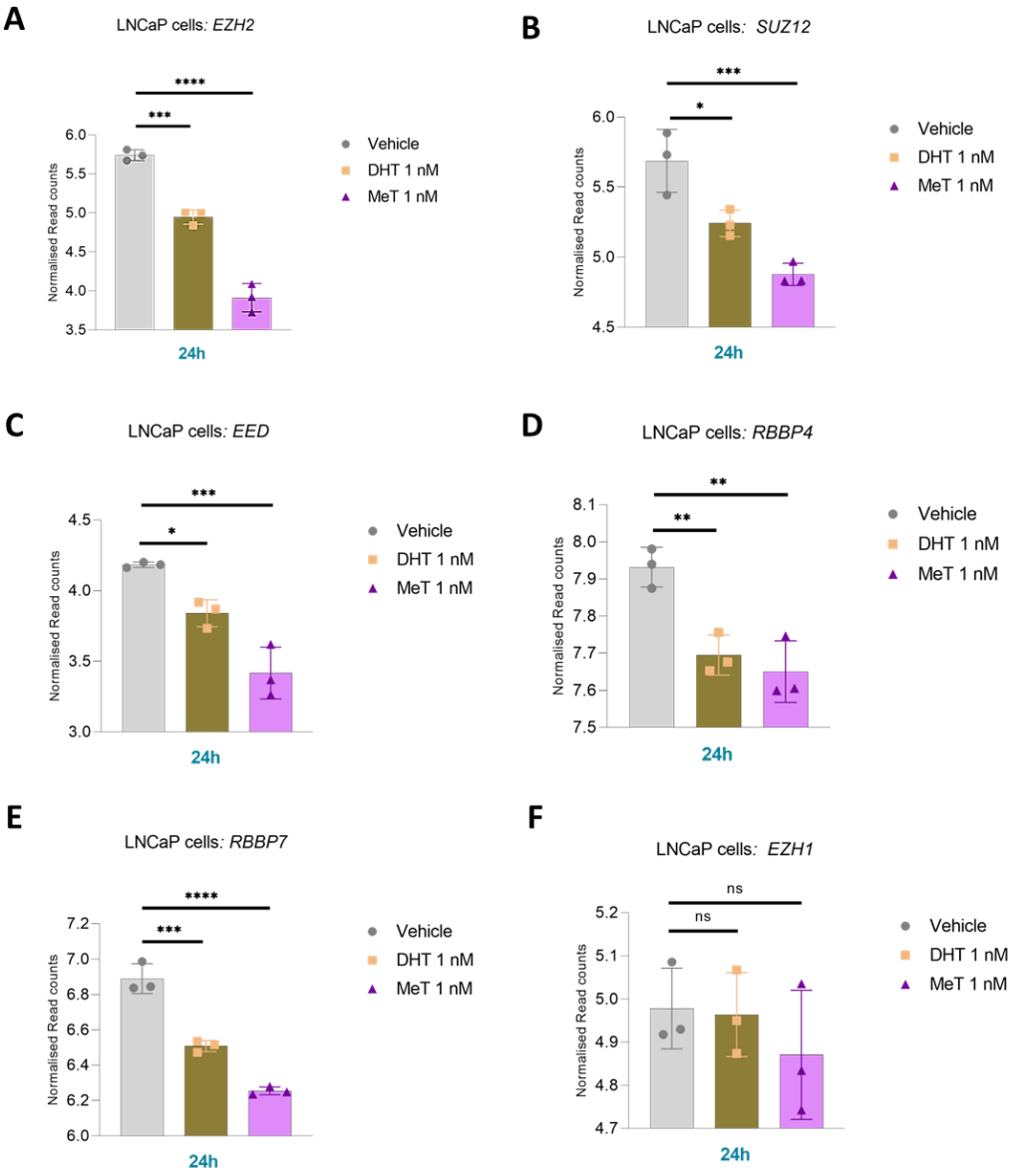

Figure 4.1. Androgens repress the expression of the PRC2 complex in LNCaP cells. A. The expression level of PRC2 complex subunits was assessed based on normalised read counts generated from the RNA-seq experiment described in Chapter 3; in this experiment, the expression of *EZH2* (A), *SUZ12* (B), *EED* (C), *RBBP4* (D), *RBBP7* (E), *and EZH1* (F) were examined 24 hours after treatment. ANOVA with Dunnett multiple comparison test was used to determine significant changes in expression (∗p < 0.05; ∗∗p < 0.01; ∗∗∗p < 0.001; ∗∗∗∗p < 0.0001).

To validate the repressive effects of MeT on the expression of *EZH2* in other prostate cancer models, a panel of prostate cancer cell lines (LNCaP, VCaP, C42B, MR49F, and V16D) were treated with different doses of MeT and DHT and expression of *EZH2* was examined at the protein level. We found that potent activation of AR using MeT (1 and 100 nM) or high-dose DHT (100 nM) caused down-regulation of *EZH2* in the LNCaP, VCaP and V16D models, but not C4-2B or MR49F (Figure 4.3), revealing that androgen-mediated repression of EZH2 is context-dependent.

A

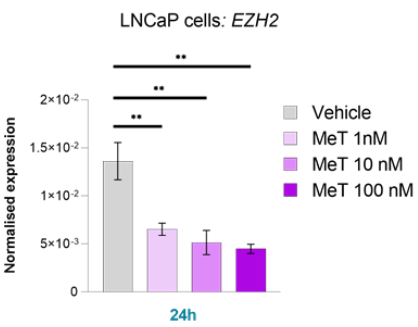
LNCaP cells: *EZH2*
Normalised expression
Vehicle
MeT 1nM
MeT 10 nM
MeT 100 nM
24h

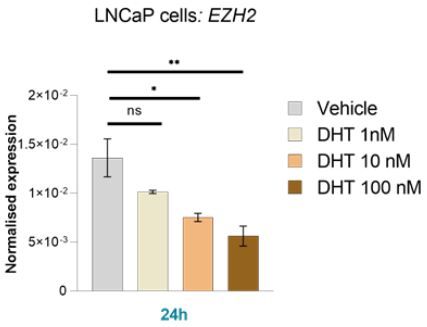
LNCaP cells: *EZH2*
Normalised expression
ns
Vehicle
DHT 1nM
DHT 10 nM
DHT 100 nM
24h

B

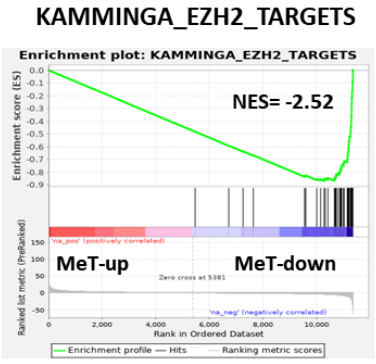
KAMMINGA_EZH2_TARGETS
Enrichment plot: KAMMINGA_EZH2_TARGETS
NES= -2.52
MeT-up
MeT-down
Rank in Ordered Dataset

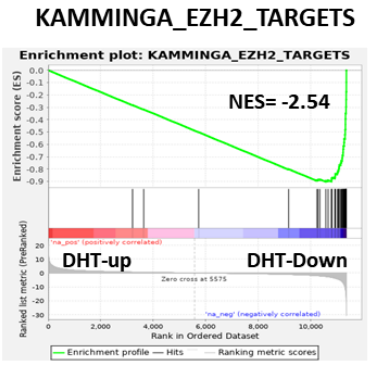
KAMMINGA_EZH2_TARGETS
Enrichment plot: KAMMINGA_EZH2_TARGETS
NES= -2.54
DHT-up
DHT-Down
Rank in Ordered Dataset

C

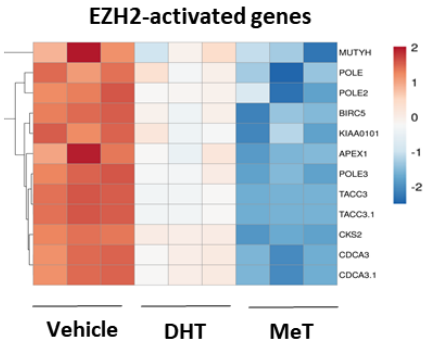
EZH2-activated genes
MUTYH
POLE
POLE2
BIRC5
KIAA0101
APEX1
POLE3
TACC3
TACC3.1
CKS2
CDCA3
CDCA3.1
Vehicle
DHT
MeT

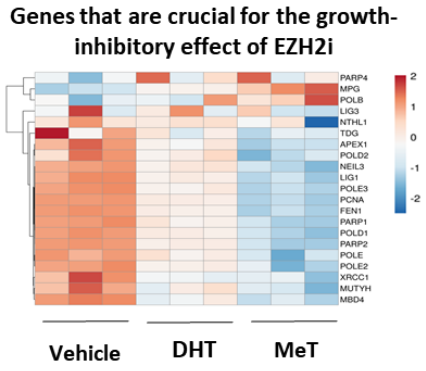
Genes that are crucial for the growth-inhibitory effect of EZH2i
PARP4
MPG
POLB
LIG3
NTHL1
TDG
APEX1
POLD2
NEIL3
LIG1
POLE3
PCNA
FEN1
PARP1
POLD1
PARP2
POLE
POLE2
XRCC1
MUTYH
MBD4
Vehicle
DHT
MeT

D

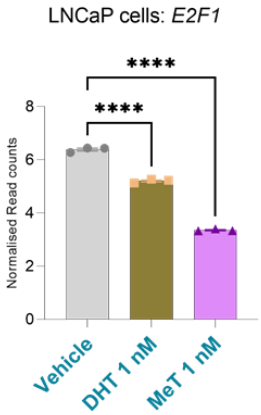
LNCaP cells: *E2F1*
Normalised Read counts
****
****
Vehicle
DHT 1 nM
MeT 1 nM

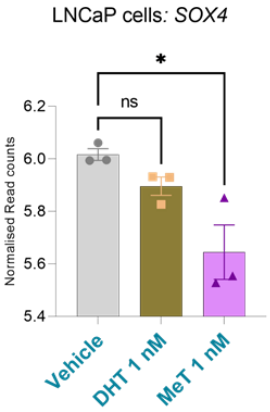
LNCaP cells: *SOX4*
Normalised Read counts
*
ns
Vehicle
DHT 1 nM
MeT 1 nM

Figure 4.2. Hyper-activation of AR leads to the suppression of *EZH2* in LNCaP cells. A. A. Validation of *EZH2* suppression using qRT-PCR in LNCaP cells treated with MeT or DHT. RNA was extracted 24 hours after treatment. p values were determined using ANOVA with Dunnett multiple comparison tests (∗p < 0.05; ∗∗p < 0.01; ∗∗∗p < 0.001; ∗∗∗∗p < 0.0001); B. MeT and DHT treatments caused significant repression of *EZH2* target genes in LNCaP cells as determined by GSEA analysis, using a published EZH2-regulated gene set (Kamminga, Bystrykh et al. 2006). C. MeT repressed the expression of genes crucial for growth inhibitory effects of EZH2 inhibitor. Heatmap generated based on normalised read counts from RNA-seq experiments described in Chapter 3 (24h time-point). Gene set has been reported previously by Liao, Yiji, et al. (Liao, Chen et al. 2020); D. The expression level of *SOX2* and *E2F1* were assessed based on normalised read counts generated from RNA-seq experiment described in Chapter 3; in this experiment, gene expression was examined 24 hours after treatment. ANOVA with Dunnett multiple comparison test was used to determine significant changes in expression (∗p < 0.05; ∗∗p < 0.01; ∗∗∗p < 0.001; ∗∗∗∗p < 0.0001).

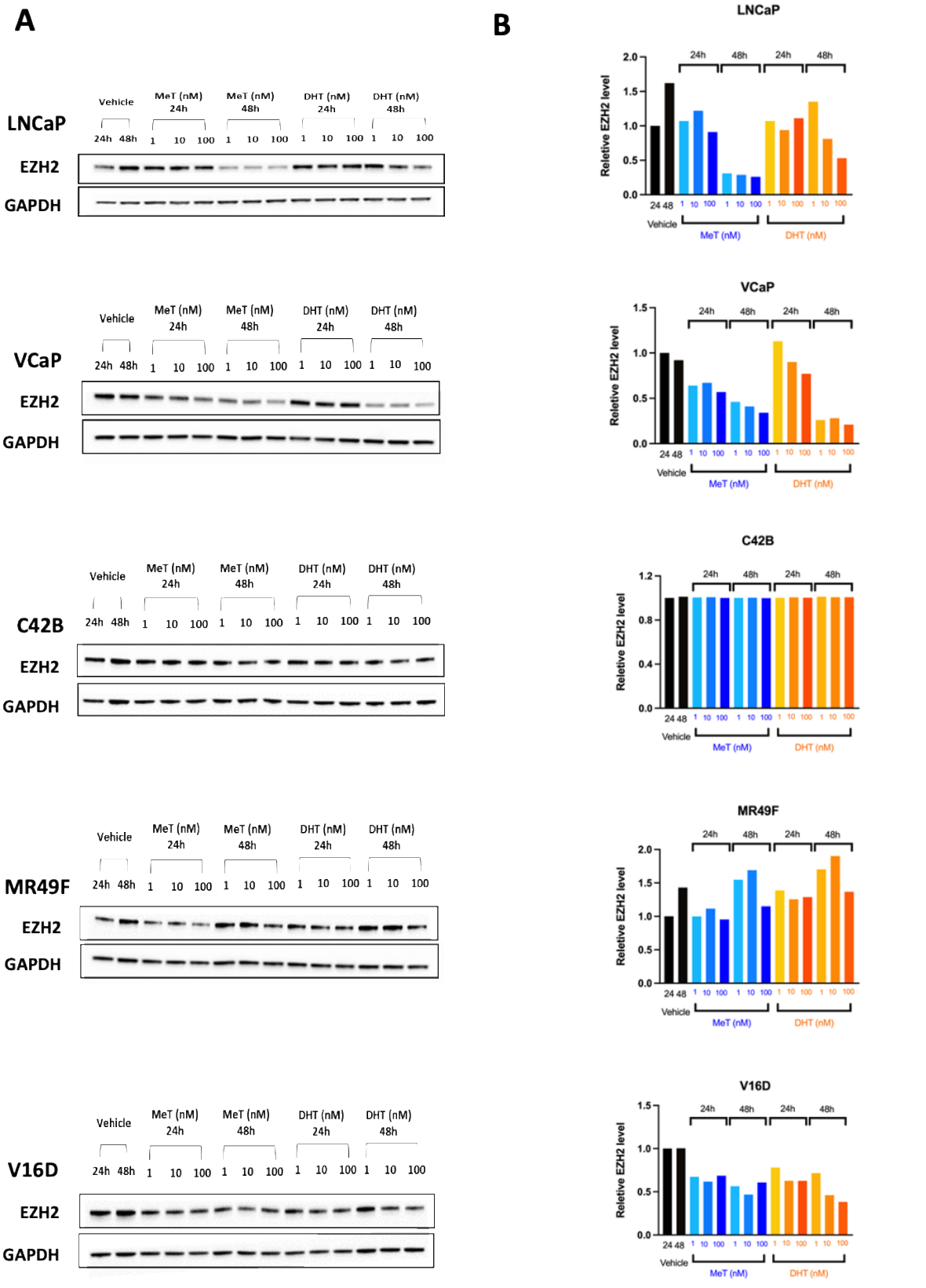
A
B
LNCaP
VCaP
C42B
MR49F
V16D
EZH2
GAPDH
Vehicle
MeT (nM) 24h
MeT (nM) 48h
DHT (nM) 24h
DHT (nM) 48h
24h 48h 1 10 100 1 10 100 1 10 100 1 10 100
Relative EZH2 level
24 48 1 10 100 1 10 100 1 10 100 1 10 100
Vehicle
MeT (nM)
DHT (nM)

Figure 4.3. Potent activation of AR represses the expression of *EZH2* in prostate cancer cell lines. A. Assessment of *EZH2* expression was carried out using Western blotting in a panel of prostate cancer models including LNCaP, VCaP, C42B, MR49F, and V16D, which were treated with different doses of MeT or DHT doses; each sample was pooled from two replicates. B. Quantification of detected bands was carried out using the ImageLab software. Signal intensity in the Vehicle sample at 24h time-point was set to 1.

4.3.2. Androgen treatment alters H3K27me3 distribution in LNCaP cells

Current evidence suggests that the oncogenic activity of EZH2, either through canonical and non-canonical functions, can lead to prostate cancer progression (Kim, Lee et al. 2018, Liao, Chen et al. 2020). To identify the consequence of *EZH2* repression by androgens, we first assessed H3K27me3 protein levels - as a read-out for the canonical activity of EZH2-by Western blotting in LNCaP cells. Consistent with decreased EZH2, androgens reduced the global level of H3K27me3 at 24 and 72 hours post-treatment (Figure 4.4 A and B). These findings suggest that the canonical activity of EZH2 is affected by high-dose androgens in LNCaP cells. Subsequently, to evaluate H3K27me3 status at specific loci, we undertook ChIP-seq as a means to examine the genome-wide deposition of this histone mark. The LNCaP cell line, which was the most sensitive model to MeT/high-dose DHT in terms of growth-inhibitory effects, repression of *EZH2*, and viral mimicry response (Chapter 3), was chosen for this experiment. A 72-hour treatment of LNCaP cells cultured in 10% FBS supplemented RPMI-1640 was chosen for the ChIP-seq experiment since MeT-induced loss of H3K27me3 (Figure 4.4) and viral mimicry response (Chapter 3) was detected at this time-point. Following the preparation of nuclear lysate for the ChIP experiment, we checked the status of *EZH2* expression and H3K27me3 in the nuclear lysates that were to be used for ChIP, which confirmed repression of *EZH2* and a decrease in H3K27me3 level by MeT and high-dose DHT (100 nM) (Figure 4.4C). We subsequently performed H3K27me3 immunoprecipitation and sequenced the co-precipitating DNA.

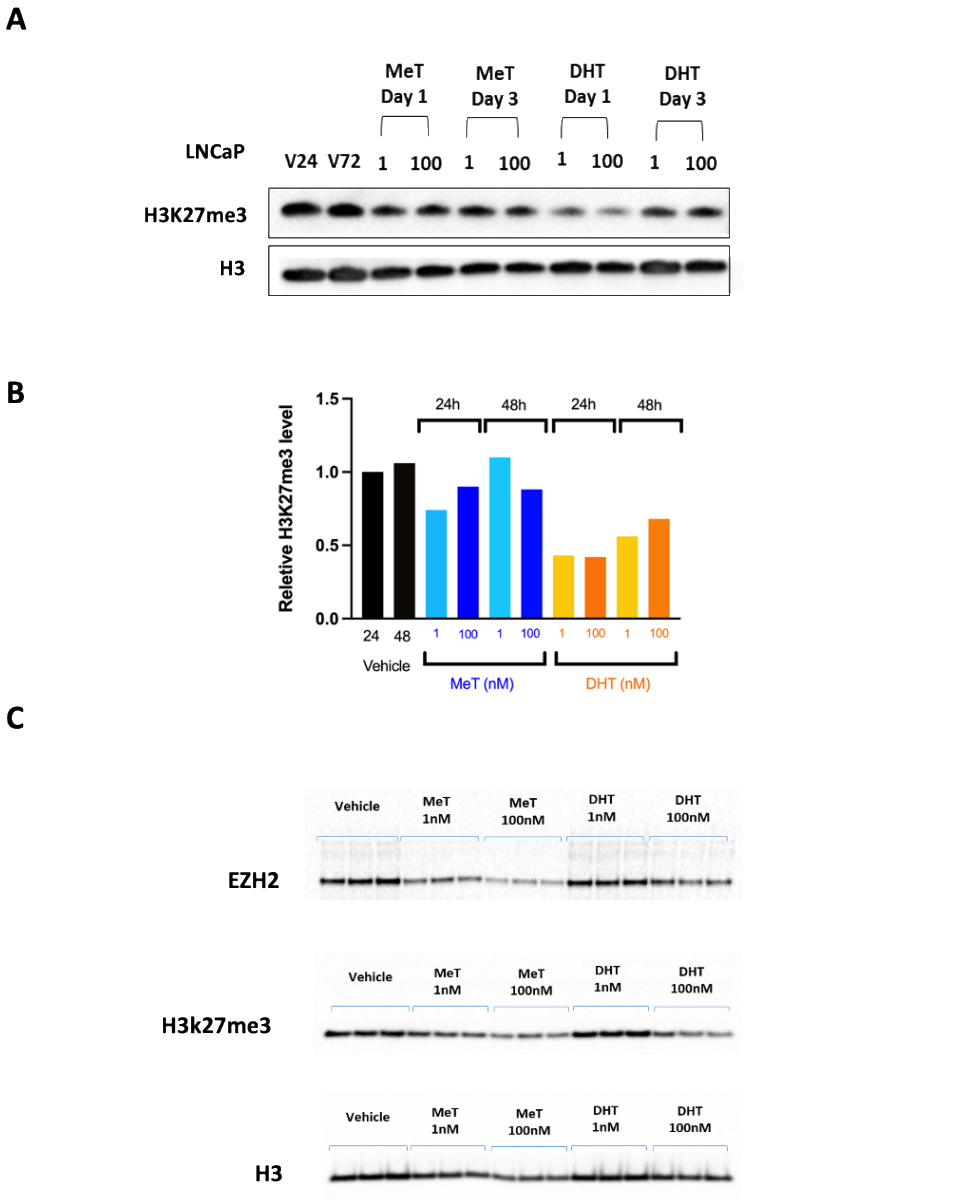

Figure 4.4. Androgen treatments alter the global level of H3K27me3 in LNCaP cells. A. Total nucleoplasmic level of H3K27me3 histone modification and histone H3 24 hours and 72 hours after treatment with MeT or DHT; each sample was pooled from two replicates. **B.** Quantification of detected bands detected in the assessment of global H3K27me3 level using the western blotting. Quantification was carried out using ImageLab software. Quantification of detected bands was carried out using the ImageLab software. Signal intensity in the Vehicle sample at 24h time-point was set to 1**. C.** Western blotting-based assessment of *EZH2* expression and H3K27me3 histone modification status using the nuclear lysates that were to be used for ChIP experiment 72h after androgen treatments.

In vehicle-treated LNCaP cells, 40,367 consensus H3K27me3 peaks were identified. Surprisingly given the loss of bulk H3K27me3, treatment with DHT 1 nM led to an increase in the number of peaks to 46,288. To confirm whether our data was consistent with other reported studies, we first compared the number and locations of H3K27me3 peaks in vehicle and DHT 1 nM treatment groups with two publicly available H3K27me3 ChIP-seq data, GSM969571 and GSE117430. The GSM969571 dataset was generated from LNCaP cells treated with DHT 10 nM (for 24h) in Charcoal DCC-FBS-supplemented media and GSE117430 data was generated from LNCaP cells treated with DHT 10 nM (for 3h) in FBS-supplemented media (Table 4.1). Overall, our H3K27me3 cistrome was more similar to that from GSE117430 in terms of the number of peaks (Table 4.1) but overlapped more strongly with GSM969571 (Table 4.1; Figure 4.5). Notably, the overlap between GSM969571 and GSE117430 was minimal (Table 4.1; Figure 4.5). Collectively, these studies suggest that our H3K27me3 data is robust and can be used to evaluate the effects of high dose androgen therapy on this histone mark.

Table 4.1. Comparison of H3K27me3 distribution in LNCaP cells

H3K27me3 peaks	Vehicle	DHT 1 nM	GSE117430 (Augello, Liu et al. 2019)	GSM969571 (Xu, Wu et al. 2012)
Number of identified peaks	40,367	46,288	51,556	16,459
Media	10% FBS/RPMI	10% FBS/RPMI	5% FBS/RPMI	10% DCC-FBS/RPMI
Treatment	-	DHT 1 nM (72h)	DHT 1 nM (3h)	DHT 1 nM (24h)
Overlapped peaks with Vehicle	-	31,233 (68.66%)	8,873 (19.55%)	5,586 (45.88%)
Overlapped peaks with DHT 1nM	31,233 (81.12%)	-	10,338 (23.76%)	6,043 (51.77%)
Intergenic (%)	61.58	61.88	65.93	57.58
Intragenic (%)	38.41	38.11	34.06	42.41
Exon (%)	6.43	5.83	2.78	7.49
Intron (%)	32.60	32.82	31.47	35.65
CDS (%)	4.17	3.76	1.92	5.31
UTR (%)	2.34	2.13	0.89	2.30
5'UTR (%)	1.49	1.29	0.26	1.40
3'UTR (%)	0.86	0.84	0.63	0.89

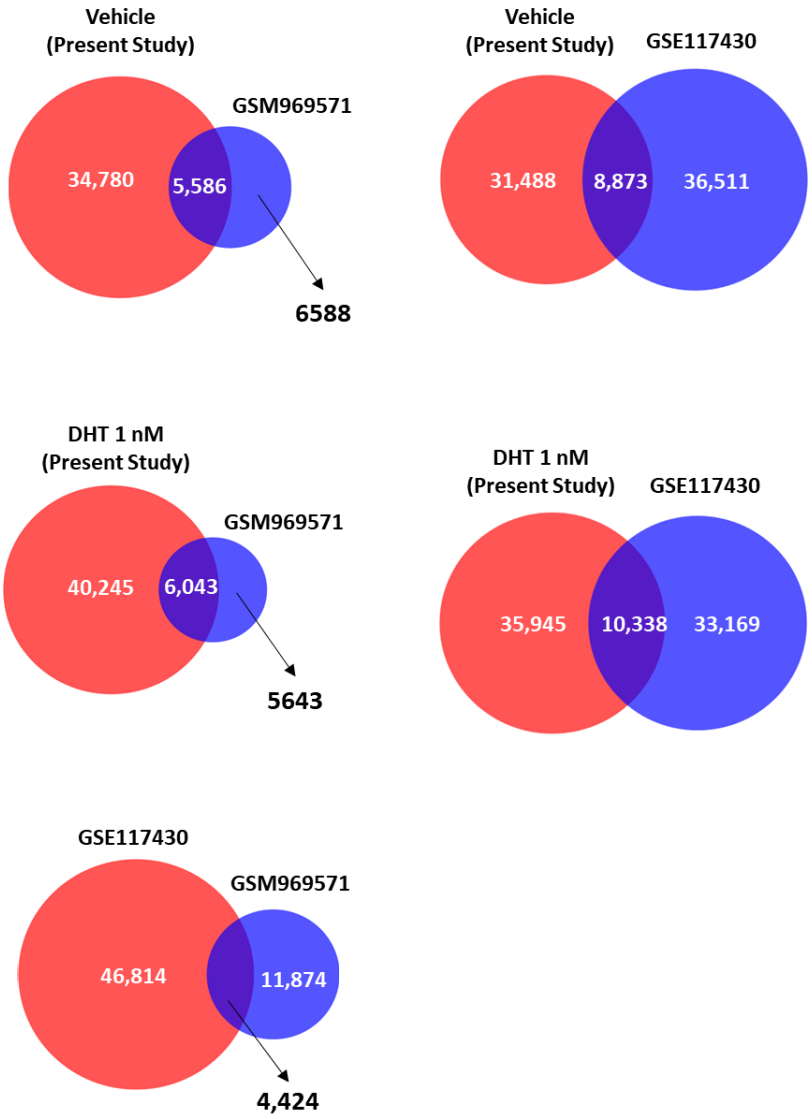

Figure 4.5. Cell growth condition can change the deposition pattern and distribution of H3k27me3 histone modification. Venn diagrams illustrating the overlap of consensus H3K27me3 peaks with other LNCaP H3M27me3 ChIP-seq datasets ((Augello, Liu et al. 2019), GEO accession GSE117430; (Xu, Wu et al. 2012), GEO accession GSM969571). Peaks from GSM969571 were lifted over to the hg19 reference genome.

Having used published data to provide confidence in our H3K27me3 ChIP-seq experiment, we next evaluated the effect of DHT and MeT treatments on this histone mark in LNCaP cells. Androgen treatment did not dramatically alter the level of chromatin-bound H3K27me3, as determined by a relatively consistent number of H3K27me3 peaks detected in each of the different treatment groups (Table 4.2). Figure 4.6 shows the deposition status of H3K27me3 on *FOXC1* and *LHX6* genes, two genes reported being regulated by EZH2 and H3K27me3 (Boshans, Factor et al. 2019, Zheng, Li et al. 2020). Evaluation of the H3K27me3 signal proximal to genes reported to be marker by this histone mark in LNCaP cells (Hawkins, Hon et al. 2010) and hESCs (Xu, Wu et al. 2012) (Figure 4.7) provided further evidence that androgen treatment had minimal effect on this histone mark. Although H3K27me3 did not dramatically change with any of the treatments, we did observe a slight decrease in terms of peak number and signal with the higher dose treatments (Table 4.2 and Table 4.3). In all treatment groups, the vast majority of peaks were in intergenic regions and introns, with only on average ~37% found at intragenic regions (Table 4.2). Overall, these findings suggest that H3K27me3 is not significantly altered, either at a qualitative or quantitative level, by MeT/DHT, which was unexpected due to significant repression of EZH2 at RNA and protein level and bulk levels of H3K27me3 measured by Western blotting.

Table 4.2. Number and location of H3K27me3 deposition 72 hours after treatment with MeT and DHT

Consensus H3K27me3 peaks*	Vehicle	MeT 1 nM	MeT 100 nM	DHT 1 nM	DHT 100 nM
Total Peak number (FDR < 0.05)	40367	43389	37351	46288	40138
Intergenic (%)	61.5825	61.7161	62.1001	61.8821	63.2493
Intragenic (%)	38.4175	38.2839	37.8999	38.1179	36.7507
Exon (%)	6.4384	6.5961	6.3666	5.8309	4.2304
Intron (%)	32.6058	32.3146	32.0928	32.8228	32.9513
CDS (%)	4.1717	4.2522	4.1123	3.7634	2.4864
UTR (%)	2.341	2.4223	2.3293	2.1345	1.7863
5'UTR (%)	1.4913	1.5672	1.5662	1.2984	1.293
3'UTR (%)	0.8646	0.8666	0.7711	0.8447	0.5008

* Peak locations were assessed using the CisGenome software.

H3K27me3 peaks deposited at *FOXC1* gene

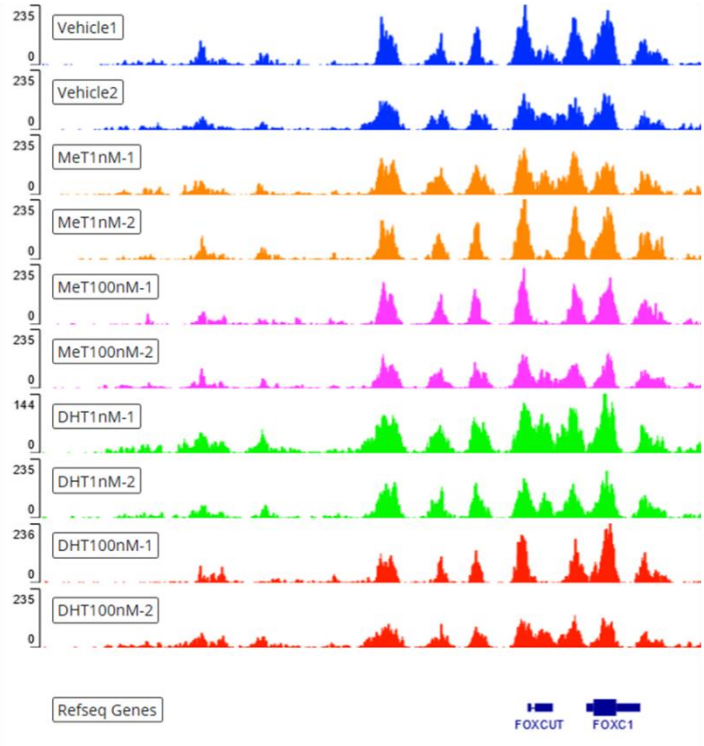

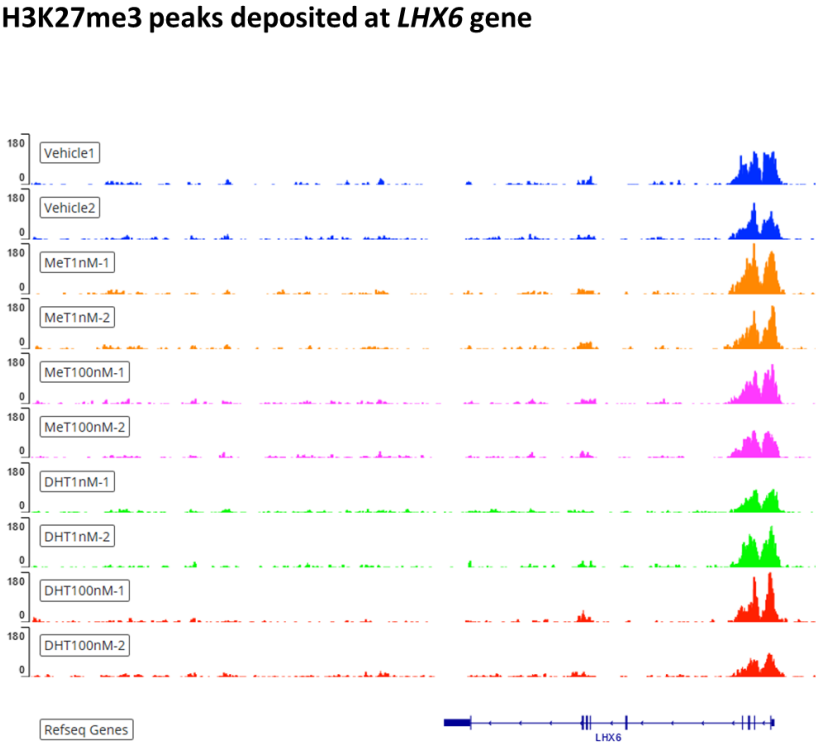

Figure 4.6. Androgen treatments did not attenuate the level of chromatin-bound H3K27me3 deposition at key EZH2 target genes. Genome browser images showing H3k27me3 ChIP-seq signals at binding sites associated with *FOXC1* and *LHX6* in two replicates of LNCaP cells treated with Vehicle, MeT (1 and 100nM) and DHT (1 and 100nM).

A. H3K27me3 status at a reported gene set associated with H3K27me3 in LNCaP cells

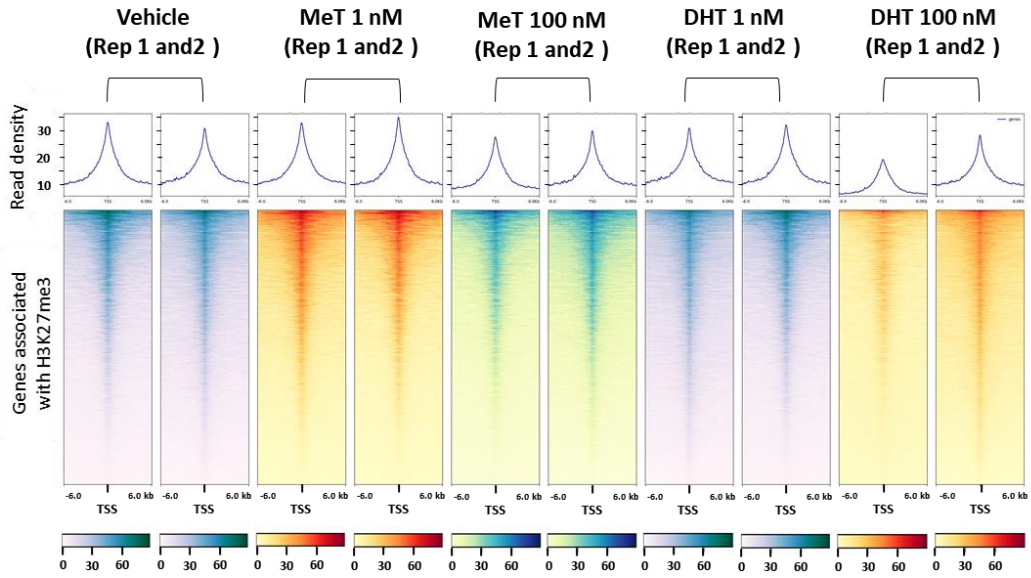

B. H3K27me3 status at a reported gene set associated with H3K27me3 in hESCs cells

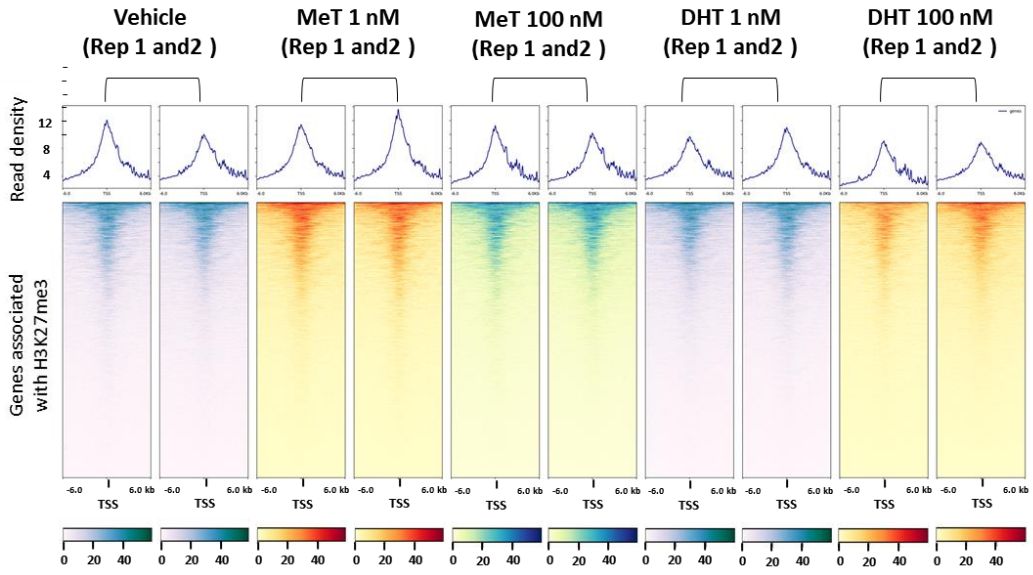

Figure 4.7. Androgen treatments did not change the genome-wide binding profile of H3K27me3. Heatmaps show the enrichment of H3K27me3 around the TSS (+/-6kb) of previously reported gene sets associated with H3K27me3 in LNCaP (Hawkins, Hon et al. 2010) and hESCs cells (Xu, Wu et al. 2012).

Table 4.3. Overlapped H3K27me3 peaks after androgen treatments

Consensus H3K27me3 peaks	Vehicle	MeT 1 nM	MeT 100 nM	DHT 1 nM	DHT 100 nM
Shared with Vehicle (%)	100	71.43	75.06	68.66	57.27
Shared with MeT 1 nM (%)	75.83	100	78.57	66.22	57.36
Shared with MeT 100 nM (%)	67.07	66.12	100	58.52	56.85
Shared with DHT 1 nM (%)	81.12	73.16	76.80	100	61.73
Shared with DHT 100 nM (%)	54.66	51.50	59.97	50.56	100

4.3.3. Functional analysis of genes associated with H3K27me3 histone mark

Although our ChIP-seq data did not identify any major quantitative change to genome-wide H3K27me3 in response to MeT or DHT, we did observe a certain level of re-distribution with androgen treatments (Figure 4.8). To measure loss and gain of H3K27me3 more quantitatively, we used the Diffreps (Shen, Shao et al. 2013), which identified 1,502, 2,031, 1,446, and 7,681 regions with differential levels of H3K27me3 after treatment with MeT 1 nM, MeT 100 nM, DHT 1 nM, and DHT 100 nM, respectively. Analysis of intersections between gained or lost H3K27me3 sites revealed that the vast majority were treatment-specific (Figure 4.9). We annotated the lost/gained sites to genomic regions known to be associated with H3K27me3: CpG islands, transcriptional start sites (TSSs), and promoters (100 to 10,000bp from TSS) (Deblois, Tonekaboni et al. 2020). This analysis reinforced that most H3K27me3 sites were distal from genes and only a small proportion was in CpG islands (Figure 4.10). More importantly, this analysis revealed that in cells treated with a low dose (1 nM) of MeT or DHT, there were more gained H3K27me3 peaks relative to lost peaks at intergenic DNA regions, suggesting that low-dose androgens caused an enrichment of H3K27me3 peaks at regulatory regions of DNA. Inversely, treatment with a high-dose of androgens caused more lost H3K27me3 peaks relative to gained peaks at the same regions. Collectively, these findings suggest that androgens exerts a dose-dependent effect on re-distribution of H3K7me3 at intergenic regions.

We then annotated the differentially marked regions with proximal genes and determined whether specific gene ontology (GO) groups were particularly associated with re-distributed

H3K27me3 (Mi, Muruganujan et al. 2019). This functional analysis strategy showed significant enrichment of genes involved in development (the nervous system, differentiation, and embryogenesis) having “re-distributed” H3K27me3 (Figure 4.11), a finding consistent with other studies suggesting the role of H3K27me3 in the development of the nervous system and anatomical structures (Hawkins, Hon et al. 2010, Zeng, Zhang et al. 2019).

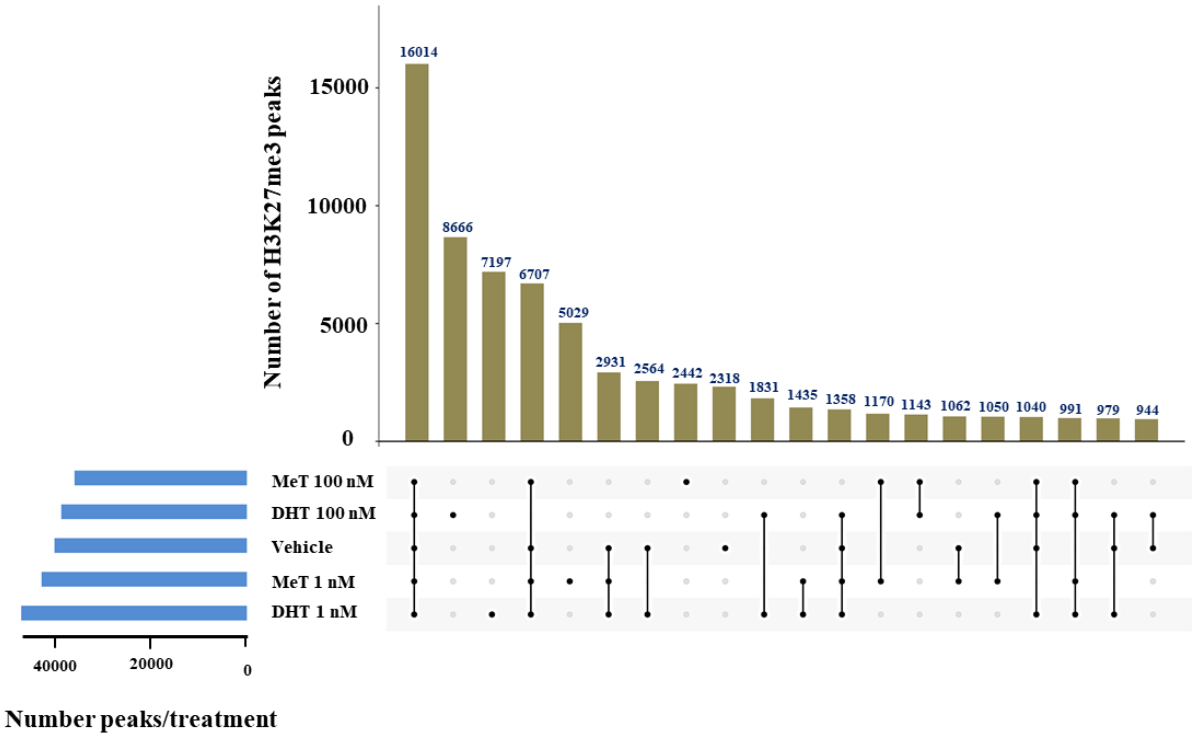

Figure 4.8. Androgen treatments changed the genome-wide distribution of H3k27me3 histone modification. UpSet plots illustrated the overlap of consensus H3K27me3 peaks in LNCaP cells treated *in vitro* with Vehicle, MeT (1 and 100 nM) or DHT (1 and 100 nM).

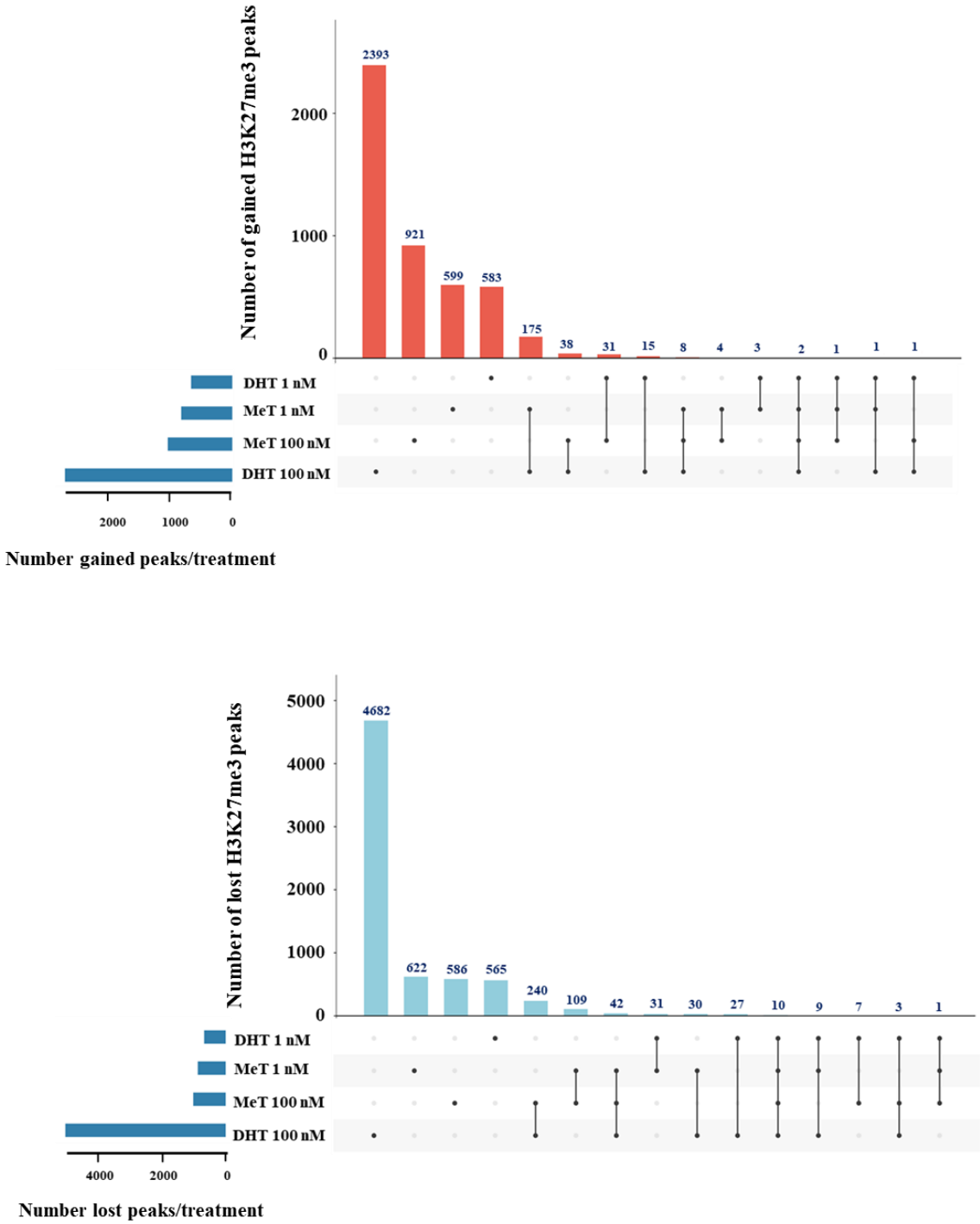

Figure 4.9. The difference in type and doses of androgens causes unique differentially modified DNA regions by H3K27me3. The overlapping of differentially gained or lost H3K27me3 by MeT and DHT was illustrated using the UpSet plots.

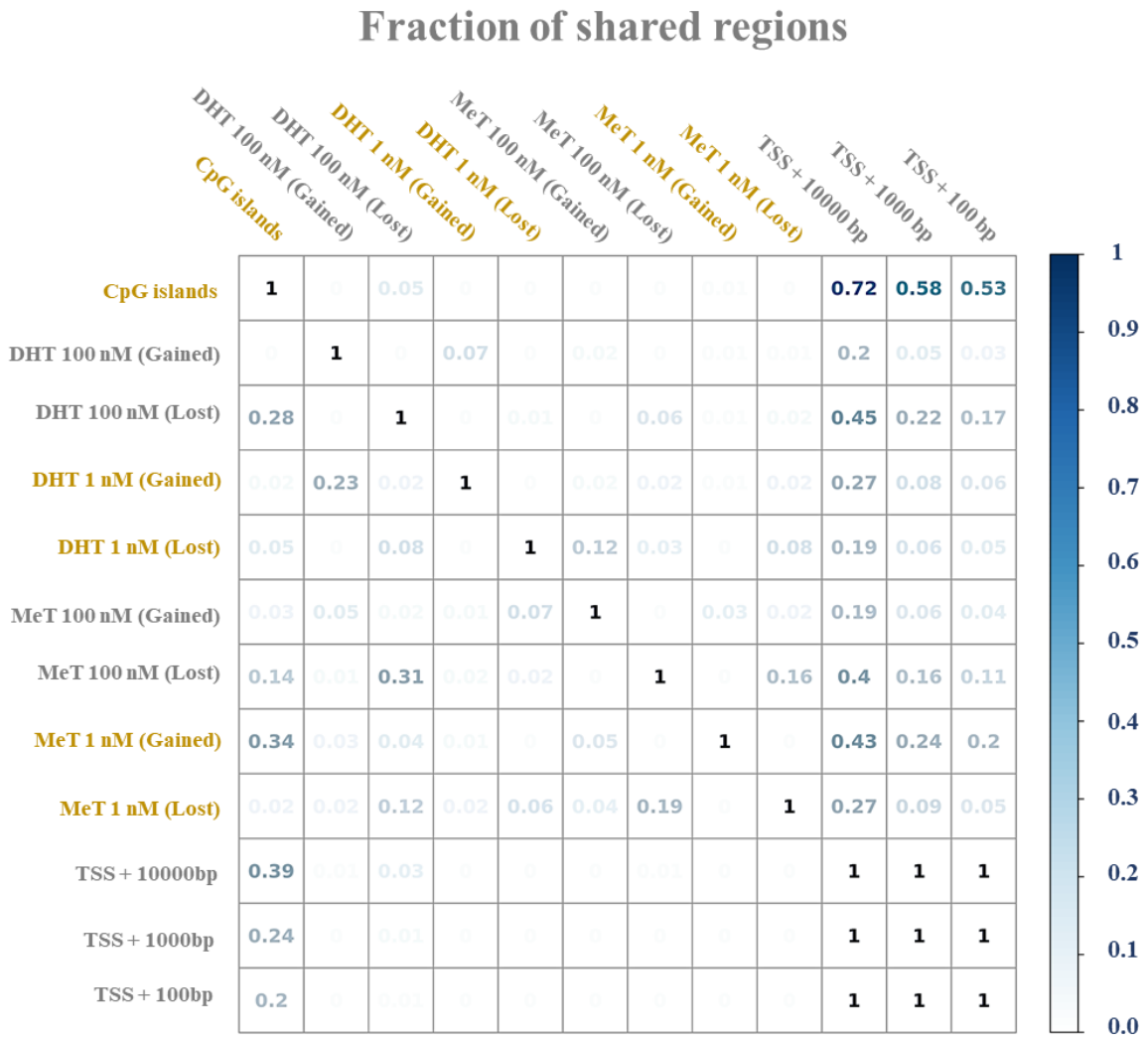

Figure 4.10. Treatment with high-dose androgens causes an increase in differentially lost peaks at intergenic regions. A pairwise plot was used to compare the overlapping of differentially gained or lost H3K27me3 peaks with each other and also with some regulatory regions including TSS, upstream of TSS, and CpG islands. The fraction of regions in the X-axis which is shared with regions in the Y-axis was shown as a fraction of 1, which is equal to 100% overlapping.

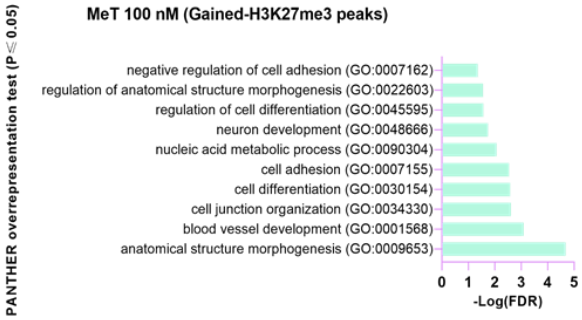
MeT 100 nM (Gained-H3K27me3 peaks)
PANTHER overrepresentation test (P ⩽ 0.05)
negative regulation of cell adhesion (GO:0007162)
regulation of anatomical structure morphogenesis (GO:0022603)
regulation of cell differentiation (GO:0045595)
neuron development (GO:0048666)
nucleic acid metabolic process (GO:0090304)
cell adhesion (GO:0007155)
cell differentiation (GO:0030154)
cell junction organization (GO:0034330)
blood vessel development (GO:0001568)
anatomical structure morphogenesis (GO:0009653)
0 1 2 3 4 5
-Log(FDR)

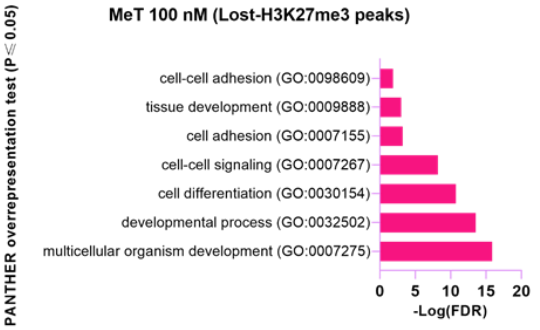
MeT 100 nM (Lost-H3K27me3 peaks)
PANTHER overrepresentation test (P ⩽ 0.05)
cell-cell adhesion (GO:0098609)
tissue development (GO:0009888)
cell adhesion (GO:0007155)
cell-cell signaling (GO:0007267)
cell differentiation (GO:0030154)
developmental process (GO:0032502)
multicellular organism development (GO:0007275)
0 5 10 15 20
-Log(FDR)

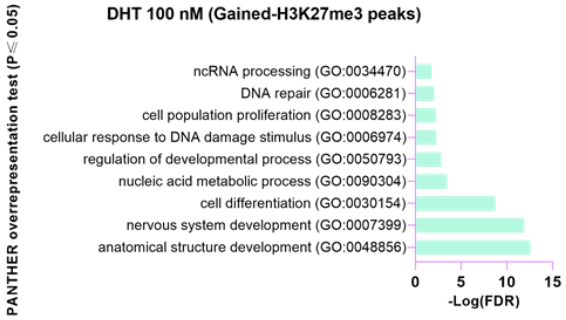
DHT 100 nM (Gained-H3K27me3 peaks)
PANTHER overrepresentation test (P ⩽ 0.05)
ncRNA processing (GO:0034470)
DNA repair (GO:0006281)
cell population proliferation (GO:0008283)
cellular response to DNA damage stimulus (GO:0006974)
regulation of developmental process (GO:0050793)
nucleic acid metabolic process (GO:0090304)
cell differentiation (GO:0030154)
nervous system development (GO:0007399)
anatomical structure development (GO:0048856)
0 5 10 15
-Log(FDR)

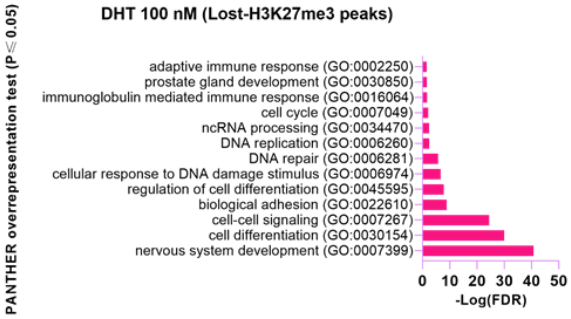
DHT 100 nM (Lost-H3K27me3 peaks)
PANTHER overrepresentation test (P ⩽ 0.05)
adaptive immune response (GO:0002250)
prostate gland development (GO:0030850)
immunoglobulin mediated immune response (GO:0016064)
cell cycle (GO:0007049)
ncRNA processing (GO:0034470)
DNA replication (GO:0006260)
DNA repair (GO:0006281)
cellular response to DNA damage stimulus (GO:0006974)
regulation of cell differentiation (GO:0045595)
biological adhesion (GO:0022610)
cell-cell signaling (GO:0007267)
cell differentiation (GO:0030154)
nervous system development (GO:0007399)
0 10 20 30 40 50
-Log(FDR)

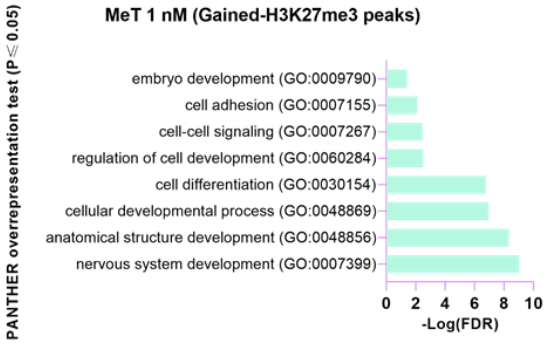
MeT 1 nM (Gained-H3K27me3 peaks)
PANTHER overrepresentation test (P ⩽ 0.05)
embryo development (GO:0009790)
cell adhesion (GO:0007155)
cell-cell signaling (GO:0007267)
regulation of cell development (GO:0060284)
cell differentiation (GO:0030154)
cellular developmental process (GO:0048869)
anatomical structure development (GO:0048856)
nervous system development (GO:0007399)
0 2 4 6 8 10
-Log(FDR)

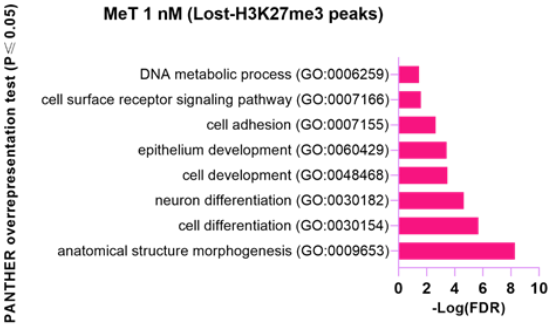
MeT 1 nM (Lost-H3K27me3 peaks)
PANTHER overrepresentation test (P ⩽ 0.05)
DNA metabolic process (GO:0006259)
cell surface receptor signaling pathway (GO:0007166)
cell adhesion (GO:0007155)
epithelium development (GO:0060429)
cell development (GO:0048468)
neuron differentiation (GO:0030182)
cell differentiation (GO:0030154)
anatomical structure morphogenesis (GO:0009653)
0 2 4 6 8 10
-Log(FDR)

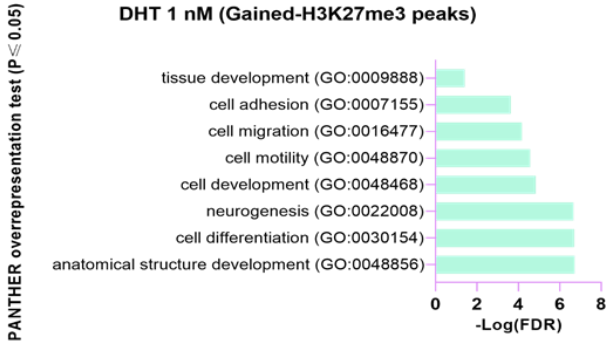
DHT 1 nM (Gained-H3K27me3 peaks)
PANTHER overrepresentation test (P ⩽ 0.05)
tissue development (GO:0009888)
cell adhesion (GO:0007155)
cell migration (GO:0016477)
cell motility (GO:0048870)
cell development (GO:0048468)
neurogenesis (GO:0022008)
cell differentiation (GO:0030154)
anatomical structure development (GO:0048856)
0 2 4 6 8
-Log(FDR)

Figure 4.11. Gene ontology enrichment analysis showed the significant enrichment of developmental pathways for regions marked by H3K27me3. The heatmap shows significantly overrepresented biological processes in different treatment groups, which was analysed using online PANTHER overrepresentation platform (Mi, Muruganujan et al. 2019). Enrichment test was performed using Fisher's exact test; FDR p-values were calculated as -log10 FDR.

4.3.4. No evidence for altered H3K27me3 at endogenous retrovirus elements

As shown in Chapter 3, MeT and high-dose androgens caused hypo-methylation of DNA and dysregulation of repetitive elements, resulting in activation of a viral mimicry response in prostate cancer cells. The repressive histone mark H3K27me3 has also been linked to repression of *ERV* transcription (Walter, Teissandier et al. 2016). Therefore, we examined H3K27me3 at different repetitive elements. Surprisingly, the analysis of the different class of repetitive elements including *DNA* class, *Long interspersed nuclear elements (LINEs)*, *long terminal repeat (LTR)*, *Short interspersed nuclear elements (SINEs)*, and *SINE-VNTR-Alus (SVAs)* revealed two distinct shapes of H3K27me3 signals (Figure 4.12). Interestingly, in DNA, LINE, and LTR classes, the peak densities were very low, exhibiting a peak-valley-peak signal pattern with depletion of H3K27me3 towards the centre of these elements. By contrast, in *SVA* and *SINE* classes, which are generally enriched with GC content (Gu, Jin et al. 2016), H3K27me3 formed sharp peaks at the centre. Similar to *SINEs* and *SVAs*, H3K27me3 was also enriched in CpG islands with sharp peaks at the centre, suggesting that the distribution pattern of H3K27me3 in LNCaP cells depends on the GC content of the targeted region. Interestingly, in the majority of regions with H3K27me3 peaks, the H3K27me3 signal from the MeT 1 nM treatment group was higher than other treatments, which is consistent with the results of pairwise analysis. Treatment with higher doses of MeT or DHT did not cause any substantial decrease to the level of H3K27me3 deposition at these elements, which is consistent with our earlier analyses but inconsistent with the hypothesis that altered distribution of this histone mark at repetitive elements results in changes to their transcription.

H3K27me3 deposition at DNA Class

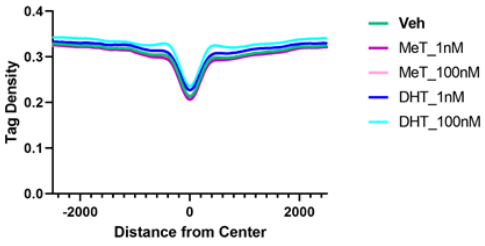

H3K27me3 deposition at CpG islands

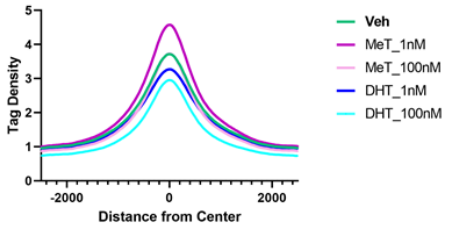

H3K27me3 deposition at LINE Class

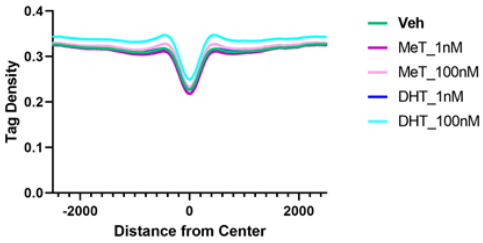

H3K27me3 deposition at SVA-C

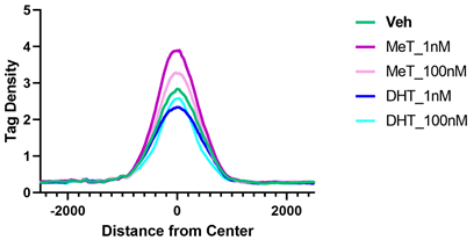

H3K27me3 deposition at LTR Class

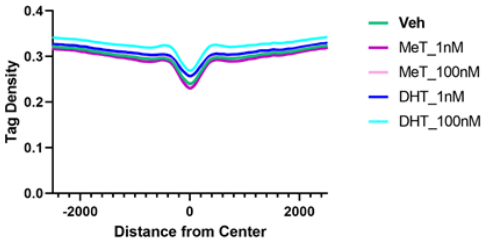

H3K27me3 deposition at SVA-D

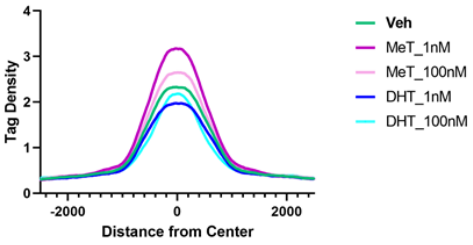

H3K27me3 deposition at SINE Class

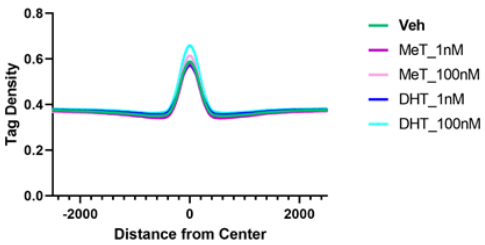

H3K27me3 deposition at SVA-F

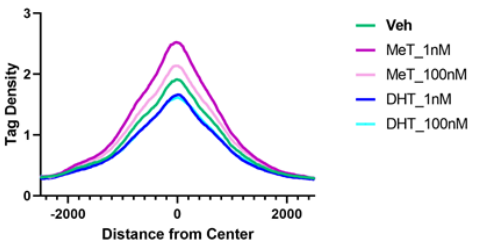

H3K27me3 deposition at AluSg

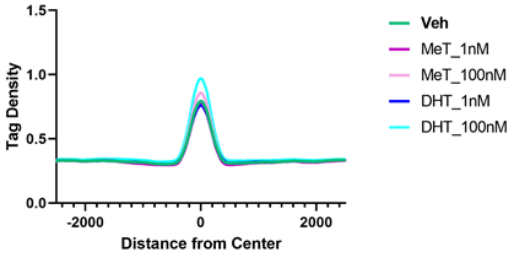

H3K27me3 deposition at AluSq

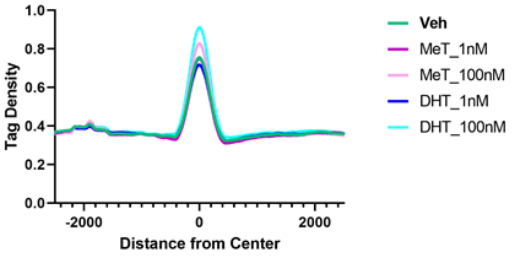

H3K27me3 deposition at ERV1

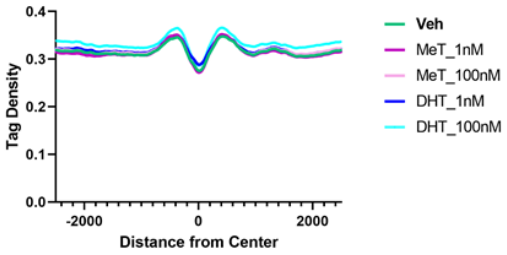

H3K27me3 deposition at ERVL

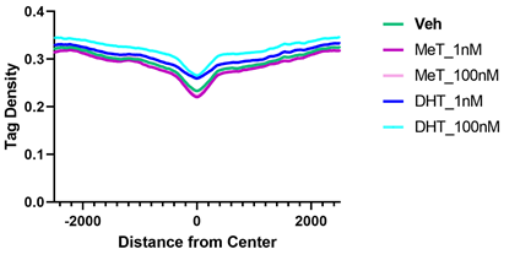

H3K27me3 deposition at AluYb8

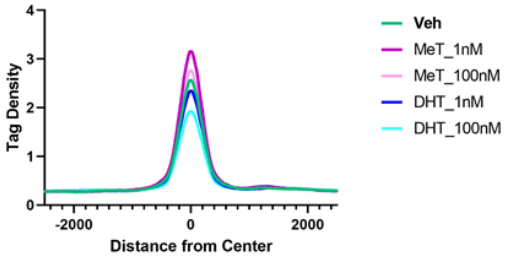

H3K27me3 deposition at HERVK-int

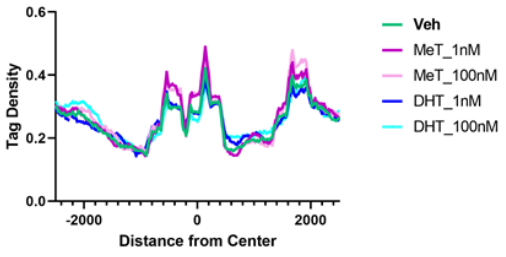

H3K27me3 deposition at HERV3-int

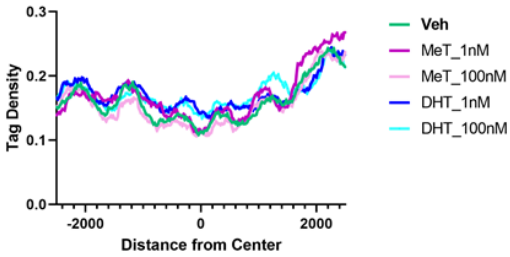

H3K27me3 deposition at HERVH-int

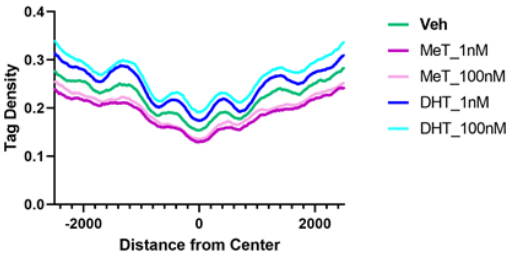

Figure 4.12. Deposition status of H3K27me3 at repetitive elements. HOMER was used to visualise the deposition status of H3K27me3 at repetitive elements in LNCaP cells treated with vehicle, MeT (1 nM and 100 nM) or DHT (1 nM and 100 nM) for 72h. Average read density plots were generated for H3K27me3 binding to DNA class, LINE class, LTR class, SINE class, CpG islands, SVA family members, Alu family members (AluSq, AluSq, and AluYb8), ERVL, HERVK-int, HERV3-int (ERV3-1), and HERVH-int. The coordinates of repetitive elements were downloaded from the UCSC Table Browser (Karolchik, Hinrichs et al. 2004).

4.3.5. Deposition pattern of H3K27me3 was not associated with enhanced expression of MHC-I and MHC-II

As demonstrated in Chapter 3, MeT and high-dose DHT increased the expression of MHC-I proteins. Previous studies demonstrated that the expression of *HLA* genes in colorectal cancer cells can be induced by decreasing the levels of H3K27me3 by pharmacological inhibition of EZH2 (Burr, Sparbier et al. 2019). Therefore, we speculated that androgen-mediated repression of EZH2 may be a reason for observed up-regulation of MHC-I and MHC-II genes (refer to Chapter 3, Figure 7A). Therefore, we examined the distribution of H3K27me3 at the promoter of gene sets associated with *MHC-I* and *MHC-II* (Reactome). However, as shown in Figure 4.13, we did not observe a loss of H3K27me3 signal at the promoters of *MHC-I* and *MHC-II* genes in response to androgen treatments. Figure 4.14 shows an example of the deposition pattern of H3K27me3 at the *HLA-B* gene following androgen treatment.

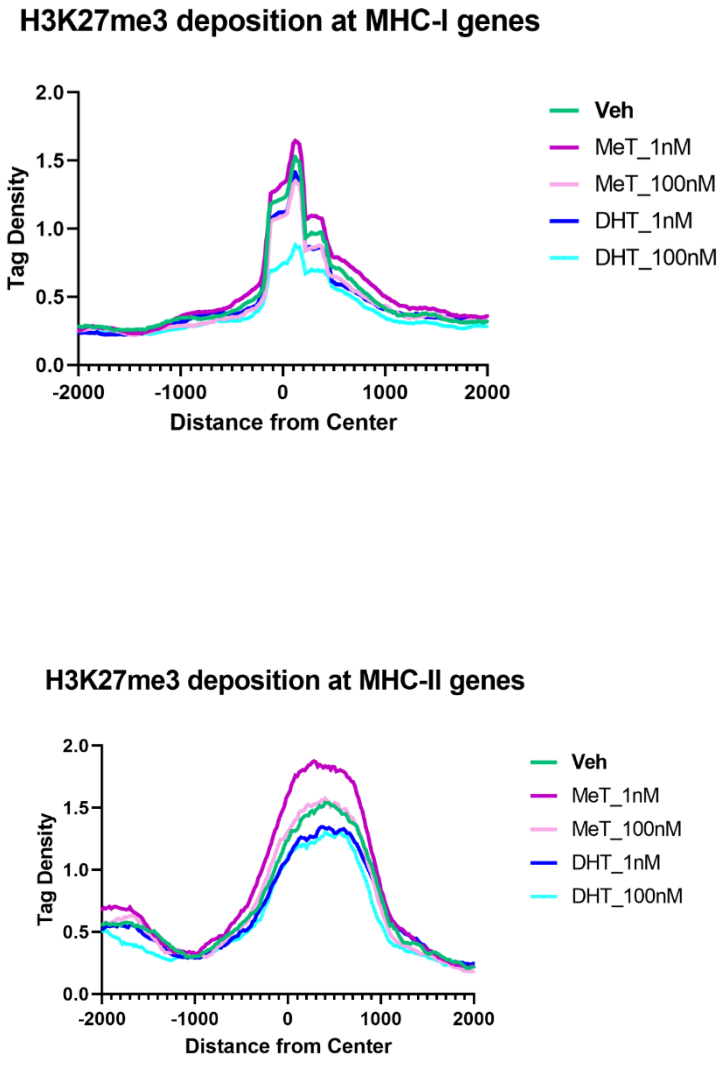

Figure 4.13. Promoter analysis showed that androgens did not change the deposition pattern of H3K27me3 at the promoter of genes associated with MHC-I and MHC-II. Average read density plots for H3K27me3 to genes associated with MHC-I and MHC-II in LNCaP cells treated with vehicle, MeT (1 nM and 100 nM) or DHT (1 nM and 100 nM) for 72h.

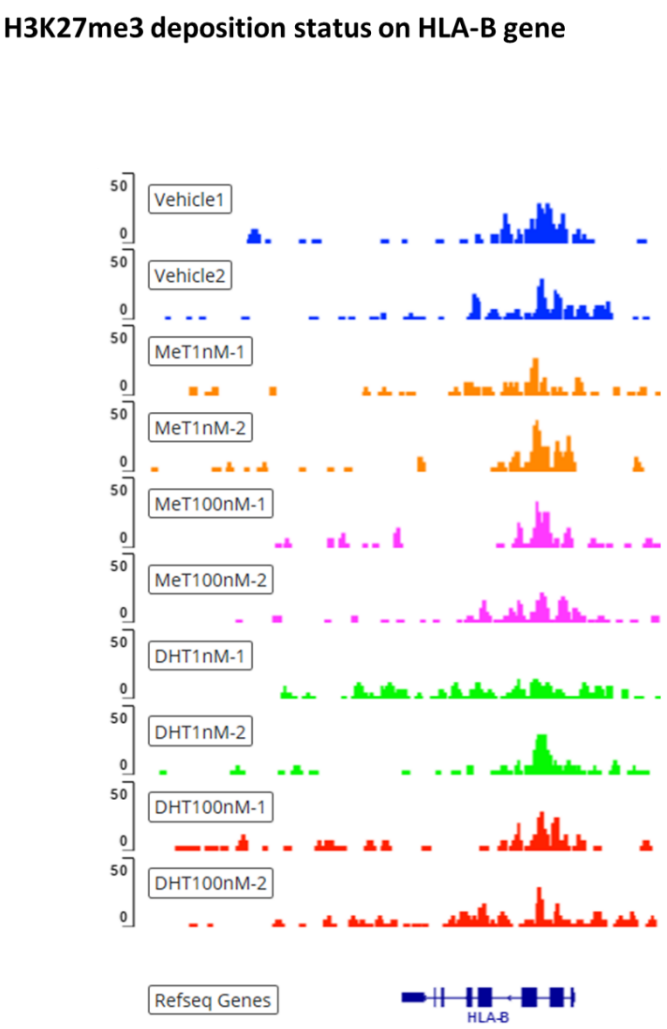

Figure 4.14. Androgen treatment did not change the deposition pattern of H3K27me3 at *HLA-B* in LNCaP cells. Genome browser image showing H3k27me3 ChIP-seq signals at binding sites associated with HLA-B in two replicates of LNCaP cells treated with Vehicle, MeT (1 and 100 nM) and DHT (1 and 100 nM).

4.4. Discussion

Epigenetic modifications, including DNA methylation and histone modifications, regulate the accessibility of chromatin for gene expression (Adam and Fuchs 2016). One of the mechanisms underlying chromatin compaction is the deposition of H3K27me3 by the PRC2 complex, which has EZH2 and EZH1 as its catalytic subunits (Rizq, Mimura et al. 2017). Overexpressed in CRPC tumours, EZH2 is considered a *bona fide* oncogene in PCa and CRPC, with its primary oncogenic function thought to be silencing of tumour suppressor genes (Varambally, Dhanasekaran et al. 2002).

Given the notion that EZH2 inhibition can make prostate cancer cells vulnerable to high-dose androgens (Nyquist, Corella et al. 2019), we were therefore intrigued to understand how *EZH2* suppression by androgens affects prostate cancer cell growth. In this study, we have shown that hyper-activation of AR causes down-regulation of *EZH2* in different prostate cancer cell lines. Also, we found that down-regulation of *EZH2* was associated with reduced total levels of nucleoplasmic H3K27me3 (as shown by Western blotting of histone acid extracts) but did not have a substantive effect on the level and distribution of chromatin-associated H3K27me3 (as shown by ChIP-seq). This finding indicates that *EZH2* repression by high-dose androgens caused a reduced level of H3K27me3 in soluble nucleoplasmic fraction rather than insoluble chromatin compartments. We envision a number of possible explanations for this apparently contradictory finding. Given that methylation of pre-deposition H3 soluble histones has been described for H3K9 histones (Loyola, Bonaldi et al. 2006), one possibility is that in LNCaP cells,

non-DNA bound H3K27 histones may be targeted by EZH2. However, this hypothesis is not consistent with previous findings in mouse embryonic stem cells (Ferrari, Scelfo et al. 2014, Juan, Wang et al. 2016), indicating that H3K27 histones are not methylated before nucleosome assembly. Therefore, in future studies, I propose that high-dose androgens effects on methylation of H3K27 should be examined in cytoplasmic, nucleoplasmic, and chromatin-bound fractions of PCa cells.

Second, the disparity between total H3K27me3 and chromatin-bound H3K27me3 may relate to DNA methylation status. Mechanistically, it has been shown that in the absence of DNA methylation, the canonical activity of EZH2 underlies a compensation mechanism, reallocating H3K27me3 to maintain the repressive chromatin state (18). With this background in mind, we showed in Chapter 3 that androgens affect the global methylation level of DNA, so it is possible that this leads to a re-distribution of H3K27me3 to compensate for DNA hypomethylation. Demonstrating the importance of this compensation mechanism in sustaining the repression of repetitive elements, Deblois G, et al., (Deblois, Tonekaboni et al. 2020) showed that in taxane-resistant triple-negative breast cancer cells, inhibiting H3K27me3 deposition through pharmacologic inhibition of EZH2 can re-activate the expression of hypo-methylated transposon elements through viral mimicry response. Supporting this possibility, we found that H3K27me3 was gained at GC rich regions such as CpG islands and SVA elements, which can be potentially related to their low DNA methylation level. In future studies, the deposition pattern of H3K27me3 should be examined after DNA hypomethylation with DNA demethylating agents in the presence and/or absence of EZH2,

which would determine how the canonical activity of EZH2 changes in hypo-methylated DNA condition. Also, genome-wide DNA methylation should be investigated to more precisely determine the interplay between H3K27me3 deposition pattern and DNA methylation status.

Finally, the simplest explanation for the apparent disparity between H3K27me3 levels in soluble nuclear fractions versus chromatin-bound could relate to experimental conditions i.e. time-point and growth conditions. It is known that the interaction of PRC2 with chromatin and deposition of H3K27me3 is a highly dynamic process that is influenced by growth conditions (Adriaens, Prickaerts et al. 2016). To overcome this issue, in future work I propose to carefully tailor the experimental conditions to decrease variability resulting from the mechanism of action of EZH2/PRC2.

The basis for the work in this chapter was that modulation of EZH2 and H3K27me3 could explain the induction of ERVs. This hypothesis was based on previous studies in other cancer models showing that this histone mark plays a key role in repressing ERV transcription (Deblois, Tonekaboni et al. 2020). Unexpectedly, we found that *ERVs* in this model were not marked by H3K27me3. This suggests that DNA methylation could be the key mechanism controlling the expression of *ERVs*, as described in Chapter 3. Other reports are consistent with this hypothesis: for example, low-resolution analysis of chromosome 17 in a mouse model revealed that H3K27me3 is depleted at *ERVs*, but enriched at broad localized regions termed BLOCs that were found primarily within *SINEs* (Pauler, Sloane et al. 2009). This study also revealed that repressive H3K27me3 BLOCs were distributed over genes and intergenic

regions and H3K27me3 peaks rarely marked the gene promoters, accounting for only 10%–15% of the promoters, which is also consistent with our findings. Another study also demonstrated that PRC2 complex / H3K27me3 is not involved in silencing repetitive elements in spermatocytes (Mu, Starmer et al. 2014) showed. Taken together, our findings do not support H3K27me3 playing a major role in ERV transcription in PCa cells. Notably, other histone modifications, such as H3K9me3 and/or H4K20me3, have been reported to play a role in the transcription of repetitive elements (Mikkelsen, Ku et al. 2007); I propose that a more comprehensive analysis of the epigenome is required to accurately determine how MeT leads to de-repression of *ERVs* and other repetitive elements (e.g. LINEs).

It is important to note that both catalytic (canonical) and non-catalytic (non-canonical; i.e. collaboration with *AR*) activities of EZH2 have been identified in PCa cells (Kim, Lee et al. 2018). Given that MeT repressed the expression of genes that are activated by EZH2; this supports the hypothesis that high-dose androgens may primarily disrupt the non-canonical activity of EZH2, as opposed to the canonical function. To test this hypothesis, I propose that assessing EZH2 interaction with AR and also its genome-wide DNA binding profile (i.e. using ChIP-seq) could be examined in response to MeT treatment.

Gene ontology analysis suggested a significant overrepresentation of biological processes involved in development, differentiation, and lineage-specification process, which are consistent with the proposed role of H3K27me3 in regulating the expression of genes involved in of nervous system and anatomical structures (Hawkins, Hon et al. 2010, Zeng, Zhang et al.

2019). However, in future studies, to examine any association between H3K27me3 re-distribution and alteration in the function of a pathway, matched transcriptomic data is needed. Unfortunately, the RNA-seq we carried out (see Chapter 3) was done at a much earlier time-point compared to the H3K27me3 ChIP-seq, which precluded integration of these datasets.

Overall, our study showed that potent activation of AR caused down-regulation of EZH2 and a concomitant decrease in the global H3K27me3 level. However, the lack of substantial impact on the level and distribution of chromatin-associated H3K27me3 means that it is not possible to know whether repression of EZH2 has any role in mediating the growth-suppressive or immunomodulatory effects of MeT. Since EZH2 inhibitors are being developed to treat PCa (Morel, Sheahan et al. 2021), this remains an important question to definitively answer.

Chapter 5: General Discussion

5. General Discussion

Prostate cancer is the second most common cancer worldwide in men and has one of the highest age-standardized incidence and mortality rates of all cancers in Australian men (Organization 2012). Current treatment strategies for patients with localized prostate cancer, including radical prostatectomy and radiotherapy, are curative in a substantial proportion of men; however, approximately 30% experience recurrence with metastatic disease (Singh, Febbo et al. 2002). As described in chapter 1, ADT is a standard-of-care treatment for metastatic PCa, which aims to inhibit the activity of a major oncogenic driver of this disease, AR. However, ADT is never curative, with all patients eventually acquiring resistance to therapy and relapsing with lethal castration-resistant prostate cancer (CRPC). Enigmatically, recent studies have suggested that potent activation of AR using high doses of androgens can, similarly to AR suppression, also inhibit the growth of CRPC (Schweizer, Antonarakis et al. 2015). However, the exact tumour suppressive effect(s) of high-dose androgen therapy remain largely uncharacterised. This study aimed to investigate the mechanisms underlying PCa growth suppression in response to hyperactivation of AR by a potent androgen, methyltestosterone (MeT).

5.1. MeT potently suppresses the growth of PCa cells

Investigation into the effects of MeT on prostate cancer cell growth revealed that MeT suppressed the growth of AR-positive PCa cell line models more potently than the physiological androgen DHT. Consistent with this finding, transcriptional activation assays showed that MeT is a more potent transcriptional activator of AR, an observation supported

by earlier studies (Sonneveld, Jansen et al. 2005, Wolf, Diel et al. 2011, Wang, Lawless et al. 2020), indicating that MeT shows more AR agonistic effects in comparison with DHT. Given the higher AR binding affinity of DHT relative to MeT (Liao, Liang et al. 1973, Saartok, Dahlberg et al. 1984, Fang, Tong et al. 2003), this was an unexpected result. However, it has been reported that MeT cannot be metabolised by Glucuronyl-transferase enzymes, which are the major mediators of androgen inactivation in prostate cancer cells (Smith, Ballard et al. 1994, Kuuranne, Kurkela et al. 2003, Chouinard, Barbier et al. 2007). Thus, I propose that MeT's greater androgenic potency is largely related to its increased stability in the models used in my project. However, in future studies, I propose that MeT and DHT should be measured in PCa cells to validate this hypothesis. Toward this end, the androgen levels can be measured in cell culture media by liquid chromatography tandem mass spectrometry (LC-MSMS), which is considered the gold standard method (Matsumoto and Bremner 2004, Harwood and Handelsman 2009).

Using an integrated genomic approach that includes ChIP-seq and RNA-seq, I found that MeT regulates a canonical set of AR-regulated genes and leads to a similar genome-wide AR DNA binding profile, but it does so much more potently than DHT. Molecularly, extreme activation of AR with MeT is linked to the repression of previously reported AR target genes that are associated with cell cycle, DNA replication, and DNA repair (Gao, Gao et al. 2016, Chatterjee, Schweizer et al. 2019, Lam, Nguyen et al. 2020). Supporting the idea that these are direct target genes, I found that MeT-activated AR was strongly recruited to the promoter of these genes. Mechanistically, repression of genes associated with cell cycle and DNA replication is

linked to cell cycle arrest (Engeland 2018), which we confirmed with FACS analysis following treatment of cells with MeT.

Preclinical studies have proposed that AR-mediated repression of genes associated with DNA damage response is linked to the therapeutic effects of high-dose androgens (Chatterjee, Schweizer et al. 2019, Lam, Nguyen et al. 2020). Consistent with this idea, some clinical studies also suggested that patients with deficiency in DNA repair genes may exhibit a better response to high-dose androgen therapies (Teply, Kachhap et al. 2017). Indeed, a prevailing dogma posits that AR-induced DNA damage is the major therapeutic mediator of high-dose androgen treatment and hence that deficiency in the DNA repair system can enhance therapeutic benefit (Chatterjee, Schweizer et al. 2019, Nyquist, Corella et al. 2019). However, we did not observe an increased level of γH2AX in response to MeT treatment. This observation aligns with other studies indicating that AR activation by androgens cannot induce persistent dsDNA breaks (Lin, Yang et al. 2009, Polkinghorn, Parker et al. 2013, Nyquist, Corella et al. 2017). Moreover, genomic analysis of circulating-tumour DNA isolated from CRPC patients who were treated with high-dose androgen therapy revealed that there was no significant association between baseline AR and DNA repair alterations with PSA response (Chatterjee, Schweizer et al. 2019, Moses, Koksal et al. 2020). Regarding the relevance of AR-induced DNA damage to BAT response in CRPC patients, next-generation sequencing of samples from patients who received BAT revealed an enormous variation among patients with different genomic aberrations (Schweizer, Antonarakis et al. 2019). Overall, the question as to whether AR-induced DNA damage is the key mechanism exerting anti-proliferative

effects in prostate cancer cells remains unanswered. Therefore, in future studies, DNA repair defects should be measured in much larger cohorts of men treated with BAT to provide definitive evidence that such defects could be used to predict response. Also, DNA damage should be examined more directly (eg using a COMET assay) in both cells and patient tumours treated with high-dose androgens.

5.2. Hyper-activation of AR triggers viral mimicry response in PCa cells

Prostate cancer is immunologically characterised as a "cold tumour", indicating that tumour cells cannot be effectively killed by immune cells. Mechanistically, the immunological "coldness" of PCa tumours, which mediates resistance to immunotherapies, can be induced by a network of different but intertwined factors including the presence of immunosuppressive cells in the tumour microenvironment, low expression of tumour-associated antigens, and dysfunctional antigen presentation system in cancer cells (Bronte, Kasic et al. 2005). Immunosuppressive cells that are enriched in prostate tumours include cancer-associated fibroblasts (CAFs), regulatory T cells, tumour-associated macrophages (TAMs), and myeloid-derived suppressor cells (MDSCs), all of which can induce immune evasion phenotypes by impeding the differentiation, activation, and interaction of cytotoxic T cells against tumour cells (Lu, Rong et al. 2019, Zhao, Lehrer et al. 2019, Li, Jiang et al. 2020). Another important immune evasion mechanisms in prostate cancer cells is loss of major histocompatibility complex (MHC) expression, which can be potentially impaired either by tumour microenvironment or intrinsic factors such as genetic/epigenetic aberrations (Sanda, Restifo et al. 1995, Bander, Yao et al. 1997, Dhatchinamoorthy, Colbert et al. 2021). It has

been reported that in primary prostate cancer tumours, low expression of MHC-I genes was associated with high Gleason score, bone metastasis, and short cancer-specific survival (Ylitalo, Thysell et al. 2017). Expression of MHC-I genes can be induced by different mechanisms including IFN signalling, which can cause a robust immune response by CD8+ T cells (Martini, Testi et al. 2010). However, it has been demonstrated that in metastatic prostate cancer cells tumour-intrinsic type I IFN and associated immune signalling is epigenetically suppressed (Owen, Gearing et al. 2020).

In my PhD studies, RNA-seq data revealed that MeT treatment induced the expression of interferon-stimulated genes (ISGs), suggesting that extreme activation of AR leads to the activation of IFN signalling pathways. Indeed, I found in multiple *in vitro* prostate cancer models that potent activation of AR induced expression of IFN-β and ISGs concomitantly with dysregulation in the expression pattern of repetitive elements. More specifically, my PhD work demonstrated that potent activation of AR triggers the activation of a viral mimicry response in prostate cancer cells, which was characterised by upregulation of ERVs, accumulation of viral dsRNAs in cells, activation of interferon signalling, upregulation of MHC Class I and activation of T cells (Figure 5.1).

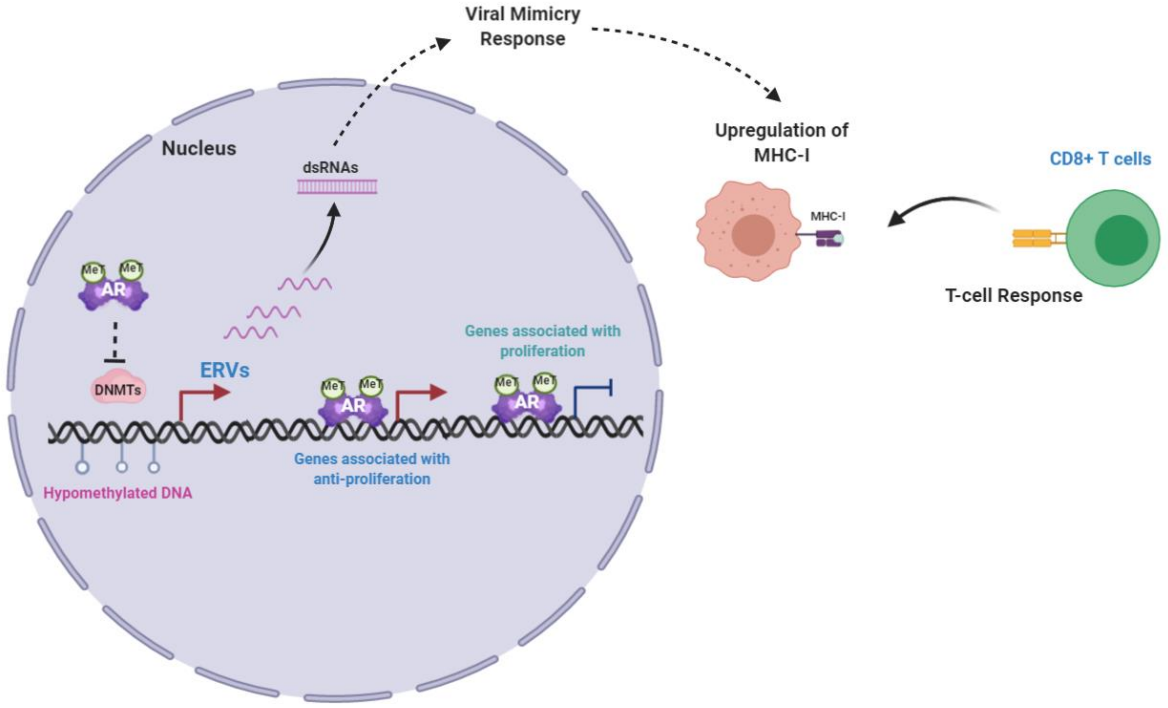

Figure 5.1. Schematic depicting the role of AR in immunosensitizing of PCa cells

Mechanistically, the expression of repetitive elements is primarily regulated by epigenetic modifications, and DNA methylation is a key mechanism conferring long-term epigenetic silencing of transposons (Yoder, Walsh et al. 1997, Reik 2007). We were therefore intrigued to discern whether high-dose androgen-mediated ERVs expression is associated with epigenetic changes in prostate cancer cells. In my PhD studies, I showed that treatment with MeT repressed the expression of key enzymes involved in the maintenance (DNMT1) and *de novo* methylation (DNMT3b) of DNA. Following this finding, we also demonstrated that treatment with androgens leads to DNA hypomethylation. Although to the best of my knowledge this is the first report of androgen-mediated hypomethylation, it should be noted

that a negative correlation between AR activity and DNA methylation status has been reported previously (Dhiman, Attwood et al. 2015). Therefore, we postulate that androgen-induced hypomethylation of DNA is the key mechanism dysregulating the expression of repetitive elements, leading to activation of viral mimicry response in prostate cancer cells. However, with current data, we cannot conclude the exact mechanism of epigenetic alterations by AR. To verify the role of DNMTs in the MeT-mediated viral mimicry response, a powerful experiment would be to treat prostate cancer cells over-expressing DNMTs with MeT and see whether ERV induction and viral mimicry response is lost or weakened. Additionally, examining whether MeT can synergise with DNA de-methylating agents such as Decitabine could provide more evidence of the importance of DNMTs in these processes. Understanding how androgens suppress DNMTs could also shed light on these questions. DNMT1 is an E2F1 target genes and our transcriptomic data showed that E2F1 and its target genes were strongly repressed by MeT (33, 34). Demonstrating loss of E2F1 binding to the *DNMT1* gene (e.g. by ChIP) would provide further evidence for its role in MeT-mediated alterations to DNA methylation. Importantly, if this hypothesis could be confirmed, it would suggest that MeT could be applied in combination with CDK4/6 inhibitors, which also inactivate E2F1 and can cause a viral mimicry response (Goel, DeCristo et al. 2017).

As reported in previous studies, detection of viral dsRNA by intracellular dsRNA sensors (TLR3, RIG-I and MDA5) or dsRNA/dsDNA sensor (STING) is the trigger of innate immune response activation (Liu, Ohtani et al. 2016, Goel, DeCristo et al. 2017, Liu, Thomas et al. 2018). In prostate cancer cells, we showed that that potent activation of AR leads to the induction of

RIG-I and STING, which potentially detect the androgen-induced dsRNAs leading to activation of viral mimicry response. However, proving that dsRNA sensing is required for MeT-mediated viral mimicry is a crucial mechanistic experiment that I was unable to complete during my PhD. In the future, I propose to use genetic methods (i.e. siRNA, CRISPR) or pharmacological methods (i.e. STING inhibitor) for inhibition of STING/RIG-I to determine whether these factors are required for induction of innate immune responses by MeT.

Activation of innate interferon signalling in tumours cells can enhance the expression of MHC-I expression and cause the infiltration of tumour-specific cytotoxic $CD8^+$ T cells (Corrales, Matson et al. 2017). My PhD studies identified a similar mechanism whereby potent activation of AR in cancer cells caused induction of MHC-I molecules (i.e. *HLA-B* and *HLA-C*), led to enhanced tumour cell immunogenicity as demonstrated by enhanced recognition of cancer cells by tumour-specific CD 8+ T cells. This is an important finding suggesting potential clinical implications, which was supported by a case report study suggesting that bipolar androgen therapy may have immune activation effects on prostate cancer tumours (Markowski, Shenderov et al. 2020). To confirm that immunomodulatory effects of MeT are mediated by activation of IFN signalling, I propose that future studies should conduct equivalent studies using genetically engineered models that are deficient for IFN signalling (e.g C57BL/6 *Ifnar1* $^{-/-}$ (Owen, Gearing et al. 2020)). Specifically, loss of immune response in such a model can confirm the role of the proposed mechanism for IFN signalling. More broadly, the tumour microenvironment's role in immune evasion is critical and the lack of in vivo studies in my study was a major limitation. Therefore, to determine whether high-dose

androgen therapy can exert the proposed immunomodulatory effects in the presence of immunosuppressive prostate tumour microenvironment in vivo studies (e.g B6-Hi-MYC model (Morel, Sheahan et al. 2021)) are essential. Finally, given the reported anticancer and immunomodulatory effects of IFN-γ on tumour cells and also on tumour microenvironment, it would be worth considering whether a combination treatment comprising MeT and IFN-γ may cause an additive benefit in terms of immune surveillance (Selleck, Canfield et al. 2003, Cheon, Borden et al. 2014, Galon and Bruni 2019, Jorgovanovic, Song et al. 2020).

5.3 Androgen treatments modulate EZH2 function and re-distribute H3K27me3

In Chapter 4, I reported that potent activation of AR caused repression of the histone methyltransferase EZH2 in prostate cancer cells, suggesting that EZH2 repression by high-dose androgens could induce epigenetic alterations beyond DNA hypomethylation. Interestingly, genome-wide studies have shown that there is an anti-correlated relationship between DNA methylation level and H3K27 methylation enrichment (Fu, Bonora et al. 2020). Given that potent activation of AR with androgens induces a global DNA hypomethylation (please see Chapter 3), we were therefore intrigued to examine the consequence of EZH2 repression by androgens on the deposition of H3K27me3. Interestingly, H3K27me3 ChIP-seq showed a minor re-distribution of H3K27me3 by MeT and DHT but not an overall loss of chromatin-bound H3K27me3. Possible explanations for this unexpected finding were described in Section 4.4.

As shown in Chapter 3, androgen-induced DNA hypomethylation causes the activation of the viral mimicry response in prostate cancer cells. More interestingly, we showed that Decitabine-induced dsRNA are less strong than MeT 1nM, suggesting that dsRNA formation by MeT is also amplified by another mechanism. We postulated that the strong induction of dsRNAs by MeT could be potentially related to the modulation of the EZH2-associated compensation mechanism. Analysis of H3K27me3 deposition at different classes of repetitive elements, however, revealed that androgen (MeT or DHT) did not cause a significant difference in H3K27me3 profile. Despite this result, I propose that future work should evaluate how a DNA de-methylating agent (e.g. Decitabine) influences H3K27me3 to determine if a compensation mechanism is active in prostate cancer and influences expression of transposable elements.

5.4. Overall conclusion

Collectively, the work described in this thesis sheds new light on the anti-tumour mechanism of action of high dose androgens in prostate cancer cells. Most importantly, the concept for immunosensitisation of prostate tumours using MeT is pioneering and warrants further pre-clinical and clinical investigation.

References:

Aarnisalo, P., J. J. Palvimo and O. A. Jänne (1998). "CREB-binding protein in androgen receptor-mediated signaling." Proceedings of the National Academy of Sciences **95**(5): 2122-2127.
Abeshouse, A., J. Ahn, R. Akbani, A. Ally, S. Amin, C. D. Andry, M. Annala, A. Aprikian, J. Armenia and A. Arora (2015). "The molecular taxonomy of primary prostate cancer." Cell **163**(4): 1011-1025.
Adam, R. C. and E. Fuchs (2016). "The Yin and Yang of chromatin dynamics in stem cell fate selection." Trends in Genetics **32**(2): 89-100.
Adamo, P. and M. Ladomery (2016). "The oncogene ERG: a key factor in prostate cancer." Oncogene **35**(4): 403-414.
Adriaens, M. E., P. Prickaerts, M. Chan-Seng-Yue, T. van den Beucken, V. E. Dahlmans, L. M. Eijssen, T. Beck, B. G. Wouters, J. W. Voncken and C. T. Evelo (2016). "Quantitative analysis of ChIP-seq data uncovers dynamic and sustained H3K4me3 and H3K27me3 modulation in cancer cells under hypoxia." Epigenetics & chromatin **9**(1): 1-11.
Attardi, B. J., S. A. Hild and J. R. Reel (2006). "Dimethandrolone undecanoate: a new potent orally active androgen with progestational activity." Endocrinology **147**(6): 3016-3026.
Auchus, R. J. and N. Sharifi (2020). "Sex Hormones and Prostate Cancer." Annu Rev Med **71**: 33-45.
Augello, M. A., D. Liu, L. D. Deonarine, B. D. Robinson, D. Huang, S. Stelloo, M. Blattner, A. S. Doane, E. W. Wong and Y. Chen (2019). "CHD1 loss alters AR binding at lineage-specific enhancers and modulates distinct transcriptional programs to drive prostate tumorigenesis." Cancer Cell **35**(4): 603-617. e608.
Aus, G., D. Robinson, J. Rosell, G. Sandblom and E. Varenhorst (2005). "Survival in prostate carcinoma—Outcomes from a prospective, population-based cohort of 8887 men with up to 15 years of follow-up." Cancer **103**(5): 943-951.
Baek, S. H., K. A. Ohgi, C. A. Nelson, D. Welsbie, C. Chen, C. L. Sawyers, D. W. Rose and M. G. Rosenfeld (2006). "Ligand-specific allosteric regulation of coactivator functions of androgen receptor in prostate cancer cells." Proceedings of the National Academy of Sciences **103**(9): 3100-3105.
Bagshaw, M. A., I. D. Kaplan and R. C. Cox (1993). "Radiation therapy for localized disease." Cancer **71**(S3): 939-952.
Bander, N. H., D. Yao, H. Liu, Y. T. Chen, M. Steiner, W. Zuccaro and P. Moy (1997). "MHC class I and II expression in prostate carcinoma and modulation by interferon-alpha and-gamma." The Prostate **33**(4): 233-239.
Bannert, N., H. Hofmann, A. Block and O. Hohn (2018). "HERVs New Role in Cancer: From Accused Perpetrators to Cheerful Protectors." Front Microbiol **9**: 178.
Barbie, D. A., P. Tamayo, J. S. Boehm, S. Y. Kim, S. E. Moody, I. F. Dunn, A. C. Schinzel, P. Sandy, E. Meylan and C. Scholl (2009). "Systematic RNA interference reveals that oncogenic KRAS-driven cancers require TBK1." Nature **462**(7269): 108.
Barbieri, C. E., C. H. Bangma, A. Bjartell, J. W. Catto, Z. Culig, H. Grönberg, J. Luo, T. Visakorpi and M. A. Rubin (2013). "The mutational landscape of prostate cancer." European urology **64**(4): 567-576.
Beltran, H., R. Yelensky, G. M. Frampton, K. Park, S. R. Downing, T. Y. MacDonald, M. Jarosz, D. Lipson, S. T. Tagawa and D. M. Nanus (2013). "Targeted next-generation sequencing of advanced prostate cancer identifies potential therapeutic targets and disease heterogeneity." European urology **63**(5): 920-926.
Berger, R., P. G. Febbo, P. K. Majumder, J. J. Zhao, S. Mukherjee, S. Signoretti, K. T. Campbell, W. R. Sellers, T. M. Roberts and M. Loda (2004). "Androgen-induced differentiation and tumorigenicity of human prostate epithelial cells." Cancer research **64**(24): 8867-8875.

Bertelloni, S., G. I. Baroncelli, P. Garofalo and S. Cianfarani (2010). "Androgen therapy in hypogonadal adolescent males." Hormone research in paediatrics **74**(4): 292-296.
Bhasin, S., W. E. Taylor, R. Singh, J. Artaza, I. Sinha-Hikim, R. Jasuja, H. Choi and N. F. Gonzalez-Cadavid (2003). "The mechanisms of androgen effects on body composition: mesenchymal pluripotent cell as the target of androgen action." The Journals of Gerontology Series A: Biological Sciences and Medical Sciences **58**(12): M1103-M1110.
Bidwell, B. N., C. Y. Slaney, N. P. Withana, S. Forster, Y. Cao, S. Loi, D. Andrews, T. Mikeska, N. E. Mangan, S. A. Samarajiwa, N. A. de Weerd, J. Gould, P. Argani, A. Moller, M. J. Smyth, R. L. Anderson, P. J. Hertzog and B. S. Parker (2012). "Silencing of Irf7 pathways in breast cancer cells promotes bone metastasis through immune escape." Nat Med **18**(8): 1224-1231.
Bill-Axelson, A., L. Holmberg, M. Ruutu, M. Häggman, S.-O. Andersson, S. Bratell, A. Spångberg, C. Busch, S. Nordling and H. Garmo (2005). "Radical prostatectomy versus watchful waiting in early prostate cancer." New England journal of medicine **352**(19): 1977-1984.
Bishop, J. L., D. Thaper, S. Vahid, A. Davies, K. Ketola, H. Kuruma, R. Jama, K. M. Nip, A. Angeles, F. Johnson, A. W. Wyatt, L. Fazli, M. E. Gleave, D. Lin, M. A. Rubin, C. C. Collins, Y. Wang, H. Beltran and A. Zoubeidi (2017). "The Master Neural Transcription Factor BRN2 Is an Androgen Receptor-Suppressed Driver of Neuroendocrine Differentiation in Prostate Cancer." Cancer Discov **7**(1): 54-71.
Blais, A., C. J. van Oevelen, R. Margueron, D. Acosta-Alvear and B. D. Dynlacht (2007). "Retinoblastoma tumor suppressor protein–dependent methylation of histone H3 lysine 27 is associated with irreversible cell cycle exit." The Journal of cell biology **179**(7): 1399-1412.
Blanco, E., M. González-Ramírez, A. Alcaine-Colet, S. Aranda and L. Di Croce (2020). "The bivalent genome: characterization, structure, and regulation." Trends in Genetics **36**(2): 118-131.
Bolger, A. M., M. Lohse and B. Usadel (2014). "Trimmomatic: a flexible trimmer for Illumina sequence data." Bioinformatics **30**(15): 2114-2120.
Boshans, L. L., D. C. Factor, V. Singh, J. Liu, C. Zhao, I. Mandoiu, Q. R. Lu, P. Casaccia, P. J. Tesar and A. Nishiyama (2019). "The chromatin environment around interneuron genes in oligodendrocyte precursor cells and their potential for interneuron reprograming." Frontiers in neuroscience **13**: 829.
Bostwick, D. G. and L. Cheng (2008). Urologic surgical pathology, Elsevier Health Sciences.
Bracken, A. P., D. Pasini, M. Capra, E. Prosperini, E. Colli and K. Helin (2003). "EZH2 is downstream of the pRB-E2F pathway, essential for proliferation and amplified in cancer." The EMBO journal **22**(20): 5323-5335.
Bray, F., J. Ferlay, I. Soerjomataram, R. L. Siegel, L. A. Torre and A. Jemal (2018). "Global cancer statistics 2018: GLOBOCAN estimates of incidence and mortality worldwide for 36 cancers in 185 countries." CA: a cancer journal for clinicians **68**(6): 394-424.
Bronte, V., T. Kasic, G. Gri, K. Gallana, G. Borsellino, I. Marigo, L. Battistini, M. Iafrate, T. Prayer-Galetti and F. Pagano (2005). "Boosting antitumor responses of T lymphocytes infiltrating human prostate cancers." The Journal of experimental medicine **201**(8): 1257-1268.
Buchanan, G., M. Yang, A. Cheong, J. M. Harris, R. A. Irvine, P. F. Lambert, N. L. Moore, M. Raynor, P. J. Neufing and G. A. Coetzee (2004). "Structural and functional consequences of glutamine tract variation in the androgen receptor." Human molecular genetics **13**(16): 1677-1692.
Bui, A. T., M. E. Huang, M. Havard, F. Laurent-Tchenio, F. Dautry and T. Tchenio (2017). "Transient exposure to androgens induces a remarkable self-sustained quiescent state in dispersed prostate cancer cells." Cell Cycle **16**(9): 879-893.
Burr, M. L., C. E. Sparbier, K. L. Chan, Y.-C. Chan, A. Kersbergen, E. Y. Lam, E. Azidis-Yates, D. Vassiliadis, C. C. Bell and O. Gilan (2019). "An evolutionarily conserved function of polycomb silences the MHC Class I antigen presentation pathway and enables immune evasion in cancer." Cancer Cell **36**(4): 385-401. e388.

Cai, C., H. H. He, S. Chen, I. Coleman, H. Wang, Z. Fang, S. Chen, P. S. Nelson, X. S. Liu and M. Brown (2011). "Androgen receptor gene expression in prostate cancer is directly suppressed by the androgen receptor through recruitment of lysine-specific demethylase 1." Cancer cell **20**(4): 457-471.
Cai, C., X. Yuan and S. P. Balk (2013). "Androgen receptor epigenetics." Transl Androl Urol **2**(3): 148-157.
Carson, C. and R. Rittmaster (2003). "The role of dihydrotestosterone in benign prostatic hyperplasia." Urology **61**(4): 2-7.
Carver, B. S., J. Tran, Z. Chen, A. Carracedo-Perez, A. Alimonti, C. Nardella, A. Gopalan, P. T. Scardino, C. Cordon-Cardo and W. Gerald (2009). "ETS rearrangements and prostate cancer initiation." Nature **457**(7231): E1-E1.
Chan, S. C., L. A. Selth, Y. Li, M. D. Nyquist, L. Miao, J. E. Bradner, G. V. Raj, W. D. Tilley and S. M. Dehm (2015). "Targeting chromatin binding regulation of constitutively active AR variants to overcome prostate cancer resistance to endocrine-based therapies." Nucleic Acids Res.
Chandrasekar, T., J. C. Yang, A. C. Gao and C. P. Evans (2015). "Mechanisms of resistance in castration-resistant prostate cancer (CRPC)." Translational andrology and urology **4**(3): 365.
Chang, C.-Y. and D. P. McDonnell (2002). "Evaluation of ligand-dependent changes in AR structure using peptide probes." Molecular Endocrinology **16**(4): 647-660.
Chang, C.-y., J. D. Norris, H. Grøn, L. A. Paige, P. T. Hamilton, D. J. Kenan, D. Fowlkes and D. P. McDonnell (1999). "Dissection of the LXXLL nuclear receptor-coactivator interaction motif using combinatorial peptide libraries: discovery of peptide antagonists of estrogen receptors α and β." Molecular and cellular biology **19**(12): 8226-8239.
Chatterjee, P., M. T. Schweizer, J. M. Lucas, I. Coleman, M. D. Nyquist, S. B. Frank, R. Tharakan, E. Mostaghel, J. Luo and C. C. Pritchard (2019). "Supraphysiological androgens suppress prostate cancer growth through androgen receptor–mediated DNA damage." The Journal of clinical investigation **129**(10).
Chatterjee, P., M. T. Schweizer, J. M. Lucas, I. Coleman, M. D. Nyquist, S. B. Frank, R. Tharakan, E. Mostaghel, J. Luo and C. C. Pritchard (2019). "Supraphysiological androgens suppress prostate cancer growth through androgen receptor–mediated DNA damage." The Journal of clinical investigation **129**(10): 4245-4260.
Chatterjee, P., M. T. Schweizer, J. M. Lucas, I. Coleman, M. D. Nyquist, S. B. Frank, R. Tharakan, E. Mostaghel, J. Luo, C. C. Pritchard, H. M. Lam, E. Corey, E. S. Antonarakis, S. R. Denmeade and P. S. Nelson (2019). "Supraphysiological androgens suppress prostate cancer growth through androgen receptor-mediated DNA damage." J Clin Invest **129**(10): 4245-4260.
Chen, R., X. Dong and M. Gleave (2018). "Molecular model for neuroendocrine prostate cancer progression." BJU international **122**(4): 560-570.
Chen, S., S. Gulla, C. Cai and S. P. Balk (2012). "Androgen receptor serine 81 phosphorylation mediates chromatin binding and transcriptional activation." Journal of Biological Chemistry **287**(11): 8571-8583.
Chen, S., Y. Xu, X. Yuan, G. J. Bubley and S. P. Balk (2006). "Androgen receptor phosphorylation and stabilization in prostate cancer by cyclin-dependent kinase 1." Proceedings of the National Academy of Sciences **103**(43): 15969-15974.
Cheon, H., E. C. Borden and G. R. Stark (2014). Interferons and their stimulated genes in the tumor microenvironment. Seminars in oncology, Elsevier.
Chiappinelli, K. B., P. L. Strissel, A. Desrichard, H. Li, C. Henke, B. Akman, A. Hein, N. S. Rote, L. M. Cope, A. Snyder, V. Makarov, S. Budhu, D. J. Slamon, J. D. Wolchok, D. M. Pardoll, M. W. Beckmann, C. A. Zahnow, T. Merghoub, T. A. Chan, S. B. Baylin and R. Strick (2015). "Inhibiting DNA Methylation

Causes an Interferon Response in Cancer via dsRNA Including Endogenous Retroviruses." Cell **162**(5): 974-986.
Chiuve, S. E., L. A. Martin, H. Campos and F. M. Sacks (2004). "Effect of the combination of methyltestosterone and esterified estrogens compared with esterified estrogens alone on apolipoprotein CIII and other apolipoproteins in very low density, low density, and high density lipoproteins in surgically postmenopausal women." J Clin Endocrinol Metab **89**(5): 2207-2213.
Chouinard, S., O. Barbier and A. Bélanger (2007). "UDP-glucuronosyltransferase 2B15 (UGT2B15) and UGT2B17 enzymes are major determinants of the androgen response in prostate cancer LNCaP cells." Journal of Biological Chemistry **282**(46): 33466-33474.
Christiansen, A. R., L. I. Lipshultz, J. M. Hotaling and A. W. Pastuszak (2020). "Selective androgen receptor modulators: the future of androgen therapy?" Transl Androl Urol **9**(Suppl 2): S135-S148.
Chu, M., Y. Chang, P. Li, Y. Guo, K. Zhang and W. Gao (2014). "Androgen receptor is negatively correlated with the methylation-mediated transcriptional repression of miR-375 in human prostate cancer cells." Oncol Rep **31**(1): 34-40.
Cichocki, F., R. Bjordahl, S. Gaidarova, S. Mahmood, R. Abujarour, H. Wang, K. Tuininga, M. Felices, Z. B. Davis and L. Bendzick (2020). "iPSC-derived NK cells maintain high cytotoxicity and enhance in vivo tumor control in concert with T cells and anti–PD-1 therapy." Science Translational Medicine **12**(568).
Coleman, D. J., K. Van Hook, C. J. King, J. Schwartzman, R. Lisac, J. Urrutia, A. Sehrawat, J. Woodward, N. J. Wang and R. Gulati (2016). "Cellular androgen content influences enzalutamide agonism of F877L mutant androgen receptor." Oncotarget **7**(26): 40690.
Conway, J. R., A. Lex and N. Gehlenborg (2017). "UpSetR: an R package for the visualization of intersecting sets and their properties." Bioinformatics **33**(18): 2938-2940.
Corrales, L., V. Matson, B. Flood, S. Spranger and T. F. Gajewski (2017). "Innate immune signaling and regulation in cancer immunotherapy." Cell research **27**(1): 96-108.
Coutinho, I., T. K. Day, W. D. Tilley and L. A. Selth (2016). "Androgen receptor signaling in castration-resistant prostate cancer: a lesson in persistence." Endocr Relat Cancer **23**(12): T179-T197.
Coutinho, I., T. K. Day, W. D. Tilley and L. A. Selth (2016). "Androgen receptor signaling in castration-resistant prostate cancer: a lesson in persistence." Endocrine-related cancer **23**(12): T179-T197.
Crea, F., N. R. N. Saidy, C. C. Collins and Y. Wang (2015). "The epigenetic/noncoding origin of tumor dormancy." Trends in molecular medicine **21**(4): 206-211.
Criscione, S. W., Y. Zhang, W. Thompson, J. M. Sedivy and N. Neretti (2014). "Transcriptional landscape of repetitive elements in normal and cancer human cells." BMC Genomics **15**: 583.
D'Antonio, J. M., D. J. Vander Griend and J. T. Isaacs (2009). "DNA licensing as a novel androgen receptor mediated therapeutic target for prostate cancer." Endocr Relat Cancer **16**(2): 325-332.
D'Antonio, J. M., D. J. Vander Griend and J. T. Isaacs (2009). "DNA licensing as a novel androgen receptor mediated therapeutic target for prostate cancer." Endocrine-related cancer **16**(2): 325-332.
Das, R., P. A. Gregory, R. C. Fernandes, I. Denis, Q. Wang, S. L. Townley, S. G. Zhao, A. R. Hanson, M. A. Pickering, H. K. Armstrong, N. A. Lokman, E. Ebrahimie, E. Davicioni, R. B. Jenkins, R. J. Karnes, A. E. Ross, R. B. Den, E. A. Klein, K. N. Chi, H. S. Ramshaw, E. D. Williams, A. Zoubeidi, G. J. Goodall, F. Y. Feng, L. M. Butler, W. D. Tilley and L. A. Selth (2017). "MicroRNA-194 Promotes Prostate Cancer Metastasis by Inhibiting SOCS2." Cancer Res **77**(4): 1021-1034.
de Almeida, D. V. P., L. Fong, M. B. Rettig and K. A. Autio (2020). "Immune Checkpoint Blockade for Prostate Cancer: Niche Role or Next Breakthrough?" Am Soc Clin Oncol Educ Book **40**: 1-18.
De Bono, J. S., C. J. Logothetis, A. Molina, K. Fizazi, S. North, L. Chu, K. N. Chi, R. J. Jones, O. B. Goodman Jr and F. Saad (2011). "Abiraterone and increased survival in metastatic prostate cancer." New England Journal of Medicine **364**(21): 1995-2005.

De Launoit, Y., R. Veilleux, M. Dufour, J. Simard and F. Labrie (1991). "Characteristics of the biphasic action of androgens and of the potent antiproliferative effects of the new pure antiestrogen EM-139 on cell cycle kinetic parameters in LNCaP human prostatic cancer cells." Cancer research **51**(19): 5165-5170.
De Mol, E., E. Szulc, C. Di Sanza, P. Martínez-Cristóbal, C. W. Bertoncini, R. B. Fenwick, M. Frigolé-Vivas, M. Masín, I. Hunter and V. Buzón (2018). "Regulation of androgen receptor activity by transient interactions of its transactivation domain with general transcription regulators." Structure **26**(1): 145-152. e143.
Deblois, G., S. A. M. Tonekaboni, G. Grillo, C. Martinez, Y. I. Kao, F. Tai, I. Ettayebi, A.-M. Fortier, P. Savage and A. N. Fedor (2020). "Epigenetic switch–induced viral mimicry evasion in chemotherapy-resistant breast cancer." Cancer discovery **10**(9): 1312-1329.
Denmeade, S. R., H. Wang, N. Agarwal, D. C. Smith, M. T. Schweizer, M. N. Stein, V. Assikis, P. W. Twardowski, T. W. Flaig, R. Z. Szmulewitz, J. M. Holzbeierlein, R. J. Hauke, G. Sonpavde, J. A. Garcia, A. Hussain, O. Sartor, S. Mao, H. Cao, W. Fu, T. Wang, R. Abdallah, S. J. Lim, V. Bolejack, C. J. Paller, M. A. Carducci, M. C. Markowski, M. A. Eisenberger and E. S. Antonarakis (2021). "TRANSFORMER: A Randomized Phase II Study Comparing Bipolar Androgen Therapy Versus Enzalutamide in Asymptomatic Men With Castration-Resistant Metastatic Prostate Cancer." J Clin Oncol **39**(12): 1371-1382.
Dhatchinamoorthy, K., J. D. Colbert and K. L. Rock (2021). "Cancer Immune Evasion Through Loss of MHC Class I Antigen Presentation." Frontiers in Immunology **12**: 469.
Dhiman, V. K., K. Attwood, M. J. Campbell and D. J. Smiraglia (2015). "Hormone stimulation of androgen receptor mediates dynamic changes in DNA methylation patterns at regulatory elements." Oncotarget **6**(40): 42575.
Dobin, A., C. A. Davis, F. Schlesinger, J. Drenkow, C. Zaleski, S. Jha, P. Batut, M. Chaisson and T. R. Gingeras (2013). "STAR: ultrafast universal RNA-seq aligner." Bioinformatics **29**(1): 15-21.
Egevad, L., B. Delahunt, J. R. Srigley and H. Samaratunga (2016). International Society of Urological Pathology (ISUP) grading of prostate cancer–An ISUP consensus on contemporary grading, Wiley Online Library.
El-Desoky el, S. I., M. Reyad, E. M. Afsah and A. A. Dawidar (2016). "Synthesis and chemical reactions of the steroidal hormone 17alpha-methyltestosterone." Steroids **105**: 68-95.
Engeland, K. (2018). "Cell cycle arrest through indirect transcriptional repression by p53: I have a DREAM." Cell Death & Differentiation **25**(1): 114-132.
Ezhkova, E., H. A. Pasolli, J. S. Parker, N. Stokes, I.-h. Su, G. Hannon, A. Tarakhovsky and E. Fuchs (2009). "Ezh2 orchestrates gene expression for the stepwise differentiation of tissue-specific stem cells." Cell **136**(6): 1122-1135.
Ezponda, T. and J. D. Licht (2014). "Molecular pathways: Deregulation of histone H3 lysine 27 methylation in cancer—Different paths, same destination." Clinical Cancer Research **20**(19): 5001-5008.
Fang, H., W. Tong, W. S. Branham, C. L. Moland, S. L. Dial, H. Hong, Q. Xie, R. Perkins, W. Owens and D. M. Sheehan (2003). "Study of 202 natural, synthetic, and environmental chemicals for binding to the androgen receptor." Chemical research in toxicology **16**(10): 1338-1358.
Fang, H., W. Tong, W. S. Branham, C. L. Moland, S. L. Dial, H. Hong, Q. Xie, R. Perkins, W. Owens and D. M. Sheehan (2003). "Study of 202 natural, synthetic, and environmental chemicals for binding to the androgen receptor." Chem Res Toxicol **16**(10): 1338-1358.
Feng, J., T. Liu, B. Qin, Y. Zhang and X. S. Liu (2012). "Identifying ChIP-seq enrichment using MACS." Nature protocols **7**(9): 1728-1740.

Feng, Q. and B. He (2019). "Androgen receptor signaling in the development of castration-resistant prostate cancer." Frontiers in Oncology **9**: 858.
Ferrari, K. J., A. Scelfo, S. Jammula, A. Cuomo, I. Barozzi, A. Stützer, W. Fischle, T. Bonaldi and D. Pasini (2014). "Polycomb-dependent H3K27me1 and H3K27me2 regulate active transcription and enhancer fidelity." Molecular cell **53**(1): 49-62.
Fizazi, K., C. Massard, M. Smith, M. Rader, J. Brown, P. Milecki, N. Shore, S. Oudard, L. Karsh and M. Carducci (2015). "Bone-related parameters are the main prognostic factors for overall survival in men with bone metastases from castration-resistant prostate cancer." European urology **68**(1): 42-50.
Fonseca, G. W. P. d., E. Dworatzek, N. Ebner and S. von Haehling (2020). "Selective androgen receptor modulators (SARMs) as pharmacological treatment for muscle wasting in ongoing clinical trials." Expert Opinion on Investigational Drugs.
Fragkaki, A., Y. Angelis, M. Koupparis, A. Tsantili-Kakoulidou, G. Kokotos and C. Georgakopoulos (2009). "Structural characteristics of anabolic androgenic steroids contributing to binding to the androgen receptor and to their anabolic and androgenic activities: applied modifications in the steroidal structure." Steroids **74**(2): 172-197.
Fu, K., G. Bonora and M. Pellegrini (2020). "Interactions between core histone marks and DNA methyltransferases predict DNA methylation patterns observed in human cells and tissues." Epigenetics **15**(3): 272-282.
Galon, J. and D. Bruni (2019). "Approaches to treat immune hot, altered and cold tumours with combination immunotherapies." Nature reviews Drug discovery **18**(3): 197-218.
Galvao, D. A., K. Nosaka, D. R. Taaffe, N. Spry, L. J. Kristjanson, M. R. McGuigan, K. Suzuki, K. Yamaya and R. U. Newton (2006). "Resistance training and reduction of treatment side effects in prostate cancer patients." Medicine & Science in Sports & Exercise **38**(12): 2045-2052.
Gao, J., B. A. Aksoy, U. Dogrusoz, G. Dresdner, B. Gross, S. O. Sumer, Y. Sun, A. Jacobsen, R. Sinha, E. Larsson, E. Cerami, C. Sander and N. Schultz (2013). "Integrative analysis of complex cancer genomics and clinical profiles using the cBioPortal." Sci Signal **6**(269): pl1.
Gao, L. and J. Alumkal (2010). "Epigenetic regulation of androgen receptor signaling in prostate cancer." Epigenetics **5**(2): 100-104.
Gao, S., Y. Gao, H. H. He, D. Han, W. Han, A. Avery, J. A. Macoska, X. Liu, S. Chen and F. Ma (2016). "Androgen receptor tumor suppressor function is mediated by recruitment of retinoblastoma protein." Cell reports **17**(4): 966-976.
Gao, S., Y. Gao, H. H. He, D. Han, W. Han, A. Avery, J. A. Macoska, X. Liu, S. Chen, F. Ma, S. Chen, S. P. Balk and C. Cai (2016). "Androgen Receptor Tumor Suppressor Function Is Mediated by Recruitment of Retinoblastoma Protein." Cell Rep **17**(4): 966-976.
Gao, W., J. Kim and J. T. Dalton (2006). "Pharmacokinetics and pharmacodynamics of nonsteroidal androgen receptor ligands." Pharmaceutical research **23**(8): 1641-1658.
Gelmann, E. P., C. L. Sawyers and F. J. Rauscher III (2013). Molecular oncology: causes of cancer and targets for treatment, Cambridge University Press.
Goel, S., M. J. DeCristo, A. C. Watt, H. BrinJones, J. Sceneay, B. B. Li, N. Khan, J. M. Ubellacker, S. Xie and O. Metzger-Filho (2017). "CDK4/6 inhibition triggers anti-tumour immunity." Nature **548**(7668): 471-475.
Gonzalez-Cao, M., N. Karachaliou, M. Santarpia, S. Viteri, A. Meyerhans and R. Rosell (2018). "Activation of viral defense signaling in cancer." Ther Adv Med Oncol **10**: 1758835918793105.
Graff, J. N., J. J. Alumkal, C. G. Drake, G. V. Thomas, W. L. Redmond, M. Farhad, J. P. Cetnar, F. S. Ey, R. C. Bergan, R. Slottke and T. M. Beer (2016). "Early evidence of anti-PD-1 activity in enzalutamide-resistant prostate cancer." Oncotarget **7**(33): 52810-52817.

Granger, J. E. and D. M. Appledorn (2021). Kinetic Measurement of Apoptosis and Immune Cell Killing Using Live-Cell Imaging and Analysis. Detection of Cell Death Mechanisms, Springer**:** 197-212.
Grigore, A. D., E. Ben-Jacob and M. C. Farach-Carson (2015). "Prostate cancer and neuroendocrine differentiation: more neuronal, less endocrine?" Frontiers in oncology **5**: 37.
Gu, Z., K. Jin, M. J. C. Crabbe, Y. Zhang, X. Liu, Y. Huang, M. Hua, P. Nan, Z. Zhang and Y. Zhong (2016). "Enrichment analysis of Alu elements with different spatial chromatin proximity in the human genome." Protein & cell **7**(4): 250-266.
Haffner, M. C., A. M. De Marzo, A. K. Meeker, W. G. Nelson and S. Yegnasubramanian (2011). "Transcription-induced DNA double strand breaks: both oncogenic force and potential therapeutic target?" Clin Cancer Res **17**(12): 3858-3864.
Haffner, M. C., A. M. De Marzo, A. K. Meeker, W. G. Nelson and S. Yegnasubramanian (2011). "Transcription-induced DNA double strand breaks: both oncogenic force and potential therapeutic target?" Clinical Cancer Research **17**(12): 3858-3864.
Hamdy, F. C., J. L. Donovan, J. Lane, M. Mason, C. Metcalfe, P. Holding, M. Davis, T. J. Peters, E. L. Turner and R. M. Martin (2016). "10-year outcomes after monitoring, surgery, or radiotherapy for localized prostate cancer." N Engl J Med **375**: 1415-1424.
Handle, F., S. Prekovic, C. Helsen, T. Van den Broeck, E. Smeets, L. Moris, R. Eerlings, S. El Kharraz, A. Urbanucci and I. G. Mills (2019). "Drivers of AR indifferent anti-androgen resistance in prostate cancer cells." Scientific reports **9**(1): 1-11.
Harwood, D. T. and D. J. Handelsman (2009). "Development and validation of a sensitive liquid chromatography–tandem mass spectrometry assay to simultaneously measure androgens and estrogens in serum without derivatization." Clinica Chimica Acta **409**(1-2): 78-84.
Hawkins, R. D., G. C. Hon, L. K. Lee, Q. Ngo, R. Lister, M. Pelizzola, L. E. Edsall, S. Kuan, Y. Luu and S. Klugman (2010). "Distinct epigenomic landscapes of pluripotent and lineage-committed human cells." Cell stem cell **6**(5): 479-491.
Haymart, M. R., D. C. Miller and S. T. Hawley (2017). "Active Surveillance for Low-Risk Cancers-A Viable Solution to Overtreatment?" The New England journal of medicine **377**(3): 203.
He, B., J. A. Kemppainen and E. M. Wilson (2000). "FXXLF and WXXLF sequences mediate the NH2-terminal interaction with the ligand binding domain of the androgen receptor." Journal of Biological Chemistry **275**(30): 22986-22994.
Hedayati, M., M. C. Haffner, J. B. Coulter, R. R. Raval, Y. Zhang, H. Zhou, O. Mian, E. J. Knight, N. Razavi and S. Dalrymple (2016). "Androgen deprivation followed by acute androgen stimulation selectively sensitizes AR-positive prostate cancer cells to ionizing radiation." Clinical Cancer Research **22**(13): 3310-3319.
Heemers, H. V. and D. J. Tindall (2007). "Androgen receptor (AR) coregulators: a diversity of functions converging on and regulating the AR transcriptional complex." Endocrine reviews **28**(7): 778-808.
Heinlein, C. A. and C. Chang (2002). "Androgen receptor (AR) coregulators: an overview." Endocrine reviews **23**(2): 175-200.
Heinlein, C. A. and C. Chang (2004). "Androgen receptor in prostate cancer." Endocrine reviews **25**(2): 276-308.
Heinz, S., C. Benner, N. Spann, E. Bertolino, Y. C. Lin, P. Laslo, J. X. Cheng, C. Murre, H. Singh and C. K. Glass (2010). "Simple combinations of lineage-determining transcription factors prime cis-regulatory elements required for macrophage and B cell identities." Mol Cell **38**(4): 576-589.
Heinz, S., C. Benner, N. Spann, E. Bertolino, Y. C. Lin, P. Laslo, J. X. Cheng, C. Murre, H. Singh and C. K. Glass (2010). "Simple combinations of lineage-determining transcription factors prime cis-regulatory elements required for macrophage and B cell identities." Molecular cell **38**(4): 576-589.

Heise, K., H. Oppermann, J. Meixensberger, R. Gebhardt and F. Gaunitz (2013). "Dual luciferase assay for secreted luciferases based on Gaussia and NanoLuc." Assay and drug development technologies **11**(4): 244-252.
Henderson, L., C. Penatti, B. Jones, P. Yang and A. Clark (2006). "Anabolic androgenic steroids and forebrain GABAergic transmission." Neuroscience **138**(3): 793-799.
Hoskin, P., O. Sartor, J. M. O'Sullivan, D. C. Johannessen, S. I. Helle, J. Logue, D. Bottomley, S. Nilsson, N. J. Vogelzang and F. Fang (2014). "Efficacy and safety of radium-223 dichloride in patients with castration-resistant prostate cancer and symptomatic bone metastases, with or without previous docetaxel use: a prespecified subgroup analysis from the randomised, double-blind, phase 3 ALSYMPCA trial." The Lancet Oncology **15**(12): 1397-1406.
Houghton, P., R. Fang, I. Techatanawat, G. Steventon, P. J. Hylands and C. C. Lee (2007). "The sulphorhodamine (SRB) assay and other approaches to testing plant extracts and derived compounds for activities related to reputed anticancer activity." Methods **42**(4): 377-387.
Hsu, F.-N., M.-C. Chen, M.-C. Chiang, E. Lin, Y.-T. Lee, P.-H. Huang, G.-S. Lee and H. Lin (2011). "Regulation of androgen receptor and prostate cancer growth by cyclin-dependent kinase 5." Journal of Biological Chemistry **286**(38): 33141-33149.
Hudson, D. (2004). "Epithelial stem cells in human prostate growth and disease." Prostate cancer and prostatic diseases **7**(3): 188-194.
Huggins, C. (1965). "Two principles in endocrine therapy of cancers: hormone deprival and hormone interference." Cancer Res **25**(7): 1163-1167.
Hur, J. and E. Giovannucci (2020). "Racial differences in prostate cancer: does timing of puberty play a role?" British Journal of Cancer **123**(3): 349-354.
Imamura, Y. and M. D. Sadar (2016). "Androgen receptor targeted therapies in castration-resistant prostate cancer: bench to clinic." International Journal of Urology **23**(8): 654-665.
Isaacs, J. T. and W. B. Isaacs (2004). "Androgen receptor outwits prostate cancer drugs." Nature medicine **10**(1): 26-27.
Ishak, C. A., A. E. Marshall, D. T. Passos, C. R. White, S. J. Kim, M. J. Cecchini, S. Ferwati, W. A. MacDonald, C. J. Howlett and I. D. Welch (2016). "An RB-EZH2 complex mediates silencing of repetitive DNA sequences." Molecular cell **64**(6): 1074-1087.
Ishiguro, K., H. Kitajima, T. Niinuma, R. Maruyama, N. Nishiyama, H. Ohtani, G. Sudo, M. Toyota, H. Sasaki and E. Yamamoto (2021). "Dual EZH2 and G9a inhibition suppresses multiple myeloma cell proliferation by regulating the interferon signal and IRF4-MYC axis." Cell death discovery **7**(1): 1-13.
Jaaskelainen, J., A. Deeb, J. Schwabe, N. Mongan, H. Martin and I. Hughes (2006). "Human androgen receptor gene ligand-binding-domain mutations leading to disrupted interaction between the N-and C-terminal domains." Journal of molecular endocrinology **36**(2): 361-368.
Janin, M. and M. Esteller (2020). "Epigenetic Awakening of Viral Mimicry in Cancer." Cancer Discovery **10**(9): 1258-1260.
Jenster, G., H. A. van der Korput, J. Trapman and A. O. Brinkmann (1995). "Identification of two transcription activation units in the N-terminal domain of the human androgen receptor." Journal of Biological Chemistry **270**(13): 7341-7346.
Jernberg, E., A. Bergh and P. Wikström (2017). "Clinical relevance of androgen receptor alterations in prostate cancer." Endocrine connections **6**(8): R146-R161.
Ji, H., H. Jiang, W. Ma, D. S. Johnson, R. M. Myers and W. H. Wong (2008). "An integrated software system for analyzing ChIP-chip and ChIP-seq data." Nature biotechnology **26**(11): 1293-1300.
Jia, L., J. Kim, H. Shen, P. E. Clark, W. D. Tilley and G. A. Coetzee (2003). "Androgen receptor activity at the prostate specific antigen locus: steroidal and non-steroidal mechanisms." Mol Cancer Res **1**(5): 385-392.

Jiao, L., M. Shubbar, X. Yang, Q. Zhang, S. Chen, Q. Wu, Z. Chen, J. Rizo and X. Liu (2020). "A partially disordered region connects gene repression and activation functions of EZH2." Proceedings of the National Academy of Sciences **117**(29): 16992-17002.
Jin, F. and J. D. Fondell (2009). "A novel androgen receptor-binding element modulates Cdc6 transcription in prostate cancer cells during cell-cycle progression." Nucleic acids research **37**(14): 4826-4838.
Joly-Pharaboz, M.-O., M.-C. Soave, B. Nicolas, F. Mebarki, M. Renaud, O. Foury, Y. Morel and J. G. Andre (1995). "Androgens inhibit the proliferation of a variant of the human prostate cancer cell line LNCaP." The Journal of Steroid Biochemistry and Molecular Biology **55**(1): 67-76.
Jorgovanovic, D., M. Song, L. Wang and Y. Zhang (2020). "Roles of IFN-γ in tumor progression and regression: a review." Biomarker Research **8**(1): 1-16.
Ju, B.-G., V. V. Lunyak, V. Perissi, I. Garcia-Bassets, D. W. Rose, C. K. Glass and M. G. Rosenfeld (2006). "A topoisomerase IIß-mediated dsDNA break required for regulated transcription." science **312**(5781): 1798-1802.
Juan, A. H., S. Wang, K. D. Ko, H. Zare, P.-F. Tsai, X. Feng, K. O. Vivanco, A. M. Ascoli, G. Gutierrez-Cruz and J. Krebs (2016). "Roles of H3K27me2 and H3K27me3 examined during fate specification of embryonic stem cells." Cell reports **17**(5): 1369-1382.
Kallio, H. M., R. Hieta, L. Latonen, A. Brofeldt, M. Annala, K. Kivinummi, T. L. Tammela, M. Nykter, W. B. Isaacs and H. G. Lilja (2018). "Constitutively active androgen receptor splice variants AR-V3, AR-V7 and AR-V9 are co-expressed in castration-resistant prostate cancer metastases." British journal of cancer **119**(3): 347-356.
Kamminga, L. M., L. V. Bystrykh, A. de Boer, S. Houwer, J. Douma, E. Weersing, B. Dontje and G. de Haan (2006). "The Polycomb group gene Ezh2 prevents hematopoietic stem cell exhaustion." Blood **107**(5): 2170-2179.
Kantoff, P. W., C. S. Higano, N. D. Shore, E. R. Berger, E. J. Small, D. F. Penson, C. H. Redfern, A. C. Ferrari, R. Dreicer, R. B. Sims, Y. Xu, M. W. Frohlich, P. F. Schellhammer and I. S. Investigators (2010). "Sipuleucel-T immunotherapy for castration-resistant prostate cancer." N Engl J Med **363**(5): 411-422.
Kareta, M. S., L. L. Gorges, S. Hafeez, B. A. Benayoun, S. Marro, A.-F. Zmoos, M. J. Cecchini, D. Spacek, L. F. Batista and M. O'Brien (2015). "Inhibition of pluripotency networks by the Rb tumor suppressor restricts reprogramming and tumorigenesis." Cell stem cell **16**(1): 39-50.
Karolchik, D., A. S. Hinrichs, T. S. Furey, K. M. Roskin, C. W. Sugnet, D. Haussler and W. J. Kent (2004). "The UCSC Table Browser data retrieval tool." Nucleic acids research **32**(suppl_1): D493-D496.
Khan, A. and A. Mathelier (2017). "Intervene: a tool for intersection and visualization of multiple gene or genomic region sets." BMC bioinformatics **18**(1): 1-8.
Khorasanizadeh, S. and F. Rastinejad (2001). "Nuclear-receptor interactions on DNA-response elements." Trends in biochemical sciences **26**(6): 384-390.
Kim, J., Y. Lee, X. Lu, B. Song, K.-W. Fong, Q. Cao, J. D. Licht, J. C. Zhao and J. Yu (2018). "Polycomb- and methylation-independent roles of EZH2 as a transcription activator." Cell reports **25**(10): 2808-2820. e2804.
Kim, T. Y., S. Zhong, C. R. Fields, J. H. Kim and K. D. Robertson (2006). "Epigenomic profiling reveals novel and frequent targets of aberrant DNA methylation-mediated silencing in malignant glioma." Cancer Res **66**(15): 7490-7501.
Kimura, H., T. Nakamura, T. Ogawa, S. Tanaka and K. Shiota (2003). "Transcription of mouse DNA methyltransferase 1 (Dnmt1) is regulated by both E2F-Rb-HDAC-dependent and -independent pathways." Nucleic Acids Res **31**(12): 3101-3113.

Kimura, T. and S. Egawa (2018). "Epidemiology of prostate cancer in Asian countries." International journal of urology **25**(6): 524-531.
Kloosterman, W. P., M. Tavakoli-Yaraki, M. J. Van Roosmalen, E. Van Binsbergen, I. Renkens, K. Duran, L. Ballarati, S. Vergult, D. Giardino and K. Hansson (2012). "Constitutional chromothripsis rearrangements involve clustered double-stranded DNA breaks and nonhomologous repair mechanisms." Cell reports **1**(6): 648-655.
Kokontis, J. M., N. Hay and S. Liao (1998). "Progression of LNCaP prostate tumor cells during androgen deprivation: hormone-independent growth, repression of proliferation by androgen, and role for p27Kip1 in androgen-induced cell cycle arrest." Mol Endocrinol **12**(7): 941-953.
Komiya, A., K. Yasuda, A. Watanabe, Y. Fujiuchi, T. Tsuzuki and H. Fuse (2013). "The prognostic significance of loss of the androgen receptor and neuroendocrine differentiation in prostate biopsy specimens among castration-resistant prostate cancer patients." Molecular and clinical oncology **1**(2): 257-262.
Korenchuk, S., J. Lehr, L. MClean, Y. Lee, S. Whitney, R. Vessella, D. Lin and K. Pienta (2001). "VCaP, a cell-based model system of human prostate cancer." In vivo (Athens, Greece) **15**(2): 163-168.
Korpal, M., J. M. Korn, X. Gao, D. P. Rakiec, D. A. Ruddy, S. Doshi, J. Yuan, S. G. Kovats, S. Kim and V. G. Cooke (2013). "An F876L mutation in androgen receptor confers genetic and phenotypic resistance to MDV3100 (enzalutamide)." Cancer discovery **3**(9): 1030-1043.
Koryakina, Y., K. E. Knudsen and D. Gioeli (2015). "Cell-cycle-dependent regulation of androgen receptor function." Endocrine-related cancer **22**(2): 249-264.
Kotredes, K. P. and A. M. Gamero (2013). "Interferons as inducers of apoptosis in malignant cells." J Interferon Cytokine Res **33**(4): 162-170.
Krug, B., N. De Jay, A. S. Harutyunyan, S. Deshmukh, D. M. Marchione, P. Guilhamon, K. C. Bertrand, L. G. Mikael, M. K. McConechy, C. C. L. Chen, S. Khazaei, R. F. Koncar, S. Agnihotri, D. Faury, B. Ellezam, A. G. Weil, J. Ursini-Siegel, D. D. De Carvalho, P. B. Dirks, P. W. Lewis, P. Salomoni, M. Lupien, C. Arrowsmith, P. F. Lasko, B. A. Garcia, C. L. Kleinman, N. Jabado and S. C. Mack (2019). "Pervasive H3K27 Acetylation Leads to ERV Expression and a Therapeutic Vulnerability in H3K27M Gliomas." Cancer Cell **35**(5): 782-797 e788.
Kumar-Sinha, C., S. A. Tomlins and A. M. Chinnaiyan (2008). "Recurrent gene fusions in prostate cancer." Nature Reviews Cancer **8**(7): 497-511.
Kumar, R., R. Betney, J. Li, E. B. Thompson and I. J. McEwan (2004). "Induced α-helix structure in AF1 of the androgen receptor upon binding transcription factor TFIIF." Biochemistry **43**(11): 3008-3013.
Kuuranne, T., M. Kurkela, M. Thevis, W. Schanzer, M. Finel and R. Kostiainen (2003). "Glucuronidation of anabolic androgenic steroids by recombinant human UDP-glucuronosyltransferases." Drug Metab Dispos **31**(9): 1117-1124.
Kuuranne, T., M. Kurkela, M. Thevis, W. Schänzer, M. Finel and R. Kostiainen (2003). "Glucuronidation of anabolic androgenic steroids by recombinant human UDP-glucuronosyltransferases." Drug metabolism and disposition **31**(9): 1117-1124.
Lallous, N., K. Dalal, A. Cherkasov and P. S. Rennie (2013). "Targeting alternative sites on the androgen receptor to treat castration-resistant prostate cancer." International journal of molecular sciences **14**(6): 12496-12519.
Lam, H.-M., H. M. Nguyen, M. P. Labrecque, L. G. Brown, I. M. Coleman, R. Gulati, B. Lakely, D. Sondheim, P. Chatterjee and B. T. Marck (2020). "Durable response of enzalutamide-resistant prostate cancer to supraphysiological testosterone is associated with a multifaceted growth suppression and impaired DNA damage response transcriptomic program in patient-derived xenografts." European urology **77**(2): 144-155.

Lam, H. M., H. M. Nguyen, M. P. Labrecque, L. G. Brown, I. M. Coleman, R. Gulati, B. Lakely, D. Sondheim, P. Chatterjee, B. T. Marck, A. M. Matsumoto, E. A. Mostaghel, M. T. Schweizer, P. S. Nelson and E. Corey (2020). "Durable Response of Enzalutamide-resistant Prostate Cancer to Supraphysiological Testosterone Is Associated with a Multifaceted Growth Suppression and Impaired DNA Damage Response Transcriptomic Program in Patient-derived Xenografts." Eur Urol **77**(2): 144-155.
Lang, S., F. Frame and A. Collins (2009). "Prostate cancer stem cells." The Journal of Pathology: A Journal of the Pathological Society of Great Britain and Ireland **217**(2): 299-306.
Langeler, E. G., C. J. van Uffelen, M. A. Blankenstein, G. J. van Steenbrugge and E. Mulder (1993). "Effect of culture conditions on androgen sensitivity of the human prostatic cancer cell line LNCaP." Prostate **23**(3): 213-223.
Langmead, B., C. Trapnell, M. Pop and S. L. Salzberg (2009). "Ultrafast and memory-efficient alignment of short DNA sequences to the human genome." Genome biology **10**(3): 1-10.
Lanzuolo, C., F. L. Sardo, A. Diamantini and V. Orlando (2011). "PcG complexes set the stage for epigenetic inheritance of gene silencing in early S phase before replication." PLoS Genet **7**(11): e1002370.
Lavery, D. N. and I. J. McEwan (2008). "Structural characterization of the native NH2-terminal transactivation domain of the human androgen receptor: a collapsed disordered conformation underlies structural plasticity and protein-induced folding." Biochemistry **47**(11): 3360-3369.
Lee, D. K. and C. Chang (2003). "Expression and degradation of androgen receptor: mechanism and clinical implication." The Journal of Clinical Endocrinology & Metabolism **88**(9): 4043-4054.
Leung, J., G. Ehmann, P. Giangrande and J. Nevins (2008). "A role for Myc in facilitating transcription activation by E2F1." Oncogene **27**(30): 4172-4179.
Li, C., P. Jiang, S. Wei, X. Xu and J. Wang (2020). "Regulatory T cells in tumor microenvironment: new mechanisms, potential therapeutic strategies and future prospects." Molecular cancer **19**(1): 1-23.
Li, F., Q. Yuan, W. Di, X. Xia, Z. Liu, N. Mao, L. Li, C. Li, J. He and Y. Li (2020). "ERG orchestrates chromatin interactions to drive prostate cell fate reprogramming." The Journal of Clinical Investigation **130**(11).
Li, H., B. Handsaker, A. Wysoker, T. Fennell, J. Ruan, N. Homer, G. Marth, G. Abecasis and R. Durbin (2009). "The sequence alignment/map format and SAMtools." Bioinformatics **25**(16): 2078-2079.
Li, Y., S. C. Chan, L. J. Brand, T. H. Hwang, K. A. Silverstein and S. M. Dehm (2013). "Androgen receptor splice variants mediate enzalutamide resistance in castration-resistant prostate cancer cell lines." Cancer research **73**(2): 483-489.
Liao, S., T. Liang, S. Fang, E. Castañeda and T.-C. Shao (1973). "Steroid structure and androgenic activity: specificities involved in the receptor binding and nuclear retention of various androgens." Journal of Biological Chemistry **248**(17): 6154-6162.
Liao, Y., C.-H. Chen, N. Shah, T. Xiao, A. Feit, M. Yang, C. Cai, S. Gao, P. Xue and Z. Liu (2020). "A non-canonical EZH2 function sensitizes solid tumors to genotoxic stress." bioRxiv.
Liao, Y., G. K. Smyth and W. Shi (2014). "featureCounts: an efficient general purpose program for assigning sequence reads to genomic features." Bioinformatics **30**(7): 923-930.
Liberzon, A., C. Birger, H. Thorvaldsdottir, M. Ghandi, J. P. Mesirov and P. Tamayo (2015). "The Molecular Signatures Database (MSigDB) hallmark gene set collection." Cell Syst **1**(6): 417-425.
Lin, C., L. Yang, B. Tanasa, K. Hutt, B.-g. Ju, K. A. Ohgi, J. Zhang, D. W. Rose, X.-D. Fu and C. K. Glass (2009). "Nuclear receptor-induced chromosomal proximity and DNA breaks underlie specific translocations in cancer." Cell **139**(6): 1069-1083.

Litvinov, I. V., D. J. Vander Griend, L. Antony, S. Dalrymple, A. M. De Marzo, C. G. Drake and J. T. Isaacs (2006). "Androgen receptor as a licensing factor for DNA replication in androgen-sensitive prostate cancer cells." Proceedings of the National Academy of Sciences **103**(41): 15085-15090.
Liu, M., H. Ohtani, W. Zhou, A. D. Ørskov, J. Charlet, Y. W. Zhang, H. Shen, S. B. Baylin, G. Liang and K. Grønbæk (2016). "Vitamin C increases viral mimicry induced by 5-aza-2'-deoxycytidine." Proceedings of the National Academy of Sciences **113**(37): 10238-10244.
Liu, M., S. L. Thomas, A. K. DeWitt, W. Zhou, Z. B. Madaj, H. Ohtani, S. B. Baylin, G. Liang and P. A. Jones (2018). "Dual inhibition of DNA and histone methyltransferases increases viral mimicry in ovarian cancer cells." Cancer research **78**(20): 5754-5766.
Liu, P., T. Kao and H. Huang (2008). "CDK1 promotes cell proliferation and survival via phosphorylation and inhibition of FOXO1 transcription factor." Oncogene **27**(34): 4733-4744.
Liu, S., S. Kumari, Q. Hu, D. Senapati, V. B. Venkadakrishnan, D. Wang, A. D. DePriest, S. E. Schlanger, S. Ben-Salem, M. M. Valenzuela, B. Willard, S. Mudambi, W. M. Swetzig, G. M. Das, M. Shourideh, S. Koochekpour, S. M. Falzarano, C. Magi-Galluzzi, N. Yadav, X. Chen, C. Lao, J. Wang, J. N. Billaud and H. V. Heemers (2017). "A comprehensive analysis of coregulator recruitment, androgen receptor function and gene expression in prostate cancer." Elife **6**.
Liu, T., J. A. Ortiz, L. Taing, C. A. Meyer, B. Lee, Y. Zhang, H. Shin, S. S. Wong, J. Ma and Y. Lei (2011). "Cistrome: an integrative platform for transcriptional regulation studies." Genome biology **12**(8): 1-10.
Liu, W., C. C. Xie, Y. Zhu, T. Li, J. Sun, Y. Cheng, C. M. Ewing, S. Dalrymple, A. R. Turner and J. Sun (2008). "Homozygous deletions and recurrent amplifications implicate new genes involved in prostate cancer." Neoplasia **10**(8): 897-IN837.
Liu, X., Y. Gao, H. Ye, S. Gerrin, F. Ma, Y. Wu, T. Zhang, J. Russo, C. Cai and X. Yuan (2017). "Positive feedback loop mediated by protein phosphatase 1α mobilization of P-TEFb and basal CDK1 drives androgen receptor in prostate cancer." Nucleic acids research **45**(7): 3738-3751.
Loeb, S., M. A. Bjurlin, J. Nicholson, T. L. Tammela, D. F. Penson, H. B. Carter, P. Carroll and R. Etzioni (2014). "Overdiagnosis and overtreatment of prostate cancer." European urology **65**(6): 1046-1055.
Lorente, D., J. Mateo, Z. Zafeiriou, A. D. Smith, S. Sandhu, R. Ferraldeschi and J. S. De Bono (2015). "Switching and withdrawing hormonal agents for castration-resistant prostate cancer." Nature Reviews Urology **12**(1): 37-47.
Love, M. I., W. Huber and S. Anders (2014). "Moderated estimation of fold change and dispersion for RNA-seq data with DESeq2." Genome biology **15**(12): 1-21.
Loyola, A., T. Bonaldi, D. Roche, A. Imhof and G. Almouzni (2006). "PTMs on H3 variants before chromatin assembly potentiate their final epigenetic state." Molecular cell **24**(2): 309-316.
Lu, C., D. Rong, B. Zhang, W. Zheng, X. Wang, Z. Chen and W. Tang (2019). "Current perspectives on the immunosuppressive tumor microenvironment in hepatocellular carcinoma: challenges and opportunities." Molecular cancer **18**(1): 1-12.
Lun, A. T., Y. Chen and G. K. Smyth (2016). It's DE-licious: a recipe for differential expression analyses of RNA-seq experiments using quasi-likelihood methods in edgeR. Statistical genomics, Springer**:** 391-416.
Marcias, G., E. Erdmann, G. Lapouge, C. Siebert, P. Barthélémy, B. Duclos, J. P. Bergerat, J. Céraline and J. E. Kurtz (2010). "Identification of novel truncated androgen receptor (AR) mutants including unreported pre-mRNA splicing variants in the 22Rv1 hormone-refractory prostate cancer (PCa) cell line." Human mutation **31**(1): 74-80.
Markowski, M. C., E. Shenderov, M. A. Eisenberger, S. Kachhap, D. M. Pardoll, S. R. Denmeade and E. S. Antonarakis (2020). "Extreme responses to immune checkpoint blockade following bipolar

androgen therapy and enzalutamide in patients with metastatic castration resistant prostate cancer." Prostate **80**(5): 407-411.
Markowski, M. C., E. Shenderov, M. A. Eisenberger, S. Kachhap, D. M. Pardoll, S. R. Denmeade and E. S. Antonarakis (2020). "Extreme responses to immune checkpoint blockade following bipolar androgen therapy and enzalutamide in patients with metastatic castration resistant prostate cancer." The Prostate **80**(5): 407-411.
Markowski, M. C., H. Wang, R. Sullivan, I. Rifkind, V. Sinibaldi, M. T. Schweizer, B. A. Teply, N. Ngomba, W. Fu, M. A. Carducci, C. J. Paller, C. H. Marshall, M. A. Eisenberger, J. Luo, E. S. Antonarakis and S. R. Denmeade (2021). "A Multicohort Open-label Phase II Trial of Bipolar Androgen Therapy in Men with Metastatic Castration-resistant Prostate Cancer (RESTORE): A Comparison of Post-abiraterone Versus Post-enzalutamide Cohorts." Eur Urol **79**(5): 692-699.
Martin, M. (2011). "Cutadapt removes adapter sequences from high-throughput sequencing reads." EMBnet. journal **17**(1): 10-12.
Martini, M., M. G. Testi, M. Pasetto, M. C. Picchio, G. Innamorati, M. Mazzocco, S. Ugel, S. Cingarlini, V. Bronte and P. Zanovello (2010). "IFN-γ-mediated upmodulation of MHC class I expression activates tumor-specific immune response in a mouse model of prostate cancer." Vaccine **28**(20): 3548-3557.
Marx, J. (2005). "Fused genes may help explain the origins of prostate cancer." Science **310**(5748): 603-603.
Matsumoto, A. M. and W. J. Bremner (2004). "Serum testosterone assays—accuracy matters." The Journal of Clinical Endocrinology & Metabolism **89**(2): 520-524.
Mattsson, J. M., S. Ravela, C. Hekim, M. Jonsson, J. Malm, A. Närvänen, U.-H. Stenman and H. Koistinen (2014). "Proteolytic activity of prostate-specific antigen (PSA) towards protein substrates and effect of peptides stimulating PSA activity." PloS one **9**(9): e107819.
McCabe, M. T., J. N. Davis and M. L. Day (2005). "Regulation of DNA methyltransferase 1 by the pRb/E2F1 pathway." Cancer Res **65**(9): 3624-3632.
McEwan, I. J. and J.-Å. Gustafsson (1997). "Interaction of the human androgen receptor transactivation function with the general transcription factor TFIIF." Proceedings of the National Academy of Sciences **94**(16): 8485-8490.
McNair, C., A. Urbanucci, C. E. Comstock, M. A. Augello, J. F. Goodwin, R. Launchbury, S. Zhao, M. J. Schiewer, A. Ertel and J. Karnes (2017). "Cell cycle-coupled expansion of AR activity promotes cancer progression." Oncogene **36**(12): 1655-1668.
McNair, C., K. Xu, A. C. Mandigo, M. Benelli, B. Leiby, D. Rodrigues, J. Lindberg, H. Gronberg, M. Crespo and B. De Laere (2018). "Differential impact of RB status on E2F1 reprogramming in human cancer." The Journal of clinical investigation **128**(1): 341-358.
Meliani, A., C. Leborgne, S. Triffault, L. Jeanson-Leh, P. Veron and F. Mingozzi (2015). "Determination of anti-adeno-associated virus vector neutralizing antibody titer with an in vitro reporter system." Human gene therapy methods **26**(2): 45-53.
Metsalu, T. and J. Vilo (2015). "ClustVis: a web tool for visualizing clustering of multivariate data using Principal Component Analysis and heatmap." Nucleic acids research **43**(W1): W566-W570.
Metsalu, T. and J. Vilo (2015). "ClustVis: a web tool for visualizing clustering of multivariate data using Principal Component Analysis and heatmap." Nucleic Acids Res **43**(W1): W566-570.
Mi, H., A. Muruganujan, D. Ebert, X. Huang and P. D. Thomas (2019). "PANTHER version 14: more genomes, a new PANTHER GO-slim and improvements in enrichment analysis tools." Nucleic acids research **47**(D1): D419-D426.

Mi, H., A. Muruganujan, X. Huang, D. Ebert, C. Mills, X. Guo and P. D. Thomas (2019). "Protocol Update for large-scale genome and gene function analysis with the PANTHER classification system (v. 14.0)." Nature protocols **14**(3): 703-721.
Mikkelsen, T. S., M. Ku, D. B. Jaffe, B. Issac, E. Lieberman, G. Giannoukos, P. Alvarez, W. Brockman, T.-K. Kim and R. P. Koche (2007). "Genome-wide maps of chromatin state in pluripotent and lineage-committed cells." Nature **448**(7153): 553-560.
Missiaglia, E., M. Donadelli, M. Palmieri, T. Crnogorac-Jurcevic, A. Scarpa and N. R. Lemoine (2005). "Growth delay of human pancreatic cancer cells by methylase inhibitor 5-aza-2'-deoxycytidine treatment is associated with activation of the interferon signalling pathway." Oncogene **24**(1): 199-211.
Mohammad, O. S., M. D. Nyquist, M. T. Schweizer, S. P. Balk, E. Corey, S. Plymate, P. S. Nelson and E. A. Mostaghel (2017). "Supraphysiologic Testosterone Therapy in the Treatment of Prostate Cancer: Models, Mechanisms and Questions." Cancers (Basel) **9**(12).
Moore, N. L., G. Buchanan, J. M. Harris, L. A. Selth, T. Bianco-Miotto, A. R. Hanson, S. N. Birrell, L. M. Butler, T. E. Hickey and W. D. Tilley (2012). "An androgen receptor mutation in the MDA-MB-453 cell line model of molecular apocrine breast cancer compromises receptor activity." Endocrine related cancer **19**(4): 599.
Morel, K. L., A. V. Sheahan, D. L. Burkhart, S. C. Baca, N. Boufaied, Y. Liu, X. Qiu, I. Cañadas, K. Roehle and M. Heckler (2021). "EZH2 inhibition activates a dsRNA–STING–interferon stress axis that potentiates response to PD-1 checkpoint blockade in prostate cancer." Nature Cancer: 1-13.
Morel, K. L., A. V. Sheahan, D. L. Burkhart, S. C. Baca, N. Boufaied, Y. Liu, X. Qiu, I. Cañadas, K. Roehle and M. Heckler (2021). "EZH2 inhibition activates a dsRNA–STING–interferon stress axis that potentiates response to PD-1 checkpoint blockade in prostate cancer." Nature cancer **2**(4): 444-456.
Morel, K. L., A. V. Sheahan, D. L. Burkhart, S. C. Baca, N. Boufaied, Y. Liu, X. Qiu, I. Canadas, K. Roehle, M. Heckler, C. Calagua, H. Ye, C. Pantelidou, P. Galbo, S. Panja, A. Mitrofanova, S. Wilkinson, N. C. Whitlock, S. Y. Trostel, A. A. Hamid, A. S. Kibel, D. A. Barbie, A. D. Choudhury, M. M. Pomerantz, C. J. Sweeney, H. W. Long, D. J. Einstein, G. I. Shapiro, S. K. Dougan, A. G. Sowalsky, H. H. He, M. L. Freedman, S. P. Balk, M. Loda, D. P. Labbe, B. M. Olson and L. Ellis (2021). "EZH2 inhibition activates a dsRNA-STING-interferon stress axis that potentiates response to PD-1 checkpoint blockade in prostate cancer." Nat Cancer **2**(4): 444-456.
Moses, M., U. Koksal, E. Ledet, C. Manogue, P. Cotogno, B. Lewis, J. Layton, A. O. Sartor and P. Barata (2020). "Evaluation of the genomic alterations in the androgen receptor gene during treatment with high-dose testosterone for metastatic castrate-resistant prostate cancer." Oncotarget **11**(1): 15.
Mottet, N., J. Bellmunt, M. Bolla, E. Briers, M. G. Cumberbatch, M. De Santis, N. Fossati, T. Gross, A. M. Henry and S. Joniau (2017). "EAU-ESTRO-SIOG guidelines on prostate cancer. Part 1: screening, diagnosis, and local treatment with curative intent." European urology **71**(4): 618-629.
Mu, W., J. Starmer, A. M. Fedoriw, D. Yee and T. Magnuson (2014). "Repression of the soma-specific transcriptome by Polycomb-repressive complex 2 promotes male germ cell development." Genes & development **28**(18): 2056-2069.
Mu, W., J. Starmer, D. Yee and T. Magnuson (2018). "EZH2 variants differentially regulate polycomb repressive complex 2 in histone methylation and cell differentiation." Epigenetics & chromatin **11**(1): 1-14.
Murthy, S., M. Wu, V. U. Bai, Z. Hou, M. Menon, E. R. Barrack, S.-H. Kim and G. P.-V. Reddy (2013). "Role of Androgen Receptor in Progression of LNCaP Prostate Cancer Cells from G 1 to S Phase." PloS one **8**(2): e56692.

Nakada, S. Y., P. di Sant'Agnese, R. A. Moynes, R. A. Hiipakka, S. Liao, A. T. Cockett and P.-A. Abrahamsson (1993). "The androgen receptor status of neuroendocrine cells in human benign and malignant prostatic tissue." Cancer research **53**(9): 1967-1970.
Nevinny-Stickel, H. B., M. M. Dederick, C. R. Haines and T. C. Hall (1964). "Comparative Study of 6-Dehydro-17alpha-Methyltestosterone and Testosterone Propionate in Human Breast Cancer." Cancer **17**: 95-99.
Ni, G., Z. Ma and B. Damania (2018). "cGAS and STING: At the intersection of DNA and RNA virus-sensing networks." PLoS Pathog **14**(8): e1007148.
Niu, Y., S. Altuwaijri, K.-P. Lai, C.-T. Wu, W. A. Ricke, E. M. Messing, J. Yao, S. Yeh and C. Chang (2008). "Androgen receptor is a tumor suppressor and proliferator in prostate cancer." Proceedings of the National Academy of Sciences **105**(34): 12182-12187.
Nyquist, M. D., A. Corella, J. Burns, I. Coleman, S. Gao, R. Tharakan, L. Riggan, C. Cai, E. Corey and P. S. Nelson (2017). "Exploiting AR-regulated drug transport to induce sensitivity to the survivin inhibitor YM155." Molecular Cancer Research **15**(5): 521-531.
Nyquist, M. D., A. Corella, O. Mohamad, I. Coleman, A. Kaipainen, D. A. Kuppers, J. M. Lucas, P. J. Paddison, S. R. Plymate and P. S. Nelson (2019). "Molecular determinants of response to high-dose androgen therapy in prostate cancer." JCI insight **4**(19).
Nyquist, M. D., A. Corella, O. Mohamad, I. Coleman, A. Kaipainen, D. A. Kuppers, J. M. Lucas, P. J. Paddison, S. R. Plymate, P. S. Nelson and E. A. Mostaghel (2019). "Molecular determinants of response to high-dose androgen therapy in prostate cancer." JCI Insight **4**(19).
Nyquist, M. D., Y. Li, T. H. Hwang, L. S. Manlove, R. L. Vessella, K. A. Silverstein, D. F. Voytas and S. M. Dehm (2013). "TALEN-engineered AR gene rearrangements reveal endocrine uncoupling of androgen receptor in prostate cancer." Proc Natl Acad Sci U S A **110**(43): 17492-17497.
Organization, W. H. (2012). International Agency For Research on Cancer GLOBOCAN 2012: estimated cancer incidence, mortality and prevalence worldwide in 2012, Geneva.
Owen, K. L., L. J. Gearing, D. J. Zanker, N. K. Brockwell, W. H. Khoo, D. L. Roden, M. Cmero, S. Mangiola, M. K. Hong and A. J. Spurling (2020). "Prostate cancer cell-intrinsic interferon signaling regulates dormancy and metastatic outgrowth in bone." EMBO reports **21**(6): e50162.
Owen, K. L., L. J. Gearing, D. J. Zanker, N. K. Brockwell, W. H. Khoo, D. L. Roden, M. Cmero, S. Mangiola, M. K. Hong, A. J. Spurling, M. McDonald, C. L. Chan, A. Pasam, R. J. Lyons, H. M. Duivenvoorden, A. Ryan, L. M. Butler, J. M. Mariadason, T. Giang Phan, V. M. Hayes, S. Sandhu, A. Swarbrick, N. M. Corcoran, P. J. Hertzog, P. I. Croucher, C. Hovens and B. S. Parker (2020). "Prostate cancer cell-intrinsic interferon signaling regulates dormancy and metastatic outgrowth in bone." EMBO Rep **21**(6): e50162.
Paltoglou, S., R. Das, S. L. Townley, T. E. Hickey, G. A. Tarulli, I. Coutinho, R. Fernandes, A. R. Hanson, I. Denis and J. S. Carroll (2017). "Novel androgen receptor coregulator GRHL2 exerts both oncogenic and antimetastatic functions in prostate cancer." Cancer research **77**(13): 3417-3430.
Panda, A. K., D. Chakraborty, I. Sarkar, T. Khan and G. Sa (2017). "New insights into therapeutic activity and anticancer properties of curcumin." Journal of experimental pharmacology **9**: 31.
Parolia, A., M. Cieslik, S.-C. Chu, L. Xiao, T. Ouchi, Y. Zhang, X. Wang, P. Vats, X. Cao and S. Pitchiaya (2019). "Distinct structural classes of activating FOXA1 alterations in advanced prostate cancer." Nature **571**(7765): 413-418.
Patt, M., K. R. Beck, T. Di Marco, M.-C. Jäger, V. González-Ruiz, J. Boccard, S. Rudaz, R. W. Hartmann, M. Salah and C. J. van Koppen (2020). "Profiling of anabolic androgenic steroids and selective androgen receptor modulators for interference with adrenal steroidogenesis." Biochemical Pharmacology **172**: 113781.

Pauler, F. M., M. A. Sloane, R. Huang, K. Regha, M. V. Koerner, I. Tamir, A. Sommer, A. Aszodi, T. Jenuwein and D. P. Barlow (2009). "H3K27me3 forms BLOCs over silent genes and intergenic regions and specifies a histone banding pattern on a mouse autosomal chromosome." Genome research **19**(2): 221-233.
Pereira de Jésus-Tran, K., P. L. Côté, L. Cantin, J. Blanchet, F. Labrie and R. Breton (2006). "Comparison of crystal structures of human androgen receptor ligand-binding domain complexed with various agonists reveals molecular determinants responsible for binding affinity." Protein Science **15**(5): 987-999.
Pihlajamaa, P., B. Sahu and O. A. Jänne (2015). "Determinants of receptor-and tissue-specific actions in androgen signaling." Endocrine reviews **36**(4): 357-384.
Polkinghorn, W. R., J. S. Parker, M. X. Lee, E. M. Kass, D. E. Spratt, P. J. Iaquinta, V. K. Arora, W.-F. Yen, L. Cai and D. Zheng (2013). "Androgen receptor signaling regulates DNA repair in prostate cancers." Cancer discovery **3**(11): 1245-1253.
Polkinghorn, W. R., J. S. Parker, M. X. Lee, E. M. Kass, D. E. Spratt, P. J. Iaquinta, V. K. Arora, W. F. Yen, L. Cai, D. Zheng, B. S. Carver, Y. Chen, P. A. Watson, N. P. Shah, S. Fujisawa, A. G. Goglia, A. Gopalan, H. Hieronymus, J. Wongvipat, P. T. Scardino, M. J. Zelefsky, M. Jasin, J. Chaudhuri, S. N. Powell and C. L. Sawyers (2013). "Androgen receptor signaling regulates DNA repair in prostate cancers." Cancer Discov **3**(11): 1245-1253.
Pomerantz, M. M., F. Li, D. Y. Takeda, R. Lenci, A. Chonkar, M. Chabot, P. Cejas, F. Vazquez, J. Cook and R. A. Shivdasani (2015). "The androgen receptor cistrome is extensively reprogrammed in human prostate tumorigenesis." Nature genetics **47**(11): 1346.
Prekovic, S., T. Van den Broeck, L. Moris, E. Smeets, F. Claessens, S. Joniau, C. Helsen and G. Attard (2018). "Treatment-induced changes in the androgen receptor axis: Liquid biopsies as diagnostic/prognostic tools for prostate cancer." Molecular and cellular endocrinology **462**: 56-63.
Quinlan, A. R. and I. M. Hall (2010). "BEDTools: a flexible suite of utilities for comparing genomic features." Bioinformatics **26**(6): 841-842.
Rakotondrafara, A. M. and W. A. Miller (2008). In vitro analysis of translation enhancers. Plant Virology Protocols, Springer**:** 113-124.
Ramírez, F., D. P. Ryan, B. Grüning, V. Bhardwaj, F. Kilpert, A. S. Richter, S. Heyne, F. Dündar and T. Manke (2016). "deepTools2: a next generation web server for deep-sequencing data analysis." Nucleic acids research **44**(W1): W160-W165.
Rebello, R. J., C. Oing, K. E. Knudsen, S. Loeb, D. C. Johnson, R. E. Reiter, S. Gillessen, T. Van der Kwast and R. G. Bristow (2021). "Prostate cancer." Nat Rev Dis Primers **7**(1): 9.
Rehwinkel, J. and M. U. Gack (2020). "RIG-I-like receptors: their regulation and roles in RNA sensing." Nat Rev Immunol **20**(9): 537-551.
Reid, J., I. Murray, K. Watt, R. Betney and I. J. McEwan (2002). "The androgen receptor interacts with multiple regions of the large subunit of general transcription factor TFIIF." Journal of Biological Chemistry **277**(43): 41247-41253.
Reik, W. (2007). "Stability and flexibility of epigenetic gene regulation in mammalian development." Nature **447**(7143): 425-432.
Reik, W. (2007). "Stability and flexibility of epigenetic gene regulation in mammalian development." Nature **447**(7143): 425-432.
Resnick, M. I. and I. M. Thompson (2000). Advanced therapy of prostate disease, PMPH-USA.
Reusswig, K.-U., F. Zimmermann, L. Galanti and B. Pfander (2016). "Robust replication control is generated by temporal gaps between licensing and firing phases and depends on degradation of firing factor Sld2." Cell reports **17**(2): 556-569.

Rizq, O., N. Mimura, M. Oshima, A. Saraya, S. Koide, Y. Kato, K. Aoyama, Y. Nakajima-Takagi, C. Wang and T. Chiba (2017). "Dual inhibition of EZH2 and EZH1 sensitizes PRC2-dependent tumors to proteasome inhibition." Clinical Cancer Research **23**(16): 4817-4830.
Robinson, D., E. M. Van Allen, Y.-M. Wu, N. Schultz, R. J. Lonigro, J.-M. Mosquera, B. Montgomery, M.-E. Taplin, C. C. Pritchard and G. Attard (2015). "Integrative clinical genomics of advanced prostate cancer." Cell **161**(5): 1215-1228.
Robinson, E. J., D. E. Neal and A. T. Collins (1998). "Basal cells are progenitors of luminal cells in primary cultures of differentiating human prostatic epithelium." The Prostate **37**(3): 149-160.
Robinson, J. T., H. Thorvaldsdóttir, W. Winckler, M. Guttman, E. S. Lander, G. Getz and J. P. Mesirov (2011). "Integrative genomics viewer." Nature biotechnology **29**(1): 24-26.
Robinson, M. D., D. J. McCarthy and G. K. Smyth (2010). "edgeR: a Bioconductor package for differential expression analysis of digital gene expression data." Bioinformatics **26**(1): 139-140.
Roediger, J., W. Hessenkemper, S. Bartsch, M. Manvelyan, S. S. Huettner, T. Liehr, M. Esmaeili, S. Foller, I. Petersen and M.-O. Grimm (2014). "Supraphysiological androgen levels induce cellular senescence in human prostate cancer cells through the Src-Akt pathway." Molecular cancer **13**(1): 214.
Rooney, M. S., S. A. Shukla, C. J. Wu, G. Getz and N. Hacohen (2015). "Molecular and genetic properties of tumors associated with local immune cytolytic activity." Cell **160**(1-2): 48-61.
Roulois, D., H. Loo Yau, R. Singhania, Y. Wang, A. Danesh, S. Y. Shen, H. Han, G. Liang, P. A. Jones, T. J. Pugh, C. O'Brien and D. D. De Carvalho (2015). "DNA-Demethylating Agents Target Colorectal Cancer Cells by Inducing Viral Mimicry by Endogenous Transcripts." Cell **162**(5): 961-973.
Saartok, T., E. Dahlberg and J.-Å. GUSTAFSSON (1984). "Relative binding affinity of anabolic-androgenic steroids: comparison of the binding to the androgen receptors in skeletal muscle and in prostate, as well as to sex hormone-binding globulin." Endocrinology **114**(6): 2100-2106.
Saartok, T., E. Dahlberg and J. A. Gustafsson (1984). "Relative binding affinity of anabolic-androgenic steroids: comparison of the binding to the androgen receptors in skeletal muscle and in prostate, as well as to sex hormone-binding globulin." Endocrinology **114**(6): 2100-2106.
Salerno, M., O. Cascio, G. Bertozzi, F. Sessa, A. Messina, V. Monda, L. Cipolloni, A. Biondi, A. Daniele and C. Pomara (2018). "Anabolic androgenic steroids and carcinogenicity focusing on Leydig cell: a literature review." Oncotarget **9**(27): 19415.
Sanchez-Osorio, M., A. Duarte-Rojo, B. Martinez-Benitez, A. Torre and M. Uribe (2008). "Anabolic-androgenic steroids and liver injury." Liver Int **28**(2): 278-282.
Sanda, M. G., N. P. Restifo, J. C. Walsh, Y. Kawakami, W. G. Nelson, D. M. Pardoll and J. W. Simons (1995). "Molecular characterization of defective antigen processing in human prostate cancer." JNCI: Journal of the National Cancer Institute **87**(4): 280-285.
Scher, H. I., G. Buchanan, W. Gerald, L. M. Butler and W. D. Tilley (2004). "Targeting the androgen receptor: improving outcomes for castration-resistant prostate cancer." Endocrine-related cancer **11**(3): 459-476.
Scher, H. I., K. Fizazi, F. Saad, M.-E. Taplin, C. N. Sternberg, K. Miller, R. de Wit, P. Mulders, K. N. Chi and N. D. Shore (2012). "Increased survival with enzalutamide in prostate cancer after chemotherapy." New England Journal of Medicine **367**(13): 1187-1197.
Schmittgen, T. D. and K. J. Livak (2008). "Analyzing real-time PCR data by the comparative C T method." Nature protocols **3**(6): 1101.
Schneider, C. A., W. S. Rasband and K. W. Eliceiri (2012). "NIH Image to ImageJ: 25 years of image analysis." Nature methods **9**(7): 671-675.

Schweizer, M. T., E. S. Antonarakis, M. A. Eisenberger, P. Nelson, J. Luo, C. Pritchard and S. R. Denmeade (2019). "Genomic determinants of sensitivity to bipolar androgen therapy (BAT) in castrate-resistant prostate cancer (CRPC)." Journal of Clinical Oncology **37**(7_suppl): 200-200.
Schweizer, M. T., E. S. Antonarakis, M. A. Eisenberger, P. Nelson, J. Luo, C. Pritchard and S. R. Denmeade (2019). Genomic determinants of sensitivity to bipolar androgen therapy (BAT) in castrate-resistant prostate cancer (CRPC), American Society of Clinical Oncology.
Schweizer, M. T., E. S. Antonarakis, H. Wang, A. S. Ajiboye, A. Spitz, H. Cao, J. Luo, M. C. Haffner, S. Yegnasubramanian and M. A. Carducci (2015). "Effect of bipolar androgen therapy for asymptomatic men with castration-resistant prostate cancer: results from a pilot clinical study." Science translational medicine **7**(269): 269ra262-269ra262.
Schweizer, M. T., E. S. Antonarakis, H. Wang, A. S. Ajiboye, A. Spitz, H. Cao, J. Luo, M. C. Haffner, S. Yegnasubramanian, M. A. Carducci, M. A. Eisenberger, J. T. Isaacs and S. R. Denmeade (2015). "Effect of bipolar androgen therapy for asymptomatic men with castration-resistant prostate cancer: results from a pilot clinical study." Sci Transl Med **7**(269): 269ra262.
Selleck, W. A., S. E. Canfield, W. A. Hassen, M. Meseck, A. I. Kuzmin, R. C. Eisensmith, S.-H. Chen and S. J. Hall (2003). "IFN-γ sensitization of prostate cancer cells to Fas-mediated death: a gene therapy approach." Molecular Therapy **7**(2): 185-192.
Sena, L. A., H. Wang, M. S. Lim Sc, I. Rifkind, N. Ngomba, J. T. Isaacs, J. Luo, C. Pratz, V. Sinibaldi, M. A. Carducci, C. J. Paller, M. A. Eisenberger, M. C. Markowski, E. S. Antonarakis and S. R. Denmeade (2021). "Bipolar androgen therapy sensitizes castration-resistant prostate cancer to subsequent androgen receptor ablative therapy." Eur J Cancer **144**: 302-309.
Shaffer, P. L., A. Jivan, D. E. Dollins, F. Claessens and D. T. Gewirth (2004). "Structural basis of androgen receptor binding to selective androgen response elements." Proceedings of the National Academy of Sciences **101**(14): 4758-4763.
Shah, R. B. and M. Zhou (2012). Anatomy and Normal Histology of the Prostate Pertinent to Biopsy Practice. Prostate Biopsy Interpretation: An Illustrated Guide, Springer**:** 1-10.
Sharma, A., W.-S. Yeow, A. Ertel, I. Coleman, N. Clegg, C. Thangavel, C. Morrissey, X. Zhang, C. E. Comstock and A. K. Witkiewicz (2010). "The retinoblastoma tumor suppressor controls androgen signaling and human prostate cancer progression." The Journal of clinical investigation **120**(12): 4478-4492.
Shen, L., N.-Y. Shao, X. Liu, I. Maze, J. Feng and E. J. Nestler (2013). "diffReps: detecting differential chromatin modification sites from ChIP-seq data with biological replicates." PloS one **8**(6): e65598.
Sheng, W., M. W. LaFleur, T. H. Nguyen, S. Chen, A. Chakravarthy, J. R. Conway, Y. Li, H. Chen, H. Yang, P. H. Hsu, E. M. Van Allen, G. J. Freeman, D. D. De Carvalho, H. H. He, A. H. Sharpe and Y. Shi (2018). "LSD1 Ablation Stimulates Anti-tumor Immunity and Enables Checkpoint Blockade." Cell **174**(3): 549-563 e519.
Shi, Y.-K., P. Y. Yan, Z.-H. Zhu, Y.-C. Han, B. Ren, J. B. Nelson and J.-H. Luo (2008). "MCM7 interacts with androgen receptor." The American journal of pathology **173**(6): 1758-1767.
Shiota, M., A. Yokomizo and M. Eto (2016). "Taxane chemotherapy for hormone-naive prostate cancer with its expanding role as breakthrough strategy." Frontiers in oncology **5**: 304.
Short, E., A. Y. Warren and M. Varma (2019). "Gleason grading of prostate cancer: a pragmatic approach." Diagnostic Histopathology **25**(10): 371-378.
Siegel, R. L., K. D. Miller and A. Jemal (2016). "Cancer statistics, 2016." CA: a cancer journal for clinicians **66**(1): 7-30.
Singh, D., P. G. Febbo, K. Ross, D. G. Jackson, J. Manola, C. Ladd, P. Tamayo, A. A. Renshaw, A. V. D'Amico and J. P. Richie (2002). "Gene expression correlates of clinical prostate cancer behavior." Cancer cell **1**(2): 203-209.

Smith, C., S. Ballard, M. Wyllie and J. Masters (1994). "Comparison of testosterone metabolism in benign prostatic hyperplasia and human prostate cancer cell lines in vitro." The Journal of steroid biochemistry and molecular biology **50**(3-4): 151-159.
Smith, C. M., S. A. Ballard, M. G. Wyllie and J. R. Masters (1994). "Comparison of testosterone metabolism in benign prostatic hyperplasia and human prostate cancer cell lines in vitro." J Steroid Biochem Mol Biol **50**(3-4): 151-159.
Sonneveld, E., H. J. Jansen, J. A. Riteco, A. Brouwer and B. van der Burg (2005). "Development of androgen-and estrogen-responsive bioassays, members of a panel of human cell line-based highly selective steroid-responsive bioassays." Toxicological Sciences **83**(1): 136-148.
Sowalsky, A. G., H. Ye, M. Bhasin, E. M. Van Allen, M. Loda, R. T. Lis, L. Montaser-Kouhsari, C. Calagua, F. Ma, J. W. Russo, R. J. Schaefer, O. S. Voznesensky, Z. Zhang, G. J. Bubley, B. Montgomery, E. A. Mostaghel, P. S. Nelson, M. E. Taplin and S. P. Balk (2018). "Neoadjuvant-Intensive Androgen Deprivation Therapy Selects for Prostate Tumor Foci with Diverse Subclonal Oncogenic Alterations." Cancer Res **78**(16): 4716-4730.
Spencer, T. E., G. Jenster, M. M. Burcin, C. D. Allis, J. Zhou, C. A. Mizzen, N. J. McKenna, S. A. Onate, S. Y. Tsai and M.-J. Tsai (1997). "Steroid receptor coactivator-1 is a histone acetyltransferase." Nature **389**(6647): 194-198.
Stelloo, S., A. M. Bergman and W. Zwart (2019). "Androgen receptor enhancer usage and the chromatin regulatory landscape in human prostate cancers." Endocrine-related cancer **26**(5): R267-R285.
Stone, M. L., K. B. Chiappinelli, H. Li, L. M. Murphy, M. E. Travers, M. J. Topper, D. Mathios, M. Lim, I. M. Shih, T. L. Wang, C. F. Hung, V. Bhargava, K. R. Wiehagen, G. S. Cowley, K. E. Bachman, R. Strick, P. L. Strissel, S. B. Baylin and C. A. Zahnow (2017). "Epigenetic therapy activates type I interferon signaling in murine ovarian cancer to reduce immunosuppression and tumor burden." Proc Natl Acad Sci U S A **114**(51): E10981-E10990.
Subramanian, A., P. Tamayo, V. K. Mootha, S. Mukherjee, B. L. Ebert, M. A. Gillette, A. Paulovich, S. L. Pomeroy, T. R. Golub and E. S. Lander (2005). "Gene set enrichment analysis: a knowledge-based approach for interpreting genome-wide expression profiles." Proceedings of the National Academy of Sciences **102**(43): 15545-15550.
Sugawara, T., S. J. Baumgart, E. Nevedomskaya, K. Reichert, H. Steuber, P. Lejeune, D. Mumberg and B. Haendler (2019). "Darolutamide is a potent androgen receptor antagonist with strong efficacy in prostate cancer models." International journal of cancer **145**(5): 1382-1394.
Sumiyoshi, T., K. Mizuno, T. Yamasaki, Y. Miyazaki, Y. Makino, K. Okasho, X. Li, N. Utsunomiya, T. Goto and T. Kobayashi (2019). "Clinical utility of androgen receptor gene aberrations in circulating cell-free DNA as a biomarker for treatment of castration-resistant prostate cancer." Scientific reports **9**(1): 1-12.
Sun, Q., L. Sun, H. H. Liu, X. Chen, R. B. Seth, J. Forman and Z. J. Chen (2006). "The specific and essential role of MAVS in antiviral innate immune responses." Immunity **24**(5): 633-642.
Sweeney, C. J., Y.-H. Chen, M. Carducci, G. Liu, D. F. Jarrard, M. Eisenberger, Y.-N. Wong, N. Hahn, M. Kohli and M. M. Cooney (2015). "Chemohormonal therapy in metastatic hormone-sensitive prostate cancer." New England Journal of Medicine **373**(8): 737-746.
Tagawa, S. T., E. S. Antonarakis, A. Gjyrezi, G. Galletti, S. Kim, D. Worroll, J. Stewart, A. Zaher, T. P. Szatrowski and K. V. Ballman (2019). "Expression of AR-V7 and ARv567es in circulating tumor cells correlates with outcomes to taxane therapy in men with metastatic prostate cancer treated in TAXYNERGY." Clinical Cancer Research **25**(6): 1880-1888.
Tan, M. E., J. Li, H. E. Xu, K. Melcher and E.-l. Yong (2015). "Androgen receptor: structure, role in prostate cancer and drug discovery." Acta Pharmacologica Sinica **36**(1): 3-23.

Teply, B. A., S. Kachhap, M. A. Eisenberger and S. R. Denmeade (2017). "Extreme Response to High-dose Testosterone in BRCA2- and ATM-mutated Prostate Cancer." Eur Urol **71**(3): 499.
Teply, B. A., S. Kachhap, M. A. Eisenberger and S. R. Denmeade (2017). "Extreme response to high-dose testosterone in BRCA2-and ATM-mutated prostate cancer." European urology **71**(3): 499.
Teply, B. A., H. Wang, B. Luber, R. Sullivan, I. Rifkind, A. Bruns, A. Spitz, M. DeCarli, V. Sinibaldi, C. F. Pratz, C. Lu, J. L. Silberstein, J. Luo, M. T. Schweizer, C. G. Drake, M. A. Carducci, C. J. Paller, E. S. Antonarakis, M. A. Eisenberger and S. R. Denmeade (2018). "Bipolar androgen therapy in men with metastatic castration-resistant prostate cancer after progression on enzalutamide: an open-label, phase 2, multicohort study." Lancet Oncol **19**(1): 76-86.
Terada, N., Y. Shimizu, T. Yoshida, A. Maeno, T. Kamba, T. Inoue, E. Nakamura, T. Kamoto and O. Ogawa (2010). "Antiandrogen withdrawal syndrome and alternative antiandrogen therapy associated with the W741C mutant androgen receptor in a novel prostate cancer xenograft." The Prostate **70**(3): 252-261.
Tewari, A. K., G. G. Yardimci, Y. Shibata, N. C. Sheffield, L. Song, B. S. Taylor, S. G. Georgiev, G. A. Coetzee, U. Ohler and T. S. Furey (2012). "Chromatin accessibility reveals insights into androgen receptor activation and transcriptional specificity." Genome biology **13**(10): 1-17.
Thomas, B. C. and D. E. Neal (2013). "Androgen deprivation treatment in prostate cancer." Bmj **346**: e8555.
Thompson, I. M., P. J. Goodman, C. M. Tangen, M. S. Lucia, G. J. Miller, L. G. Ford, M. M. Lieber, R. D. Cespedes, J. N. Atkins and S. M. Lippman (2003). "The influence of finasteride on the development of prostate cancer." New England Journal of Medicine **349**(3): 215-224.
Tiwari, N., V. K. Tiwari, L. Waldmeier, P. J. Balwierz, P. Arnold, M. Pachkov, N. Meyer-Schaller, D. Schübeler, E. van Nimwegen and G. Christofori (2013). "Sox4 is a master regulator of epithelial-mesenchymal transition by controlling Ezh2 expression and epigenetic reprogramming." Cancer cell **23**(6): 768-783.
Tomlins, S. A., R. Mehra, D. R. Rhodes, X. Cao, L. Wang, S. M. Dhanasekaran, S. Kalyana-Sundaram, J. T. Wei, M. A. Rubin and K. J. Pienta (2007). "Integrative molecular concept modeling of prostate cancer progression." Nature genetics **39**(1): 41-51.
Tomlins, S. A., D. R. Rhodes, S. Perner, S. M. Dhanasekaran, R. Mehra, X.-W. Sun, S. Varambally, X. Cao, J. Tchinda and R. Kuefer (2005). "Recurrent fusion of TMPRSS2 and ETS transcription factor genes in prostate cancer." science **310**(5748): 644-648.
Topper, M. J., M. Vaz, K. B. Chiappinelli, C. E. DeStefano Shields, N. Niknafs, R. C. Yen, A. Wenzel, J. Hicks, M. Ballew, M. Stone, P. T. Tran, C. A. Zahnow, M. D. Hellmann, V. Anagnostou, P. L. Strissel, R. Strick, V. E. Velculescu and S. B. Baylin (2017). "Epigenetic Therapy Ties MYC Depletion to Reversing Immune Evasion and Treating Lung Cancer." Cell **171**(6): 1284-1300 e1221.
Tsihlias, J., W. Zhang, N. Bhattacharya, M. Flanagan, L. Klotz and J. Slingerland (2000). "Involvement of p27Kip1 in G1 arrest by high dose 5 alpha-dihydrotestosterone in LNCaP human prostate cancer cells." Oncogene **19**(5): 670-679.
Umesono, K. and R. M. Evans (1989). "Determinants of target gene specificity for steroid/thyroid hormone receptors." Cell **57**(7): 1139-1146.
van de Wijngaart, D. J., M. Molier, S. J. Lusher, R. Hersmus, G. Jenster, J. Trapman and H. J. Dubbink (2010). "Systematic structure-function analysis of androgen receptor Leu701 mutants explains the properties of the prostate cancer mutant L701H." Journal of Biological Chemistry **285**(7): 5097-5105.
Van Leenders, G. J., W. R. Gage, J. L. Hicks, B. Van Balken, T. W. Aalders, J. A. Schalken and A. M. De Marzo (2003). "Intermediate cells in human prostate epithelium are enriched in proliferative inflammatory atrophy." The American journal of pathology **162**(5): 1529-1537.

Vander Griend, D. J., I. V. Litvinov and J. T. Isaacs (2014). "Conversion of androgen receptor signaling from a growth suppressor in normal prostate epithelial cells to an oncogene in prostate cancer cells involves a gain of function in c-Myc regulation." International journal of biological sciences **10**(6): 627.
Varambally, S., S. M. Dhanasekaran, M. Zhou, T. R. Barrette, C. Kumar-Sinha, M. G. Sanda, D. Ghosh, K. J. Pienta, R. G. Sewalt and A. P. Otte (2002). "The polycomb group protein EZH2 is involved in progression of prostate cancer." Nature **419**(6907): 624-629.
Veldscholte, J., C. Ris-Stalpers, G. Kuiper, G. Jenster, C. Berrevoets, E. Claassen, H. Van Rooij, J. Trapman, A. Brinkmann and E. Mulder (1990). "A mutation in the ligand binding domain of the androgen receptor of human INCaP cells affects steroid binding characteristics and response to anti-androgens." Biochemical and biophysical research communications **173**(2): 534-540.
Vignozzi, L., G. Rastrelli, G. Corona, M. Gacci, G. Forti and M. Maggi (2014). "Benign prostatic hyperplasia: a new metabolic disease?" Journal of endocrinological investigation **37**(4): 313-322.
Walter, M., A. Teissandier, R. Pérez-Palacios and D. Bourc'his (2016). "An epigenetic switch ensures transposon repression upon dynamic loss of DNA methylation in embryonic stem cells." Elife **5**: e11418.
Wang, J., Y. Cai, W. Yu, C. Ren, D. M. Spencer and M. Ittmann (2008). "Pleiotropic biological activities of alternatively spliced TMPRSS2/ERG fusion gene transcripts." Cancer research **68**(20): 8516-8524.
Wang, L., C. L. Hsu and C. Chang (2005). "Androgen receptor corepressors: an overview." The Prostate **63**(2): 117-130.
Wang, Q., W. Li, Y. Zhang, X. Yuan, K. Xu, J. Yu, Z. Chen, R. Beroukhim, H. Wang and M. Lupien (2009). "Androgen receptor regulates a distinct transcription program in androgen-independent prostate cancer." Cell **138**(2): 245-256.
Wang, S., J. Lawless and Z. Zheng (2020). "Prenatal low-dose methyltestosterone, but not dihydrotestosterone, treatment induces penile formation in female mice and guinea pigs." Biology of reproduction **102**(6): 1248-1260.
Wassef, M., A. Luscan, S. Aflaki, D. Zielinski, P. W. Jansen, H. I. Baymaz, A. Battistella, C. Kersouani, N. Servant and M. R. Wallace (2019). "EZH1/2 function mostly within canonical PRC2 and exhibit proliferation-dependent redundancy that shapes mutational signatures in cancer." Proceedings of the National Academy of Sciences **116**(13): 6075-6080.
Watson, P. A., V. K. Arora and C. L. Sawyers (2015). "Emerging mechanisms of resistance to androgen receptor inhibitors in prostate cancer." Nature Reviews Cancer **15**(12): 701-711.
Wen, S., Y. Niu and H. Huang (2019). "Posttranslational regulation of androgen dependent and independent androgen receptor activities in prostate cancer." Asian Journal of Urology.
Whittemore, A. S., L. N. Kolonel, A. H. Wu, E. M. John, R. P. Gallagher, G. R. Howe, J. D. Burch, J. Hankin, D. M. Dreon and D. W. West (1995). "Prostate cancer in relation to diet, physical activity, and body size in blacks, whites, and Asians in the United States and Canada." JNCI: Journal of the National Cancer Institute **87**(9): 652-661.
Wolf, S., P. Diel, M. K. Parr, F. Rataj, W. Schanzer, G. Vollmer and O. Zierau (2011). "Long-term detection of methyltestosterone (ab-) use by a yeast transactivation system." Arch Toxicol **85**(4): 285-292.
Wolf, S., P. Diel, M. K. Parr, F. Rataj, W. Schänzer, G. Vollmer and O. Zierau (2011). "Long-term detection of methyltestosterone (ab-) use by a yeast transactivation system." Archives of toxicology **85**(4): 285-292.
Xu, K., H. Shimelis, D. E. Linn, R. Jiang, X. Yang, F. Sun, Z. Guo, H. Chen, W. Li and H. Chen (2009). "Regulation of androgen receptor transcriptional activity and specificity by RNF6-induced ubiquitination." Cancer cell **15**(4): 270-282.

Xu, K., Z. J. Wu, A. C. Groner, H. H. He, C. Cai, R. T. Lis, X. Wu, E. C. Stack, M. Loda and T. Liu (2012). "EZH2 oncogenic activity in castration-resistant prostate cancer cells is Polycomb-independent." Science **338**(6113): 1465-1469.
Ylitalo, E. B., E. Thysell, E. Jernberg, M. Lundholm, S. Crnalic, L. Egevad, P. Stattin, A. Widmark, A. Bergh and P. Wikström (2017). "Subgroups of castration-resistant prostate cancer bone metastases defined through an inverse relationship between androgen receptor activity and immune response." European urology **71**(5): 776-787.
Yoder, J. A., C. P. Walsh and T. H. Bestor (1997). "Cytosine methylation and the ecology of intragenomic parasites." Trends in genetics **13**(8): 335-340.
Yu, J., J. Yu, R.-S. Mani, Q. Cao, C. J. Brenner, X. Cao, X. Wang, L. Wu, J. Li and M. Hu (2010). "An integrated network of androgen receptor, polycomb, and TMPRSS2-ERG gene fusions in prostate cancer progression." Cancer cell **17**(5): 443-454.
Yu, J., J. Yu, D. R. Rhodes, S. A. Tomlins, X. Cao, G. Chen, R. Mehra, X. Wang, D. Ghosh and R. B. Shah (2007). "A polycomb repression signature in metastatic prostate cancer predicts cancer outcome." Cancer research **67**(22): 10657-10663.
Zeng, Z., W. Zhang, A. P. Marand, B. Zhu, C. R. Buell and J. Jiang (2019). "Cold stress induces enhanced chromatin accessibility and bivalent histone modifications H3K4me3 and H3K27me3 of active genes in potato." Genome biology **20**(1): 1-17.
Zhang, Y., T. Liu, C. A. Meyer, J. Eeckhoute, D. S. Johnson, B. E. Bernstein, C. Nusbaum, R. M. Myers, M. Brown and W. Li (2008). "Model-based analysis of ChIP-Seq (MACS)." Genome biology **9**(9): 1-9.
Zhao, S. G., J. Lehrer, S. L. Chang, R. Das, N. Erho, Y. Liu, M. Sjöström, R. B. Den, S. J. Freedland and E. A. Klein (2019). "The immune landscape of prostate cancer and nomination of PD-L2 as a potential therapeutic target." JNCI: Journal of the National Cancer Institute **111**(3): 301-310.
Zheng, X.-j., W. Li, J. Yi, J.-y. Liu, L.-w. Ren, X.-m. Zhu, S.-w. Liu, J.-h. Wang and G.-h. Du (2020). "EZH2 regulates expression of FOXC1 by mediating H3K27me3 in breast cancers." Acta Pharmacologica Sinica: 1-9.
Zhou, L., T. Mudianto, X. Ma, R. Riley and R. Uppaluri (2020). "Targeting EZH2 Enhances Antigen Presentation, Antitumor Immunity, and Circumvents Anti–PD-1 Resistance in Head and Neck Cancer." Clinical Cancer Research **26**(1): 290-300.
Zhou, X. E., K. M. Suino-Powell, J. Li, Y. He, J. P. MacKeigan, K. Melcher, E.-L. Yong and H. E. Xu (2010). "Identification of SRC3/AIB1 as a preferred coactivator for hormone-activated androgen receptor." Journal of biological chemistry **285**(12): 9161-9171.